



Universiteit  
Leiden  
The Netherlands

## **Modelling the role of cytotoxic T lymphocytes in tumour regression**

Beck, R.J.

### **Citation**

Beck, R. J. (2021, June 22). *Modelling the role of cytotoxic T lymphocytes in tumour regression*. Retrieved from <https://hdl.handle.net/1887/3185765>

Version: Publisher's Version

License: [Licence agreement concerning inclusion of doctoral thesis in the Institutional Repository of the University of Leiden](#)

Downloaded from: <https://hdl.handle.net/1887/3185765>

**Note:** To cite this publication please use the final published version (if applicable).

Cover Page



Universiteit Leiden



The handle <http://hdl.handle.net/1887/3185765> holds various files of this Leiden University dissertation.

**Author:** Beck, R.J.

**Title:** Modelling the role of cytotoxic T lymphocytes in tumour regression

**Issue date:** 2021-06-22

Printing: [printenbind.nl](http://printenbind.nl)

© Copyright, Richard Beck, 2021

All rights reserved. No part of this book may be reproduced in any form or by any means without permission of the author.

# **Modelling the role of cytotoxic T lymphocytes in tumour regression**

Proefschrift

ter verkrijging van

de graad van doctor aan de Universiteit Leiden,

op gezag van rector magnificus prof.dr.ir. H. Bijl,

volgens besluit van het college voor promoties

te verdedigen op dinsdag 22 juni 2021

klokke 11.15 uur

door

Richard J. Beck



Promotor

Prof. Dr. B. van de Water      LACDR, Leiden University

Co-promotor

Dr. J.B. Beltman                  LACDR, Leiden University

Promotion committee

Prof. Dr. H. Irth                  LACDR, Leiden University (chair)

Prof. Dr. J.A. Bouwstra          LACDR, Leiden University (secretary)

Prof. Dr. R. Merks                Mathematical Institute, Leiden University

Prof. Dr. R.J. de Boer            Theoretical Biology and Bioinformatics, Utrecht University

Prof. Dr. A.J. Yates                Pathology and Cell Biology, Columbia University

This research was conducted at the Division of Drug Discovery and Safety of the Leiden Academic Centre for Drug Research, Leiden University, Leiden, The Netherlands

# Table of contents

<b>Chapter 1</b>	<b>1</b>
Introduction, aim and scope of the thesis	
<b>Chapter 2</b>	<b>15</b>
Heterogeneous, delayed-onset killing by multiple-hitting T cells: Stochastic simulations to assess methods for analysis of imaging data	
<b>Chapter 3</b>	<b>53</b>
Contact-Dependent Killing by Cytotoxic T Lymphocytes Is Insufficient for EL4 Tumor Regression in vivo	
<b>Chapter 4</b>	<b>75</b>
CD137-stimulated cytotoxic T lymphocytes exert superior tumour control due to an enhanced antimitotic effect on tumour cells	
<b>Chapter 5</b>	<b>101</b>
Quantification of T cell exhaustion in B16F10 melanoma through mathematical modeling	
<b>Chapter 6</b>	<b>129</b>
Discussion	
<b>Thesis summary</b>	<b>141</b>

# Chapter 1

## Introduction, aim and scope of the thesis

### Summary

- Immunotherapies are an emerging treatment paradigm with potential application to many cancer types.
- Currently, only a subset of patients responds to immunotherapy. Moreover, only a subset of cancers are currently treatable with immunotherapies.
- Greater insight into T cell interactions with cancer will inform and improve immunotherapeutic strategies.
- In this thesis, mathematical and computational models are applied to *in vivo* or *in vitro* datasets containing measurements of T cells.
- By quantifying T cell interactions using models, this thesis aims to improve understanding of T cell behaviour and thus contribute to the rational design of immunotherapies.

### Immunotherapies for cancer

The “immune surveillance” hypothesis was developed in the 1950’s and 1960’s in response to a number of studies which showed that mice could develop immunity to chemically induced tumours[1–3], as well as an increased understanding developed from homografts that the immune system could discriminate between cells which were native and non-native to the host[4]. The immune surveillance hypothesis was first proposed by Thomas Lewis[5] and later developed by Sir Macfarlane Burnet, who stated the following in 1964[6]:

“The phenomena manifested in homograft immunity, tolerance and the like are based on the existence of a process of immunological surveillance, which eliminates cells with surface antigenic structure recognizably different from that normal to the individual. Any carcinogenic process will be successful only if this control can be overcome: (i) by inhibition of the effector process of control which is presumed to be by the direct action of immunologically competent cells; (ii) by loss of any antigens recognizable as foreign; (iii) by the development of growth potential capable of overriding any immunological control.”

The immune surveillance hypothesis seemed to provide an explanation for several observations about the incidence of cancer in humans. Cancers occurred most frequently in the very young and old - when the immune system was just developing, or was in decline. Moreover, it had been noted that tumours occurred more frequently in patients with immune-deficiency disorders or those who had been administered immunosuppressive drugs[7]. In the following years a surge of interest followed, which is well exemplified by a rather pointed quote published in *Immunological Reviews* in 1971[8]:

“The theory of immunosurveillance of neoplasia is so well established that its further discussion and demonstration risk becoming rather boring. Any-one with the temerity to question its overriding importance is likely to be the subject of discrete but possibly well-deserved ridicule.”

A body of scientists willing to risk ridicule apparently existed, because by the mid 1970's the immune surveillance hypothesis was under attack. Other explanations for increased cancer frequency in immune-compromised humans were given: for example it was considered that cancer and immune-deficiency disorders may share a common cause, or that perhaps immunosuppressive drugs may themselves have had carcinogenic effects[9]. Studies which claimed to have demonstrated immunogenicity of tumours in mouse models were also called into question. Most evidence came from either allograft, chemically induced, or virally induced tumours in mice. It was argued that the process of allografting may have potentiated an immune response[10], or that tumours of chemical or viral origin were abnormally immunogenic and thus unrepresentative of spontaneously arising tumours[11]. The discovery of the nude mouse, which lacked a thymus and therefore was severely deficient in mature thymus cells (T cells)[12], provided evidence against the immune surveillance hypothesis: Nude mice showed no deficits in their ability to control chemically induced tumours[13] and no enhanced frequency of spontaneous tumour formation[14]. The immune surveillance hypothesis fell from favour, since the prevailing wisdom at the time was that the immune response simply discriminated between “self” and “nonself” - cancers were “self”, thus not usually recognised by the immune system.

Several developments in the late 1980's and the 1990's led to renewed interest in the possibility that tumours could be recognised by the immune system. First, tumour infiltrating lymphocytes - isolated from human melanoma tumours and expanded *ex vivo* - exerted cytolytic activity against fresh melanoma cells[15]. Second, certain antigens were identified on tumour cells to which T cells reacted[16,17]. Third, perforin and interferon- $\gamma$  (IFN- $\gamma$ ), known components of the immune system, were shown to be important in defending the host against tumorigenesis[18–21]. Fourth, tumours which developed in immunocompromised hosts were significantly more immunogenic[22], showing that tumours were sculpted by an immunogenic environment.

On the basis of these results, new theoretical frameworks were proposed. The “laws of lymphotics” gave an alternative perspective on the requirements for T cell responses - rather than simply responding to “self” or “nonself”, it was proposed that the immune system should respond instead to “danger”[23]. The idea was that T cells exist with the capacity to recognise a broad range of antigens, including those derived from the host. However, when a T cell meets an antigen-presenting cell there is a requirement for costimulatory signals in order for the T cell to become activated. If these signals are not supplied, tolerance is promoted instead. A refined version of the immunosurveillance hypothesis, the immunoediting hypothesis, was put forward to explain 1) why immunocompetent individuals experience cancer and 2) why most tumours are immunologically silent[24]. In the immunoediting hypothesis, nascent tumours are surveilled by the immune system and may be eliminated. However, the immune system exerts a strong selection pressure on tumours, so that any tumour which has progressed enough to be clinically detectable must have acquired features which allow it to evade an immune response. The knowledge that tumours are potentially immunogenic, but have evolved strategies to suppress

and evade an immune response, suggests that a broad range of cancers may be treatable if only the relevant immunosuppressive mechanisms can be identified and removed.

Today, research efforts focussed on immunotherapy aim to characterise the interaction between the immune system and malignancies, to identify factors which may be limiting the immune response, and to devise strategies to augment the immune response to tumours. These strategies can be contextualised and understood by considering the “cancer-immunity cycle”[25]. The cancer-immunity cycle is a modern framework proposed to describe the self-reinforcing process which occurs after recognition of a malignancy by the immune system. Tumour antigens arrive in the draining lymph nodes where they are sampled by dendritic cells and then presented to naive CD8+ T cells. When presented with cognate antigen in the presence of appropriate costimulatory signals, T cells become activated and undergo rapid clonal expansion. The resulting clones recognize the antigen which triggered the expansion, thus they can attack the tumour. After T cells infiltrate the tumour and begin to kill tumour cells, further tumour antigens are released, thereby reinforcing the immune response. Any of these steps in the cancer-immunity cycle may be defective and could represent a therapeutic target. In a recent series of publications attempting to define the clinical immuno-oncology landscape[26–28], immunotherapeutic strategies for cancer treatment were stratified into 6 categories:

1. **Cell therapies** utilise engineered T cells to attack cancer cells.
2. **T cell targeted immunomodulators** modify T cell activity by activating stimulatory receptors or inhibiting suppressive receptors expressed on T cells.
3. **Other immunomodulators** enhance immunity by modulating immune cells other than T cells (e.g. tumour associated macrophages).
4. **Cancer vaccines** *prime the immune system to respond to tumour-associated antigens*[29]
5. **Oncolytic viruses** selectively infect and kill tumour cells, resulting in subsequent engagement of the immune system at the site of the tumour[30].
6. **CD3 targeted bispecific antibodies** are designed to simultaneously engage tumour antigens and the T cell co-receptor CD3, thus redirecting the immune response towards a tumour[31].

Some of these strategies have now begun to see clinical success, and amongst the most successful have been a class of T cell targeted immunomodulators known as immune checkpoint inhibitors which function by suppressing inhibitory receptors expressed on T cells. Ipilimumab, an antibody targeting the inhibitory receptor cytotoxic-T-lymphocyte-antigen-4 (CTLA-4), was the first immune checkpoint inhibitor to be approved for treatment of advanced melanoma in 2011. A phase III study showed that median overall survival increased to 11.1 months in the study group treated with ipilimumab plus dacarbazine, compared with 9.1 months in the trial arm treated with dacarbazine plus placebo[32]. In another phase III study conducted at around the same time, ipilimumab was compared to the glycoprotein 100 vaccine and improved survival from 6.4 months to 10.1 months[33]. Since the approval of ipilimumab, other immune checkpoint inhibitors have been approved, most notably inhibitors for the programmed death receptor-1 (PD-1) and its ligand, PD-L1. The checkmate 067 trial (ClinicalTrials.gov Identifier: NCT01844505) initiated in 2013 tested ipilimumab and the PD-1 inhibitor nivolumab either as monotherapies or in combination. At the recently published five year follow up, median overall survival was 19.9

months in the ipilimumab treated group; 36.9 months in the nivolumab treated group, and had not been reached in the combination treatment group (thus was greater than 60 months)[34].

Despite the extremely encouraging results demonstrated by the marked improvement in median survival time in the checkmate 067 study, not all patients responded to the therapy. Patient response was graded according to the RECIST criteria[35] which has 4 categories: Complete Response (CR), where no evidence of the disease remains; Partial Response (PR), where there is a measurable reduction in disease burden and no new lesions; Progressive Disease (PD), where there is a greater than 50% increase in the size of any existing lesion or there are new lesions; Stable Disease (SD), where none of the three other criteria have been met. The best responses achieved for the ipilimumab plus nivolumab combination in the checkmate 067 study were[34]: CR - 22%; PR - 36%; SD - 12%; PD - 24%, thus a significant number of patients did not respond to treatment. Indeed, a significant outstanding question in the field of immunotherapy is whether biomarkers can be found which predict which patients are most likely to benefit from treatment. Another question is whether other combinations exist that might yield enhanced clinical benefit, for example other immune checkpoints such as TIM-3 and LAG-3 which are both under investigation in combination with PD-1 inhibitors[36]. Further, although most successful so far in melanoma, immunotherapies are currently also employed in many other other types of cancer e.g. bladder cancer[37] and there is work to be done to expand the scope of immunotherapies further to other types of tumour. Improvements in our understanding of the interactions of T cells with tumours will be vital for the rational design of immunotherapies.

## **The role of Computational Models**

Theories provide an objective framework for interpreting experimental data[38]. An important feature of theories is that by logically following their consequences, predictions can be made. The iterative process of developing and revising theories, and then testing their consequences, is the basis for advancement of scientific knowledge. Therefore, theories are an indispensable component of the scientific method. Mathematical and computational models can be regarded as a class of theory, whose predictions are quantitative, specific, and precise. As such, mathematical modelling of the interaction between cancer and the immune system has an important role in guiding experimentation and generating new hypotheses. Mathematical modelling can incorporate processes believed to explain the dynamics of the system, and test whether these are indeed sufficient to explain what is actually observed. If the developed model can explain all the dynamics, the model is a cheap and convenient tool to study and predict the expected effect of different perturbations to the system. If the model cannot explain the system dynamics, new processes can be introduced into the model. In either case, the model should generate new and specific predictions which can be experimentally verified, in turn leading to new knowledge.

## **Computational Models of Cytotoxic T Cells**

Computational models have been developed to address several of the obstacles facing the development of successful immunotherapies[39]. Examples are models which have identified patient specific parameters such as antigenicity[40] or tumour size[41] which might be predictive of response to treatment. Other models have been developed to identify optimal dosage and

scheduling for immunotherapies[42], or to identify promising combination strategies for immunotherapeutic treatments[43]. Different model formalisms are typically employed depending on the studied phenomena of interest. For example, for the modelling of homogenous cell populations ordinary differential equation (ODE) models are typically applied[40,43,44]. When modelling populations of cells which are spatially heterogeneous but homogeneous otherwise, partial differential equation (PDE) models are employed[45,46]. When heterogeneous populations of cells are under consideration, agent based models (ABM) are applicable[47,48]. Different types of ABM are typically employed depending on the granularity required to describe the phenomena of interest. Cells are often represented as entities on two-dimensional or three-dimensional lattices, with a set of rules specified to determine permissible interactions between individual entities. When only the spatial location of a cell is of interest each cell may be adequately described by assigning it only a single lattice site[49,50]. In contrast, when a more realistic description of the interaction between individual cells is desired[51,52], formalisms such as the cellular Potts model[53] may be employed in which many lattice sites are assigned to represent a single cell.

In this thesis, we develop ODE models and ABMs of Cytotoxic T Lymphocytes (CTLs), otherwise known as “killer T cells” or CD8<sup>+</sup> T cells. CTLs are key players in the immune response, since their specificity combined with their ability to form a long lasting memory holds promise for long lasting and highly targeted interventions. In broad terms, there are only two ways by which a tumour may conceivably be controlled. Tumour cells may either be killed, or their proliferation may be suppressed. This leads to a very simple calculus for describing the evolution of a tumour over time, when considering only the dynamics of the tumour:

$$\frac{dT}{dt} = (g - d)T, \quad \text{Eq. 1}$$

where  $T$  is the number of tumour cells,  $g$  is the proliferation rate of the tumour cells, and  $d$  is the death rate of tumour cells. Noting that  $g$  and  $d$  are not necessarily constant and may depend on other cell types (see Eq’s 2-3 below), the model is extremely general and can be adapted to a wide range of realistic scenarios, and assumes only that “tumour cells” can be clearly defined and separated from normal (non malignant) cells. The model can exhibit 4 different types of behaviour corresponding to biologically relevant scenarios and analogous to the RECIST criteria for evaluating tumour response to therapy[35]. If  $g > d$ , then tumour cells proliferate faster than they die, so the tumour is progressing analogously to the PD RECIST evaluation. When  $g = d$ , the proliferation rate of tumour cells is exactly matched by their death rate, analogously to the SD RECIST evaluation. In the case where  $g < d$ , tumour cells die at a rate greater than they proliferate, so the tumour is in a regressing state, analogously to the PR RECIST evaluation. Should the tumour remain in the regressing state for a sufficient duration, then  $T \rightarrow 0$  and the tumour will be eliminated, corresponding to the CR RECIST evaluation.

In order to introduce CTLs into this calculus, our general strategy is to consider the growth and death rates of the tumour as functions depending on the presence of CTLs inside the tumour, which are denoted  $E$  (effectors) throughout this thesis:

$$g = f_g(E, \dots), \quad \text{Eq. 2}$$

$$d = f_d(E, \dots), \quad \text{Eq. 3}$$

thus  $f_g$  and  $f_d$  are functions representing the tumour growth and death rates (respectively), modified by the presence of CTLs. Our methodology is to study experimental data in which measurements of  $E$  and  $T$  are available or can be estimated. We will then attempt to determine forms for the functions  $f_g$  and  $f_d$  which are capable of matching the measurements made from the experimental data, subject to any other constraints which can be placed on the model. The resulting models should contain the minimum possible set of elements required to describe a given set of observations. Thus we will be able to test whether known interactions are minimally sufficient to quantitatively describe tumour progression in the presence of CTLs. We will also be able to assess, among a group of interactions, which play the greatest role in control of a tumour. Finally, if known interactions do not appear to be consistent with observed dynamics, our models will provide insights into the type of interactions which might explain the data, which will lead to new hypotheses and directions for experimental work.

## Research questions

Although the mathematical framework we have just established is simple, within it there lies scope for considerable complexity due to the plethora of pathways through which CTLs may be able to modify the proliferation or death rate of tumour cells. Within this scope, a number of specific research questions can be identified which will be addressed in this thesis. Below, the background of these questions is discussed, after which a thesis outline is provided.

### How can the rate at which CTLs kill target cells be quantified and what is the rate at which CTLs kill tumour cells?

The canonical function of CTLs is their ability to recognise and kill antigen presenting targets. CTLs are able to do this in a number of ways: secretion of the cytotoxic perforin and granzyme molecules towards the target cell membrane[54,55], induction of death via Fas-ligand[20,56,57], or release of soluble factors such as tumour necrosis factor which may facilitate target cell death[58]. Although the ability to directly kill antigen presenting cells is perhaps the most well recognised function of CTLs, quantifying this behaviour may be difficult. For example, it has been reported that CTLs can require multiple hits to kill target cells[59,60] (the ‘multiple-hitting hypothesis’), which can influence the dynamics of the killing process[51,61] and thus may hamper accurate determination of the underlying killing rate of the CTLs. In this thesis we devote substantial effort to characterising the killing rate of CTLs.



## **How important is the contribution of CTL mediated killing towards control of tumours?**

In addition to the “direct” means of killing tumour cells discussed in the previous paragraph, the arrival of CTLs at the tumour may lead to further downstream events which increase the rate at which tumour cells die - for example by recruitment of innate effectors into the tumour which go on to kill tumour cells[62]. Thus in this thesis we aim to quantify the importance of direct killing of tumour cells by CTLs, and ask whether such killing is sufficient to account for the reduction in tumour growth following adoptive transfer of CTLs.

## **How important are the antiproliferative effects that CTLs exert upon tumour cells?**

In addition to increasing the rate at which tumour cells die, there are also reported means by which CTLs may alter the growth rate of tumour cells. Activated CTLs secrete interferon- $\gamma$ , which has an antiproliferative effect on some tumour cells[63–65]. Additionally, the presence of CTLs inside the tumour has been linked to destruction of tumour vasculature which should exert an antiproliferative effect on tumour cells by depriving them of nutrients required for proliferation[66]. Thus, in this thesis we aim to identify and quantify the importance of antiproliferative effects exerted by CTLs upon tumour CTLs towards tumour regression.

## **What is the effect of CTL stimulation on their *in vivo* functionality?**

Since there is significant clinical interest in modulating the functions of CTLs to improve their anti-tumoural potential, we also ask how CTL functions could be modulated *in vivo*. In this thesis, we address that question in two ways. First, we study how CTL functions are modified after administration of a stimulating compound. For this we analyse a series of experiments wherein rates relevant for various aspects of the CTL:tumour interaction (i.e. CTL and tumour cell apoptosis/mitosis rates) are recorded in the presence or absence of agonist antibody anti-CD137. Initial clinical trials of such antibodies as a potential immune stimulatory therapy led to liver damage due to an inflammatory response in that organ, yet modified approaches that aim to target CD137 agonists specifically to the tumour are ongoing, e.g., by using bispecific constructs [67,68].

## **What is the contribution of immune checkpoint molecules towards CTL exhaustion?**

In our second approach to understanding potential for modulating CTL function, we studied the development of the “exhausted” phenotype among adoptively transferred CTLs. CTL exhaustion is characterised by a progressive loss of effector function alongside upregulation of inhibitory receptors among chronically stimulated populations of CTLs[69–71]. CTL exhaustion is currently of particular relevance due to the large number of immune checkpoint inhibitors currently being explored as immunotherapeutic strategies which aim to inhibit suppressive receptors expressed on CTLs and thereby reinvigorate exhausted CTLs. In this thesis we examine how CTL effector functions *in vivo* are diminished as the expression of several well known immune molecules increases, in order to characterise the contribution of these different immune checkpoints towards CTL exhaustion.

## Thesis outline

In the first section of this thesis (chapter 2), we study the killing behaviour of individual CTLs using stochastic models. Moreover, we develop statistical procedures which could be used to test for the multiple hitting hypothesis in future. In the second section of the thesis (chapters 3-5), we apply models to various *in vivo* datasets where CTLs were observed after adoptive transfer into tumours. By integrating data from different modalities to estimate values for key parameters which should determine tumour progression (e.g. the killing rate of CTLs and the proliferation rate of the tumour), we investigate the relationship between the estimated parameters and the progression of the tumours. This thesis concludes with a discussion of our findings, limitations of the work, and future research directions (chapter 6).

In chapter 2, we develop stochastic models of individual CTLs in order to better characterise the expected killing kinetics of multiple hitting CTLs. With the aid of these models, we re-examined a previously published *in vitro* dataset where CTLs were confined with antigen presenting targets and their killing kinetics were monitored over a period of 12 hours. In that dataset, the killing kinetics of the CTLs could not be explained by existing models. Therefore, a subpopulation of “high rate killer” CTLs had been invoked to explain the kinetics, despite the fact that no other evidence could be provided for such a hypothesis. Applying our models to this data, we show that the multiple hitting hypothesis was sufficient to account for the unexplained CTL kinetics, without any requirement to invoke a subpopulation of “high rate killer” CTLs. Moreover, we developed statistical procedures to be used for identification of multiple hitting CTLs in imaging data, and suggested experimental strategies for determining the presence of multiple hitting in future experiments.

In chapter 3, we study progression of a murine thymoma after adoptive transfer of CTLs. We parameterised spatial and nonspatial models with estimates of tumour proliferation rate, CTL killing rate, and estimates of the density of CTLs inside the tumours. In doing so, we showed that the reported killing rate of the CTLs was insufficient to account for the tumour regression that occurred in the experimental data. After also investigating whether uncertainties in the killing estimate due to multiple hitting could account for the apparent insufficiency in killing, we found that the discrepancy between the estimated versus observed rates of killing were too large to permit this explanation. Using a spatially explicit agent based model, we showed how an antiproliferative effect exerted by CTLs on the tumour could account for the discrepancy.

In chapter 4, we develop ordinary differential equation models applied to an experimental murine model of B16F10 melanoma. In these experiments, CTLs were adoptively transferred to melanoma bearing mice in the presence or absence of a stimulating antibody targeting the CD137 receptor. Our analysis revealed an extremely low killing rate of CTLs, and our models demonstrated that such a low killing rate combined with relatively low infiltration of CTLs should not have any important impact on tumour progression whatsoever. We also investigated the mechanisms underpinning the reduced rate of tumour progression in mice treated with CTLs alongside the stimulatory CD137 antibody. We found that CD137 antibody stimulation did not enhance the killing of transferred CTLs, but rather found that an improved antiproliferative effect or enhanced recruitment of CTLs to the site of the tumour was most compatible with the data.

In chapter 5, we again apply ordinary differential equation models applied to another experimental murine model of B16F10 melanoma following adoptive transfer of CTLs. In this series of experiments, a Fucci sensor was used allowing tracking of melanoma cells through the cell cycle. Additionally, transcript data was available to quantify the production of IFN- $\gamma$  inside the tumour. These data allowed us to refine the models developed in chapters 3-4 to include an explicit description of the cell cycle and the effect of IFN- $\gamma$  thereupon. The results obtained with this second B16F10 dataset agreed with those in chapter 4, i.e. an extremely low killing rate of CTLs meant that the IFN- $\gamma$  mediated antiproliferative effect of CTLs had the most substantial effect on tumour progression. Moreover, we found evidence of the development of an exhausted state amongst the tumour infiltrating CTLs, and using transcriptomics data we characterised the immune checkpoint molecules which best defined the development of the exhausted state amongst tumour infiltrating CTLs. This thesis concludes with a discussion of our findings, limitations of the work, and future research directions (chapter 6).

1. Gross L. Intradermal Immunization of C3H Mice against a Sarcoma That Originated in an Animal of the Same Line. *Cancer Res.* 1943;3: 326–333.
2. Prehn RT, Main JM. Immunity to methylcholanthrene-induced sarcomas. *J Natl Cancer Inst.* 1957;18: 769–778.
3. Foley EJ. Antigenic properties of methylcholanthrene-induced tumors in mice of the strain of origin. *Cancer Res.* 1953;13: 835–837.
4. Medawar PB. The Croonian Lecture: The homograft reaction. *Proceedings of the Royal Society of London Series B - Biological Sciences.* 1958;149: 145–166.
5. Thomas L, Lawrence HS. Cellular and humoral aspects of the hypersensitive states. New York: Hoeber-Harper. 1959; 529–532.
6. Burnet M. IMMUNOLOGICAL FACTORS IN THE PROCESS OF CARCINOGENESIS. *Br Med Bull.* 1964;20: 154–158.
7. Keast D. Immunosurveillance and cancer. *Lancet.* 1970;2: 710–712.
8. Prehn RT, Lappé MA. An immunostimulation theory of tumor development. *Transplant Rev.* 1971;7: 26–54.
9. Doll R, Kinlen L. Immunosurveillance and cancer: epidemiological evidence. *Br Med J.* 1970;4: 420–422.
10. Andrews EJ. Failure of immunosurveillance against chemically induced in situ tumors in mice. *J Natl Cancer Inst.* 1974;52: 729–732.

11. Hewitt HB, Blake ER, Walder AS. A critique of the evidence for active host defence against cancer, based on personal studies of 27 murine tumours of spontaneous origin. *Br J Cancer*. 1976;33: 241–259.
12. Pantelouris EM. Absence of thymus in a mouse mutant. *Nature*. 1968;217: 370–371.
13. Stutman O. Tumor development after 3-methylcholanthrene in immunologically deficient athymic-nude mice. *Science*. 1974;183: 534–536.
14. Rygaard J, Povlsen CO. The mouse mutant nude does not develop spontaneous tumours. An argument against immunological surveillance. *Acta Pathol Microbiol Scand B Microbiol Immunol*. 1974;82: 99–106.
15. Muul LM, Spiess PJ, Director EP, Rosenberg SA. Identification of specific cytolytic immune responses against autologous tumor in humans bearing malignant melanoma. *J Immunol*. 1987;138: 989–995.
16. Barnd DL, Lan MS, Metzgar RS, Finn OJ. Specific, major histocompatibility complex-unrestricted recognition of tumor-associated mucins by human cytotoxic T cells. *Proc Natl Acad Sci U S A*. 1989;86: 7159–7163.
17. van der Bruggen P, Traversari C, Chomez P, Lurquin C, De Plaen E, Van den Eynde B, et al. A gene encoding an antigen recognized by cytolytic T lymphocytes on a human melanoma. *Science*. 1991;254: 1643–1647.
18. Dighe AS, Richards E, Old LJ, Schreiber RD. Enhanced in vivo growth and resistance to rejection of tumor cells expressing dominant negative IFN $\gamma$  receptors. *Immunity*. 1994;1: 447–456.
19. Kaplan DH, Shankaran V, Dighe AS, Stockert E, Aguet M, Old LJ, et al. Demonstration of an interferon gamma-dependent tumor surveillance system in immunocompetent mice. *Proc Natl Acad Sci U S A*. 1998;95: 7556–7561.
20. van den Broek ME, Kägi D, Ossendorp F, Toes R, Vamvakas S, Lutz WK, et al. Decreased tumor surveillance in perforin-deficient mice. *J Exp Med*. 1996;184: 1781–1790.
21. Smyth MJ, Thia KY, Street SE, MacGregor D, Godfrey DI, Trapani JA. Perforin-mediated cytotoxicity is critical for surveillance of spontaneous lymphoma. *J Exp Med*. 2000;192: 755–760.
22. Shankaran V, Ikeda H, Bruce AT, White JM, Swanson PE, Old LJ, et al. IFN $\gamma$  and lymphocytes prevent primary tumour development and shape tumour immunogenicity. *Nature*. 2001;410: 1107–1111.
23. Matzinger P. Tolerance, danger, and the extended family. *Annu Rev Immunol*. 1994;12: 991–1045.

24. Dunn GP, Bruce AT, Ikeda H, Old LJ, Schreiber RD. Cancer immunoediting: from immunosurveillance to tumor escape. *Nat Immunol.* 2002;3: 991–998.
25. Chen DS, Mellman I. Oncology meets immunology: the cancer-immunity cycle. *Immunity.* 2013;39: 1–10.
26. Tang J, Shalabi A, Hubbard-Lucey VM. Comprehensive analysis of the clinical immuno-oncology landscape. *Ann Oncol.* 2018;29: 84–91.
27. Tang J, Pearce L, O'Donnell-Tormey J, Hubbard-Lucey VM. Trends in the global immuno-oncology landscape. *Nat Rev Drug Discov.* 2018;17: 783–784.
28. Xin Yu J, Hubbard-Lucey VM, Tang J. Immuno-oncology drug development goes global. *Nat Rev Drug Discov.* 2019;18: 899–900.
29. Finn OJ. Cancer vaccines: between the idea and the reality. *Nat Rev Immunol.* 2003;3: 630–641.
30. Kaufman HL, Kohlhapp FJ, Zloza A. Oncolytic viruses: a new class of immunotherapy drugs. *Nat Rev Drug Discov.* 2015;14: 642–662.
31. Yuraszeck T, Kasichayanula S, Benjamin JE. Translation and Clinical Development of Bispecific T-cell Engaging Antibodies for Cancer Treatment. *Clin Pharmacol Ther.* 2017;101: 634–645.
32. Robert C, Thomas L, Bondarenko I, O'Day S, Weber J, Garbe C, et al. Ipilimumab plus dacarbazine for previously untreated metastatic melanoma. *N Engl J Med.* 2011;364: 2517–2526.
33. Hodi FS, O'Day SJ, McDermott DF, Weber RW, Sosman JA, Haanen JB, et al. Improved survival with ipilimumab in patients with metastatic melanoma. *N Engl J Med.* 2010;363: 711–723.
34. Larkin J, Chiarion-Sileni V, Gonzalez R, Grob J-J, Rutkowski P, Lao CD, et al. Five-Year Survival with Combined Nivolumab and Ipilimumab in Advanced Melanoma. *N Engl J Med.* 2019;381: 1535–1546.
35. Eisenhauer EA, Therasse P, Bogaerts J, Schwartz LH, Sargent D, Ford R, et al. New response evaluation criteria in solid tumours: revised RECIST guideline (version 1.1). *Eur J Cancer.* 2009;45: 228–247.
36. Khair DO, Bax HJ, Mele S, Crescioli S, Pellizzari G, Khiabany A, et al. Combining Immune Checkpoint Inhibitors: Established and Emerging Targets and Strategies to Improve Outcomes in Melanoma. *Front Immunol.* 2019;10: 453.
37. Ghatalia P, Zibelman M, Geynisman DM, Plimack E. Approved checkpoint inhibitors in bladder cancer: which drug should be used when? *Ther Adv Med Oncol.* 2018;10: 1758835918788310.

38. Longo G, Soto AM. Why do we need theories? *Prog Biophys Mol Biol.* 2016;122: 4–10.
39. Konstorum A, Vella AT, Adler AJ, Laubenbacher RC. Addressing current challenges in cancer immunotherapy with mathematical and computational modelling. *J R Soc Interface.* 2017;14. doi:10.1098/rsif.2017.0150
40. Kirschner D, Panetta JC. Modeling immunotherapy of the tumor--immune interaction. *J Math Biol.* 1998;37: 235–252.
41. Kronik N, Kogan Y, Vainstein V, Agur Z. Improving alloreactive CTL immunotherapy for malignant gliomas using a simulation model of their interactive dynamics. *Cancer Immunol Immunother.* 2008;57: 425–439.
42. Ghaffari A, Naserifar N. Optimal therapeutic protocols in cancer immunotherapy. *Comput Biol Med.* 2010;40: 261–270.
43. de Pillis LG, Gu W, Radunskaya AE. Mixed immunotherapy and chemotherapy of tumors: modeling, applications and biological interpretations. *J Theor Biol.* 2006;238: 841–862.
44. Talkington A, Dantoin C, Durrett R. Ordinary Differential Equation Models for Adoptive Immunotherapy. *Bull Math Biol.* 2018;80: 1059–1083.
45. Lai X, Friedman A. Combination therapy of cancer with cancer vaccine and immune checkpoint inhibitors: A mathematical model. *PLoS One.* 2017;12: e0178479.
46. Matzavinos A, Chaplain MAJ, Kuznetsov VA. Mathematical modelling of the spatio-temporal response of cytotoxic T-lymphocytes to a solid tumour. *Math Med Biol.* 2004;21: 1–34.
47. Gong C, Milberg O, Wang B, Vicini P, Narwal R, Roskos L, et al. A computational multiscale agent-based model for simulating spatio-temporal tumour immune response to PD1 and PDL1 inhibition. *J R Soc Interface.* 2017;14. doi:10.1098/rsif.2017.0320
48. Kim PS, Lee PP. Modeling protective anti-tumor immunity via preventative cancer vaccines using a hybrid agent-based and delay differential equation approach. *PLoS Comput Biol.* 2012;8: e1002742.
49. Gerlee P, Anderson ARA. An evolutionary hybrid cellular automaton model of solid tumour growth. *J Theor Biol.* 2007;246: 583–603.
50. Monteagudo Á, Santos J. Treatment Analysis in a Cancer Stem Cell Context Using a Tumor Growth Model Based on Cellular Automata. *PLoS One.* 2015;10: e0132306.
51. Gadhamsetty S, Marée AFM, Beltman JB, de Boer RJ. A general functional response of cytotoxic T lymphocyte-mediated killing of target cells. *Biophys J.* 2014;106: 1780–1791.

52. Gadhamsetty S, Marée AFM, de Boer RJ, Beltman JB. Tissue Dimensionality Influences the Functional Response of Cytotoxic T Lymphocyte-Mediated Killing of Targets. *Front Immunol.* 2016;7: 668.
53. Graner F, Glazier JA. Simulation of biological cell sorting using a two-dimensional extended Potts model. *Phys Rev Lett.* 1992;69: 2013–2016.
54. Cullen SP, Brunet M, Martin SJ. Granzymes in cancer and immunity. *Cell Death Differ.* 2010;17: 616–623.
55. Voskoboinik I, Whisstock JC, Trapani JA. Perforin and granzymes: function, dysfunction and human pathology. *Nat Rev Immunol.* 2015;15: 388–400.
56. Caldwell SA, Ryan MH, McDuffie E, Abrams SI. The Fas/Fas ligand pathway is important for optimal tumor regression in a mouse model of CTL adoptive immunotherapy of experimental CMS4 lung metastases. *J Immunol.* 2003;171: 2402–2412.
57. Zhu Y, Huang B, Shi J. Fas ligand and lytic granule differentially control cytotoxic dynamics of natural killer cell against cancer target. *Oncotarget.* 2016;7: 47163–47172.
58. Faletti L, Peintner L, Neumann S, Sandler S, Grabinger T, Mac Nelly S, et al. TNF $\alpha$  sensitizes hepatocytes to FasL-induced apoptosis by NF $\kappa$ B-mediated Fas upregulation. *Cell Death Dis.* 2018;9: 909.
59. Caramalho I, Faroudi M, Padovan E, Müller S, Valitutti S. Visualizing CTL/melanoma cell interactions: multiple hits must be delivered for tumour cell annihilation. *J Cell Mol Med.* 2009;13: 3834–3846.
60. Halle S, Keyser KA, Stahl FR, Busche A, Marquardt A, Zheng X, et al. In Vivo Killing Capacity of Cytotoxic T Cells Is Limited and Involves Dynamic Interactions and T Cell Cooperativity. *Immunity.* 2016;44: 233–245.
61. Gadhamsetty S, Marée AFM, Beltman JB, de Boer RJ. A Sigmoid Functional Response Emerges When Cytotoxic T Lymphocytes Start Killing Fresh Target Cells. *Biophys J.* 2017;112: 1221–1235.
62. Nagoshi M, Sadanaga N, Joo HG, Goedegebuure PS, Eberlein TJ. Tumor-specific cytokine release by donor T cells induces an effective host anti-tumor response through recruitment of host naive antigen presenting cells. *Int J Cancer.* 1999;80: 308–314.
63. Chin YE, Kitagawa M, Su WC, You ZH, Iwamoto Y, Fu XY. Cell growth arrest and induction of cyclin-dependent kinase inhibitor p21 WAF1/CIP1 mediated by STAT1. *Science.* 1996;272: 719–722.

64. Harvat BL, Seth P, Jetten AM. The role of p27Kip1 in gamma interferon-mediated growth arrest of mammary epithelial cells and related defects in mammary carcinoma cells. *Oncogene*. 1997;14: 2111–2122.
65. Matsushita H, Hosoi A, Ueha S, Abe J, Fujieda N, Tomura M, et al. Cytotoxic T lymphocytes block tumor growth both by lytic activity and IFN $\gamma$ -dependent cell-cycle arrest. *Cancer Immunol Res*. 2015;3: 26–36.
66. Schietinger A, Arina A, Liu RB, Wells S, Huang J, Engels B, et al. Longitudinal confocal microscopy imaging of solid tumor destruction following adoptive T cell transfer. *Oncoimmunology*. 2013;2: e26677.
67. Makkouk A, Chester C, Kohrt HE. Rationale for anti-CD137 cancer immunotherapy. *Eur J Cancer*. 2016;54: 112–119.
68. Etxeberria I, Glez-Vaz J, Teijeira Á, Melero I. New emerging targets in cancer immunotherapy: CD137/4-1BB costimulatory axis. *ESMO Open*. 2020;4. doi:10.1136/esmoopen-2020-000733
69. Blank CU, Haining WN, Held W, Hogan PG, Kallies A, Lugli E, et al. Defining “T cell exhaustion.” *Nat Rev Immunol*. 2019;19: 665–674.
70. Thommen DS, Schumacher TN. T Cell Dysfunction in Cancer. *Cancer Cell*. 2018;33: 547–562.
71. Wherry EJ, Kurachi M. Molecular and cellular insights into T cell exhaustion. *Nat Rev Immunol*. 2015;15: 486–499.



# Chapter 2

## Heterogeneous, delayed-onset killing by multiple-hitting T cells: Stochastic simulations to assess methods for analysis of imaging data

Richard J. Beck, Dario I. Bijker and Joost B. Beltman

Division of Drug Discovery and Safety, Leiden Academic Centre for Drug Research, Leiden University, Leiden, The Netherlands

*PLoS computational biology* 16.7 (2020): e1007972.

### Abstract

Although quantitative insights into the killing behaviour of Cytotoxic T Lymphocytes (CTLs) are necessary for the rational design of immune-based therapies, CTL killing function remains insufficiently characterised. One established model of CTL killing treats CTL cytotoxicity as a Poisson process, based on the assumption that CTLs serially kill antigen-presenting target cells via delivery of lethal hits, each lethal hit corresponding to a single injection of cytotoxic proteins into the target cell cytoplasm. Contradicting this model, a recent *in vitro* study of individual CTLs killing targets over a 12-hour period found significantly greater heterogeneity in CTL killing performance than predicted by Poisson-based killing. The observed killing process was dynamic and varied between CTLs, with the best performing CTLs exhibiting a marked increase in killing during the final hours of the experiments, along with a “burst killing” kinetic. Despite a search for potential differences between CTLs, no mechanistic explanation for the heterogeneous killing kinetics was found. Here we have used stochastic simulations to assess whether target cells might require multiple hits from CTLs before undergoing apoptosis, in order to verify whether multiple-hitting could explain the late onset, burst killing dynamics observed *in vitro*. We found that multiple-hitting from CTLs was entirely consistent with the observed killing kinetics. Moreover, the number of available targets and the spatiotemporal kinetics of CTL:target interactions

influenced the realised CTL killing rate. We subsequently used realistic, spatial simulations to assess methods for estimating the hitting rate and the number of hits required for target death, to be applied to microscopy data of individual CTLs killing targets. We found that measuring the cumulative duration of individual contacts that targets have with CTLs would substantially improve accuracy when estimating the killing kinetics of CTLs.

## Introduction

Cytotoxic T Lymphocytes (CTLs) are key effectors in the adaptive immune response, therefore CTL function - or lack thereof - is relevant in many pathologies. A greater quantitative understanding of CTL effector function will aid in interpretation of prior experiments and should yield useful insights for the treatment of diseases in the future. However, the rate at which CTLs kill infected or malignant cells remains poorly characterised. Estimates of CTL killing based on *in vitro* and *in vivo* CTL killing assays vary, with some variation explained by e.g. different susceptibility of target cells to CTL killing or the type of antigen expressed by the targets [1,2]. Moreover, especially *in vivo* the presence of stimulatory or suppressive factors and difficulty in controlling or estimating the ratio of CTLs to target cells at the site of killing might confound CTL killing estimates [1,2].

As a frequently discussed example, consider the *in vivo* CTL killing assay of Barber *et. al.* [3], in which CTLs demonstrated rapid killing against Lymphocytic Choriomeningitic Virus (LCMV). Although Barber *et. al.* initially estimated that CTLs took 15 minutes to kill targets, subsequent modelling studies based on the same data have estimated much faster killing rates [4,5,6], with one study implying an expected target survival time of 16 seconds after contact from a CTL [4] (see also [1] for a detailed summary of these estimates). Given that killing in those experiments was perforin-dependent[3], these fast estimates seem to contradict recent *in-vivo* imaging showing that the perforin-dependent killing process requires a minimal contact time. For example, long-lasting (median: 80s) calcium fluxes linked with CTL killing of virally infected cells occurred, on average, 480s (median) after CTLs established contact with virally infected targets[7]. Such killing times of around 10 minutes are consistent with the duration of killing events that can be observed in various supplemental videos elsewhere [8,9]. Given this lower bound it is difficult to see how solely granule-mediated killing could plausibly lead to killing rates in excess of  $\sim 6 \text{ hour}^{-1}$ , even in optimal situations where CTLs are not limited in their supply of targets and do not require time to search for new targets between killing events.

A major limitation of many prior estimates of CTL killing is that analysis is performed on population level data in *in vivo* settings, with no direct measurements of the killing process. This approach has a number of drawbacks: First, it can be challenging to accurately assess the frequency of CTLs and target cells. Second, other immune cells may contribute to the killing process, confounding estimates of the true CTL killing rate. Third, the processes underlying CTL killing are complex and it may be insufficient to describe them with a single, time invariant rate constant. Indeed, recent observations have indicated that target cells may require multiple hits before death either *in vitro* [10], or *in vivo* [7]. We have previously shown that such multiple-hitting can lead to

a time-increasing killing kinetic when CTLs are exposed to fresh targets [11,12], further complicating the killing rate estimation procedure.

Besides analysing CTL killing performance at the population level, a potentially useful approach is to analyse CTL killing at the single cell level. Such analysis can yield greater insights into the dynamics of the killing process. This was exemplified in studies undertaken in the 1970's in which the killing kinetics of CTLs conjugated with 1-4 EL4 tumour cell targets were examined under the microscope for a period of 3 hours [13,14]. Subsequent mathematical analysis of these studies indicated that the CTL killing process was well described as a Poisson process [15], indicating that CTLs kill targets sequentially rather than simultaneously. This analysis allowed the authors to conclude that CTL killing was mediated by secretory lysosomes, several years before this was demonstrated conclusively [16]. The aforementioned studies also revealed that the rate of CTL killing was not diminished after target lysis, an observation which led the authors to deduce that CTLs were able to discriminate between viable and killed targets. More recently, *in vitro* studies of individual natural killer cells have shown that killing occurs via both granzyme and death receptor mediated pathways, each having different kinetics [17,18].

Despite the utility of studying CTL killing at the single-cell level, there remains a shortage of *in vitro* CTL killing studies with statistical power sufficient to check the validity of the Poisson model first proposed in the 1980's by Perelson et. al. [15]. Recently one such a study was performed: Over a 12 hour period, image-based killing measurements were taken from human-derived CTL clones, each CTL being separately confined within small micro-wells that contained an excess of JY target cells [19]. During the studied time period, the killing rate of CTLs was dynamic, exhibiting a marked increase in the final hours of the experiment. The total number of targets killed per CTL was overdispersed compared to the Poisson distribution, implying greater heterogeneity between individual CTL killing performance than anticipated. Vasconcelos et. al. (Vasconcelos et al. 2015) found the data was well described by a Poisson mixture model, and they postulated the existence of a subset of "high rate killers" comprising 30% of the population that emerged 8-10 hours after first exposure to target cells. However, no mechanistic explanation could be found to explain this result, despite a search for membrane markers that might identify and/or explain the variability of CTL killing characteristics.

We hypothesised that a requirement for "multiple hits" to kill targets before apoptosis induction might explain heterogeneous killing amongst clonal CTLs *in vitro*. Perelson et. al. [20] previously considered the possibility of multiple-hitting, noting however that such a model was excessively complex to describe the limited experimental data available at that time. Recent evidence has directly shown that multiple-hitting does occur at least in some settings [7,10,21], and our previous modelling work has demonstrated that multiple-hitting can indeed lead to population-level killing kinetics increasing over time when CTLs are exposed to fresh targets [11]. Therefore, we here used stochastic simulations to investigate the compatibility of the multiple-hitting hypothesis with the findings of Vasconcelos et. al. [19]. We found that multiple-hitting was indeed able to explain the late onset, high-rate bursting kinetic of individual CTLs, with physiologically plausible parameters. We also highlight that multiple-hitting is expected to lead to a complex dependence of realised killing rate upon the number of available targets and on the ability of individual CTLs to form and abort conjugates with target cells. We subsequently developed spatially explicit, agent

based simulations of CTLs killing targets in micro-wells as a means of generating realistic yet noisy artificial data and assessing methods of recovering CTL hitting parameters from future microscopy data. Using these spatial simulations, we demonstrate how parameter estimation is substantially improved if contacts of individual targets with CTLs can be tracked throughout the duration of the experiments.

## Results

### Multiple-hitting CTLs exhibit heterogeneous late onset killing

We first sought to establish whether the multiple-hitting hypothesis was a feasible explanation for the heterogeneous, delayed onset, “burst” killing kinetics observed and defined by Vasconcelos *et. al.* [19]. In brief, these high rate killer CTLs were a subset among a clonal population whose killing suddenly accelerated after 8-10 hours of experimentation, with no explanation readily apparent (Methods). In the current study, we used Monte Carlo simulations of individual CTLs killing targets to identify conditions under which multiple-hitting might lead to heterogeneous, “burst” killing. In these Monte Carlo simulations, CTLs hit targets at a constant rate  $\lambda$ , then targets died after receiving  $\eta$  hits. We simulated single- and multiple-hitting scenarios on the basis that the expected (mean) time for one target in contact with a CTL to be killed was 1 hour, i.e., we set  $\lambda / \eta = 1$  (valid for entire Fig. 1).

Firstly we simulated CTLs with  $\eta=1,2$ , or 10, with each simulation containing one CTL interacting with a single target. For such a strictly 1:1 CTL:target ratio, the waiting times for target death were gamma distributed with rate parameter  $\lambda$  and shape parameter  $\eta$  (Fig. 1A). The gamma distributions (Fig. 1B, top panel), together with their accompanying survival probability functions (Fig. 1B, middle panel), define the hazard function (Fig. 1B, bottom panel), which is the momentary rate of death experienced by a target, given that the target has already survived an interaction for some time,  $t$ . When  $\eta = 1$ , the hazard experienced by contacted targets does not change with time. In contrast, when  $\eta > 1$  the hazard experienced by contacted targets increases over time, as contacted targets become increasingly likely to have received  $(\eta - 1)$  hits and thus be killed by the next hit. For the case where CTLs interact with targets in a strictly 1:1 ratio, the gamma( $\eta$ ,  $\lambda$ ) distribution parameters could be estimated from the mean and variance of the samples of the waiting time ( $y_o$ ):  $\overline{y_o} = \frac{\eta}{\lambda}$  and  $Var(y_o) = \frac{\eta}{\lambda^2}$  (Fig. 1C).

We next extended our Monte Carlo simulations to allow CTL:target interactions in a 1: $n$  ratio, for variable numbers of targets,  $n$ . CTLs were individually assigned their initial number of targets by drawing  $n$  from a Poisson distribution, with mean  $\bar{n} = 16$  (Fig. 1D, blue bars). The total number of targets killed by a CTL during one simulation,  $x$ , should also follow the Poisson distribution, if the killing rate of each simulated CTL would be the same. Moreover, the mean and variance should be approximately equal for any set of Poisson distributed samples. Therefore, observation of a ratio  $\frac{var(x)}{\bar{x}} > 1$  for a set of killed targets would imply that the killing was more heterogeneous than expected under Poisson assumptions. For single-hit killing ( $\eta = 1$ ), the variance of the 12 hour

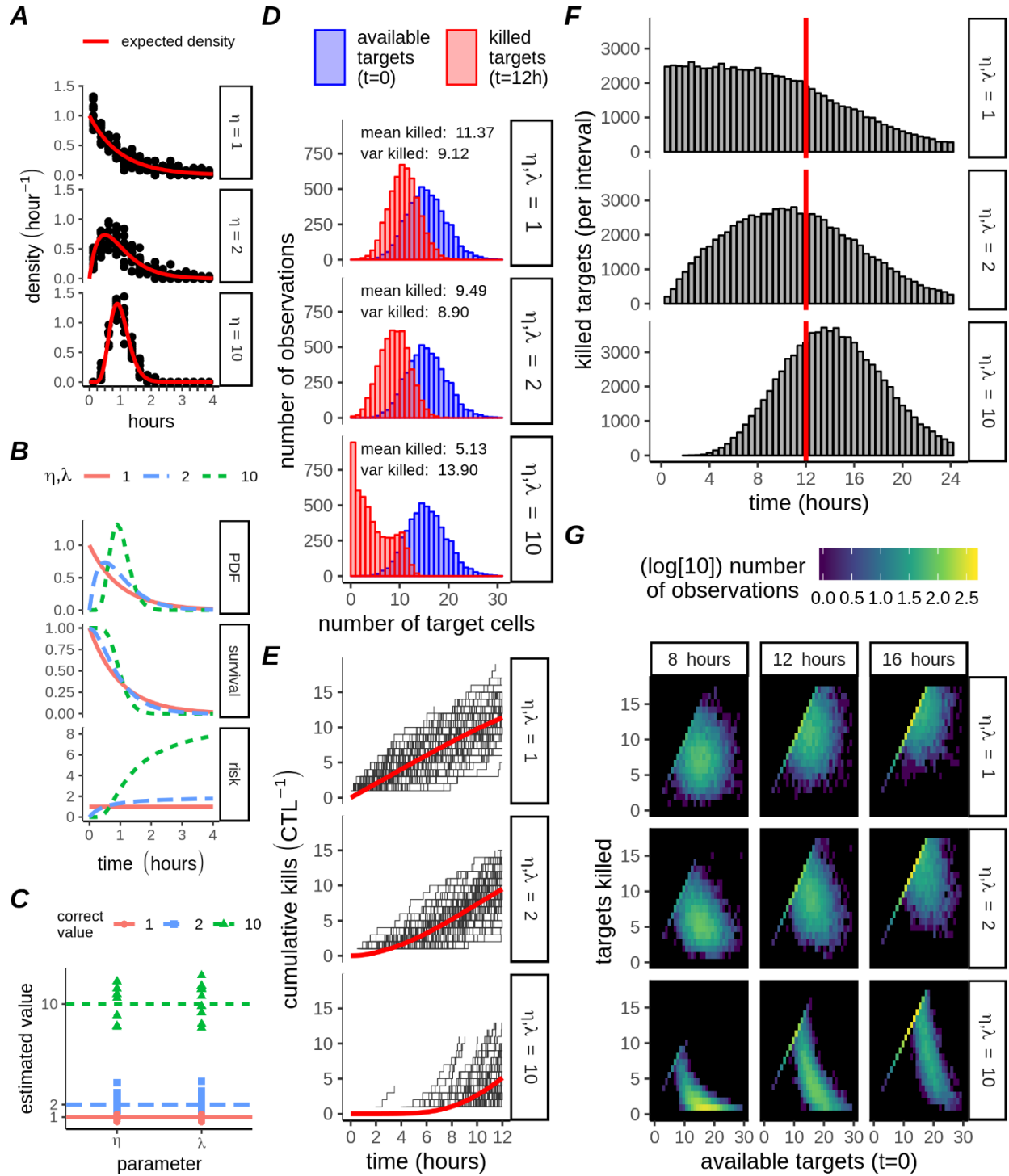


**Figure 1. Killing kinetics and heterogeneity of multiple-hitting CTLs.** A) Gamma probability density functions describing expected time for a CTL to kill 1 target in monogamous contact (red lines). Each point represents the sample killing density of one series of simulations ( $N_s=10$ ), each series comprising  $N_w=100$  CTL:target pairs. Observations were binned at 15 minute intervals. B) Theoretical Gamma probability density function (PDF), survival function, and hazard function for different values of  $\eta$  as indicated. C) Estimation of parameters from simulations in panel A, by equating the first two moments (the mean and variance) with their estimators. D) Distribution of targets killed per CTL at 12 hours (red bars), with Poisson

distributions for the initial number of targets (using the same initialising distribution for all  $\eta$ ; blue bars). Each panel contains results from  $N_w=5000$  CTLs for different  $\eta$ , as indicated by facet labels on the right. Text inside panels indicates the mean and variance of the killed targets. E) Cumulative killing performance of  $N_w = 100$  members (thin black lines) of the population shown in D; the red line is the mean calculated for the entire population ( $N_w=5000$ ). F) Distribution of target killing times over extended (24 hours) simulations with CTL parameters matching D, with the 12 hour censorship indicated by a red line ( $N_w=5000$ , bars are kills per 30 min interval). G) Heatmap of the probability density for each simulation in C-D. Observations were binned according to unique combinations of the initial number of targets (individual columns), together with the number of killed targets at the indicated interval (individual rows). Thus, summing across columns will recover the initial Poisson distribution (blue bars in D), and summing across rows will produce the distribution of killed cells at the indicated time (e.g red bars in D at 12 hours).

killing samples was in fact slightly below the mean (Fig. 1D, upper row), resulting from some simulations where CTLs killed all their targets before the simulation had finished. However, for  $\eta = 2$  (Fig. 1D, central row), the variance approached the mean and for  $\eta = 10$  far exceeded the mean (Fig. 1D, bottom row). In the latter case, a bimodal distribution occurred, which could be interpreted as a subpopulation of high-rate killers, yet importantly such a population did not exist in our simulations.

In our simulations, the additional variability in killing performance of multiple-hitting CTLs was due to the allocation of subsequent hits amongst several different targets. When a group of targets share hits evenly, the time for a specified target to be hit is proportional to the number of other targets sharing. This has no effect on the killing rate observed if  $\eta = 1$ , so the mean killing rate for our simulated single-hitting CTLs initially remained constant over time (Fig. 1E-F, top row; time<8h), gradually decreasing as some CTLs eliminated all their targets (Fig. 1E-F, top row; time>8h). In contrast, hit sharing in the case of multiple-hitting CTLs led to a delayed onset of killing (Fig. 1E-F), with the length of the delay dependent on the number of targets sharing hits (compare Figs 1A-B with single targets to Fig. 1F with multiple targets, for identical  $\eta$ ). The interaction between  $\eta$  and the number of initial targets can also be understood from heatmaps of targets killed (Fig. 1G). The expected cumulative number of kills increases over time for  $\eta, \lambda = 1$ , but this increase is independent of the initial number of targets except for the censorship implying a maximum target number that can be killed. For  $\eta, \lambda = 10$ , the dependency of the observed kills on the initial number of targets is very clear, with killing happening earlier in those wells with initially fewer targets. Moreover, these effects did not only depend on the initial number of targets. When we performed simulations with the hitting rate  $\lambda$  a random variable, this in turn increased the variability of killing amongst multiple-hitting CTLs to a greater extent than was the case for single-hitting CTLs (S1 Fig), implying that the killing of multiple-hitting CTLs is more sensitive to environmental variables than the single-hitting CTLs. Taken together, these results imply that multiple-hitting CTLs could explain both heterogeneous and delayed onset killing among clonal CTL populations.

## Multiple-hitting is not identifiable based on population killing statistics only

We asked if population-level killing statistics (as e.g. examined in [19] )) could be used to identify the hitting parameters ( $\lambda$  and  $\eta$ ) of CTLs. In our previous simulations (Fig. 1) we studied a scenario of simultaneous risk for target cells, yet this may be an oversimplification. For example, due to physical constraints the number of targets CTLs can simultaneously contact and thus hit must be limited. Therefore, we extended our  $1:n$  Monte Carlo simulations to allow dynamic contacts between CTLs and targets, in order to check how the parameter estimates ( $\lambda$  and  $\eta$ ) would be impacted. To achieve this, we included an additional state for target cells, now distinguishing between targets that are contacting the CTL, versus those not in-contact (Fig. 2A; Methods). The killing kinetics realized by CTLs in these dynamic simulations indeed differed from those in our previous simulations (Fig. 1), where all the targets shared risk and so the killing rate of each CTL was dictated by the total number of yet-living targets. In contrast, for our Monte Carlo simulations allowing dynamic conjugate formation, only the targets presently being contacted were relevant. Here, small bursting events occurred throughout the simulations, which was the result of accumulating hits followed by rapid sequential killing among a subset of contacted targets (Fig. 2B).

Using our simulations including dynamic conjugate formation we searched for parameters consistent with the statistics reported previously [19] concerning high rate “burst killing” CTLs. For fitting we used the reported group mean (4) and variance (6.9) of the number of killed targets per CTL over 12 hours. Additionally, we aimed for a breakpoint in the mean killing rate such that half (2) of the observed kills occurred in the interval 0-9 hours and the other half in the interval 9-12 hours (see Methods). We performed this fit using different values for  $\eta$  (ranging from 1-5, or 10), and a Poisson variable with  $\bar{n} = 16$  for the initial number of targets (S2 Fig). We obtained good fits for different values of  $\eta$ ; in particular for all  $\eta > 2$  the cumulative killing was very closely matched (Fig. 2C, intersecting lines for  $\bar{n} = 16$ ). Moreover, for values  $\eta > 3$  the fits to the mean and variance for cumulative targets killed at 12 hours were all similarly close to their target values of 4 and 6.9, respectively (Fig. 2D). Some differences for different  $\eta$  were apparent, for example as the number of hits increased towards  $\eta = 10$  the breakpoint marking transition from low to high rate was more distinct (Fig. 2E). However, overall differences between  $\eta$  were quite small (Fig. 2F), and many simulated CTLs were required for these differences to emerge consistently (at least  $N_w=10^3$  CTLs). Our results were also sensitive to the distribution for the initial number of targets per CTL: for simulations with  $\bar{n} = 12$  or 20, substantial differences in the cumulative kills over time occurred (Fig. 2C). Thus, we conclude that multiple-hitting is not only qualitatively, but also quantitatively consistent with the experimental results reported previously (Vasconcelos et al. 2015). However, our analysis shows that the mean and variance of the killing process measured for a group of CTLs are insufficient statistics to determine the number of hits CTLs require to kill targets, so CTL:target interactions should be explicitly accounted for if killing due to multiple-hitting is to be modelled accurately.

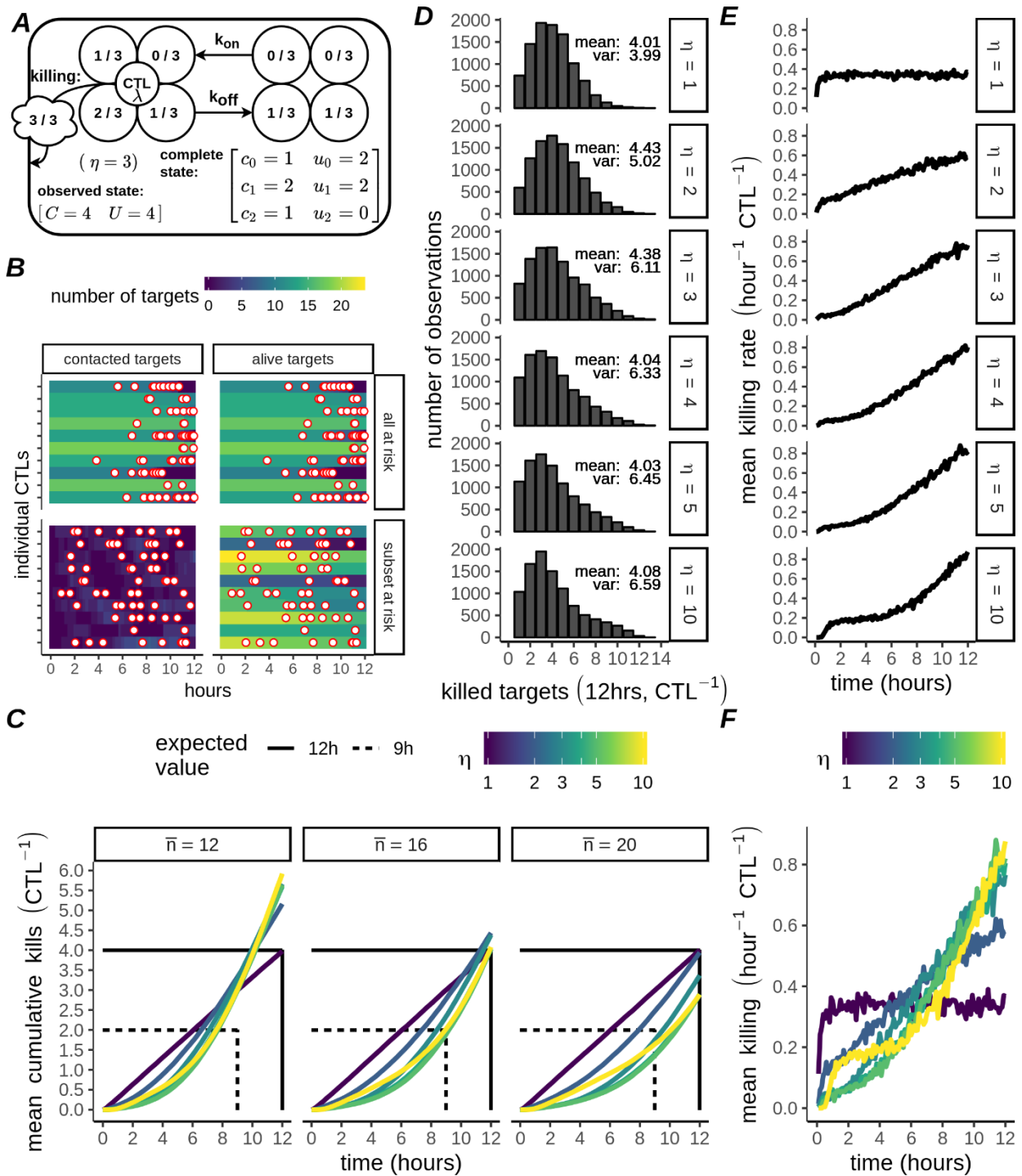


**Figure 2. Burst killing and non-identifiability of dynamically interacting, multiple hitting CTLs.** A) Schematic of the dynamic model (example with  $\eta = 3$ ). Target cells are represented by circles containing fractions (numerator: hits received; denominator:  $\eta$ ). The observable state  $[C \ U]$  consists of the total number of contacting,  $C$ , and non-contacting targets,  $U$ . The complete state of the system is represented by a matrix, with  $\eta$  rows indicating the number of hits received (subscript) and with columns indicating whether the target is contacting ( $c_i$ ) or non-contacting ( $u_i$ ). B) Measured killing events (red dots, filled white) during Monte Carlo simulations with  $N_w=10$  CTLs and the number of targets drawn from a Poisson



distribution with mean  $\bar{n} = 16$  (top panels;  $\lambda, \eta = 10, k_{off} = 0, k_{on} \rightarrow \infty$ ), or a subset of targets at risk (bottom panels;  $\lambda, \eta = 10, k_{on} = 1hr^{-1}, k_{off} = 0.3hr^{-1}$ ). Each horizontal strip is one single simulation, the right panel strips are colored according to the total number of alive targets and the left panel strips are colored according to the number of targets that are in contact with a CTL. C) Each line (coloured according to  $\eta$ ) is the mean cumulative killing over time ( $CTL^{-1}$ ) from  $N_w=10^4$  CTLs, simulated using parameters estimated by fitting the case with  $\bar{n} = 16$  targets (central column). Straight lines show target values for fitting. All parameters except  $\bar{n}$  are constant across columns. D-F) Measured statistics within simulations with  $\bar{n} = 16$  shown in the central column of C. Shown are the distribution of killed targets after 12 hours, with the mean and variance as indicated for each  $\eta$  (D), and the mean killing rate over time for CTLs grouped by  $\eta$  and shown either separately (E, rows), or together (F, colors), calculated as  $(kills \cdot (6 \text{ min} \cdot N_w)^{-1})$ .

## An Agent Based Model of Multiple-hitting CTLs to test methods for estimation of killing parameters

Since we found that in many situations the true hitting parameters for CTLs could not be determined based on group level killing mean and variance, we sought methods to compare the likelihood of different hitting models. We did not wish to consider a particular model for the process of CTLs finding targets, preferring a method that could be applied to determine the CTL hitting behaviour in general situations (i.e., in the absence of knowledge on contact dynamics). As a framework for testing we employed an agent based cellular Potts model (CPM) to generate 2D simulations of CTLs interacting with and killing targets (Fig. 3A). The resulting datasets were visually similar to realistic microscopy data and could be used to investigate methods for recovering the hitting parameters ( $\eta$  and  $\lambda$ ) of CTLs from experimental data under various conditions. For all CPM simulations we maintained the same underlying gamma model of CTL hit generation as was used for our Monte-Carlo simulations (Fig. 1-2), however we made several modifications that would lead to different (yet not predictable a priori) distributions of hits amongst targets. Specifically, instead of allocating hits to all contacted targets with equal probability, target risk of receiving a hit was proportional to the length of the interface between CTL and target at the moment of hit generation (Fig. 3A, target coloring on left images indicates interface length). We also considered the effect of a lower bound on the time required for a CTL to complete a hit, by introducing a delay condition that prohibited targets from being hit within an initial time window after contacting a CTL, which was reset every time the target broke contact with the CTL (Fig. 3A, target coloring on right images). Note that the delay condition was applied per target and therefore does not preclude the possibility of CTLs hitting other contacted targets simultaneously.

Finally we varied CTL migration to create two groups of CTLs which we termed “high-motility” (Fig. 3B, S1 Video) or “low-motility” (Fig. 3C, S2 Video) CTLs. For both motility conditions the migration of the CTLs was influenced by the presence of the targets, as CTLs became corralled by surrounding targets. The difference between these models was that high-motility CTLs exhibited an increased propensity to break free from confinement and roam the well. This roaming ensured that over the course of 12 hours the high-motility CTL made new contacts with far greater frequency than low-motility CTLs (Fig. 3D), although the average number of simultaneously contacted targets at any time was similar (Fig. 3E). Thus, the high-motility CTL is expected to

approach the previously modeled ‘all targets at risk’ scenario more closely than the low-motility CTLs.

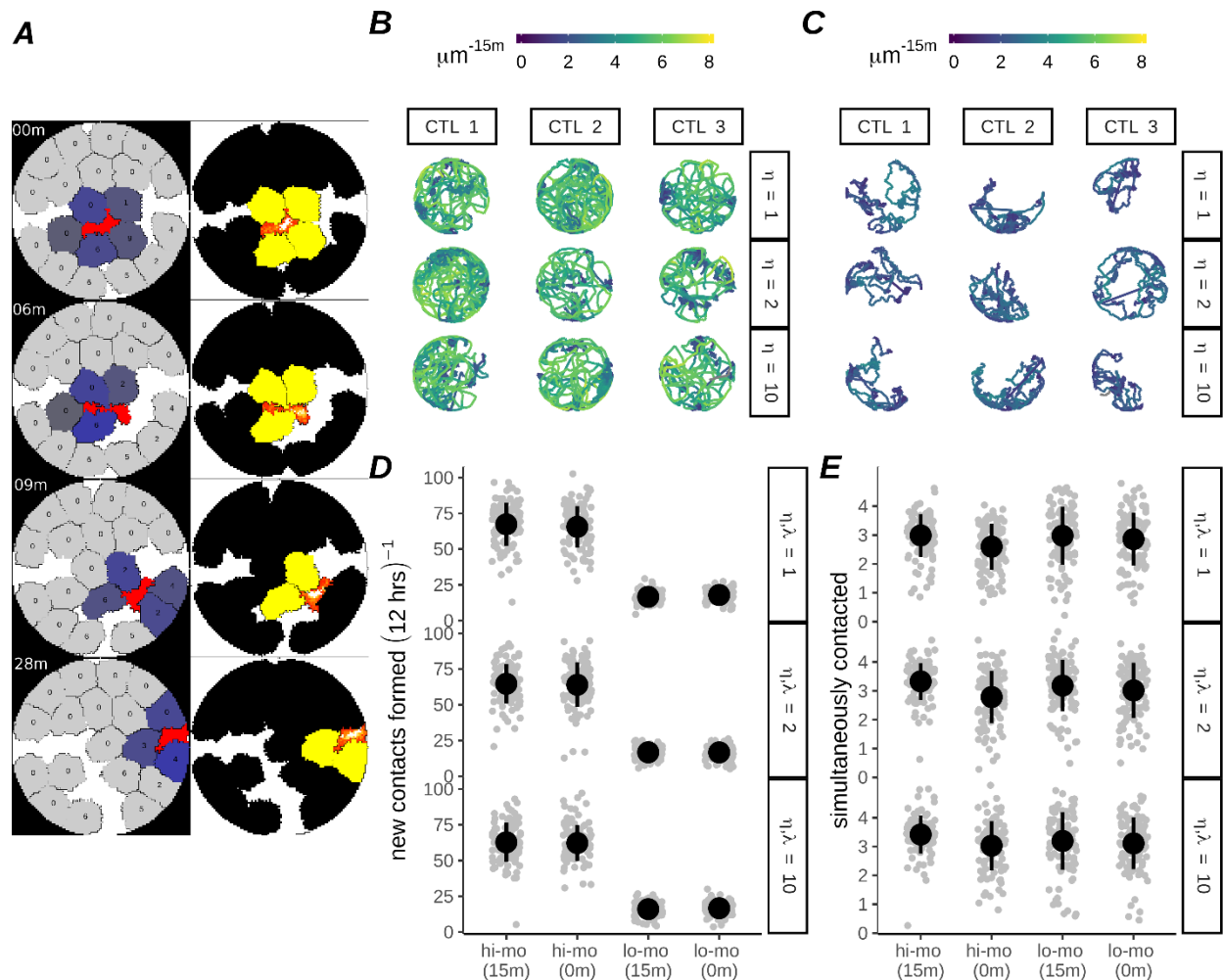


**Figure 3. Characterisation of high- and low-motility *in silico* CTLs within CPM simulations.** A) Still images of a high motility CTL with 15 minute minimal hitting time, interacting with targets. Left color scheme: CTLs are red, uncontacted targets are grey, and contacted targets have various shades of blue based on their share of total CTL:target interface, which determines their probability of receiving a hit. Targets are overlaid with the number of hits they have received. Right color scheme: Lattice sites inhabited by the CTL are colored according to actin activity [22]. Targets are black, turning yellow after 15 minutes of continuous contact with the CTL. Elapsed simulation time is displayed in the upper left corner of the stills, presented in minutes since the first frame shown. B-C) Track plots showing movement of 3 randomly sampled CTLs of high (B) and low (C) motility throughout a simulation, for simulated  $\eta$  as shown. D-E) Frequency at which CTLs form new conjugates (D) and mean number of simultaneously contacted targets per CTL (E) for low- and high-motility CTLs. Plots are based on 100 simulations per condition, with each dot representing one CTL, and circles and error bars indicating mean  $\pm$  SD.

We used the CPM model to simulate CTLs (with  $\eta, \lambda = 1, 2, \text{ or } 10$ ), in either high- or low-motility scenarios. The total amount of targets killed by each CTL depended on the interaction between the parameters  $\lambda$  and  $\eta$ , the CTL motility, and the presence or absence of the delay condition. In particular, the combination of high motility plus 15 minute delay resulted in a substantial decrease in killing in comparison to the other simulation groups, for all values of  $\eta$  (Fig. 4A). Together with the high rate of contact formation in that group (Fig. 3D), this is consistent with targets spending significant time in transient contacts with the CTL, too short to result in successful hit delivery. The killing rate of the low-motility CTLs was initially greater than of high-motility CTLs, in particular for large  $\eta$  (Fig. 4B), due to the more stable nature of the contacts leading to greater accumulation of hits among the contacted targets (Fig. 4C). High-motility CTLs reduced this deficit over the course of the simulations due to an accumulation of latent hits among uncontacted targets (Fig. 4D). These spatial simulations therefore illustrate how CTL:target contact dynamics can play a role in determining killing performance. Moreover, since in these models CTLs with the same killing parameters - but different motility parameters - generated different killing kinetics, they are useful to test how underlying killing parameters might be recovered from microscopy data that are similar to data emanating from our realistic simulations.

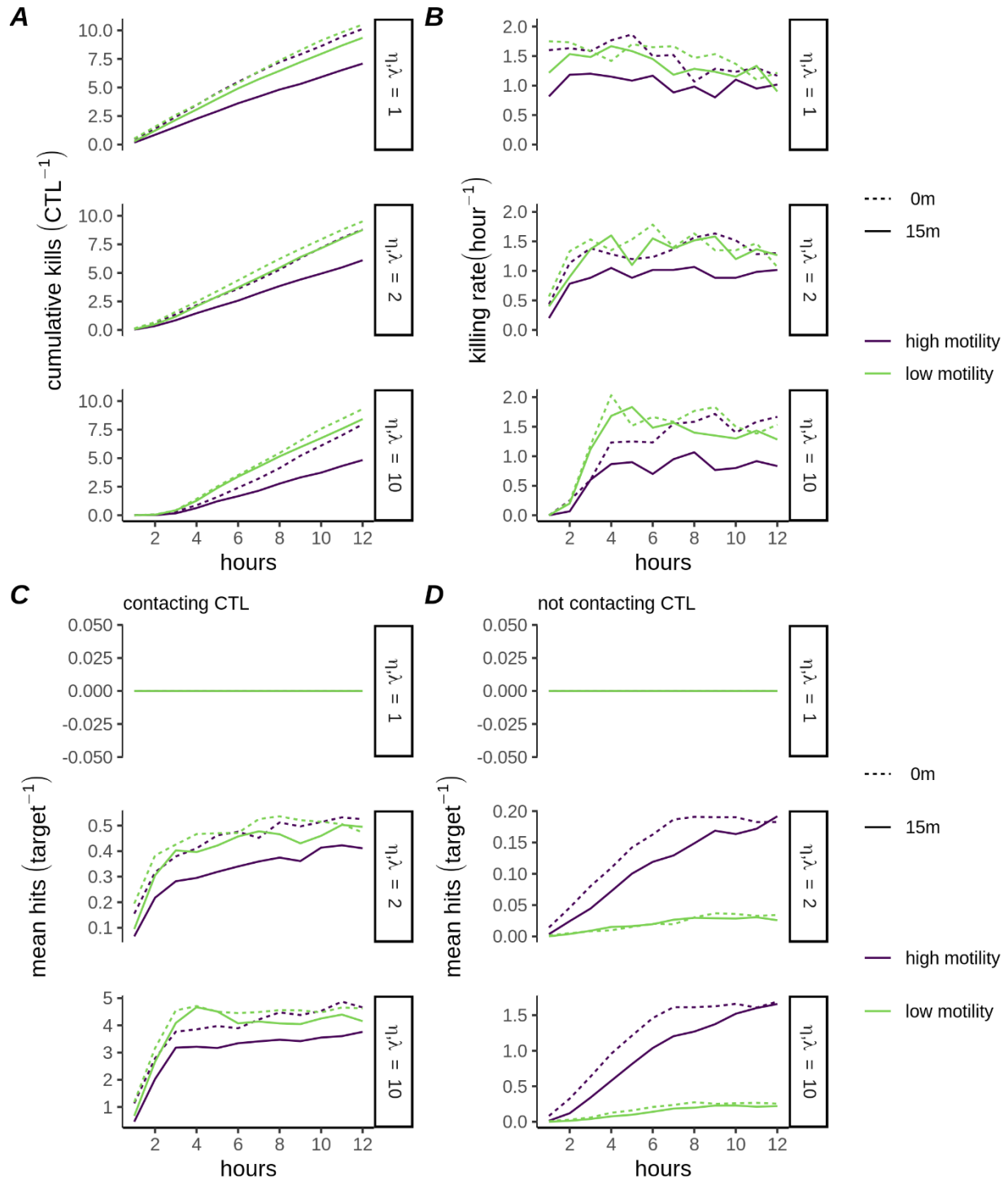


**Figure 4. Killing performance of multiple-hitting CTLs depends on motility.** A) Mean cumulative killing over time (CTL<sup>-1</sup>) for CPM simulations of high- and low- motility CTLs ( $\eta, \lambda = 1, 2$ , or  $10$ ) B) Mean killing rate (CTL<sup>-1</sup>) for each simulated condition in A. C-D) Mean number of hits received per target, sampled over targets currently contacting the CTL (C) or over targets not currently contacting the CTL (D).

## Estimating CTL hitting parameters through analysis of contact time and target survival

Since we found that hitting parameters  $\eta$  and  $\lambda$  could not be recovered via analysis of population averages only, we employed a parametric survival analysis to study the hazard experienced by individual targets contacting CTLs. Our analysis considers the different hazard functions identified earlier (Fig. 1B), which distinguish CTLs on the basis of their intrinsic hitting rate  $\lambda$  and the number of hits required for killing targets,  $\eta$ . Specifically, we analyse the cumulative duration of CTL:target contact events from the perspective of the target cells (example in Fig. 5A). To take into account shared hazard amongst a set of co-contacting targets, we recorded for each sampled frame the statistic  $\theta = (c)^{-1}$ (per-target), representing the probability that each separate target out of the subset of  $c$  targets co-contacting the CTL is presently being hit (Fig. 5B). Note that targets not in contact with the CTL were assigned  $\theta = 0$ . Subsequently, we integrated the  $\theta$  values over time to arrive at a set of ‘adjusted’ contact times,  $\tau$ , for each target (Fig. 5C), which takes into account uncertainty with respect to hitting of multiple co-contacted targets (Fig. 5C). This approach has the advantage that no explicit account needs to be taken of the CTL-target interaction dynamics. Moreover, estimation of cellular contact times occurs already frequently in time-lapse imaging data [7,23], hence is feasible.

Applying the concept of adjusted contact times,  $\tau$ , on all our CPM simulations, we established maximum likelihood estimates for the hitting parameters within the simulations (S1 Text; S3 Fig). This yielded excellent estimates for the parameters in simulations without delay (Fig. 5D;  $\eta_{CPM}, \lambda_{CPM}$  indicate input CPM parameter values, and  $\hat{\lambda}, \hat{\eta}$  indicate estimated values). We also tested our method of parameter recovery by fitting our model to small subsets taken from the CPM simulations each containing only  $N_w=10$  CTLs (Fig. 5E), which led to good estimates. Additionally, we tested our model on sample data generated from a mixed dataset with two subpopulations of single-hitting CTLs, each with a different killing rate (S1 Text), in order to examine the high-rate-killer hypothesis put forth by Vasconcelos *et. al.* [19]. We found that the multiple-hitting model would not predict multiple-hitting unless multiple-hitting was indeed underlying the data, instead predicting a single-hitting population whose killing rate was the mean of the individual subpopulations (S1 Text; S4 Fig, S5 Fig). Thus, our maximum likelihood approach based on contact time monitoring can distinguish multiple-hitting from alternative hypotheses and is expected to work for a relatively small number of samples.

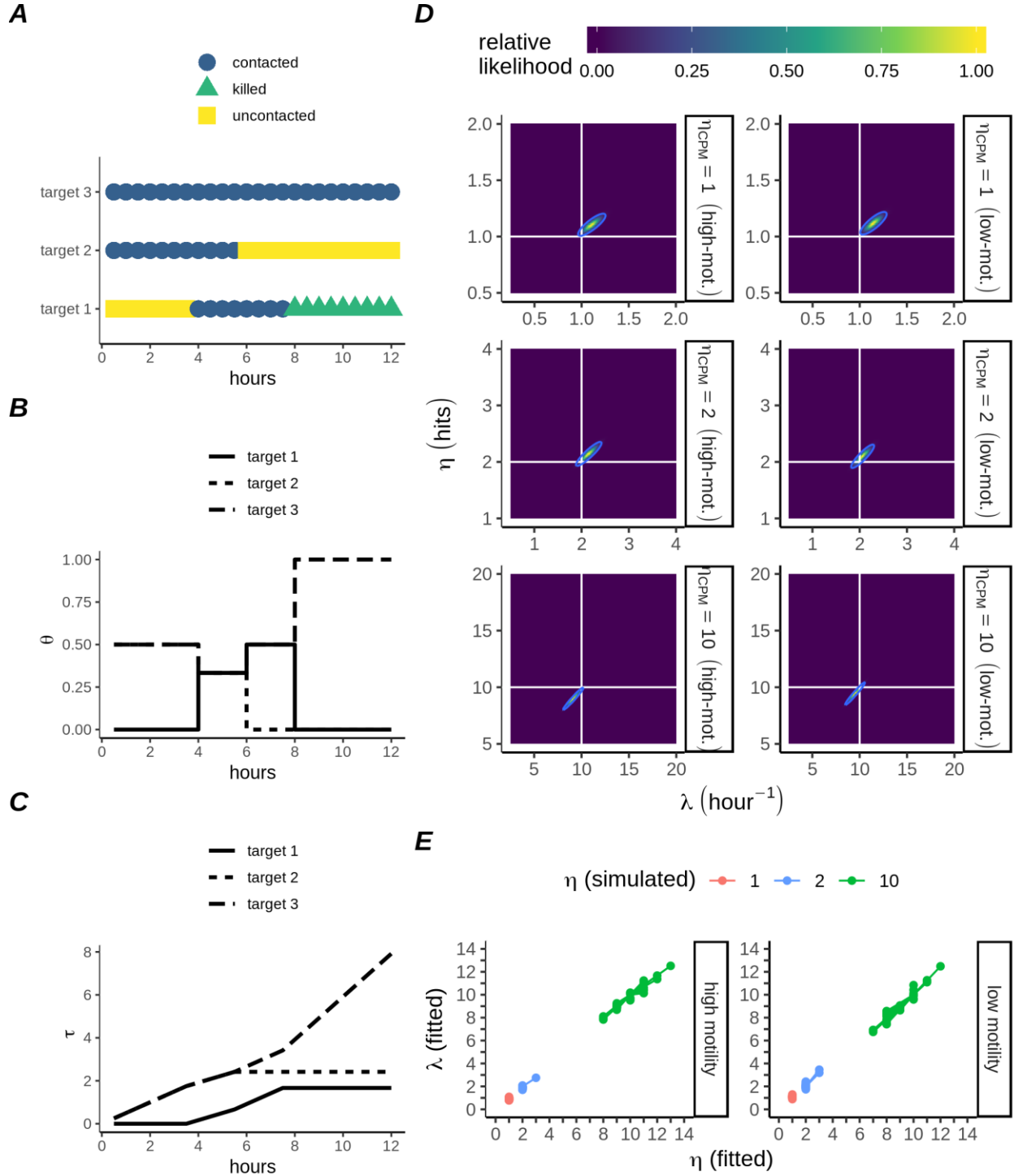


**Figure 5. Parameter retrieval for multiple-hitting CTLs based on adjusted contact time.** A) Hypothetical example illustrating sharing of subsequent CTL hits by target cells. Interaction history during a period of 12 hours for each of three target cells contacted by a single CTL, sampled at 30 minute intervals. B) Estimated probability (expressed as fraction  $\theta$ ) that each target is being hit by the CTL, corresponding to the hypothetical interaction history shown in A. C) The quantity  $\tau$  is defined as the cumulative sum over the course of the simulation of all sampled values of  $\theta$  associated with each individual target. The samples resulting from interaction with this CTL include target 1, which was killed after a cumulative interaction

period of ~1.7h, and targets 2 and 3, which remained alive after cumulative interaction periods of ~2.4h and ~7.9h, respectively. D) Heatmaps of the likelihood function around the maximum likelihood estimates for the killing parameters, in CPM simulations without hitting delay. Horizontal and vertical lines mark the values of the CPM parameters used to generate the data for each group. The boundary enclosing the 95% confidence region is also marked with a line. E) Results of fitting 30 randomly chosen subsets, each consisting of  $N_w=10$  simulations, of the CPM simulations without hitting delay.

## Impact of a hitting threshold on killing parameter estimation

Given the time needed for formation of a cytotoxic synapse that is required for hit delivery, brief interactions between CTLs and targets may not contribute to killing. Taking such brief interactions into account in our parameter estimation may thus interfere with correct estimation. Therefore, we tested our parameter recovery on those CPM simulations wherein a 15 minute minimal bound (+15m) was set for the time CTLs required to successfully execute each hit upon a target. In these CPM simulations, we generally obtained robust estimates for the number of hits needed to kill targets,  $\hat{\eta}$  (S6A Fig). However, after rounding to the nearest integer value for  $\eta$ , the estimated hitting rate parameter,  $\hat{\lambda}$ , was underestimated compared to the generating value ( $\lambda_{CPM}$ ) in simulations with the 15m minimal hitting time. Since the realised killing was reduced in the 15m-delay simulations, particularly for high-motility CTLs (Fig. 4), the estimated  $\hat{\lambda}$  could be considered more appropriate than the generating value  $\lambda_{CPM}$ . Nevertheless, to investigate further we performed additional simulations, using high motility CTLs, with variable hitting delays in the interval between 0-15 mins (Fig. 6A, S6B). We found that for the important boundary between single-hitting ( $\eta = 1$ ) or multiple-hitting ( $\eta = 2$ ), the estimated number of hits parameter  $\hat{\eta}$  was accurately classified for limited delays of less than 15 minutes (Fig. 6A, top row).

A particular advantage of a parametric survivorship analysis such as that we employ here is that, having estimated the hitting parameters ( $\eta, \lambda$ ), we can revisit the sample data and ask whether different subsets of targets were killed according to our expectation. We selected the high-motility +15m simulations with  $\eta_{CPM} = 1$  for further study, since for this simulation group there was an ambiguous estimate of  $\hat{\eta}$ . For comparison, we also analysed the data from CPM simulations with multiple-hitting CTLs ( $\eta_{CPM} = 2$ ). First, we inspected the Kaplan-Meier estimates of the survival functions (Fig. 6B, black lines) marking close agreement when the correct parameter estimate ( $\hat{\eta} = 2$ ) was applied to CPM data generated by multiple-hitting CTLs (Fig. 6B bottom, blue line,  $\eta_{CPM} = 2$ ), but not when the incorrect  $\hat{\eta} = 1$  was applied (Fig. 6B bottom, red line,  $\eta_{CPM} = 2$ ). For data generated by single-hitting CTLs, the Kaplan-Meier estimate lay exactly between the estimates using  $\hat{\eta} = 1$  or 2, yet the shape of the survival function over the entire length better matched that for the single-hitting estimate  $\hat{\eta} = 1$  (Fig. 6B top, red line,  $\eta_{CPM} = 1$ ) than for the estimate  $\hat{\eta} = 2$  (Fig. 6B top, blue line,  $\eta_{CPM} = 1$ ). Second, visual inspections of the hazard experienced by individual targets throughout the simulations (Fig. 6C), revealed that in many CPM simulations with  $\eta_{CPM} = 1$  and a +15m hitting delay there was substantial killing of targets that had not yet undergone long interactions with the CTL (Fig. 6C, first two grey bars), as would not be expected for multiple-hitting. Thus, both results (Fig. 6B-C) supported  $\hat{\eta} = 1$  as the most likely

candidate for the data derived from simulations with  $\eta_{CPM} = 1$ . However, the most conclusive result was obtained by evaluating the mean hazard experienced by contacted targets according to either of the two candidate estimates for the number of hits ( $\hat{\eta}=1$  or 2). Integrating this value over the duration of the experiments (Fig. 6D, black lines) led to predictions for the killing rate over time which closely followed the data whenever a correct estimate for  $\hat{\eta}$  was applied (Fig. 6D, comparing black and red lines in the upper panel, or black and blue lines below). In contrast, killing predictions from incorrect estimates of  $\hat{\eta}$  were extremely poor, thus allowing for correct identification of the underlying  $\eta$ . Thus, our analysis shows that monitoring of cumulative interaction times between targets and single CTLs allows for proper estimates of the number of hits required for target cell death even when brief contacts between CTLs and targets cannot lead to hits, although the hitting rate may be underestimated in that case.



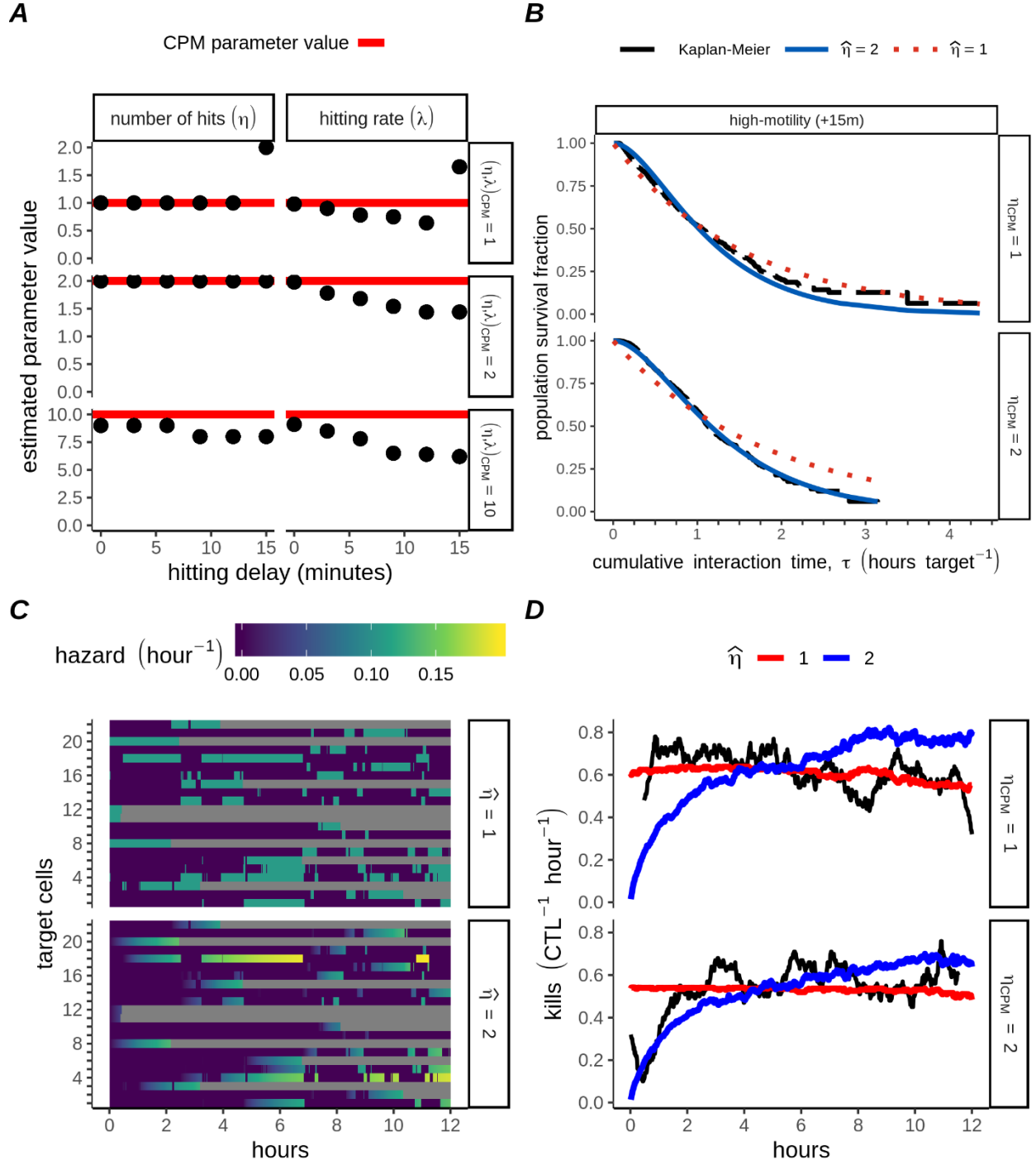


**Figure 6. Parameter retrieval for multiple-hitting CTLs with underlying hitting delay.** A) Estimated parameters (points), compared to the underlying parameter values used (red lines) in CPM simulations, featuring high-motility CTLs, in which we varied the lower bound for the time (in minutes, as indicated) needed for hitting. B) Kaplan-Meier survival functions (black lines), or survival functions plotted with estimated parameters fitted to data from  $N_w=100$  CPM simulations generated by multiple-hitting (lower row,  $\eta_{CPM} = 2$ ) or single-hitting CTLs (upper row,  $\eta_{CPM} = 1$ ). C) Heatmaps from one CPM simulation containing high-motility, single-hitting CTLs who had a 15 minute lower bound set on the hitting time. Each row

represents a single target. Target status is represented by colour: targets not-contacting the CTL are deep purple, and killed targets are grey. Contacted targets are coloured according to their momentary hazard according to two candidate parameter sets (top panel:  $\hat{\eta} = 1, \hat{\lambda} = 0.65$ ; bottom panel:  $\hat{\eta} = 2, \hat{\lambda} = 1.65$ ). D) Predicted killing rate according to two different candidate parameter sets ( $\hat{\eta} = 1$ , red lines;  $\hat{\eta} = 2$ , blue lines), candidates being themselves applied to CPM simulations with high-motility, +15m CTLs ( $\eta_{CPM} = 1$ , top panel;  $\eta_{CPM} = 2$ , bottom panel).

## Discussion

Here we have used stochastic simulations to show that ‘multiple-hitting’ is a plausible explanation for the heterogeneous and time-inhomogeneous killing activity recently observed for CTLs *in vitro* [19]. We showed that multiple-hitting leads to an increase in realised killing rate over time. Moreover, the extent of this late onset killing increases when more hits are required to kill targets, or when a greater number of antigen-presenting targets are simultaneously contacted. Furthermore, identical CTLs displayed varying killing performance depending on the number of targets available. Simulating CTLs with variable hitting rates, we also found that the killing performance of multiple-hitting CTLs is more heterogeneous than killing of single-hitting CTLs, given similar variation in underlying hitting rate. Overall, we conclude that multiple-hitting is sufficient to explain heterogeneous killing amongst clonal CTLs and there is no need to invoke an unobserved subpopulation of high-rate killers.

Given the dependence of the killing performance of multiple-hitting CTLs on several parameters that we describe here, we developed spatially explicit CPM simulations to assess methods for investigating whether multiple hitting occurs *in vitro* or *in vivo*. Our specific goal was retrieval of the hitting rate and number of hits required for CTLs to kill targets. Our model of dynamic conjugate formation can be conceptualised using Kendall’s notation as an M/E<sub>r</sub>/1 queue [24]. Within this framework there is 1 “server” (in our case the CTL), with markovian arrival times (M: in our case conjugate formation events), and Erlang distributed (E<sub>r</sub>) “service times” which represent the killing process. It is known that for such models, the mean and variance (or any similar measure of variability) are insufficient for estimating the true parameters, and can only be used to approximate the distribution [24]. Instead of using population-level killing statistics, we were able to accurately recover model parameters from the CPM data by analysing the ‘adjusted’ cumulative contact durations between CTLs and individual targets, i.e. the total length of the interaction until either the target was killed or the experiment ended. Importantly, we found that measurements for both killed and surviving cells are required for this approach to be successful. This is because the limited time window of observation renders data that are in part censored, yet elapsed contacts that have not yet resulted in killed targets also contain information on underlying killing parameters. In a similar fashion, we previously developed a method to estimate absolute (i.e., not cumulative) cellular interaction times based on time lapse imaging data [23].

Although CTL cooperativity and multiple-hitting have now been described in a number of settings [7,10-12], a detailed quantitative description of the sequence of intracellular events which might underlie multiple-hitting does not yet exist. Several mechanisms can be envisaged which

separately or collectively might result in target cells enduring sustained attacks from CTLs before death. A first factor which may explain the ability of target cells to endure sustained attacks is death occurring via the 'extrinsic apoptosis pathway', i.e., via tumour necrosis factor (TNF) or FAS-L. In the study of Vasconcelos et. al. [19], blockade of FAS-L did not diminish overall killing, suggesting that FAS-L was not involved in CTL killing. Moreover, separation of CTLs and targets in a transwell assay showed that contact was required before target cell apoptosis could occur. Although this result suggests that diffusible TNF did not contribute to target cell apoptosis, TNF is also expressed in transmembrane form [25] and may have contributed to contact-dependent killing, or could have synergised with other effector pathways. Furthermore, TNF or interferon- $\gamma$  - another hallmark cytokine produced by activated CTLs - have been linked to an upregulation of FAS-L receptors in different cell types [26,27], or might otherwise synergise with FAS-L to induce target cell apoptosis [28]. The possibility of synergistic activators of the extrinsic apoptosis pathway is intriguing since activation of such mechanisms might explain delayed onset of burst-killing. This was observed in recent studies in which natural killer cells initially controlled tumour cell targets with a fast-acting, perforin-dependent mechanism, before switching to a mechanism primarily depending on engagement of death receptors [17,18]. It would be useful to investigate whether CTLs also utilise this mechanism.

A second factor which may account for multiple-hitting is heterogeneity in delivery of perforin and granzymes. Perforin alone induces rapid pore formation in target cell membranes, with such membrane disruption expected to increase the metabolic burden on target cells. Even if insufficient to directly induce apoptosis, one would expect such depletion to divert resources from adaptive cellular stress responses, thereby sensitising cells to death from other mechanisms. Granzymes are a diverse set of cytotoxic proteases with a broad array of intracellular targets [29]. A recent review highlights that perforin-mediated pore formation may or may not be accompanied by delivery of granzyme molecules into the cytosol [30]; a requirement for granzyme delivery appears to be the establishment of a sufficiently large pore at the point of contact between CTL and target. Examination of recent 4D images of CTL–target engagement highlight potential for heterogeneous delivery of cytotoxic molecules [8]. That study showed the capability of a single CTL to rapidly organise lytic molecules around the centrosome upon initial target recognition and to subsequently polarise the centrosome towards the target. This sequence of events results in a strong and stable cytotoxic synapse with a high local density of perforin and granzymes. Anecdotal evidence from this same work indicates that there can also be an alternative outcome: In one observation a CTL attempted to form two immunological synapses with one target, with the result that effective centrosome polarisation towards either synapse did not occur and ultimately both synapses were aborted without target cell death (see Video S8 in reference [8]). Other observations of CTLs simultaneously polarising granules towards multiple targets [9] demonstrate that the formation of multiple immunological synapses does not necessarily preclude CTLs from killing. Taken together, these observations suggest that due to the diversity of possible damage pathways activated by CTLs as well as the potential for heterogeneity in delivery of granules, several mechanistic explanations for multiple-hit induced killing remain open.

Given the breadth of cytotoxic weaponry available to a single CTL, it is apparent that experimental interference with one or more CTL effector functions is insufficient to conclude that one or another pathway is primarily involved in target cell death in a given experiment. We suggest high

resolution, *in vitro* imaging as an effective means of achieving insight into the CTL killing process. Such high-resolution imaging would have several benefits: clear visualization of the polarisation of the lytic granules towards target cells would allow acquisition of statistics regarding the lethality of hits. Moreover, monitoring of individual target cells over time would provide statistics regarding the formation and abortion rates of immunological synapses and regarding the probability of target cell death after multiple hits. In addition, such approaches would allow investigation of the possibility of target cell recovery between successive hits, along with assessing the timescale over which such recovery might occur. Although such spatio-temporal resolution might be challenging to achieve experimentally, recent approaches using structured environments [31,32] provide a possible means of achieving more refined control of CTL-target interactions.

In conclusion, in addition to recent efforts to further characterise heterogeneity amongst CTLs, greater attention is needed to simultaneous monitoring of mechanisms activated in target cells after the target has been contacted by a CTL, assisted by statistical analyses and computational methods such as those presented here. Experimental research particularly involving use of e.g. caspase-8 reporters or reporters of granzyme activity to compare the relative importance of different killing mechanisms, as recently done in NK cells [17,18] is crucial. Computational models can then be used to compare results between different experimental assays, thereby quantitatively assessing the contribution of identified CTL effector functions in different contexts.

## Methods

### Monte Carlo simulations

We devised stochastic simulations representing different “wells” in which individual CTLs killed targets. The setup of the simulations was based on published data by Vasconcelos *et al.* [19]. In brief, Vasconcelos *et al.* incubated pre-activated human-derived CTL clones with Epstein-Barr virus transformed B cell targets for 12 hours in microwells ( $N_w=259$ ). Each microwell contained a single CTL confined with an indeterminate (approximately 10-20, see Fig. 4A in reference [19]) number of targets. Microwells were approximately cylindrical and had a cross-section diameter of approximately 100 $\mu$ m. A caspase reporter was used to determine the killing rate of individual CTLs over time. Similarly, our simulations featured  $N_w$  independent simulations, each containing  $n$  initially unhit targets and lasting for a simulated time period of 12 hours, or until all targets had been killed. The simulations proceed as follows:

1. A random variable  $x_{wait}$ , representing the waiting time until the next CTL hit, is drawn from the exponential distribution with rate parameter equal to the CTL hitting rate  $\lambda$ . The current simulation time is increased by  $x_{wait}$ .
2. A random target is selected and its number of hits is increased by one.
3. If a target has received sufficient hits for death (i.e.,  $\eta$  hits), it is immediately removed from the simulation.

In some simulations, we extended the rules in order to reflect typical *in vitro* assays more accurately:

- 1) **Variable target numbers.** Each simulation contained a single CTL and a variable number of targets  $n$ . For each well the number of targets was drawn from a Poisson distribution with mean  $\bar{n}$ .
- 2) **Variable hitting rate.** For each simulation the hitting rate  $\lambda$  of each CTL was a normally distributed random variable. The standard deviation of this distribution was used as a model parameter, with larger standard deviation reflecting CTL populations with greater intrinsic heterogeneity in killing performance between individuals.
- 3) **Dynamic conjugate formation.** We considered that hit delivery had to be preceded by conjugate formation and that at  $t = 0$  hrs the CTL has not yet encountered any targets, and that CTLs form new conjugates with targets at constant rate  $k_{on}$  and abort conjugates with constant rate  $k_{off}$ . Thus these simulations consider 4 distinct types of event: in addition to hitting and dying, we now have conjugate formation and conjugate abortion. The Gillespie algorithm was used to determine the type of event and waiting time between subsequent events [33], except for target cell death which occurs immediately after the lethal hit just as in our “all at risk” simulations. These simulations were used for estimating the parameters  $\lambda$  and  $\eta$  from our spatial simulations.

Parameter estimation for the dynamic conjugate formation model was based on four reported values from Vasconcelos *et. al.* [19]: the population killing averages for the high rate killers (6.4 targets killed per 12 hours) or low rate killers (2.8 targets killed per 12 hours), the fraction of the population reported to be high rate killers ( $1/3$ ), and the breakpoint after which the high rate phenotype appeared (8-10 hours; we took 9 hours for this value). From these 4 reported values we derived three statistics for fitting our Monte Carlo simulations with dynamic conjugate formation: the mean ( $a_1$ ) and variance ( $a_2$ ) of the number of killed targets per CTL after 12 hours, and the expected number of killed targets per CTL at the breakpoint of 9 hours ( $a_3$ ). We estimated the killing at 9 hours by noting that the high rate group had not yet emerged at 9 hours, before which all cells killed at an approximately constant rate. Thus extrapolating from the low rate killing average at 12 hours (  $2.8 \times 9/12$  ) gives approximately 2 targets killed at the 9-hour breakpoint (note that this is also consistent with Fig. 4B of Vasconcelos *et. al* [19]). Thus, the experimental estimates were:  $a_1 = 4$ ,  $a_2 = 6.9$  and  $a_3=2$ . To fit to these estimates, we measured the same statistics ( $b_{1,2,3}$ ) from our simulations and then minimised the root mean squared error:

$$RMSE = \sqrt{(1/3 \cdot \sum_{i=1,2,3} (a_i - b_i)^2)}, \quad \text{Eq. 1}$$

for different values of the parameters  $\eta$ ,  $\lambda$ ,  $k_{on}$ , and  $k_{off}$ . For the stochastic optimisation we performed 10 repeats for all combinations of selected discrete values of  $\eta$ ,  $k_{on}$ , and  $k_{off}$  (S2 Fig), and then for each combination we estimated  $\lambda$  based on  $N_w = 1000$  repeats and the optimise function in R. Dynamic conjugate simulations were written in C++ using the Rcpp package. Biological interpretation of parameters for the stochastic simulations are summarised in Table 1 and the parameter values used throughout the manuscript are provided in S1 Table.

**Table 1.** Stochastic simulation parameters

parameter	biological interpretation
$\eta$	number of hits required for target death
$\bar{n}$	mean number of targets in a well
$\lambda$ (hr <sup>-1</sup> )	hitting rate
$k_{on}$ (hr <sup>-1</sup> )	conjugate formation rate
$k_{off}$ (hr <sup>-1</sup> )	conjugate dissociation rate

## Spatial Simulations

We developed spatial simulations of CTLs killing in microwells, with the aim of generating noisy and undersampled artificial data representative of data generated by microscopy, data which can be used to test methods for recovery of parameters governing CTL hitting. To this end we employed the cellular Potts model (CPM) framework [34], a formalism we used previously to simulate T cell-target cell interactions [11,35,36]. The CPM is a lattice based model, with entities such as cells represented by assigning individual lattice sites a ‘spin’ value, to identify them as belonging to a specific entity. The model evolves via minimisation of an energy function, the Hamiltonian:

$$H = H_{sort} + H_l + H_{act}. \quad \text{Eq. 2}$$

Here,  $H_{sort}$  represents interactions between cell surfaces and deviations from a target cell area;  $H_{sort}$  is defined as [34]:

$$H_{sort} = \sum_{(a(\sigma) - A_{q(\sigma)})^2} J(q(\sigma(i, j)), q(\sigma(i', j'))) (1 - \delta_{\sigma(i, j), \sigma(i', j')}) + \zeta_a \sum_{spin\ types\ \sigma} (a(\sigma) - A_{q(\sigma)})^2, \quad \text{Eq. 3}$$

where  $\sigma(i, j)$  is the spin of an individual cell of type  $q$  at grid point with  $x$  coordinate  $i$  and  $y$  coordinate  $j$ ;  $J(q, q')$  is the surface energy between cells of type  $q$  and  $q'$ ;  $\delta_{\sigma, \sigma'}$  represents the Kronecker delta;  $a(\sigma)$  represents the actual area of a cell and  $A_{q(\sigma)}$  the target area for a cell of type  $q$  (we refer to this as area rather than volume because we employ 2D simulations);  $\zeta_a$  is a weighting term for the area constraint; Note that the sum of the surface energies are calculated over each third order neighbour of a 2D grid site.

Our model also includes a term for surface area conservation of individual cells [37]:

$$H_l = \zeta_l \sum_{\sigma} (l(\sigma) - L_{q(\sigma)})^2, \quad \text{Eq. 4}$$

where  $L_{q(\sigma)}$  is the target perimeter for cells of type  $q$ ,  $l(\sigma)$  is the current perimeter of a cell with type  $\sigma$  (determined as the total length of the boundary interfaces with grid sites of differing spin), and  $\zeta_l$  is the weight of the perimeter constraint. We set  $L_q = 2\pi\sqrt{A_q}$ , i.e., the ratio of a circle's perimeter to its area, so that the term  $H_l$  is minimised when cells become perfectly circular. We set  $\zeta_l$  lower for the CTLs than for the target cells, implying that the targets retained a spherical shape whereas CTLs were much more deformable in our simulations.

Finally, the Hamiltonian includes a term  $H_{Act}$  to drive the motility of CTLs [22]:

$$H_{Act} = \frac{\zeta_{Act}}{Max_{Act}} (GM_{Act}(u) - GM_{Act}(v)). \quad \text{Eq. 5}$$

This follows an actin-driven cell motility model with protrusions driving the migration of cells. In this model actin is modelled explicitly and when a cell occupies a new site on the lattice, the site is given an actin value  $Max_{Act}$ . The actin activity  $Act$  in that site then decreases by one at every Monte carlo step until it reaches 0. The function:

$$GM_{Act}(u) = \left( \prod_{y \in V(u)} Act(y) \right)^{1/|V(u)|} \quad \text{Eq. 6}$$

calculates the geometric mean actin activity around site  $u$ , where  $|V(u)|$  are the second order Moore neighbours of site  $u$  (see Fig. 1 of reference [22]). The model favours updates from sites  $u$  with high actin activity into neighbouring sites  $v$  with low actin activity, resulting in local positive feedback. The CPM parameter  $\zeta_{Act}$  is a weighting term the strength of which we varied to control

the motility of the CTLs. The  $H_{act}$  term was not applied to target cells, which are moved only passively via interactions with the CTL and other targets.

In our spatial simulations we also implemented a contact-limited hitting behaviour for the CTL. We take CTL killing of targets to occur primarily via the perforin/granzyme pathway so we consider only contacted targets to be at risk, although our model should also apply to FAS-Ligand mediated killing, which is also contact-limited. When multiple targets are contacted by a CTL, it seems likely that the risk of getting hit is not equal for all targets, as polarisation of the lysosome towards specific targets should occur in order to permit delivery of lytic molecules to the target [8,9]. Although we did not model the polarisation of the lysosome explicitly, we do take into account a tendency for CTLs to unequally distribute hits towards contacted targets. To achieve this, we implement the same baseline hitting probability as in the Gillespie simulations, and multiply this by  $\theta_i(t)$ , the proportional fraction of CTL: target membrane interface occupied by the target at time point  $t$ .

$$\theta_i(t) = \frac{l_i(t)}{L_i(t)}, \quad \text{Eq. 7}$$

where  $l_i(t)$  is the length of the interaction interface between target  $i$  and the CTL inhabiting the same well,  $L_i(t)$  the total interaction interface length of the CTL that contacts target  $i$ , including any other co-contacting targets. Because CTLs are considered to hit targets at a constant rate  $\lambda$ , for simulations without delayed hitting each target's risk of being hit during a brief time interval  $\Delta t$  equals  $\lambda \theta_i(t) \cdot \Delta t$ . For some simulations we introduced a rule preventing CTLs from hitting targets for a specified delay period each time a CTL contacted or recontacted a target. This was implemented by means of a counting variable inside each target, such that hits would not register until the target had been in continuous contact with the CTL for the specified interval.

Simulations had a spatial scale of  $1 \mu\text{m pixel}^{-1}$  and were  $100 \mu\text{m}^2$  in area. The simulation space consisted of a circular area representing a microwell within which one CTL and usually between 10-20 targets were constrained to move. Simulations had a temporal scale of 1 second per Monte Carlo step. Parameters employed in the CPM simulations are given in Table 2. Simulation output was produced every 120 Monte Carlo steps (2 minute intervals), corresponding to a typical sampling frequency in time-lapse imaging data with multiple wells [19]. CPM simulations were developed within the morpheus framework [38].



**Table 2.** Cellular Potts simulation parameters

parameter	value	description
$J_{\sigma,\sigma'}$	$J_{tar,tar} = 0.7;$ $J_{ctl,tar} = -3;$ $J_{tar,well} = 0;$ $J_{ctl,well} = 0;$	surface energies between cell types
$A_q$	$A_{ctl} = 140 \mu m^2$ $A_{tar} = 340 \mu m^2$	the target area for a cell of type $q$
$L_q$	$2\sqrt{\pi A_q}$	the target perimeter for a cell of type $q$
$\varsigma_l$	$\varsigma_{l,ctl} = 0.1$ $\varsigma_{l,tar} = 0.25$	strength of cell perimeter constraint
$\varsigma_a$	$\varsigma_{a,ctl} = 1$ $\varsigma_{a,tar} = 1$	strength of cell area constraint
$\varsigma_{Act}$	$\varsigma_{Act,low} = 2$ $\varsigma_{Act,high} = 10$	strength of actin protrusion dynamics: $\varsigma_{Act,low}$ for low-motility and $\varsigma_{Act,high}$ for high motility CTLs
$Max_{Act}$	50	Actin activity value when CTLs occupy a new lattice site

## Acknowledgements

We would like to thank Delphine Guipouy and Loïc Dupré for useful discussions on the set-up of previously published microwell experiments.

## References

1. Elemans M, Florins A, Willems L, Asquith B. Rates of CTL killing in persistent viral infection in vivo. *PLoS Comput Biol*. 2014 Apr;10(4):e1003534.
2. Regoes RR, Yates A, Antia R. Mathematical models of cytotoxic T-lymphocyte killing. *Immunol Cell Biol*. 2007 Jun;85(4):274–9.
3. Barber DL, Wherry EJ, Ahmed R. Cutting edge: rapid in vivo killing by memory CD8 T cells. *J Immunol*. 2003 Jul 1;171(1):27–31.
4. Yates A, Graw F, Barber DL, Ahmed R, Regoes RR, Antia R. Revisiting estimates of CTL killing rates in vivo. *PLoS One*. 2007 Dec 12;2(12):e1301.
5. Ganusov VV, De Boer RJ. Estimating in vivo death rates of targets due to CD8 T-cell-mediated killing. *J Virol*. 2008 Dec;82(23):11749–57.
6. Regoes RR, Barber DL, Ahmed R, Antia R. Estimation of the rate of killing by cytotoxic T lymphocytes in vivo. *Proc Natl Acad Sci U S A*. 2007 Jan 30;104(5):1599–603.
7. Halle S, Keyser KA, Stahl FR, Busche A, Marquardt A, Zheng X, et al. In Vivo Killing Capacity of Cytotoxic T Cells Is Limited and Involves Dynamic Interactions and T Cell Cooperativity. *Immunity*. 2016 Feb 16;44(2):233–45.
8. Ritter AT, Asano Y, Stinchcombe JC, Dieckmann NMG, Chen B-C, Gawden-Bone C, et al. Actin depletion initiates events leading to granule secretion at the immunological synapse. *Immunity*. 2015 May 19;42(5):864–76.
9. Wiedemann A, Depoil D, Faroudi M, Valitutti S. Cytotoxic T lymphocytes kill multiple targets simultaneously via spatiotemporal uncoupling of lytic and stimulatory synapses. *Proc Natl Acad Sci U S A*. 2006 Jul 18;103(29):10985–90.
10. Caramalho I, Faroudi M, Padovan E, Müller S, Valitutti S. Visualizing CTL/melanoma cell interactions: multiple hits must be delivered for tumour cell annihilation. *J Cell Mol Med*. 2009 Sep;13(9B):3834–46.
11. Gadhamsetty S, Marée AFM, Beltman JB, de Boer RJ. A Sigmoid Functional Response Emerges When Cytotoxic T Lymphocytes Start Killing Fresh Target Cells. *Biophys J*. 2017 Mar 28;112(6):1221–35.

12. Beck RJ, Slagter M, Beltman JB. Contact-dependent killing by cytotoxic T lymphocytes is insufficient for EL4 tumor regression in vivo. *Cancer Res* [Internet]. 2019 Apr 30; Available from: <http://dx.doi.org/10.1158/0008-5472.CAN-18-3147>
13. Zagury D, Bernard J, Thiernes N, Feldman M, Berke G. Isolation and characterization of individual functionally reactive cytotoxic T lymphocytes: conjugation, killing and recycling at the single cell level. *Eur J Immunol*. 1975 Dec;5(12):818–22.
14. Zagury D, Bernard J, Jeannesson P, Thiernes N, Cerottini JC. Studies on the mechanism of T cell-mediated lysis at the single effector cell level. I. Kinetic analysis of lethal hits and target cell lysis in multicellular conjugates. *J Immunol*. 1979 Oct;123(4):1604–9.
15. Perelson AS, Macken A. Kinetics of Cell-Mediated Cytotoxicity: Stochastic and Deterministic Multistage Models. *Math Biosci*. 1984;70:161–94.
16. Peters PJ, Borst J, Oorschot V, Fukuda M, Krähenbühl O, Tschopp J, et al. Cytotoxic T lymphocyte granules are secretory lysosomes, containing both perforin and granzymes. *J Exp Med*. 1991 May 1;173(5):1099–109.
17. Zhu Y, Huang B, Shi J. Fas ligand and lytic granule differentially control cytotoxic dynamics of natural killer cell against cancer target. *Oncotarget*. 2016 Jul 26;7(30):47163–72.
18. Prager I, Liesche C, van Ooijen H, Urlaub D, Verron Q, Sandström N, et al. NK cells switch from granzyme B to death receptor-mediated cytotoxicity during serial killing. *J Exp Med* [Internet]. 2019 Jul 3; Available from: <http://dx.doi.org/10.1084/jem.20181454>
19. Vasconcelos Z, Müller S, Guipouy D, Yu W, Christophe C, Gadat S, et al. Individual Human Cytotoxic T Lymphocytes Exhibit Intracloal Heterogeneity during Sustained Killing. *Cell Rep*. 2015 Jun 9;11(9):1474–85.
20. Macken CA, Perelson AS. Some stochastic models in immunology. *Acta Appl Math*. 1985 Sep 1;4(2):157–200.
21. Weigelin B, Bolaños E, Teixeira A, Martinez-Forero I, Labiano S, Azpilikueta A, et al. Focusing and sustaining the antitumor CTL effector killer response by agonist anti-CD137 mAb. *Proc Natl Acad Sci U S A*. 2015 Jun 16;112(24):7551–6.
22. Niculescu I, Textor J, de Boer RJ. Crawling and Gliding: A Computational Model for Shape-Driven Cell Migration. *PLoS Comput Biol*. 2015 Oct;11(10):e1004280.
23. Beltman JB, Henrickson SE, von Andrian UH, de Boer RJ, Marée AFM. Towards estimating the true duration of dendritic cell interactions with T cells. *J Immunol Methods*. 2009 Aug 15;347(1-2):54–69.

24. Adan I, Resing J. Queueing theory [Internet]. Eindhoven University of Technology Eindhoven; 2002. Available from: <https://wwwhome.ewi.utwente.nl/~scheinhardtwrw/queueingdictaat.pdf>
25. Mehta AK, Gracias DT, Croft M. TNF activity and T cells. *Cytokine*. 2018 Jan;101:14–8.
26. Faletti L, Peintner L, Neumann S, Sandler S, Grabinger T, Mac Nelly S, et al. TNF $\alpha$  sensitizes hepatocytes to FasL-induced apoptosis by NF $\kappa$ B-mediated Fas upregulation. *Cell Death Dis*. 2018 Sep 5;9(9):909.
27. Badie B, Schartner J, Vorpahl J, Preston K. Interferon-gamma induces apoptosis and augments the expression of Fas and Fas ligand by microglia in vitro. *Exp Neurol*. 2000 Apr;162(2):290–6.
28. Viard-Leveugle I, Gaide O, Jankovic D, Feldmeyer L, Kerl K, Pickard C, et al. TNF- $\alpha$  and IFN- $\gamma$  are potential inducers of Fas-mediated keratinocyte apoptosis through activation of inducible nitric oxide synthase in toxic epidermal necrolysis. *J Invest Dermatol*. 2013 Feb;133(2):489–98.
29. Cullen SP, Brunet M, Martin SJ. Granzymes in cancer and immunity. *Cell Death Differ*. 2010 Apr;17(4):616–23.
30. Voskoboinik I, Whisstock JC, Trapani JA. Perforin and granzymes: function, dysfunction and human pathology. *Nat Rev Immunol*. 2015 Jun;15(6):388–400.
31. Brückner DB, Fink A, Schreiber C, Röttgermann PJF, Rädler JO, Broedersz CP. Stochastic nonlinear dynamics of confined cell migration in two-state systems. *Nat Phys* [Internet]. 2019 Mar 4; Available from: <https://doi.org/10.1038/s41567-019-0445-4>
32. Emmert M, Witzel P, Heinrich D. Challenges in tissue engineering - towards cell control inside artificial scaffolds. *Soft Matter*. 2016 May 11;12(19):4287–94.
33. Gillespie DT. A general method for numerically simulating the stochastic time evolution of coupled chemical reactions. *J Comput Phys*. 1976 Dec 1;22(4):403–34.
34. Graner F, Glazier JA. Simulation of biological cell sorting using a two-dimensional extended Potts model. *Phys Rev Lett*. 1992 Sep 28;69(13):2013–6.
35. Gadhamsetty S, Marée AFM, Beltman JB, de Boer RJ. A general functional response of cytotoxic T lymphocyte-mediated killing of target cells. *Biophys J*. 2014 Apr 15;106(8):1780–91.
36. Gadhamsetty S, Marée AFM, de Boer RJ, Beltman JB. Tissue Dimensionality Influences the Functional Response of Cytotoxic T Lymphocyte-Mediated Killing of Targets. *Front Immunol*. 2016;7:668.

37. Ouchi NB, Glazier JA, Rieu J-P, Upadhyaya A, Sawada Y. Improving the realism of the cellular Potts model in simulations of biological cells. *Physica A: Statistical Mechanics and its Applications*. 2003 Nov 15;329(3):451–8.
38. Starrau J, de Back W, Brusch L, Deutsch A. Morpheus: a user-friendly modeling environment for multiscale and multicellular systems biology. *Bioinformatics*. 2014 May 1;30(9):1331–2.

## Supplementary Data

Additional supplementary data for this chapter are available online with the links provided below:

**S1 Table.** Summary of parameters used in stochastic simulations. Data and code used in this project are available (<http://doi.org/10.17605/OSF.IO/6GQYP>).

<https://doi.org/10.1371/journal.pcbi.1007972.s001>

**S1 Text.** Fitting procedure and hypothesis comparison for multiple-hitting model and subpopulation model.

<https://doi.org/10.1371/journal.pcbi.1007972.s002>

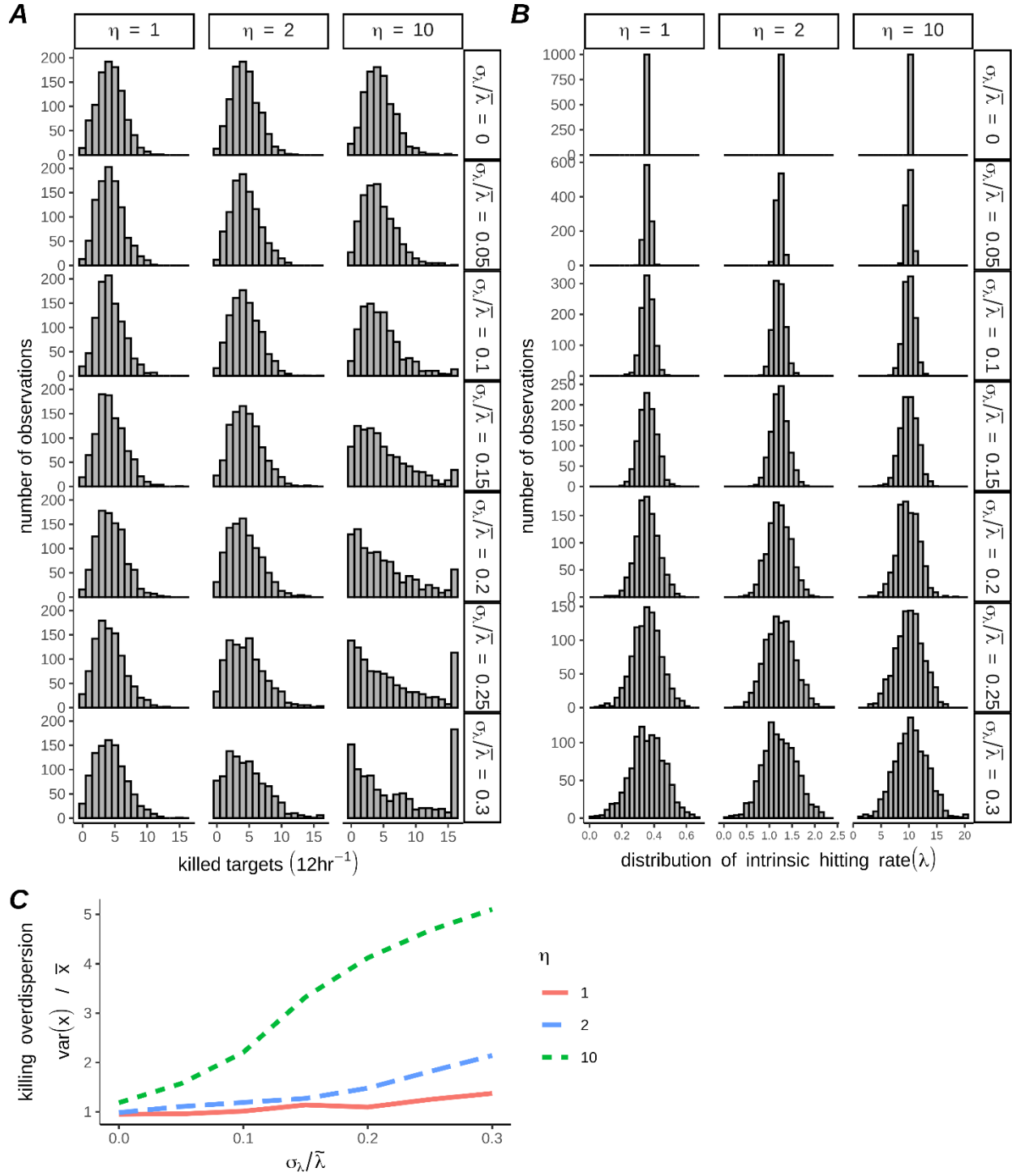
**S1 Video.** Simulation of high-motility CTL, requiring 5 hits to kill targets.

<https://doi.org/10.1371/journal.pcbi.1007972.s009>

**S2 Video.** Simulation of low-motility CTL, requiring 5 hits to kill targets.

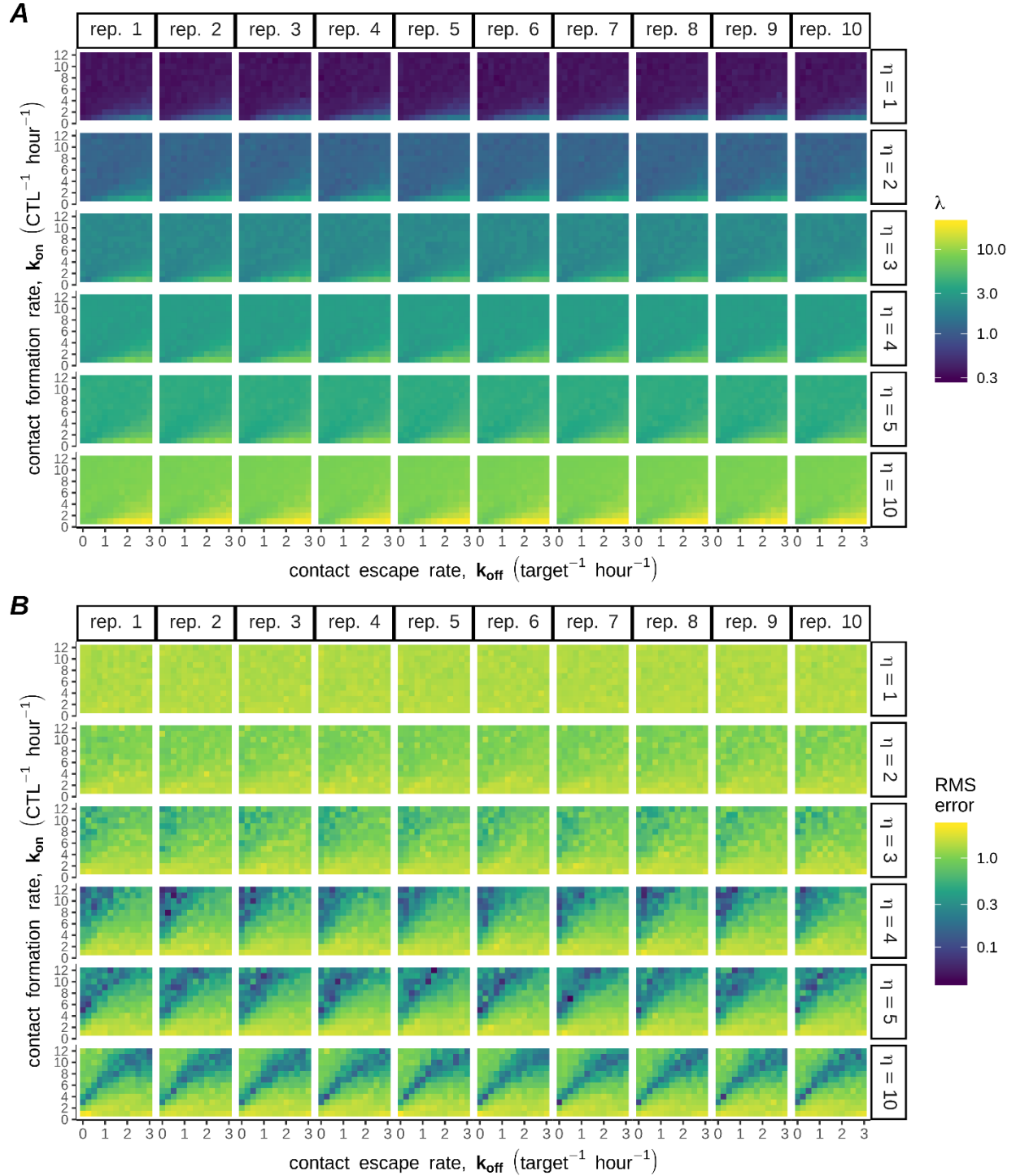
<https://doi.org/10.1371/journal.pcbi.1007972.s010>

In all videos, CTLs are shown in red whilst uncontacted targets are in grey. Contacted targets are shaded blue based on their share of total CTL:target interface, i.e. the probability that they will receive the next hit generated by the CTL. Targets are overlaid with the number of hits they have received. Elapsed simulation time (hours:minutes) is displayed in the upper right corner of the videos.



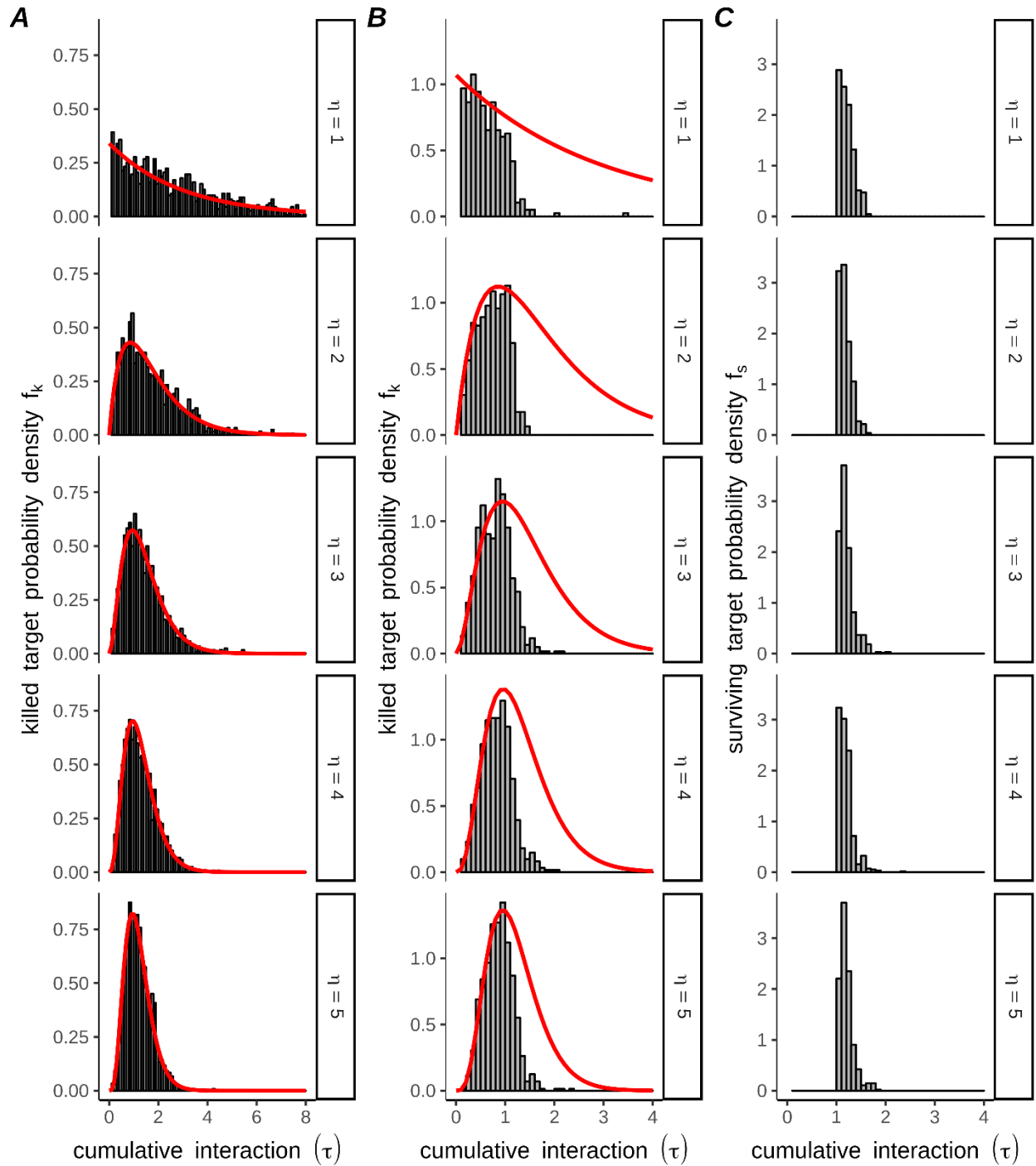
**S1 Fig. Multiple hitting increases inherent variability in killing performance between individual CTLs.** A-B) Distribution of killed target numbers after 12 hours (A) when intrinsic hitting rates  $\lambda$  (B) are drawn from a normal distribution with mean  $\bar{\lambda}$  and standard deviation  $\sigma_{\lambda}$  ( $\lambda \sim Normal(\bar{\lambda}, \sigma_{\lambda})$ ). C) Overdispersion for the variance in killed targets in A relative to the variance expected for a Poisson distribution, i.e., the ratio of the variance ( $var(x)$ ) to the mean ( $\bar{x}$ ) number of targets killed after 12 hours

(vertical axis). The horizontal axis is the ratio of the standard deviation to the mean value of the intrinsic hitting rate.



**S2 Fig. Parameter estimation for Monte Carlo simulations with dynamic contacts.** A) Estimated hitting rates ( $\lambda$ , represented by colour) for various combinations of the number of hits ( $\eta$ , rows), contact formation rates ( $k_{on}$ , vertical axes in sub-panels), or contact escape rates ( $k_{off}$ , horizontal axes in sub-panels). Ten

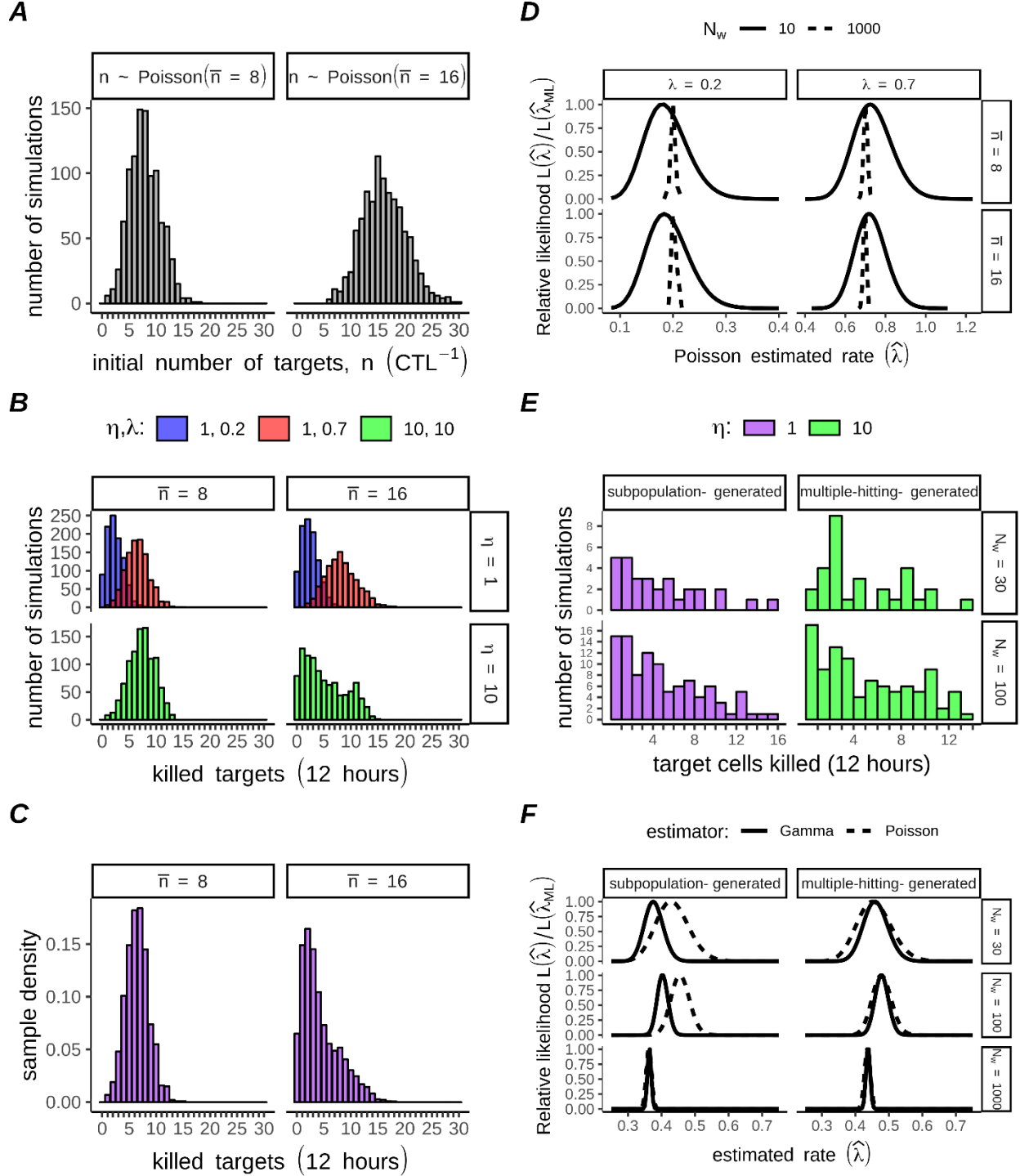
repeats (across columns) were performed for the optimisation step, using  $N_w=10^3$  CTLs per tested value of  $\lambda$ . After fitting we validated our results by performing  $N_w=10^4$  simulations with each best fitting parameter combination, which is shown here. B) Root mean square residual errors for the best fitting parameter estimates (panel arrangement is as described in S2A Fig legend). Results are from validation simulations, using  $N_w=10^4$  simulations per parameter combination.



**S3 Fig. Monte Carlo simulated CTL:target interaction durations amongst surviving and killed targets.** (displayed on previous page) A) Sample density of killed targets in Monte Carlo simulations lasting

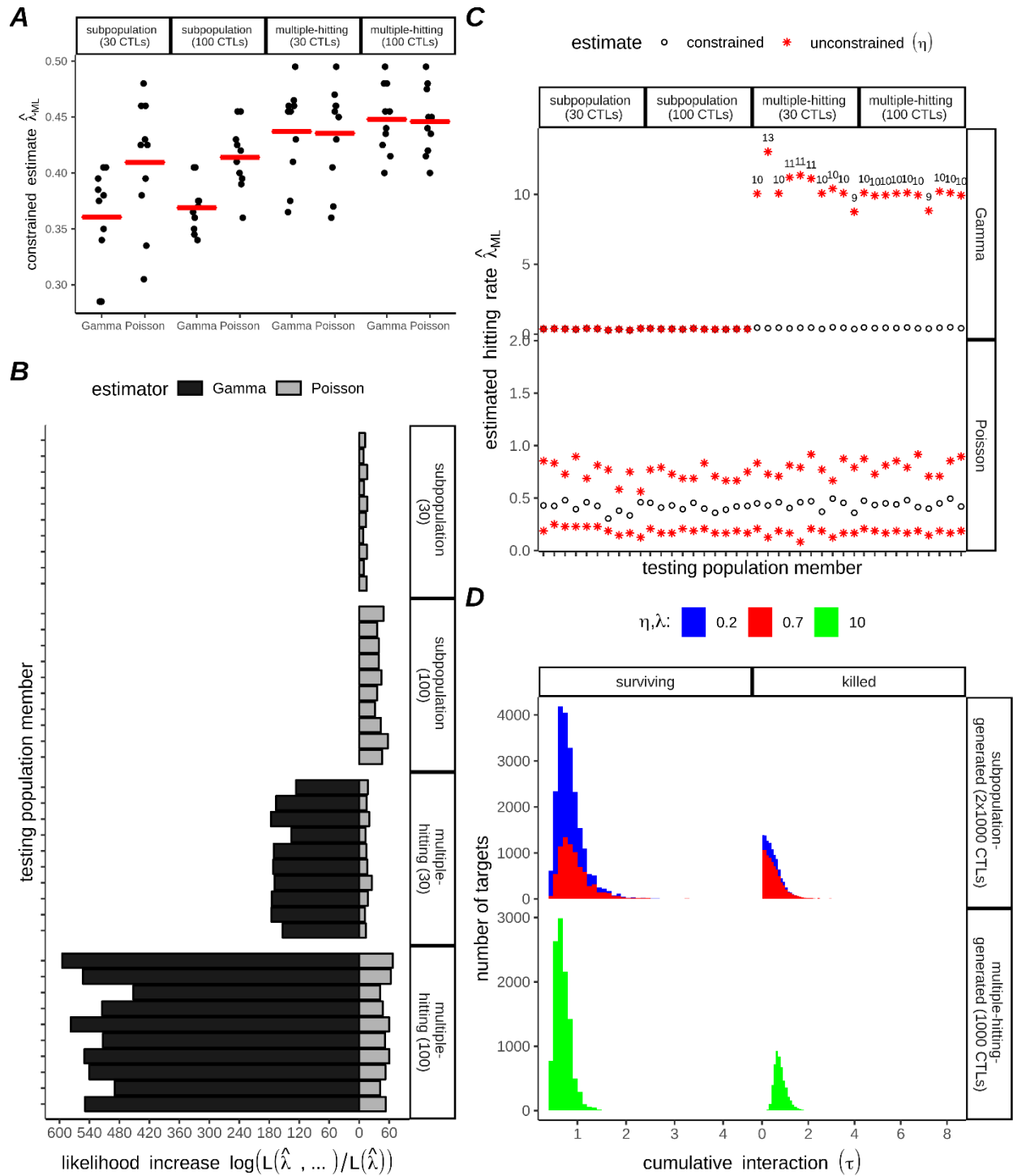


until all targets were killed, with different numbers of hits ( $\eta$ , on different rows). B) Sample density of killed targets in Monte Carlo simulations stopped after 12 hours. C) Sample density of surviving targets, corresponding to the 'absent' portion of the distribution for killed targets in B. The red line in A and B is the probability density function  $f_k$  for a gamma distributed waiting time until targets receive  $\eta$  hits arriving at a constant rate  $\lambda$ . For all S3 Fig:  $N_w=100$ ,  $n=12$  targets per well, all targets equally at risk. Parameter combinations used were: ( $\eta = 1, \lambda = 0.34$ ;  $\eta = 2, \lambda = 1.17$ ;  $\eta = 3, \lambda = 2.12$ ;  $\eta = 4, \lambda = 3.14$ ;  $\eta = 1, \lambda = 4.22$ ).



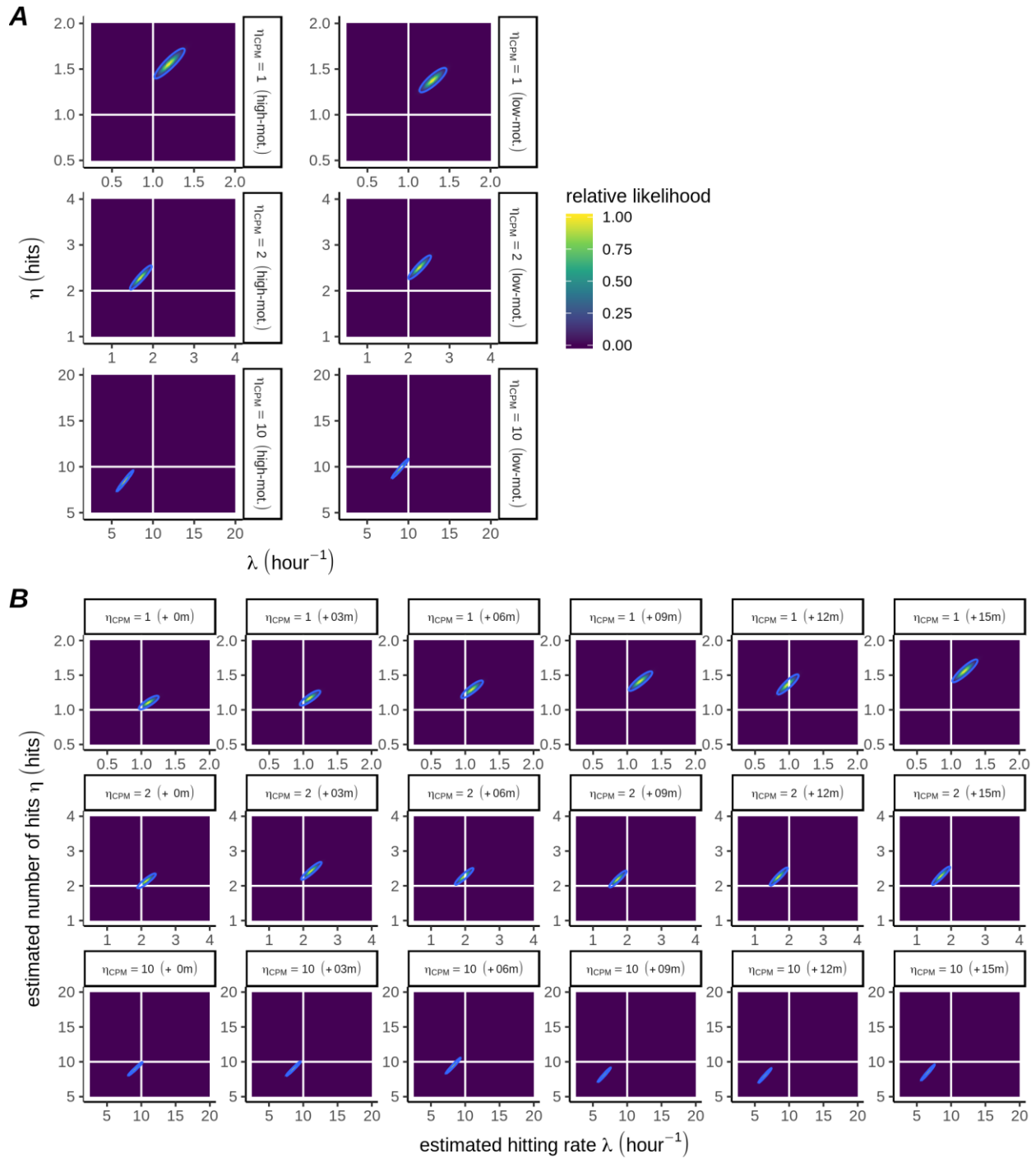
**S4 Fig. Maximum likelihood estimation for the killing rate of single-hitting CTLs.** A) Poisson distributions for the number of targets used to start simulations in Fig. S4, with mean  $\bar{n} = 8$  or 16 as shown. B) Number of killed targets after 12 hours for  $N_w = 2 \times 3 \times 1000$  simulations, each group of  $N_w = 1000$  started with one of the 2 distributions in A, and with one of the 3 indicated parameter settings. C) Density of killed targets after 12 hours from 'Mixed' distributions resulting from  $\eta = 1, \lambda_{LR} = 0.2, \lambda_{HR} = 0.7$  and either  $\bar{n} = 8$  and  $m = 0$  (left panel), or  $\bar{n} = 16$  and  $m = 0.67$  (right panel). Note that for  $\bar{n} = 8$  the killing of multiple-

hitting CTLs became greater than the high rate subpopulation of single-hitting CTLs;  $\bar{n} = 8$  was only used for testing robustness of the estimators on heavily censored data. D) Relative likelihood of candidate hitting rate estimates,  $\hat{\lambda}$ , compared to the maximum likelihood estimate,  $\hat{\lambda}_{ML}$ , resulting from application of the Poisson estimator separately to each of the single-hitting ( $\eta = 1$ ) datasets shown in B. Relative likelihood are shown either for the dataset in its entirety (dashed lines), or for a randomly selected sample of  $N_w=10$  (solid lines). E) Examples of testing datasets derived from the multiple-hitting population (B,  $\bar{n} = 16$ ,  $\eta = 10$ ) or from a mixture of single-hitting CTLs (B,  $\bar{n} = 16$ ,  $\eta = 1$ , where the true density of killed targets in the mixture distribution is in C). F) Relative likelihood of candidate hitting rate estimates,  $\hat{\lambda}$ , compared to the maximum likelihood estimate,  $\hat{\lambda}_{ML}$ , for constrained fits constructed from either the subpopulation datasets, or from multiple-hitting datasets, for three samples with either  $N_w=30, 100$ , or  $1000$  (note the multiple-hitting-generated data ( $\eta = 10$ ) is therefore fully represented by the  $N_w= 1000$  case).



**S5 Fig. Testing for multiple-hitting CTLs versus subpopulations of single-hitting CTLs.** A) Maximum likelihood estimates for the hitting rate,  $\hat{\lambda}_{ML}$ , with either the gamma or Poisson estimators, both constrained to a uniform single-hitting population (i.e. by forcing  $\eta = 1$  for the gamma estimator and by forcing  $m = 1$  for the Poisson estimator). Each of the 2x4x10=80 points represents one of the 4x10 testing populations from S4E Fig (here indicated by facet labels), fit with both of our estimators (x-axis). B) Difference between the log likelihood function evaluated with the constrained versus unconstrained Gamma estimator

$\log L(\hat{\lambda}_{ML}, \hat{\eta}_{ML})$  (dark bars); or with the constrained versus unconstrained Poisson estimator  $\log L(\hat{\lambda}_{HR,ML}, \hat{\lambda}_{LR,ML}, \hat{m}_{ML})$  (light bars). Each of the 40 testing populations occupies one horizontal bar, with the details of the testing populations as indicated in facet labels. For the x-axis scaling (negative values are not possible), the relative size of the dark v.s. light bars is proportional to the strength of the evidence for the multiple-hitting hypothesis (dark bars) versus the subpopulation hypothesis (light bars). C) The constrained estimates for the hitting rate parameters,  $\hat{\lambda}_{ML}$ , (circles; also shown in A) or their unconstrained counterparts (red asterisks) for each testing population (points on x-axis). For the Gamma estimator (top row) the estimated  $\hat{\eta}_{ML}$  is shown only where  $\hat{\eta}_{ML} > 1$ . For the Poisson estimator (bottom row), the unconstrained estimates for  $\hat{\lambda}_{HR,ML}, \hat{\lambda}_{LR,ML}$  are above and below their counterpart constrained estimates, and the Gamma and Poisson estimators can be compared per population. D) Distribution of all cumulative interaction times,  $\tau$  (killed and surviving targets shown separately in columns), for all  $N_w=1000$  members of each of the 3 generating populations (as shown in S4B Fig). Although the 2 single-hitting populations were combined (upper row), the separate contribution of the  $\lambda_{HR}$  (red) or  $\lambda_{LR}$  (blue) populations is indicated by color. Multiple-hitting CTLs (green) are shown separately (bottom row).



**S6 Fig. Maximum likelihood estimation for CPM simulations with a hitting threshold time.** A-B) Heatmaps of the likelihood function around the maximum likelihood estimates for the killing parameters  $\eta$  and  $\lambda$ , in CPM simulations under various conditions. In A, results are shown for various  $\eta$  values (rows) and for both high-motility (left column) and low-motility (right column) conditions for simulations with 15 minute hitting delay. In B, results are shown for high motility CTLs at all tested values of the delay (in range 0-15 minutes, across columns). The horizontal and vertical lines in A-B mark the values of the CPM parameters used to generate the data for each group and the boundary enclosing the 95% confidence region is marked with a thin blue line.

# Chapter 3

## Contact-Dependent Killing by Cytotoxic T Lymphocytes Is Insufficient for EL4 Tumor Regression in vivo

Richard J. Beck, Maarten Slagter and Joost B. Beltman

Division of Drug Discovery and Safety, Leiden Academic centre for Drug Research, Leiden University, Leiden, The Netherlands

*Cancer research 79.13 (2019): 3406-3416.*

### Abstract

Immunotherapies are an emerging strategy for treatment of solid tumors. Improved understanding of the mechanisms employed by cytotoxic T lymphocytes (CTLs) to control tumors will aid in the development of immunotherapies. CTLs can directly kill tumor cells in a contact-dependent manner or may exert indirect effects on tumor cells via secretion of cytokines. Here we aim to quantify the importance of these mechanisms in murine thymoma EL4/EG7 cells. We developed an agent-based model (ABM) and an ordinary differential equation (ODE) model of tumor regression after adoptive transfer of a population of CTLs. Models were parameterized based on in vivo measurements of CTL infiltration and killing rates applied to EL4/EG7 tumors and OTI T cells. We quantified whether infiltrating CTLs are capable of controlling tumors through only direct, contact-dependent killing. Both models agreed that the low measured killing rate of CTLs in vivo was insufficient to cause tumor regression. In our ABM we also simulated CTL production of the cytokine interferon gamma (IFN $\gamma$ ) in order to explore how an antiproliferative effect of IFN $\gamma$  might aid CTLs in tumor control. In this model IFN $\gamma$  substantially reduced tumor growth compared to direct killing alone. Collectively these data demonstrate that contact-dependent killing is insufficient for EL4 regression in vivo and highlight the potential importance of cytokine-induced antiproliferative effects in T cell mediated tumor control.

## Introduction

In the last decade, immunotherapies for cancer have moved into the mainstream of clinical oncology. Antibodies targeting immune checkpoints have been particularly successful, offering significant advantages over chemotherapy in a range of advanced metastatic, relapsed, and refractory solid tumors. CTLA-4, PD-1, and PD-L1 inhibitors are now approved in melanoma, non-small-cell lung cancer, renal cell carcinoma, urothelial carcinoma, merkel cell carcinoma, and some colon cancers[1]. Another promising immunotherapeutic approach has been the transfer of large numbers of cytotoxic T lymphocytes (CTLs). The transferred cells can be either autologously derived tumor infiltrating lymphocytes (TILs), or engineered with a chimeric antigen receptor (CAR) for tumor specificity. 2017 saw the first FDA approvals of CAR T cells for treatment of B cell malignancies[2]. The potential of adoptive transfer therapies for solid tumors has been highlighted in trials using TILs against melanoma[3–5], or CAR T cells against a range of solid tumors[6–8]. However, these promising early results have so far failed to transfer into the clinic.

Many attempts are being made to improve the efficacy and broaden the scope of cancer immunotherapies. For example, immunotherapies can have a synergistic effect when applied together with other immunotherapies[9,10], or with traditional treatments such as radiotherapy and chemotherapy[11,12]. Optimal treatment scheduling and dosages are yet to be determined. Given the danger of life threatening immune related adverse events following immunotherapy as well as the high costs involved, biomarkers to indicate which patients are likely to benefit from these treatments will be highly valuable. In particular, the immunosuppressive microenvironment which often characterises solid tumors represents a significant hurdle to the expansion and improvement of immunotherapies. Given the complex nature of the various mechanisms of interaction involved in determining the success of immunotherapies, a quantitative understanding of the contribution of these various mechanisms will be highly beneficial for the rational design and optimisation of cancer immunotherapies.

One highly relevant topic requiring greater quantitative insight regards the mechanisms employed by CTLs to control tumors *in vivo*. Indeed, these cells are key players in anti-tumor immune responses, which they are thought to achieve through being extremely efficient killers. This reputation has primarily been established by *in vitro* studies showing evidence of serial or simultaneous killing of several target cells in a short time frame[13,14]. Killing by CTLs is usually considered to be 'direct', i.e., contact dependent, and mediated by either perforin and granzymes, or FAS-L. Several studies have suggested that direct lysis of tumor cells by CTLs is extremely important in tumor control[15–18]. However, the reported killing rates of CTLs *in vivo* are typically low[19] and it is not clear whether these rates are indeed sufficient for control of tumors. Several studies have highlighted the importance of 'indirect' effects of cytokine signalling by activated T cells in the control of tumors, in particular IFN $\gamma$  [20,21]. IFN $\gamma$  may control tumors by exertion of an antiproliferative effect[22], sensitization of tumor cells to FAS-L mediated death[23], recruitment of effector cells of the innate immune system[24], and by causing widespread necrosis of tumor cells along with tumor vasculature destruction[25].



In the current study we quantitatively compare the importance of direct, contact dependent killing, with indirect cytokine mediated tumor control, based on published experiments in which EL4/EG7 tumor cells were infused into mice[18]. We chose to focus on the EL4 tumor cell line which, along with its transformed Ova antigen expressing derivative EG7, has been widely used to explore the anti-tumor activities of CTLs in an *in vivo* setting[18,21,26–29]. Using these cell lines, evidence has emerged supporting an important role for IFN $\gamma$  in tumor control by CTLs yet a negligible role for direct killing, along with apparently contradictory evidence suggesting an important role for direct killing. Hollenbaugh *et al.*[30] transferred perforin and FasL deficient T cells into EG7 tumor bearing mice, and these deficient T cells were able to control tumors almost as well as their wild type counterparts. However, IFN $\gamma$  deficient T cells displayed a marked reduction in tumor control, suggesting that IFN $\gamma$  rather than direct cytotoxicity was the primary mechanism used by CTLs to control the tumor. In contrast, Breart *et al.*[18] used intravital two-photon imaging to show that apoptotic events almost exclusively occurred when tumor cells were contacted by T cells, thus arguing for a major role of direct cytotoxicity. Moreover, they generated mixed tumors, comprising both Ova-expressing EG7 cells and non-Ova-expressing EL4 cells. In these mixed tumors only the antigen expressing EG7 cells were eliminated, arguing against an indiscriminate effect from IFN $\gamma$ . We integrate the data acquired at various levels into both an ordinary differential equation (ODE) model, and a spatial agent-based model (ABM). Applying these models to the *in vivo* data we show that the observed T cell densities and slow killing rate were insufficient to explain the population-level tumor regression observed in the mice. We found that an antiproliferative effect mediated through IFN $\gamma$  signalling allowed CTLs to influence far more cells than direct killing alone, therefore leading to a substantially greater impact on tumor progression. Our modelled scenario corroborated the notion that IFN $\gamma$  plays a crucial role in EL4 tumor control, and reconciles this with the apparently conflicting observation of low reported killing rates and density of infiltrating CTLs.

## Methods

### Data interpretation

Since the main aim of this work is to test whether CTLs could have controlled the tumor through the sole means of direct killing, we favoured ‘optimism’ from the CTL viewpoint wherever the *in vivo* dataset was ambiguous. Thus, we chose model assumptions that promoted tumor control through direct CTL killing.

**Tumor Cells.** Tumor volume measurements in the absence of CTL transfer were used to fit the growth rate of both our ODE model and ABM. Based on manual counting of the images, we estimated that the density of tumor cells was approximately  $10^6$  cells  $\text{mm}^{-3}$ . This value is the default used in all our models. Moreover, Breart *et al.*[18] used flow cytometry to estimate the absolute number of tumor cells inside two tumors 10 days after inception (in the absence of infused T cells). An average of  $4 \times 10^6$  cells were recovered, at a time-point where the average tumor volume was  $\sim 17 \text{mm}^3$ , corresponding to a density of approximately  $0.25 \times 10^6$  cells  $\text{mm}^{-3}$ . Given that a substantial fraction of tumor cells were likely lost during the cell isolation procedure[31], this can be viewed as an absolute underestimate of the tumor cell density. To

convert between tumor volume and number of tumor cells, we consider direct proportionality between these quantities.

Dead tumor cells are not recognised by CTLs in our models yet are not immediately removed from the models. Parnaik *et al.* [32] found that cultured rat cerebellar neurons were completely cleared within 3 hours of apoptosis by professionally phagocytic microglia, whereas the same cells were incompletely cleared after 9 hours by non-professionally phagocytic epithelial cells. We therefore considered tumor cells to persist for an average of 6 hours after apoptosis. Because the number of CTLs in our modelled tumors is proportional to the tumor volume (the sum of numbers of dead and alive cells), inclusion of dead tumor cells increases the ratio of effector : alive target (E:T ratio) and thereby increases the total killing rate.

**CTLs.** Breart *et al.*[18] transferred CTLs to mice on day 5 after tumor injection. Before this point we consider CTLs to be absent from the tumor. Because killing undertaken by any endogenous CTL should also occur in the control tumors where no CTLs were transferred, this is already accounted for in our fit to the tumor growth data in the absence of CTLs. Breart *et al.*[18] measured the density of CTLs within the tumor on days 7 (12500 CTLs mm<sup>-3</sup>) and 8 (25000 CTLs mm<sup>-3</sup>). Based on our estimate of 10<sup>6</sup> tumor cells mm<sup>-3</sup>, this corresponds to an Effector:Target ratio of 1:80 on day 7, and 1:40 on day 8. Due to the temporally sparse measurements the exact dynamics of T cell infiltration into the tumor are not known and for simplicity we linearly interpolated between the available data points. Beyond day 8, further data on the density of infiltrating CTLs was not recorded. In reality T cell numbers likely peak and then decline a few days after adoptive transfer[22], and T cells often suffer from exhaustion after extended time in the tumor[33,34]. However, it is certainly possible that CTL numbers continued to increase beyond day 8. In line with our policy of taking the most optimistic assumptions from the CTL viewpoint, we considered the ratio of effector T cells to total tumor cells (Effector:Tumor-Cell ratio) to continue to linearly increase after day 8. Also in line with our policy, we do not consider CTLs to diminish in effector function over time (which would make it more difficult to control the tumor). CTLs kill tumor cells at a default rate of  $k = 4 \text{ CTL}^{-1} \text{ day}^{-1}$ .

## ODE Model

**Model setup.** ODE simulations were performed in the R language, using the package 'deSolve 1.14'. Models were fitted using the Levenberg Marquardt algorithm in the package 'minpack.lm 1.2-1'. Our ODE model was designed to test whether CTLs could control tumors with the observed direct killing rate of  $k = 4 \text{ kills } \text{CTL}^{-1} \text{ day}^{-1}$ . Therefore, we deliberately simplified the model, with assumptions chosen to maximise the likelihood of tumor control. The model consists of two coupled equations:

$$\frac{dT}{dt} = gT - kE(t) , \quad (1)$$

$$\frac{dD}{dt} = kE(t) - dD, \quad (2)$$

Thus, tumor cells  $T$  are considered to grow exponentially with rate  $g$  ( $day^{-1}$ ) in the absence of CTLs, because the experimental tumors clearly did not yet suffer from competition for resources during the measurement interval (Fig. 1A). Tumor cells are killed at rate  $k$  ( $CTL^{-1} day^{-1}$ ) by a population of effector cells  $E(t)$ , where  $E(t)$  is determined based on the number of dead and alive tumor cells (Data Interpretation, Fig. 1B):

$$E(t) = \lambda(T + D) \begin{cases} 0 & \text{if } (t \leq 5) \\ (t - 5) & \text{if } (5 < t \leq 7) \\ 2(1 + (t - 7)) & \text{if } (7 < t), \end{cases} \quad (3)$$

with the parameter  $\lambda$  arising from interpolation of the data ( $\lambda = \frac{1}{160} cell^{-1} day^{-1}$ ), which defines the rate of increase in the Effector:Tumor-Cell ratio  $E:(T + D)$ .

Killed cells  $D$  are cleared at rate  $d$  ( $day^{-1}$ ). We took the killing rate to be proportional to the number of CTLs and independent of the number of target cells, implying that CTLs are considered to always kill at their maximal rate. In reality a dual saturation function, with saturation in both effector and tumor cell number  $T$ , is a more complete description of CTL killing (Supplementary Methods) [35,36]. However, we aimed to model a situation that favours CTL control of the tumor. In such a best-case scenario from the CTL viewpoint, CTLs always have sufficient targets to kill and need never search for targets. As such our simplified ODE model is an extremely optimistic scenario from the point of view of the CTLs. This simplification implies that our model is a good approximation as long as the E:T ratio remains sufficiently low.

## ABM

**Model setup.** ABM simulations were implemented in C++14, using boost 1.69.0. Visualisations were rendered in C++ using VTK 8.0. We use an asynchronously updating ABM to simulate tumor growth, T cell infiltration and migration, and tumor regression. Our ABM features two types of agents: CTLs and tumor cells. Tumor cells live on a regular 3D lattice where each cell occupies a single lattice site; tumor cells do not share sites with each other. Empty sites in the lattice represent extracellular matrix, or other cell types not interfering with the tumor. Lattice sites have length  $10\mu m$  by default, roughly corresponding to our default tumor cell density assumptions. Each tumor cell grid point contains information on the tumor cell type (either EG7 or EL4), the amount of damage it has sustained from CTL attacks, and whether it is alive or not. Throughout the simulation we track the displacement of the furthest tumor cell from the centre of the lattice; this measurement is used to dynamically adjust the size of the simulation domain. The domain is a sphere, extending from the lattice centre out to a radius 5 lattice sites ( $50\mu m$ ) beyond the displacement of the furthest tumor cell.

**Tumor cell behaviour.** The tumor is initialised on day 0, by filling  $70$  lattice sites with tumor cells within a radius of  $R_t$  from the lattice centre. The simulation is advanced in timesteps of 1 minute ( $\Delta t$ ). At each timestep each tumor cell is liable to replicate with probability  $g\Delta t$ . Cells replicate into a random neighbouring square if one is available. We implemented short range dispersal (similar to [37]) as a computationally inexpensive means to achieve exponential, spheroidal tumor growth whilst comfortably allowing simulation of over  $10^8$  individual agents. Candidate dividing cells whose surroundings are fully occupied attempt to disperse from the tumor with probability  $p_{disp}$ . Dispersing cells produce a daughter cell for which a new location is chosen based on a random walk with mean dispersal distance proportional to the current tumor radius. If the chosen site is vacant the daughter cell occupies this site, otherwise the dispersal attempt fails.

**CTL infiltration.** CTLs are associated with a location corresponding to a grid site, however they are not explicitly represented on the grid and as such can share space with other CTLs or tumor cells. Thus, CTLs do not contribute to the tumor mass and are able to move through tumor tissue, attempting to form conjugates with antigen expressing tumor cells. We allowed for such co-occupancy because CTLs can easily move in between other cells in densely packed environments such as a lymph node[38] or the skin epidermis[39], and are able to cooperate to kill individual targets[19]. Because of the relatively low Effector:Tumor-Cell ratios observed in the experimental data, in practise our CTLs rarely share lattice sites. Specifically, two or more CTLs share a lattice site only  $\sim 2\%$  of the time, and 3 or more share a site  $\sim 0.01\%$  of the time on day 8 of a typical simulation. Following the experimental setup, CTLs infiltrate the tumor on day 5 after tumor inception. New CTLs arrive at random points within the existing simulation domain. At each timestep a target number of CTLs is calculated based on the Effector:Tumor-Cell ratio we estimated from the data (in equivalence with the ODE model). If the number of CTLs inside the simulation is below the current target, new CTLs are added to the simulation until the target is reached. CTLs are only removed from the simulation when they migrate outside the simulation domain. The number of CTLs may therefore exceed the target density, albeit only whilst the tumor disappears more quickly than CTLs migrate out of the simulation domain.

**CTL migration.** CTLs migrate until they reach a site occupied by a tumor cell; CTLs that migrate outside the simulation domain are removed. Whilst a CTL is migrating, each time-step it randomly moves to an adjacent lattice site within its 3D Moore neighbourhood including its current location. Thus, there is a  $1/27$  probability of no movement, a  $6/27$  probability of a  $10\mu\text{m}$  movement,  $8/27$  probability of a  $10\sqrt{2}\mu\text{m}$  movement, and a  $8/27$  probability of a  $10\sqrt{3}\mu\text{m}$  movement. Therefore, the resulting migration speed is  $11.5\mu\text{m}$  per minute, which is in close agreement with previously measured values in the EL4/EG7 tumor [29]. CTLs that find tumor cells arrest with probability  $p_{arr}$ , and subsequently attack tumor cells with probability  $p_{hit}$  or detach and resume migration with probability  $p_{det}$ . By default  $p_{arr} = 1$  and  $p_{det} = 0$ , although these are varied to  $p_{arr} = 0.9$  and  $p_{det} = 0.01$  in the simulations where we examine multi hitting CTL. CTLs are immediately released from conjugates if the target cell dies.

**Effects of CTLs on tumor cells.** Tumor cells may sustain  $n_{hit}$  hits from CTLs before apoptosis occurs. By default  $n_{hit} = 1$ , in which case CTLs attack targets with an attack rate identical to the killing rate. In simulations where multiple hits are required for tumor cell death the base attack rate is multiplied by the number of hits required for apoptosis. Therefore the overall killing potential

of the CTLs is controlled between single-hit and multiple-hit simulations to obtain equal killing rates.

In simulations with IFN $\gamma$ , that cytokine is produced at a constant rate by CTLs whilst conjugated with tumor cells. IFN $\gamma$  is consumed by tumor cells, and tumor cells cannot divide when the local IFN $\gamma$  concentration exceeds a threshold value. We set the diffusion parameters such that the threshold occurs at around 3 cell lengths away from a conjugated CTL. For details see the Supplementary Methods.

**Mixed tumors.** We simulated mixed EL4/EG7 tumors by seeding a 50/50 mixture of cells on day 0. The only difference between these cell types is that EG7 cells are not recognised by CTLs.

## Results

### Direct CTL cytotoxicity is not sufficient to mediate *in vivo* regression of EG7 tumors

In the *in vivo* data of Breart *et al.*[18], transferred OTI effector T cells rapidly controlled an infused EG7 tumor, following direct contact with tumor cells. However, each infiltrating CTL killed on average only 4 tumor cells per day and it is unclear if tumor regression should be expected based on the density and cytotoxic activity observed in this *in vivo* data. To test whether CTLs could reasonably be expected to control the *in vivo* tumors, we employed an ODE model (see Methods) that integrated the measurements made at various levels. Instead of providing a detailed description of the tumor and its interactions with the immune system, the goal of this model was rather to assess the possibility that direct killing could have solely accounted for tumor regression. The simplifications that we made in the ODE model always favoured the CTLs, i.e., they made tumor regression more likely. If indeed CTLs were capable of controlling the tumor by direct killing alone, tumor regression would certainly be observed in this simplified model.

Modelling tumor growth as an exponential process resulted in a good match to the tumor measurements from Breart *et al.*[18] for the case without T cell transfer (Fig. 1A), suggesting that tumor growth was not yet inhibited by factors such as competition for nutrients. Subsequently, we introduced a population of CTLs into this model, with Effector:Tumor-Cell ratio based also upon experimental measurements (Fig. 1B). The impact on the tumor was limited when CTLs killed tumor cells at a rate of  $k=4 \text{ CTL}^{-1}\text{day}^{-1}$  as reported by Breart *et al.*[18] (Fig. 1C), despite the continuous increase in intratumoral T cell numbers (Fig. 1D). The killing rate measurements were relatively uncertain compared to the other parameters in the ODE model, perhaps having varied over time or throughout the tumor. To address that uncertainty, we simulated CTL populations killing with rate up to  $k=16 \text{ CTL}^{-1}\text{day}^{-1}$ , which is at the high end of the range of reported estimates for CTL killing performance *in vivo* [40]. As a side note, in this model such a 4-fold increase of the killing rate is equivalent to a 4-fold increase of the CTL infiltration rate. With  $k=16$  our simulated tumors were controlled, although this control occurred only at much later time points than was the case for the *in vivo* tumors. Thus, even for the extremely optimistic scenario we consider and using a substantially higher killing rate than was measured experimentally, direct CTL lysis alone could not explain the observed *in vivo* tumor regression.

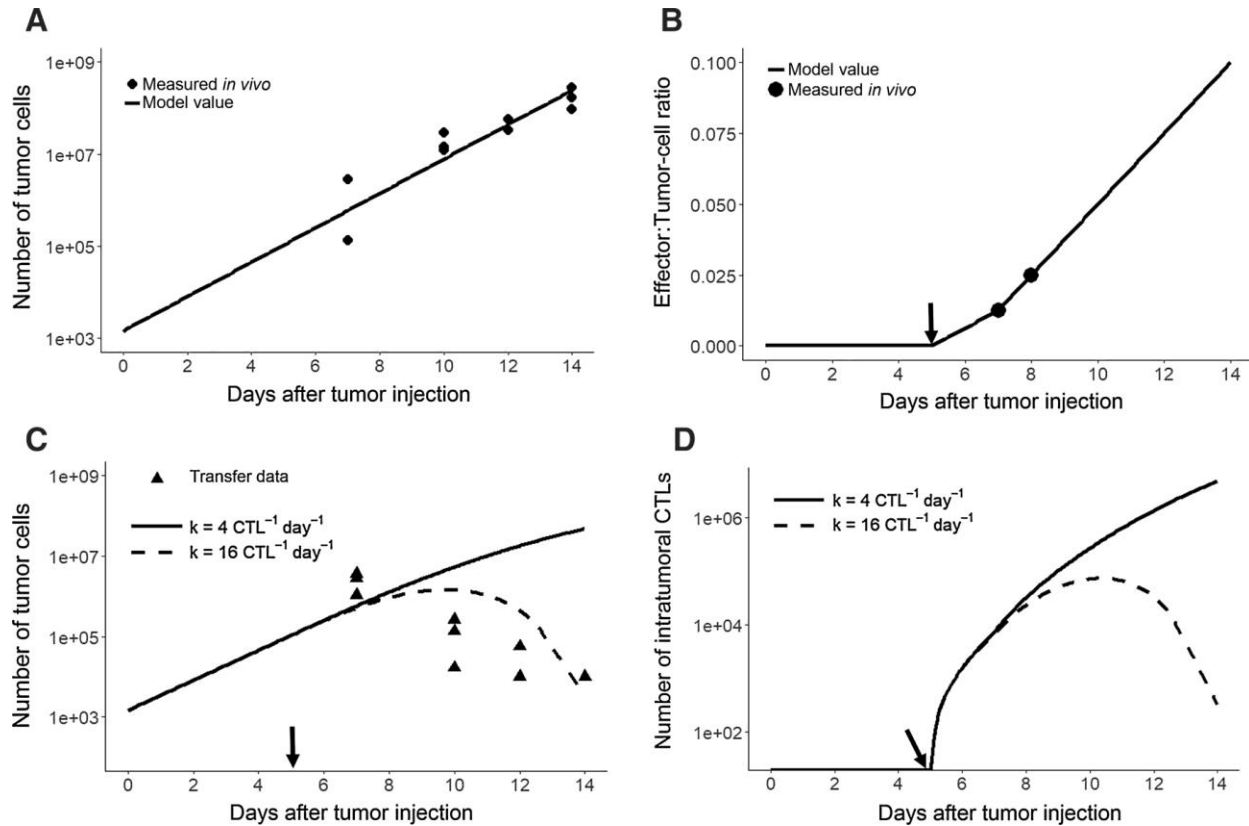


**Figure 1.** ODE model suggests direct T cell cytotoxicity is insufficient for control of EG7 tumors. **A)** Tumor growth is described as exponential growth ( $g=0.86 \text{ day}^{-1}$ ). **B)** Effector:Tumor-Cell ratio in the ODE model is estimated by linear interpolation of measured data points. After day 8, we assume a linear increase in CTL density. Arrows in **B-D** indicate time of CTL transfer. **C)** ODE simulation of tumor dynamics in the presence of actively killing CTLs, with two different killing rates. Lines represent model fits and dots represent experimental data. **D)** Total number of CTLs in simulations with killing.

## Agent Based Model supports notion that CTL cytotoxicity is insufficient to mediate *in vivo* regression of EG7 tumors

We developed a spatially explicit ABM with tumor cells and CTLs as agents to contrast against the idealised ODE model (Fig. 2A-B). As in the ODE model, in the ABM the overall growth rate of the tumor was matched to the data in the absence of CTLs (Fig. 2C), although the ABM differs in that tumor cells cannot divide when fully surrounded, i.e., there is competition for space. Tumors were much less well controlled in the ABM than they were in the ODE model (Fig. 2D); even at a killing rate of  $k=16 \text{ CTL}^{-1} \text{ day}^{-1}$  the tumor was not controlled in the ABM. There are two reasons for this discrepancy. Firstly, when compared to the ODE model, the ABM has the added requirement that CTLs must migrate in order to find tumor cells to kill. Indeed, the fraction of CTLs in conjugates was lower in simulations with  $k=16 \text{ CTL}^{-1} \text{ day}^{-1}$  than in those with  $k=4 \text{ CTL}^{-1} \text{ day}^{-1}$  (Fig. 2E), because faster killing CTLs spend less time conjugated with tumor cells. The second source of discrepancy between the ODE and ABM results stems from the competition for space between tumor cells that occurs in our ABM; CTL killing eases such competition, so tumor control is more difficult. Thus, the idealised ABM highlights that CTLs might make their own job more difficult by

being highly efficient killers. Overall, the ABM simulations confirm that CTL-mediated direct killing alone cannot explain EG7 tumor regression.

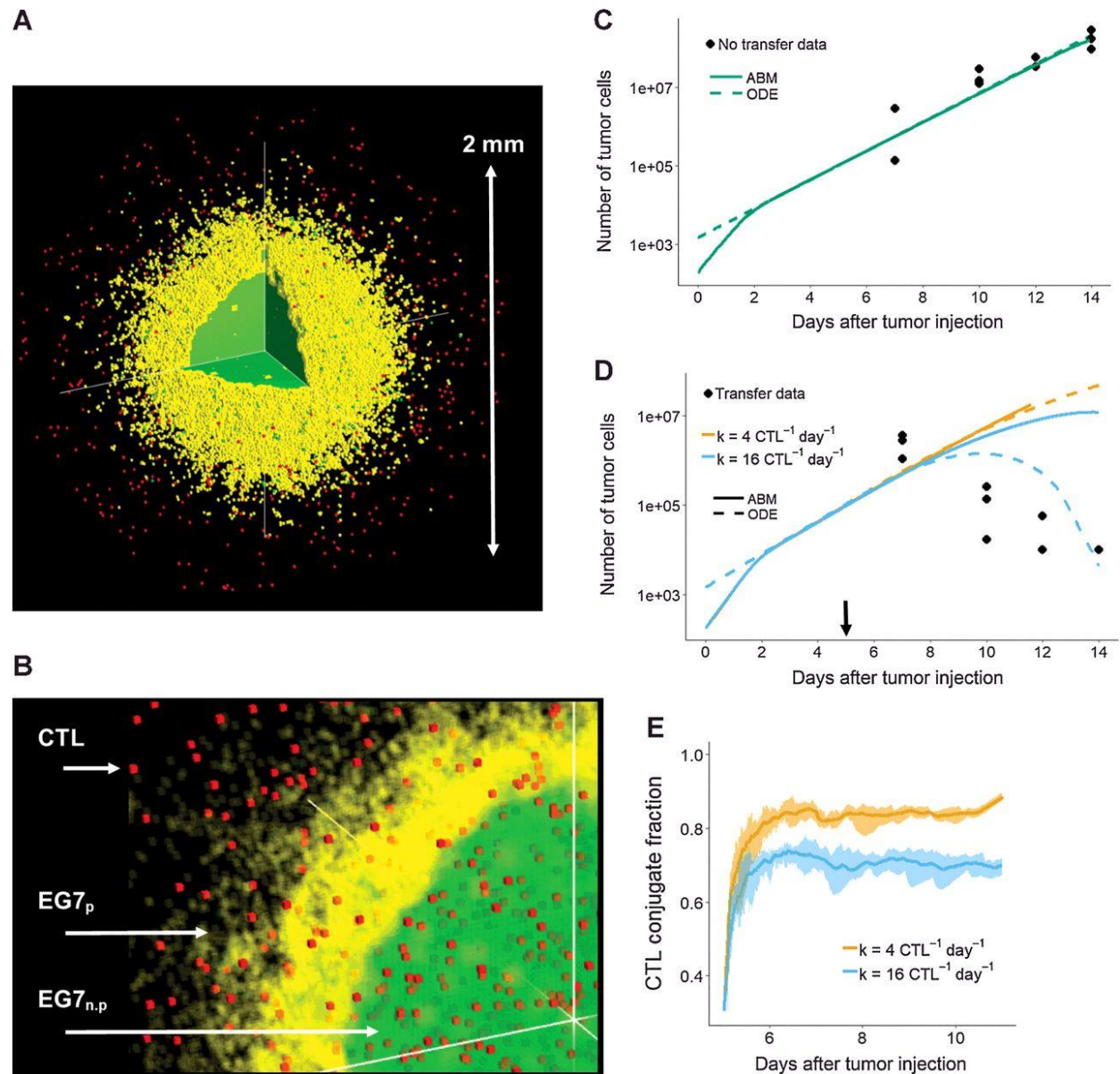


**Figure 2.** ABM confirms that direct T cell cytotoxicity is insufficient for control of EG7 tumors. **A-B)** ABM tumor infiltrated by CTLs on day 7. EG7 with free adjacent lattice sites can proliferate (EG7<sub>p</sub>). EG7 with no free adjacent lattice sites are non-proliferating (EG7<sub>n.p</sub>), although they may still disperse (see Methods). **C-D)** Comparison of tumor evolution in ABM (solid lines) and ODE model (dashed lines) without **(C)** and with **(D)** transferred CTLs, where arrow indicates time of CTL transfer. **E)** Fraction of CTLs in a conjugate with a tumor cell throughout ABM simulations.

## IFN $\gamma$ -mediated cell cycle arrest is sufficient for tumor control

Because IFN $\gamma$  has been widely implicated in tumor eradication [20,21,23–25,41], we added production and diffusion of this cytokine to our ABM. We focussed on an antiproliferative effect of IFN $\gamma$  because Breart *et al.* [18] only detected apoptosis in tumor cells directly contacted by CTLs, an observation which is inconsistent with the notion of significant IFN $\gamma$  cytotoxicity towards EG7 cells. To test the contribution of the putative antiproliferative effect of IFN $\gamma$ , we simulated tumors with  $k=4 \text{ CTL}^{-1}\text{day}^{-1}$  or  $k=16 \text{ CTL}^{-1}\text{day}^{-1}$ , in the presence or absence of IFN $\gamma$ . In our simulated tumors, the antiproliferative effect of IFN $\gamma$  was much stronger than the contact dependent CTL lysis, even with  $k=16 \text{ CTL}^{-1}\text{day}^{-1}$  (Fig. 3A). Although tumors were rapidly controlled in our model with IFN $\gamma$ , they were not entirely eradicated. This can be explained by the low number of CTLs in the IFN $\gamma$  simulations (Fig. 3B), together with the fraction of conjugated CTLs which drops after the onset of tumor regression for  $k=16 \text{ CTL}^{-1}\text{day}^{-1}$  (Fig. 3C). CTLs mostly eradicate tumor cells in the centre of the spheroid, but some pockets of tumor cells in the periphery survive and allow the tumor to escape (Fig. 3D, Video S2). These modelled behaviours are consistent with literature observations that solid tumors “melt from the inside” [42], and that EL4 tumors may rebound after an initial response to transferred CTLs [43]. In summary, tumor cell cycle arrest due to cytokine production by CTLs in addition to their cytotoxicity can explain the observed response of EG7 cells to a population of transferred CTLs.

## CTL cooperativity leads to heterogeneity in killing rate

Our ABM predicted an almost negligible role for direct killing in tumor regression, with or without the presence of IFN $\gamma$ . However, the CTL killing rate may in reality have been higher than the measured  $k=4 \text{ CTL}^{-1}\text{day}^{-1}$  and may not have been constant over time [36]. Factors that could play a role here include the ability of CTLs to kill collaboratively [19] and that of cancer cells to resist multiple CTL ‘hits’ before apoptosis is triggered [44]. We therefore used our ABM to assess whether the measurement of  $k=4 \text{ CTL}^{-1}\text{day}^{-1}$  could have resulted from a higher ‘intrinsic’ CTL killing rate. We compared simulations in which tumor cells die after a single ‘lethal hit’ with simulations where an accumulation of several hits was required for apoptosis. There was no substantive difference between the single hit and multi hit scenarios in terms of tumor growth (Fig. 4A), or number of CTLs (Fig. 4B). At early time points, the fraction of CTLs in conjugates in the multi hit model was slightly higher than in the single hit model (Fig. 4C) and the temporal pattern of killing rate per simulated CTL (Fig. 4D) or per conjugated CTL (Fig. 4E) differs between the two settings. Multi hitting CTL populations initially killed at a low rate, because targets had generally not acquired enough damage to die. Subsequently, targets accumulated damage and the manifested killing rate per conjugated CTL rose above the killing rate for the single hit scenario (Fig. 4E). Similar to the killing rate-measurement procedure of Breart *et al.* [18], we measured killing in  $100\mu\text{m} \times 100\mu\text{m} \times 30\mu\text{m}$  ‘windows’ for a two hour period at the beginning of day 8 during a cumulative total of 75 hours of conjugated CTL imaging time [18]. Our analysis shows that such sample sizes in general reflect the global killing rate well (Fig. 4F). As a side note, in our model the infiltration of the tumors by CTLs was relatively homogeneous, meaning that damage to targets occurred roughly evenly throughout the tumor (Fig. 4G). Although heterogeneous infiltration may lead to strong spatial variability in killing rate, we conclude that temporal variation in killing is likely large, especially when CTLs cooperate.



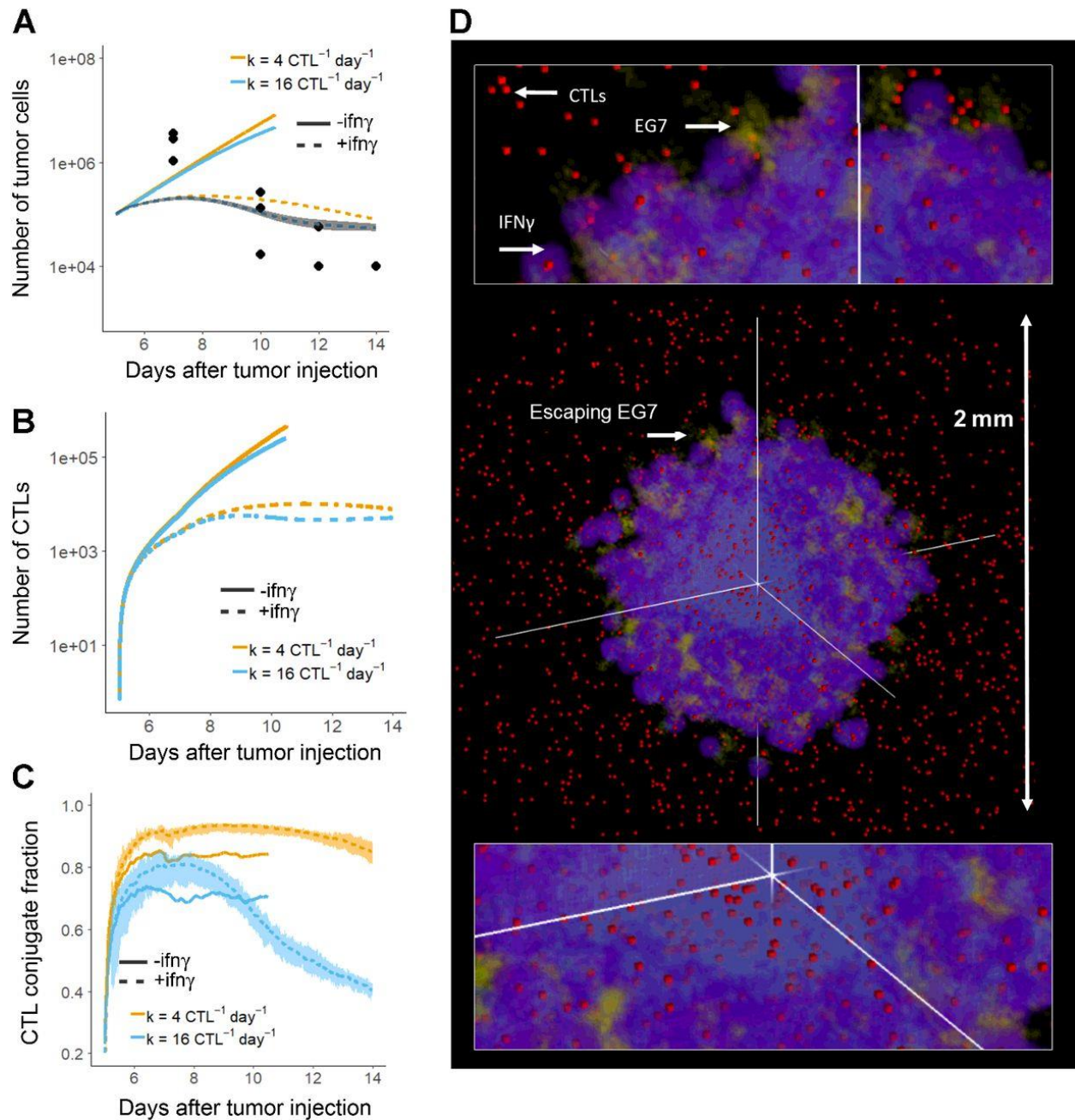


**Figure 3.** Antiproliferative IFN $\gamma$  leads to tumor control. **A)** Simulated tumor volume compared with and without IFN $\gamma$  producing CTLs. **B)** Total CTL numbers in simulations with or without IFN $\gamma$ . **C)** Fraction of CTLs in conjugates in simulations with and without IFN $\gamma$ . **D)** Tumor on day 8, in the presence of IFN $\gamma$ .

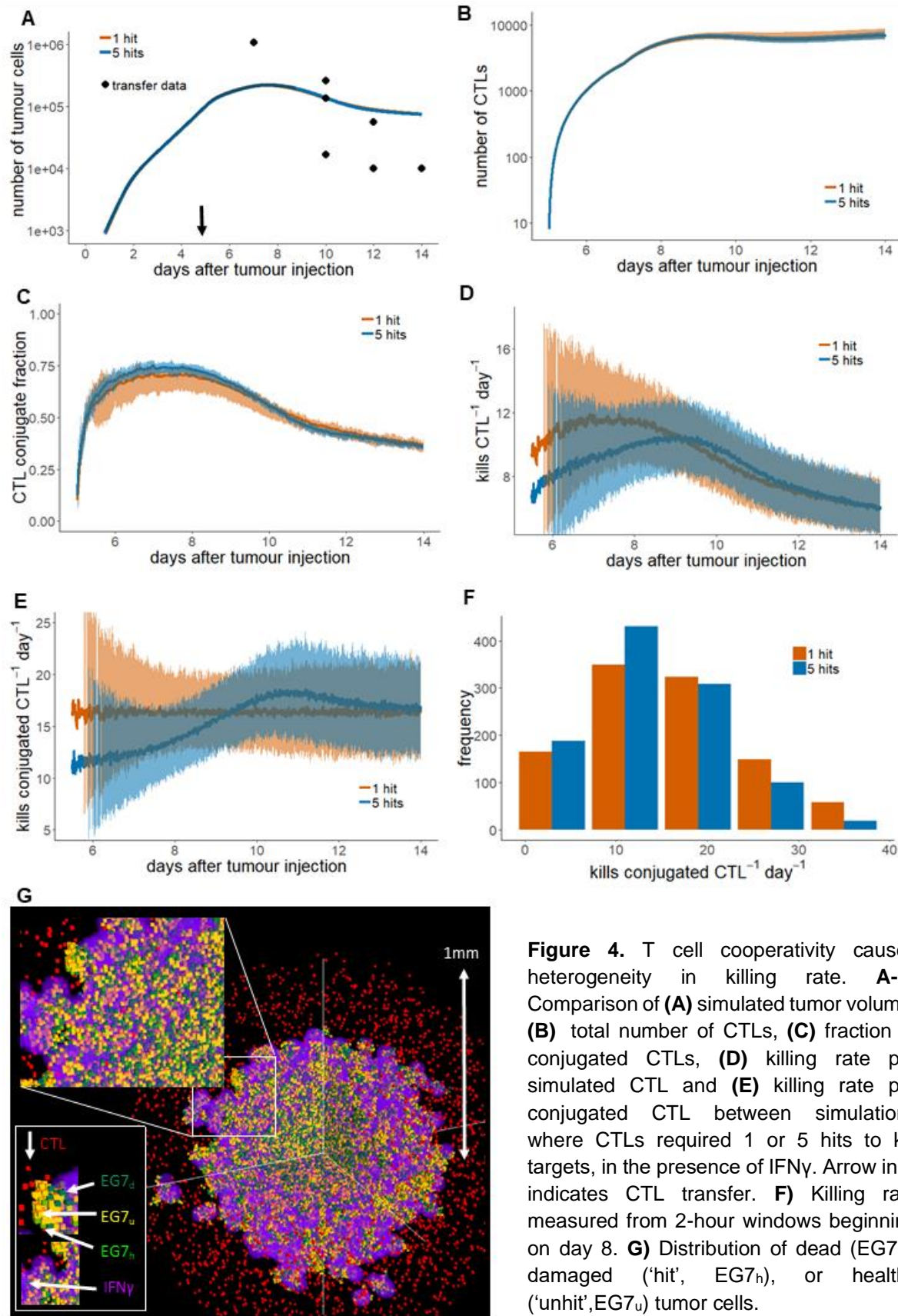


**Figure 4.** T cell cooperativity causes heterogeneity in killing rate. **A-E)** Comparison of **(A)** simulated tumor volume, **(B)** total number of CTLs, **(C)** fraction of conjugated CTLs, **(D)** killing rate per simulated CTL and **(E)** killing rate per conjugated CTL between simulations where CTLs required 1 or 5 hits to kill targets, in the presence of IFN $\gamma$ . Arrow in **A** indicates CTL transfer. **F)** Killing rate measured from 2-hour windows beginning on day 8. **G)** Distribution of dead (EG7<sub>d</sub>), damaged ('hit', EG7<sub>h</sub>), or healthy ('unhit', EG7<sub>u</sub>) tumor cells.

## **Direct killing plus antiproliferative IFN $\gamma$ accounts for selective elimination of antigen positive cells**

Breart *et al.*[18] noted that in mixed EL4/EG7 tumors, the non-cognate antigen expressing tumor cells (EL4) grew more or less unconstrained and it is unclear whether the antiproliferative effect of IFN $\gamma$  is consistent with this finding. We therefore simulated mixed tumors, containing patches of antigen positive EG7 cells or antigen negative EL4 cells. EL4 cells were considered not to be recognized and thus not affected by direct interactions with CTLs, but could be affected by IFN $\gamma$  that diffused from nearby locations. When initialised with a 50% mixture of EL4/EG7 cells, our simulated tumors form patches with similar spatial dimensions to the images from Breart *et al.* (Fig. 5A). We simulated the transfer of CTLs into the mixed tumor model, upon which CTLs preferentially accumulated in regions of Ova-expressing EG7 cells where they began killing these cells and secreting IFN $\gamma$  (Fig. 5B, Video S3). IFN $\gamma$  concentrations were generally higher in regions of EG7 cells compared to regions of EL4 cells, yet despite the limited ( $\sim 30\text{ }\mu\text{m}$ ) range of IFN $\gamma$  diffusion in our model many EL4 cells were prevented from replicating for a period of approximately 2 days, when the activity of the CTLs was greatest (Fig. 5C). By day 10 most EG7 cells were eliminated, and the CTLs, being deprived of stimulation, stopped producing IFN $\gamma$ . After this point EL4 cells resumed growth, eventually filling the spaces left behind by the dead EG7 cells. EL4 cells were thus not so much affected by the presence of the CTLs. In conclusion, local production of anti-proliferative IFN $\gamma$  is consistent with the experimental observation that within mixed tumors primarily cognate-antigen expressing cells were cleared by CTLs.



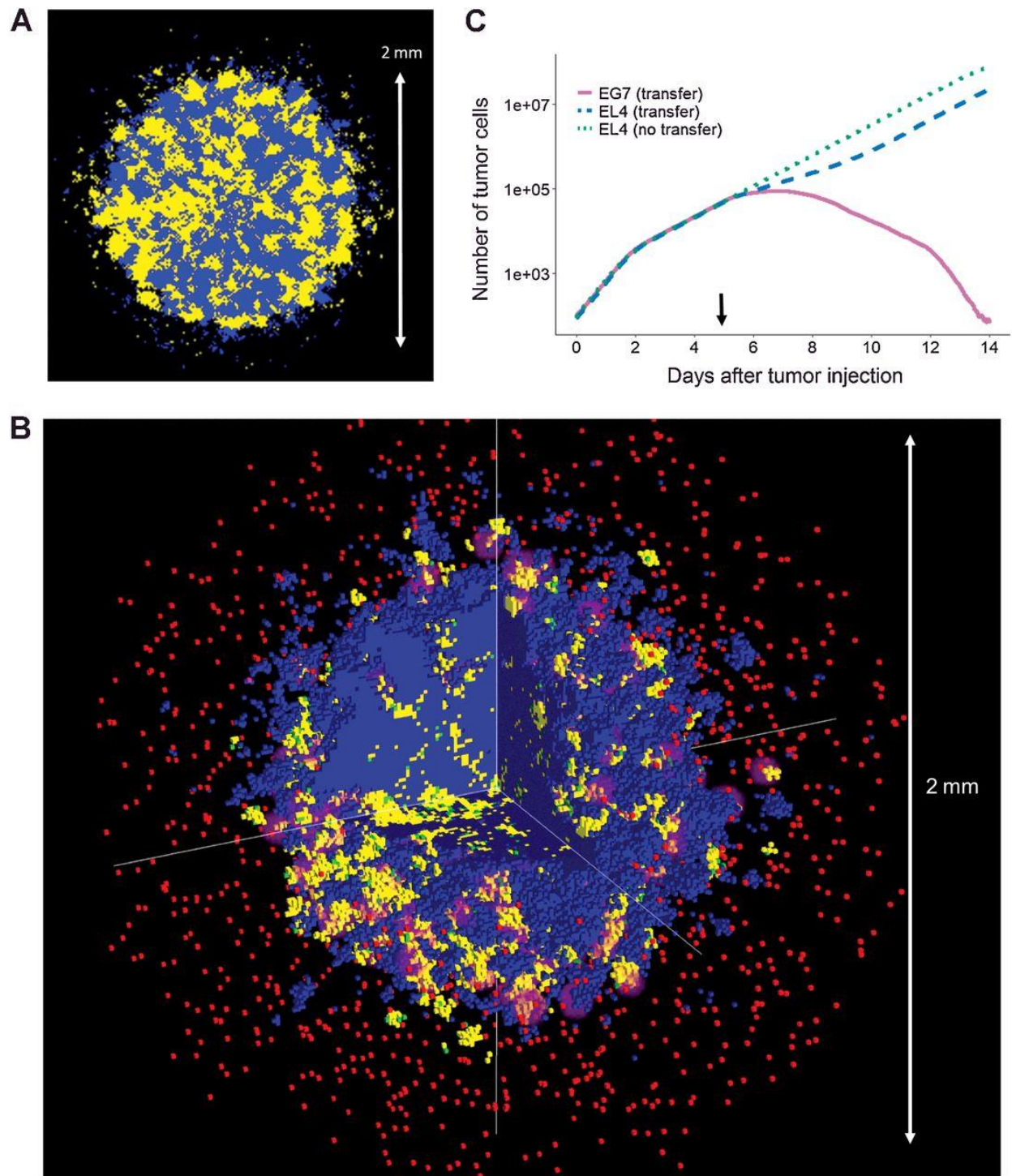


**Figure 5.** Antiproliferative IFN $\gamma$  explains selective destruction of EG7 cells within EG7/EL4 mixed tumors. **A)** Example 2D slice from the centre of a simulated mixed tumor 8 days after tumor inception. **B)** Images showing examples of tumor composition (T cells in red, EG7 cells in yellow, EL4 cells in blue and IFN $\gamma$  concentrations in purple) on day 8 during the course of EG7 regression. **C)** Evolution of the total volume of EG7 or EL4 cells in mixed tumor simulations. Arrow indicates time of CTL transfer.

## Discussion

Immunotherapies involving CTLs are able to mediate regression or tumor control in cancers that were previously out of reach for conventional treatments. Despite major progress, many patients fail to respond, and the mechanistic insight required to explain this disparity in outcomes is lacking. Lysis of infected or malignant cells following direct physical contact is the canonical CTL effector function, but indirect effects of CTLs such as production of cytokines are increasingly recognised as having an important role in CTL mediated tumor regression[21,22,25,45]. The relative importance of these different mechanisms remains unclear and is likely to depend on characteristics of both the tumor and the T cells involved. Here we developed an ABM and an ODE model of tumor regression following adoptive transfer of a population of CTLs attacking EL4/EG7 tumor cells. Using these models, we attempted to quantify the relative contribution of direct CTL killing towards tumor regression in the EL4/EG7 model. Our simulated tumors were not controlled by direct CTL killing only, so we conclude that direct killing was not a sufficient explanation for regression in the EL4 tumor model.

In our ABM we also included simulation of an antiproliferative effect of IFN $\gamma$ , because Hollenbaugh et. al.[21] observed that IFN $\gamma$  deficient T cells display substantially reduced tumor controlling abilities. We modelled an antiproliferative effect because the tumor cells were only observed to die after CTL contact, evidence against a substantial long distance cytotoxic effect of IFN $\gamma$  in this *in vivo* setting. IFN $\gamma$  secreted by CTLs has been shown to contribute to regression in a different tumor model[22], by arresting the cell cycle of tumor cells. Although IFN $\gamma$  has no direct antiproliferative effect on EL4 cells *in vitro*[22] it has been shown that nitric oxide (NO) is secreted by stromal cells after exposure to IFN $\gamma$ [21]. Such NO reduces proliferation of EL4 cells *in vitro*[21], and thereby provides a possible mechanism for the growth inhibition included in our model. Note that we incorporated a direct effect of IFN $\gamma$  on tumor proliferation rather than explicitly including this potential cascade of events, because detailed quantitative measurements on these mechanisms are currently lacking.

Although the antiproliferative effect of IFN $\gamma$  may be an important contributor to tumor control, IFN $\gamma$  may have had other effects which we did not take into account. First, although we were able to explain regression without a substantial cytotoxic effect of IFN $\gamma$ , we cannot exclude that possibility. Since such an effect does not act specifically towards tumor cells presenting cognate antigen it may be an important mechanism to control antigen loss variants, which might otherwise allow tumors to recur. Second, IFN $\gamma$  may induce immuno-tolerance leading to decreased CTL effector function[46]. Third, it has been speculated that IFN $\gamma$  aids in control of tumors by recruitment of innate effector cells[24], or destruction of tumor vasculature[45]. Our model included neither of these effects because they were not apparent in the experiments we based our model on. However, it is possible that these events happened at a later time, after observations of CTL killing were made. This further underlines that measurements are required throughout the entire course of tumor rejection, in order to gain a full understanding of the sequence of events that occurs.

Apart from the role that IFN $\gamma$  may play in tumor control, our modeling has also highlighted a potential explanation for temporal variation in measured killing rates of CTLs. Tumor cells may be able to endure multiple attacks from CTLs before apoptosis is triggered[19,44]. When we implemented such variability in our model, we indeed found an increase in killing rate over the course of tumor regression. This dependence of killing rate upon measurement time is in agreement with our previous modelling work[36] on T cell-target cell interactions.

A criticism of our approach could be that our simulations do not capture all the myriad complex interactions within the tumor microenvironment. Indeed, our models are a highly idealised representation of reality, since they contain only the mechanisms we explicitly chose to include. This would likely be a problem if using the model as a fully predictive tool for other settings, since the model predictions will not be valid in tumors where unincluded mechanisms are important. However, when applying the model as a diagnostic tool (as we have here), model simplicity is a major advantage. This approach allowed us to quantitatively test whether observations made at the cellular level could explain emergent behaviour of the tumor as a whole, without the interference of confounding variables.

Our work highlights the need for further investigation of indirect effects mediated by CTLs in an anti-tumor immune response. Although many mechanisms utilised by CTLs to control tumors have been identified, quantitative measurements detailing their contribution to regression are scarce. Such quantitative understanding would enable a more sophisticated and systems based understanding of the interplay of various mechanisms in tumor regression following immunotherapy - and likely enable better targeted interventions. Future studies should therefore aim to characterise the potential contribution of various mechanisms to tumor regression. Computational models that integrate *in vitro* and *in vivo* experiments, such as those developed here and as developed by others[47–49], can be a valuable tool to aid in this process.

## Acknowledgements

We would like to thank Beatrice Bréart and Philippe Bousso for providing their previously published data and for useful feedback on our modeling of their data. This work is supported by a Vidi grant from the Netherlands Organisation for Scientific Research (NWO; grant 864.12.013 to J.B.B.).

## References

1. Jardim DL, de Melo Gagliato D, Giles FJ, Kurzrock R. Analysis of Drug Development Paradigms for Immune Checkpoint Inhibitors. *Clin Cancer Res.* 2018;24: 1785–1794.
2. Yip A, Webster RM. The market for chimeric antigen receptor T cell therapies. *Nat Rev Drug Discov.* 2018;17: 161–162.
3. Besser MJ, Shapira-Frommer R, Treves AJ, Zippel D, Itzhaki O, Hershkovitz L, et al. Clinical responses in a phase II study using adoptive transfer of short-term cultured tumor infiltration lymphocytes in metastatic melanoma patients. *Clin Cancer Res.* 2010;16: 2646–2655.

4. Rosenberg SA, Yang JC, Sherry RM, Kammula US, Hughes MS, Phan GQ, et al. Durable complete responses in heavily pretreated patients with metastatic melanoma using T-cell transfer immunotherapy. *Clin Cancer Res*. 2011;17: 4550–4557.
5. Chandran SS, Somerville RPT, Yang JC, Sherry RM, Klebanoff CA, Goff SL, et al. Treatment of metastatic uveal melanoma with adoptive transfer of tumour-infiltrating lymphocytes: a single-centre, two-stage, single-arm, phase 2 study. *Lancet Oncol*. 2017;18: 792–802.
6. Feng K, Guo Y, Dai H, Wang Y, Li X, Jia H, et al. Chimeric antigen receptor-modified T cells for the immunotherapy of patients with EGFR-expressing advanced relapsed/refractory non-small cell lung cancer. *Sci China Life Sci*. 2016;59: 468–479.
7. Louis CU, Savoldo B, Dotti G, Pule M, Yvon E, Myers GD, et al. Antitumor activity and long-term fate of chimeric antigen receptor-positive T cells in patients with neuroblastoma. *Blood*. 2011;118: 6050–6056.
8. Ahmed N, Brawley VS, Hegde M, Robertson C, Ghazi A, Gerken C, et al. Human Epidermal Growth Factor Receptor 2 (HER2) -Specific Chimeric Antigen Receptor-Modified T Cells for the Immunotherapy of HER2-Positive Sarcoma. *J Clin Oncol*. 2015;33: 1688–1696.
9. Larkin J, Chiarion-Sileni V, Gonzalez R, Grob JJ, Cowey CL, Lao CD, et al. Combined Nivolumab and Ipilimumab or Monotherapy in Untreated Melanoma. *N Engl J Med*. 2015;373: 23–34.
10. Swart M, Verbrugge I, Beltman JB. Combination Approaches with Immune-Checkpoint Blockade in Cancer Therapy. *Front Oncol*. 2016;6: 233.
11. Pfirschke C, Engblom C, Rickelt S, Cortez-Retamozo V, Garriss C, Pucci F, et al. Immunogenic Chemotherapy Sensitizes Tumors to Checkpoint Blockade Therapy. *Immunity*. 2016;44: 343–354.
12. Weichselbaum RR, Liang H, Deng L, Fu Y-X. Radiotherapy and immunotherapy: a beneficial liaison? *Nat Rev Clin Oncol*. 2017;14: 365–379.
13. Isaacs S, Baetz K, Olsen K, Podack E, Griffiths GM. Serial killing by cytotoxic T lymphocytes: T cell receptor triggers degranulation, re-filling of the lytic granules and secretion of lytic proteins via a non-granule pathway. *Eur J Immunol*. 1995;25: 1071–1079.
14. Wiedemann A, Depoil D, Faroudi M, Valitutti S. Cytotoxic T lymphocytes kill multiple targets simultaneously via spatiotemporal uncoupling of lytic and stimulatory synapses. *Proc Natl Acad Sci U S A*. 2006;103: 10985–10990.
15. Kägi D, Ledermann B, Bürki K, Seiler P, Odermatt B, Olsen KJ, et al. Cytotoxicity mediated by T cells and natural killer cells is greatly impaired in perforin-deficient mice. *Nature*. 1994;369: 31–37.

16. Smyth MJ, Kershaw MH, Darcy PK, Trapani JA. Adoptive transfer: the role of perforin in mouse cytotoxic T lymphocyte rejection of human tumor xenografts in vivo. *Xenotransplantation*. 1998;5: 146–153.
17. Caldwell SA, Ryan MH, McDuffie E, Abrams SI. The Fas/Fas ligand pathway is important for optimal tumor regression in a mouse model of CTL adoptive immunotherapy of experimental CMS4 lung metastases. *J Immunol*. 2003;171: 2402–2412.
18. Breart B, Lemaître F, Celli S, Bousso P. Two-photon imaging of intratumoral CD8+ T cell cytotoxic activity during adoptive T cell therapy in mice. *J Clin Invest*. 2008;118: 1390–1397.
19. Halle S, Keyser KA, Stahl FR, Busche A, Marquardt A, Zheng X, et al. In Vivo Killing Capacity of Cytotoxic T Cells Is Limited and Involves Dynamic Interactions and T Cell Cooperativity. *Immunity*. 2016;44: 233–245.
20. Barth RJ Jr, Mulé JJ, Spiess PJ, Rosenberg SA. Interferon gamma and tumor necrosis factor have a role in tumor regressions mediated by murine CD8+ tumor-infiltrating lymphocytes. *J Exp Med*. 1991;173: 647–658.
21. Hollenbaugh JA, Dutton RW. IFN- $\gamma$  Regulates Donor CD8 T Cell Expansion, Migration, and Leads to Apoptosis of Cells of a Solid Tumor. *The Journal of Immunology*. 2006;177: 3004–3011.
22. Matsushita H, Hosoi A, Ueha S, Abe J, Fujieda N, Tomura M, et al. Cytotoxic T lymphocytes block tumor growth both by lytic activity and IFN $\gamma$ -dependent cell-cycle arrest. *Cancer Immunol Res*. 2015;3: 26–36.
23. Selleck WA, Canfield SE, Hassen WA, Meseck M, Kuzmin AI, Eisensmith RC, et al. IFN-gamma sensitization of prostate cancer cells to Fas-mediated death: a gene therapy approach. *Mol Ther*. 2003;7: 185–192.
24. Nagoshi M, Sadanaga N, Joo HG, Goedegebuure PS, Eberlein TJ. Tumor-specific cytokine release by donor T cells induces an effective host anti-tumor response through recruitment of host naive antigen presenting cells. *Int J Cancer*. 1999;80: 308–314.
25. Briesemeister D, Sommermeyer D, Loddenkemper C, Loew R, Uckert W, Blankenstein T, et al. Tumor rejection by local interferon gamma induction in established tumors is associated with blood vessel destruction and necrosis. *Int J Cancer*. 2011;128: 371–378.
26. Nguyen HH, Kim T, Song SY, Park S, Cho HH, Jung S-H, et al. Naïve CD8(+) T cell derived tumor-specific cytotoxic effectors as a potential remedy for overcoming TGF- $\beta$  immunosuppression in the tumor microenvironment. *Sci Rep*. 2016;6: 28208.
27. Mikucki ME, Fisher DT, Matsuzaki J, Skitzki JJ, Gaulin NB, Muhitch JB, et al. Non-redundant requirement for CXCR3 signalling during tumoricidal T-cell trafficking across tumour vascular checkpoints. *Nat Commun*. 2015;6: 7458.



28. Yao Y, Chen S, Cao M, Fan X, Yang T, Huang Y, et al. Antigen-specific CD8<sup>+</sup> T cell feedback activates NLRP3 inflammasome in antigen-presenting cells through perforin. *Nat Commun.* 2017;8: 15402.
29. Boissonnas A, Fetler L, Zeelenberg IS, Hugues S, Amigorena S. In vivo imaging of cytotoxic T cell infiltration and elimination of a solid tumor. *J Exp Med.* 2007;204: 345–356.
30. Hollenbaugh JA, Reome J, Dobrzanski M, Dutton RW. The rate of the CD8-dependent initial reduction in tumor volume is not limited by contact-dependent perforin, Fas ligand, or TNF-mediated cytotoxicity. *J Immunol.* 2004;173: 1738–1743.
31. Steinert EM, Schenkel JM, Fraser KA, Beura LK, Manlove LS, Igyártó BZ, et al. Quantifying Memory CD8 T Cells Reveals Regionalization of Immunosurveillance. *Cell.* 2015;161: 737–749.
32. Parnai R, Raff MC, Scholes J. Differences between the clearance of apoptotic cells by professional and non-professional phagocytes. *Curr Biol.* 2000;10: 857–860.
33. Hirano K, Hosoi A, Matsushita H, Iino T, Ueha S, Matsushima K, et al. The nitric oxide radical scavenger carboxy-PTIO reduces the immunosuppressive activity of myeloid-derived suppressor cells and potentiates the antitumor activity of adoptive cytotoxic T lymphocyte immunotherapy. *Oncoimmunology.* 2015;4: e1019195.
34. Pauken KE, Wherry EJ. Overcoming T cell exhaustion in infection and cancer. *Trends Immunol.* 2015;36: 265–276.
35. Gadhamsetty S, Marée AFM, Beltman JB, de Boer RJ. A general functional response of cytotoxic T lymphocyte-mediated killing of target cells. *Biophys J.* 2014;106: 1780–1791.
36. Gadhamsetty S, Marée AFM, Beltman JB, de Boer RJ. A Sigmoid Functional Response Emerges When Cytotoxic T Lymphocytes Start Killing Fresh Target Cells. *Biophys J.* 2017;112: 1221–1235.
37. Waclaw B, Bozic I, Pittman ME, Hruban RH, Vogelstein B, Nowak MA. A spatial model predicts that dispersal and cell turnover limit intratumour heterogeneity. *Nature.* 2015;525: 261–264.
38. Beltman JB, Marée AFM, Lynch JN, Miller MJ, de Boer RJ. Lymph node topology dictates T cell migration behavior. *J Exp Med.* 2007;204: 771–780.
39. Ariotti S, Beltman JB, Chodaczek G, Hoekstra ME, van Beek AE, Gomez-Eerland R, et al. Tissue-resident memory CD8<sup>+</sup> T cells continuously patrol skin epithelia to quickly recognize local antigen. *Proc Natl Acad Sci U S A.* 2012;109: 19739–19744.
40. Halle S, Halle O, Förster R. Mechanisms and Dynamics of T Cell-Mediated Cytotoxicity In Vivo. *Trends Immunol.* 2017;38: 432–443.

41. Matsushita H, Hosoi A, Ueha S, Abe J, Fujieda N. Cytotoxic T lymphocytes block tumor growth both by lytic activity and IFN $\gamma$ -dependent cell-cycle arrest. *Cancer Immunol. Res.* 3, 26–36. doi: 10.1158/2326 .... 2015.
42. Blohm U, Potthoff D, van der Kogel AJ, Pircher H. Solid tumors “melt” from the inside after successful CD8 T cell attack. *Eur J Immunol.* 2006;36: 468–477.
43. Thomas DA, Massagué J. TGF-beta directly targets cytotoxic T cell functions during tumor evasion of immune surveillance. *Cancer Cell.* 2005;8: 369–380.
44. Caramalho I, Faroudi M, Padovan E, Müller S, Valitutti S. Visualizing CTL/melanoma cell interactions: multiple hits must be delivered for tumour cell annihilation. *J Cell Mol Med.* 2009;13: 3834–3846.
45. Schietinger A, Arina A, Liu RB, Wells S, Huang J, Engels B, et al. Longitudinal confocal microscopy imaging of solid tumor destruction following adoptive T cell transfer. *Oncoimmunology.* 2013;2: e26677.
46. Benci JL, Xu B, Qiu Y, Wu TJ, Dada H, Twyman-Saint Victor C, et al. Tumor Interferon Signaling Regulates a Multigenic Resistance Program to Immune Checkpoint Blockade. *Cell.* 2016;167: 1540–1554.e12.
47. Gong C, Milberg O, Wang B, Vicini P, Narwal R, Roskos L, et al. A computational multiscale agent-based model for simulating spatio-temporal tumour immune response to PD1 and PDL1 inhibition. *J R Soc Interface.* 2017;14. doi:10.1098/rsif.2017.0320
48. Byrne HM. Dissecting cancer through mathematics: from the cell to the animal model. *Nat Rev Cancer.* 2010;10: 221–230.
49. Kather JN, Poleszczuk J, Suarez-Carmona M, Krisam J, Charoentong P, Valous NA, et al. In Silico Modeling of Immunotherapy and Stroma-Targeting Therapies in Human Colorectal Cancer. *Cancer Res.* 2017;77: 6442–6452.

**Table 1:** Overview of parameters used in models, what they represent, and their default value. Parameters apply to ABM and ODE model unless indicated otherwise. Parameter values are based on data in Breart *et al.*[18] unless indicated otherwise.

Parameter	Description	Default value
T0	Number of tumor cells at time 0	1450 (ODE) 180 (ABM)
E0	Number of CTLs at time 0	0
D0	Number of killed tumor cells at time 0	0
k	CTL killing rate	4 kills CTL <sup>-1</sup> day <sup>-1</sup>
g	Tumor growth rate	0.86 day <sup>-1</sup> (ODE) 1.97 day <sup>-1</sup> (ABM)
d <sup>a</sup>	Disappearance rate of killed tumor cells	2 day <sup>-1</sup>
p <sub>arr</sub>	Probability of conjugate formation	1 (ABM)
n <sub>hit</sub> <sup>b</sup>	Number of hits before tumor cell apoptosis	1 (ABM)
p <sub>det</sub>	Probability of conjugate splitting	0 (ABM)
p <sub>disp</sub>	Probability of tumor cell dispersal	0.03 (ABM)
R <sub>i</sub>	Initial tumor radius	120μm (ABM)

<sup>a</sup> based on Parnaik *et al.*[32]; <sup>b</sup> based on Halle *et al.*[19]

## Supplementary Data

**Video S1.** Growth of ABM tumour from day 0 to day 5. EG7 cells that have no available space to divide are indicated in green (others in yellow).

**Video S2.** CTLs (red) producing IFN $\gamma$  (purple), which prevents proliferation of EG7 cells (yellow). Video shows day 8, where almost all cells in the tumour centre are affected by IFN $\gamma$ , but isolated peripheral pockets are escaping.

**Video S3.** CTLs (red) producing IFN $\gamma$  (purple) when conjugated with EG7 cells (yellow) but not when conjugated with EL4 cells (blue), in mixed tumours on day 8. IFN $\gamma$  prevents both tumour cell types from dividing. Note that CTLs congregate in EG7 patches and many EL4 cells remain unaffected.

**Supplementary Methods.** Additional details of our modeling approach with respect to the killing term employed in the ODE model and IFN $\gamma$  production and diffusion in the ABM.

Supplementary Methods and Videos S1-S3 are available online (<https://doi.org/10.1158/0008-5472.CAN-18-3147>).

# **Chapter 4**

## **CD137-stimulated cytotoxic T lymphocytes exert superior tumour control due to an enhanced antimitotic effect on tumour cells**

**Richard J Beck<sup>1</sup>, Bettina Weigelin<sup>2</sup>, Joost B Beltman<sup>1</sup>**

- 1. Division of Drug Discovery and Safety, Leiden Academic Centre for Drug Research, Leiden University, Leiden, The Netherlands**
- 2. Department of Preclinical Imaging and Radiopharmacy, Eberhard Karls University of Tübingen, Germany**

*Cancers (in press)*

### **Abstract**

Several immunotherapeutic strategies for the treatment of cancer are under development. Two prominent strategies are adoptive cell transfer (ACT) of cytotoxic T lymphocytes (CTLs) and modulation of CTL function with immune checkpoint inhibitors or with costimulatory antibodies. Despite some success with these approaches, there remains a lack of detailed and quantitative descriptions of the events following CTL transfer and the impact of immunomodulation.

Here, we have applied ordinary differential equation models to two photon imaging data derived from a B16F10 murine melanoma. Models were parameterised with data from two different treatment conditions: either ACT-only, or ACT with intratumoural costimulation using a CD137 targeted antibody. Model dynamics and best fitting parameters were compared, in order to assess the mode of action of the CTLs and examine how the CD137 antibody influenced their activities.

We found that the cytolytic activity of the transferred CTLs was minimal without CD137 costimulation, and that the CD137 targeted antibody did not enhance the per-capita killing ability of the transferred CTLs. Instead, the results of our modelling study suggest that an antiproliferative effect of CTLs exerted upon the tumour likely accounted for the majority of the

reduction in tumour growth after CTL transfer. We found that CD137 most likely improved tumour control via enhancement of this antiproliferative effect, as well as prolonging the period in which CTLs were inside the tumour, leading to a sustained duration of their antitumour effects following CD137 stimulation.

## Introduction

The global immuno-oncology pipeline grew by 67% between 2017-2018 [1]. A substantial component of this growth came from “cell therapies”, defined in the context of immuno-oncology as therapies “that engineer immune cells such as T cells to directly attack cancer cells” [2]. Another significant component of the pipeline were therapies classified as “immunomodulators”, defined as therapies which “act on inhibitory or activating molecules expressed by T cells (...) other immune cells or the tumour immune microenvironment to unleash antitumour immunity” [2]. The rapid growth in this field reflects increasing progress in our ability to engineer Cytotoxic T Lymphocytes (CTLs) with ability to recognise and attack tumour cells, then modulate that response via therapeutic targeting of various “checkpoints”, such as the inhibitory CTLA-4 or PD-1 / PD-L1 signalling axes which are among the best known immunomodulators and have been most successful in the clinic so far [3–5]. Although rapid growth is an indicator that the field of immuno-oncology is promising, due to the burgeoning body of literature it can be difficult to achieve consensus. In that context, mathematical and computational models are a useful tool to aid reuse and integration of previous studies. Such models can be used to integrate data from multiple sources, check their consistency, and identify those mechanisms which are most important for explaining the overall dynamics of the studied system. This systems biology approach can create novel insights into biological phenomena [6–8].

One immunomodulator which has received much recent attention is CD137: in 2017 there were 9 trials with therapies targeting CD137; in 2018 there were 36 [2]. Although several anti-CD137 agonists are under clinical evaluation [9], the mechanisms through which anti-CD137 influences cancer immunotherapy remain under debate [10,11]. CD137 is a costimulatory molecule classified as a member of the Tumour Necrosis Factor Receptor superfamily, which is expressed on both innate and adaptive immune cells. Targeting the CD137 signalling domain has been linked to a gain of effector functions in CD8<sup>+</sup> T cells including enhanced proliferation and resistance to apoptosis [12–14]. A recent study examined Cytotoxic T Lymphocyte (CTL) functions in a B16F10 OVA expressing mouse melanoma, in combination with anti-CD137 agonist antibody administered intraperitoneally [13]. OT1 CTLs were adoptively transferred to tumour bearing mice in both the presence and absence of anti-CD137, after which tumour volume progression was recorded and the activities of tumour infiltrating CTLs were observed by means of intravital two-photon microscopy. In that study, anti-CD137 treated mice differed from control mice in the following respects: 1) Tumour bearing mice treated with adoptively transferred CTLs plus anti-CD137 (ACT+mAb) showed improved tumour control compared to counterparts treated with CTL but no antibody (ACT-only). 2) Flow cytometry analysis of cell suspensions retrieved from tumours revealed that CTLs from ACT+mAb tumours expressed greater levels of markers associated with the effector phenotype than did those recovered from tumours treated with ACT-only. 3) Intravital images gave evidence for altered CTL functioning in vivo after anti-CD137

treatment. Mitosis and apoptosis rates of both tumour and CTLs were affected, as was the migration behaviour of the CTLs. Taken together these findings support the idea that anti-CD137 together with adoptive CTL transfer improves the outcome of ACT. The suggestion was also that anti-CD137 treatment boosts the effector functions of CTLs *in vivo*, since anti-CD137 treatment both increased apoptosis and reduced proliferation of tumour cells compared to control. However, there was no quantification of the various effects of anti-CD137 upon CTL-mediated tumour control, so it remains unclear which enhancements to CTL effector function played the most substantial role in the improved tumour control after anti-CD137 treatment.

We previously quantified the effect of CTLs on solid tumours, considering both cytotoxicity through direct cellular interactions [6,15] and production of cytokines which inhibit tumour cell proliferation (e.g., IFN $\gamma$ ) as potential agents by which CTLs could control tumours [6]. We here provide a re-assessment of the *in vivo* melanoma data summarised above, aided by computational models. The goal was to develop a quantitative picture of the functioning of adoptively transferred CTLs *in vivo*, and of the effect that costimulatory anti-CD137 treatment had upon their functioning. Specifically, we aimed to determine the extent to which an antiproliferative effect contributed to tumour control, compared to direct cytotoxicity. We also asked whether the improvement in tumour control after anti-CD137 treatment was due to a numeric increase in CTLs, or due to a difference in CTL performance. To answer these questions, we developed an ordinary differential equation (ODE) model to describe the dynamical evolution of CTL treated tumours. We fit the ODE model to the *in-vivo* data, and examined how the model parameters differed in the presence or absence of anti-CD137. We did not find any evidence that the ability of CTLs to kill tumour cells was improved in the ACT+mAb group relative to ACT only, when killing was considered on a per-capita basis. Moreover, in both ACT-only and ACT+mAb conditions, an antiproliferative effect associated with transferred CTLs explained a far larger share of the reduction in tumour progression than did CTL cytotoxicity towards tumour cells. Finally, an increased antiproliferative effect associated with anti-CD137 treatment, together with a more sustained presence of CTLs within the tumour after anti-CD137 treatment, could explain the reduced tumour progression in our data.

## Results

### Population dynamics of tumour cells and infiltrating CTLs

In this work our aim was to integrate dynamic two-photon imaging and volumetric tumour progression data [13], to create a systems-based description of a murine melanoma after ACT. To understand the expansion and retraction of CTL populations in the tumour during therapy and in relation to local tumour response, we first plotted apoptosis against mitosis rates of tumour cells (Fig.1A) and of CTLs (Fig.1B), both stratified by mouse (Fig. 1A-B, shapes) and by the day of measurement (Fig. 1A-B, colours). Apoptosis and mitosis events were derived from 2 hour time-lapse sequences, allowing accurate calculation of net cell proliferation or regression rates. Each plot splits into two regions: net population growth when mitosis exceeded apoptosis (Fig. 1A-B, above dashed lines) and net population reduction otherwise (Fig. 1A-B, below dashed lines). There was net growth of tumour cells in all except one measured position with ACT only (Fig. 1A,

left panel), whereas with ACT+mAb this was true for only half of the measured positions (Fig. 1A, right panel). In contrast to tumour cells which were mostly proliferating, CTL apoptosis matched or exceeded mitosis in almost all measured positions (Fig. 1B), suggesting that transferred CTL populations were only able to sustain their numbers, but were not “expanding” inside the tumour. Nevertheless, we observed much higher absolute rates of apoptosis or mitosis for CTLs compared to tumour cells (compare axes values between Figs. 1A-B), suggesting that there is more potential for rapid changes in the number of CTLs compared to tumour cells inside the tumour if CTL apoptosis could be reduced relative to mitosis.

Besides mitosis and apoptosis rates (Fig. 1A-B), the intravital dataset also consists of the total numbers of each cell type which are represented by point size in separate plots for tumour cells (Fig. 1C) or CTLs (Fig. 1D). Considering the data per-mouse (Fig. 1A-B, shapes or C-D, colors), it is apparent that all measurements from the same day pertaining to a given tumour are clustered (valid for both CTLs and tumour cells). Similar measurements at different sites within one tumour indicated that tumours were spatially relatively homogeneous, at least for the peripheral areas that were imaged in the study. However, the fact that the clusters travel over time indicates that conditions inside the tumours were not temporally homogeneous. Comparing tumour cells between ACT-only and ACT+mAb (Fig. 1A,C; columns), the population dynamics appear most different in two of the mice, both corresponding to the ACT+mAb group (m65 d6&d9, m49 d6). Measurements from those mice occur in the region of the plot below the red dashed line where local tumour regression is apparent, which was barely reached in any ACT-only mouse. Interestingly, the mitosis rates of tumour cells in the ACT-only group decrease between days 6-9, yet over the same time interval TC mitosis rates in the ACT+mAb group increase (Fig. 1E). This result suggests that tumours were recovering proliferative capacity after ACT+mAb treatment faster than the ACT-only treated group, seemingly at odds with the more sustained CTL activity previously reported [13]. Similarly, there was a more sustained replacement of the CTL population in the ACT+mAb group compared to the ACT-only group (Fig. 1B and 1F, solid lines in right panels remain parallel to the dashed line), which was due mainly to an increase in mitosis rather than to a decrease in apoptosis. Overall, these results indicate that the ACT+mAb treatment improved tumour control by shifting tumour cell dynamics towards a regime where net apoptosis exceeded mitosis, but it is unclear from these data how CTLs participated in this process.



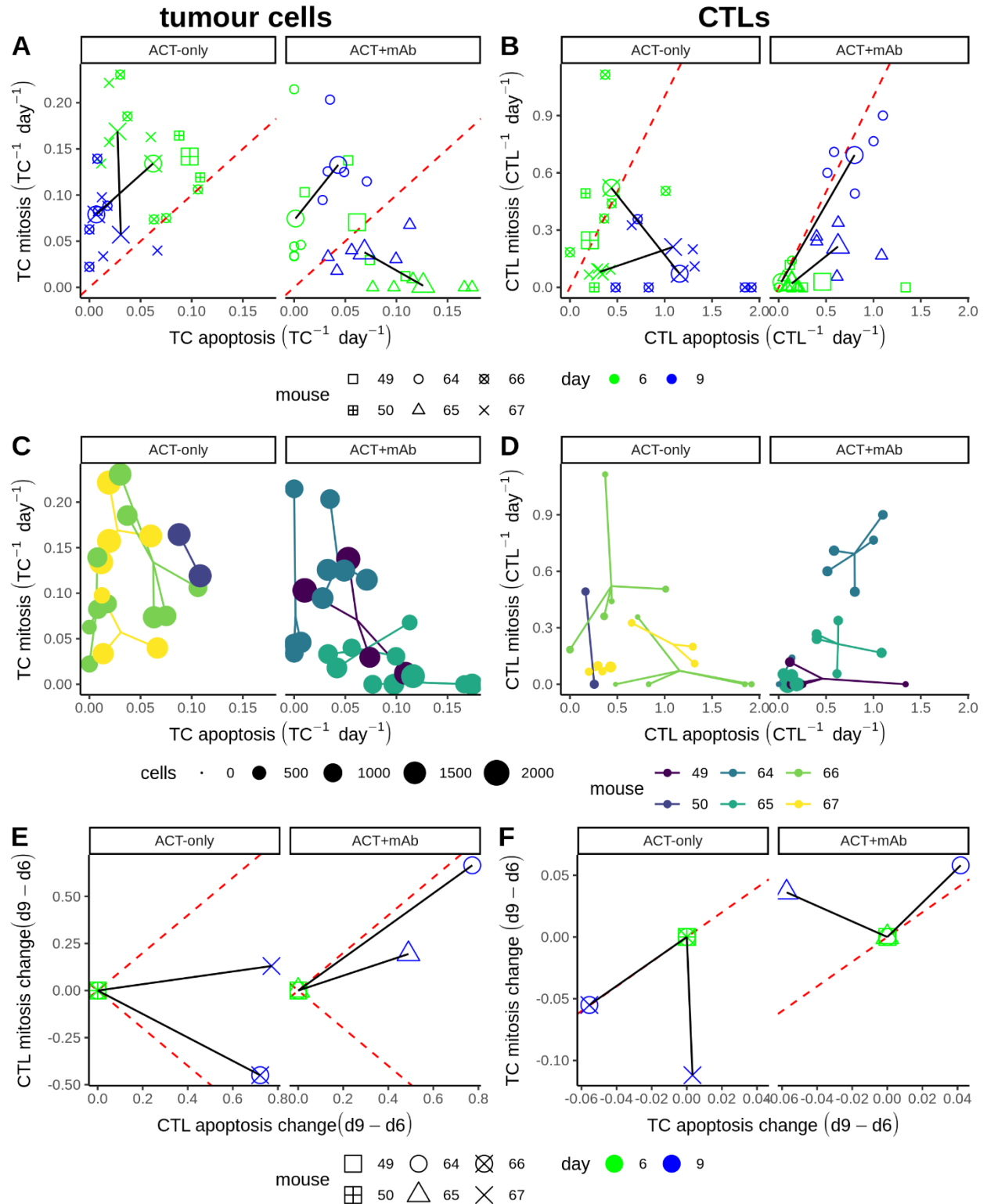


**Figure 1.** Comparison of apoptosis and mitosis rates for tumour cells and CTLs. A-B) Apoptosis and mitosis rates of tumour cells (A) or CTLs (B) with or without anti-CD137 (columns). Each small point represents two simultaneous apoptosis (x-axis) and mitosis (y-axis) rates measured at one site within a tumour. Points are coloured based on the day of measurement, and different mice are indicated by shape. Large points

are the mean values per position/day; these are connected by solid black lines for cases where we have intravital measurements on both days 6 and 9 from the same mouse. The red dashed line marks net zero population growth. C-D) Apoptosis and mitosis rates of tumour cells (C) or CTLs (D) where point size indicates the total number of cells recorded per site. Segments connect all points from the same mouse imaged on the same day. E-F) Change in the apoptosis and mitosis rates of tumour cells (E) or CTLs (F) based on intravital data for two mice per condition (constructed via linear translation of the mean values in A-B such that the day 6 measurement lies at the origin).

## **Impact of CTLs on the population dynamics of tumour cells**

In addition to the intravital statistics, volume progression data for the tumours from the same experiments were also available (Fig. 2A). There were two control conditions: one where ACT was applied on day 3 but tumour cells did not express the cognate OVA antigen for recognition by adoptively transferred CTLs (Fig. 2A, top row left), and another where tumour cells expressed OVA but mice did not receive ACT (Fig. 2A, top row right). In the middle row are the two experiments (corresponding to Fig. 1 intravital data) where ACT was applied 3 days after mice were inoculated with tumours, and in the final row ACT treatment was delayed until day 7 after tumour inoculation. Data points from mice that had not (yet) received ACT are black, whereas points from mice that had received ACT are green. To compare these volumetric data with the intravital dataset we converted the volumetric data for each mouse into growth rates (Fig. 2B), i.e. each point represents the growth rate of a single tumour between successive volume measurements. This conversion ensured that all our data points later used for model fitting would have the same units ( $\text{day}^{-1}$ ). We estimated that the growth rate of the untreated tumours was approximately  $0.5 \text{ day}^{-1}$  (Fig. 2B grey lines; also slope of grey lines in 2A). The impact of the transferred CTLs is clear from the transient decrease in volumetric growth rate observable after ACT (2A-B, green lines 2nd and 3rd rows).

To verify whether the activity of the CTLs observed in the intravital data was consistent with the measurements of tumour progression based on the volumetric data, we considered two possible effects of CTLs on tumours: either killing of tumour cells by CTLs, or prevention of proliferation. In the intravital dataset we studied whether the number of tumour cells per position influenced the killing rate of CTLs, but found no clear evidence that this was the case (S1. Fig). We found that the number of TC apoptosis events per position could be adequately described by a straightforward Poisson model [16], with the intensity of the killing directly proportional to the number of CTLs (Fig. 2C left panel). The correlation between TC mitosis and CTL numbers was less clear, although appeared to be negative since the positions with the most tumour cell mitosis were those with few CTLs (Fig 2C right panel, S2 Fig). Thus, the intravital data suggest the presence of CTLs led to killing of tumour cells and inhibition of their proliferation, which is consistent with the volumetric data. However, it was unclear which of these effects were most important in the control of the tumours.

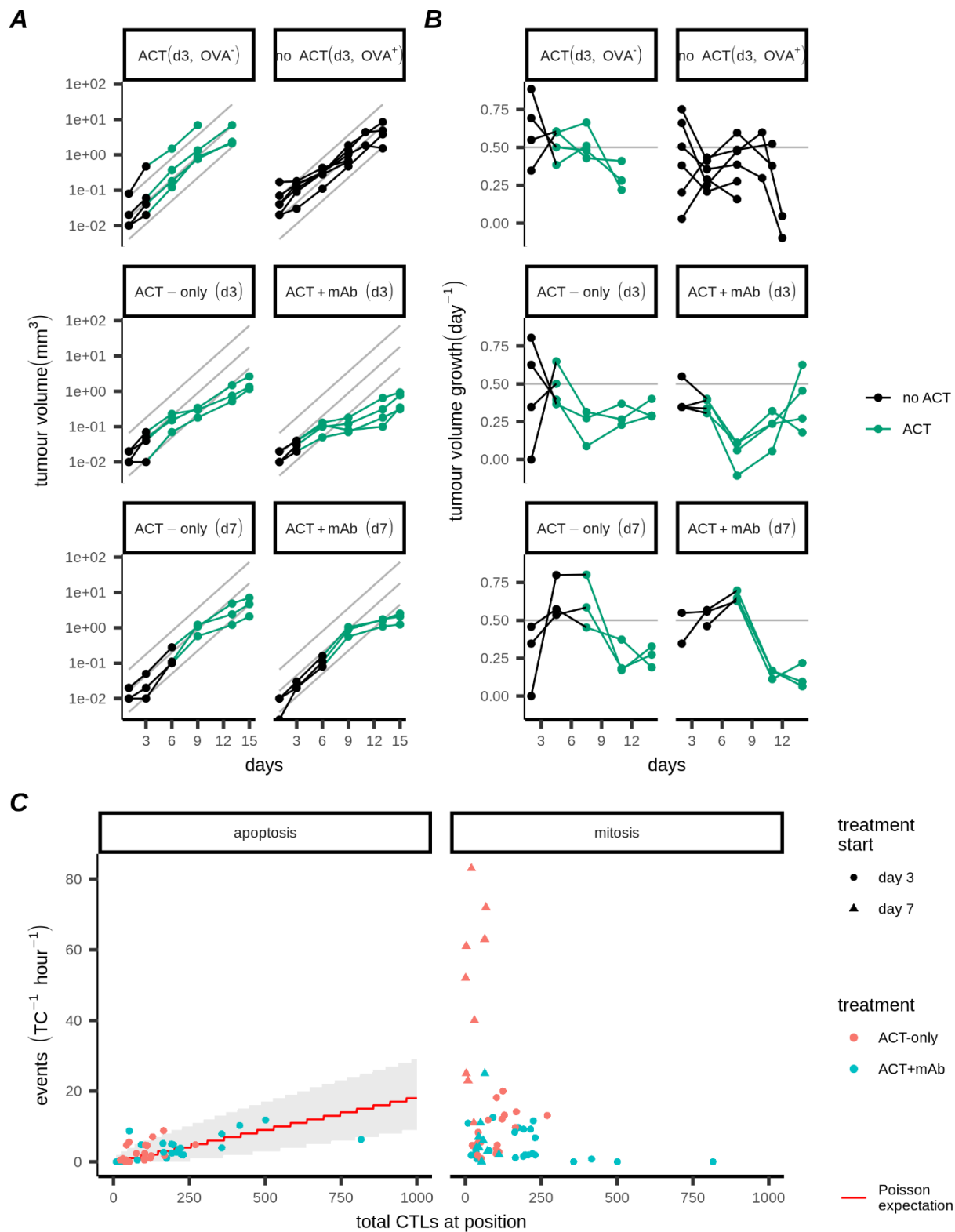


**Figure 2.** Impact of CTLs on the population dynamics of tumour cells. A) Tumour volume measurements over time. Row 1: control tumours, either treated with ACT 3 days after inoculation but not expressing OVA (top left), or OVA expressing tumours not treated with ACT (top right). Rows 2 and 3: OVA expressing

tumours treated with ACT 3 days (row 2) or 7 days (row 3) after inoculation, without anti-CD137 (left) or with anti-CD137 (right). B) Volumetric growth rates of tumours corresponding to (A). Estimates of tumour growth rate are made over the interval between two successive volume measurements. Points representing estimates are displayed at the midpoint of the interval. Treatments for conditions are indicated in facet labels as “day of ACT”. “treatment details”. Points in (A)-(B) are connected with straight lines visualizing the trajectories for individual mice. Points/lines corresponding to mice that had not (yet) received ACT are black, and green indicates that mice have received ACT. C) Relationship between the number of TC apoptosis (left panel) or mitosis (right panel) events vs. number of CTLs per position. The number of events has been normalised ( $\text{hour}^{-1}$ ) to account for differences in imaging time between positions. In the left panel the expected number of kills per hour (red line) and 5-95% confidence interval (shaded region) are shown for a Poisson process where individual CTLs kill at a constant rate ( $0.44 \text{ CTL}^{-1} \text{ day}^{-1}$ ). See also Fig. S2 for day 7 mitosis data.

## Ordinary Differential Equation model CTLs v.s. B16F10 Melanoma

In order to probe the relative contributions of these two effects (antimitotic or killing) we elected to develop an ODE model to combine all the disparate measurements together and check them for internal consistency and with other reports in the literature. The absolute number of tumour cells per field in the imaging data depended strongly on the location of the imaging windows which were sometimes located in the centre of the tumour but other times near the periphery, or contained large features like vessels (Fig. 3A). Therefore we opted to discard the absolute numbers of CTLs and tumour cells, instead using the CTL:TC (Effector:Target, E:T) ratio to develop our ODE model. A further advantage of utilising the dimensionless E:T ratio for fitting is that it prevents the physical size of the imaging windows unduly influencing our results. Our ODE model (Fig. 3B) features CTLs ( $E$ ) either killing tumour cells ( $T$ ) or preventing them from proliferating, which in our model happens via transfer of proliferating ( $T_p$ ) tumour cells into a quiescent state ( $T_q$ ). To describe the population dynamics of CTLs we considered CTLs to infiltrate across the tumour boundary at a constant rate  $s$  per unit area of boundary. Additionally, since CTL mitosis and apoptosis measurements within the tumour were available we included these processes in our model as well via incorporation of two loops. The first loop considered a factor stimulating CTL proliferation (Induction/Interleukin:  $I$ ), whereas the second loop described a tumour resistance factor ( $R$ ). The resistance factor increased over time spent with CTLs inside the tumour and led to an increase in CTL apoptosis (see Methods).

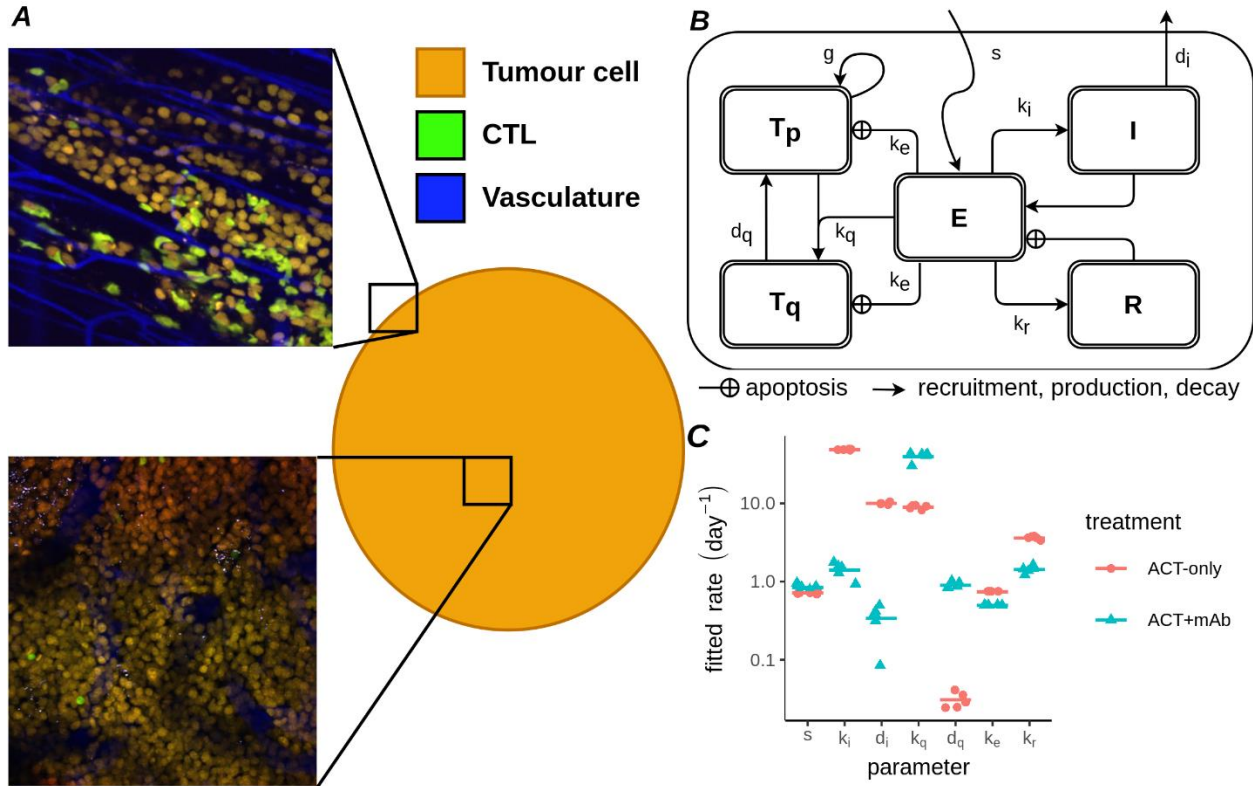


**Figure 3.** ODE model linking intravital and volumetric measurements from ACT treated tumours. A) Examples of imaged positions with varying numbers of tumour cells, shown with their presumed location inside the tumour (circle). B) Schematic of ODE model. C) Best fitting parameters for the ODE model. Each point represents 1 of 5 fits using the stochastic evolutionary algorithm. Horizontal lines represent the mean fitted parameter for either ACT-only (red) or ACT+mAb (blue) conditions.

### An antiproliferative effect of CTLs is most important for controlling tumour progression

We fit our model simultaneously to all available measurements, except for the tumour growth rate in the untreated condition, which we fixed before fitting (using  $g=0.5 \text{ day}^{-1}$ ). Overall we varied 7 parameters for either the ACT-only or the ACT+mAb condition (Fig. 3C) to obtain the best match between model and tumour data. We then studied our best fitting models to gain insight into the dynamics and activities of the transferred CTLs. When we took best fitting parameter sets for either ACT-only or ACT+mAb conditions and varied the killing rate  $k_e$ , abrogation of killing (by setting  $k_e=0$ ; Fig. 4A) had only marginal impact on the progression of the tumours. In contrast, with abrogation of CTL-induced tumour proliferation arrest (by setting  $k_q=0$ ; Fig. 4B) tumour growth progression continued virtually unaffected by the presence of the CTLs killing at the best fitted rates. This indicated that the antiproliferative effect, rather than the killing, accounted for the majority of deviation from exponential growth. Notably, when we simulated progressive increases to CTL killing we saw progressively improved tumour control for both ACT-only and ACT+mAb conditions ( $k_e>1$ ; Fig. 4A). However, the antimitotic effect appeared to be close to saturation, particularly for the ACT+mAb condition, since further increases to the  $k_q$  parameter hardly led to further improvements in tumour control ( $k_q>1$ ; Fig. 4B). These results imply that strategies for

increasing CTL killing ( $k_e$ ) could be of greater therapeutic benefit than strategies aiming to further enhance the antimitotic effect ( $k_q$ ).

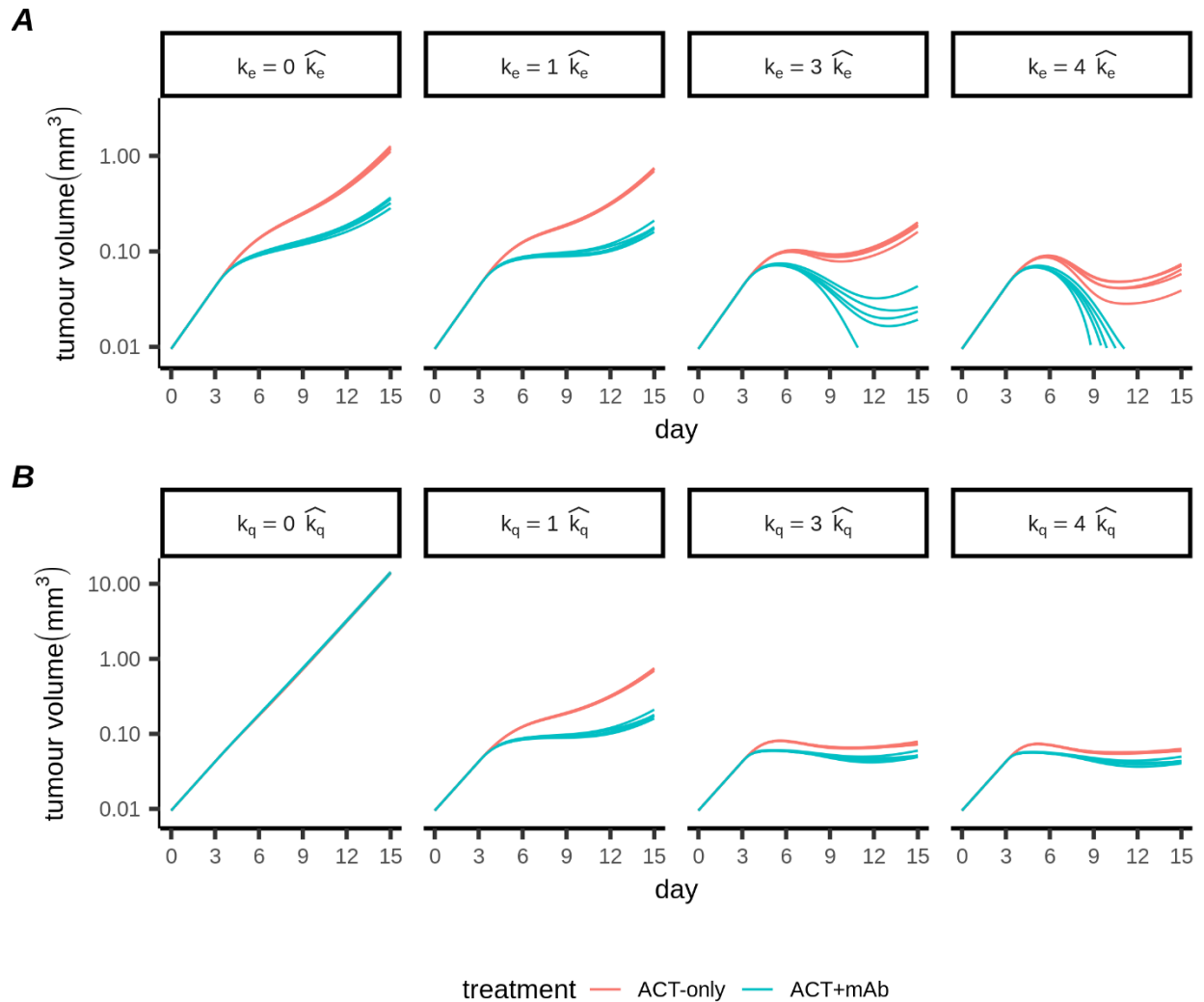


**Figure 4.** Relative impacts of antiproliferative and killing effects of adoptively transferred CTLs. A-B) Impact of varying the killing rate ( $k_e$ ; A) and the rate parameter for induction of antiproliferative effect ( $k_q$ ; B). Using the best fitting parameter sets, both rates were multiplied by a factor of 0,1,3 or 4 (indicated by columns). Hats on parameters indicate best fitting values.

### anti-CD137 leads to superior tumour control by enhancing the antiproliferative effect of CTLs

We finally sought to identify differences in the dynamics of CTLs and their interactions with the tumour after the CD137 antibody costimulation. Since abrogating killing by setting  $k_e=0$  had no substantial impact on tumour volume progression (Fig. 4A), it seemed unlikely that ACT+mAb enhanced control of the tumour by improving the ability of CTLs to kill tumour cells. Indeed, there was no improvement in the per-capita CTL killing performance of CTLs after ACT+mAb. In fact

the best fitting killing rates from ACT-only ( $k_e=0.75 \text{ day}^{-1}$ ) were even somewhat higher than for the ACT+mAb condition ( $k_e=0.5 \text{ day}^{-1}$ ) (Fig. 3B & Fig. 5A-B, row 2).

Since the E:T ratio was also higher in the ACT+mAb tumours (Fig. 5C-D) it could be that increased killing due to more CTLs could explain the improved tumour control in the ACT+mAb group. There are multiple indications that this was not the case. First, tumour growth reduction was broadly similar between tumours treated with ACT+mAb on d3 (Fig. 5E) and those treated on d7 (Fig. 5F), despite substantially lower E:T ratios in the d7 treated group - consistent with the notion of a small number of CTLs being quickly able to control a large number of tumour cells through cytostatic effects. Second, the tumour cell mitosis predicted by the best fitting models followed the volumetric tumour growth closely, leaving little room for a contribution from killing (compare Fig. 5E-F with Fig. 5A-B, top row).

Rather than an increase in killing, a stronger reduction in tumour proliferation for ACT+mAb tumours compared to ACT-only tumours accounts for the difference in results. Note that different values for the preset growth rate parameter resulted in similar best fitting parameters and similar model dynamics, therefore our conclusions about the relative importance of killing versus antiproliferative effect do not appear to be especially sensitive to our choice for the tumour growth rate (S3. Fig). Our model suggests two means by which enhanced reduction of proliferation for ACT+mAb tumours could have occurred. First, our fits resulted in larger values of  $k_q$  for the ACT+mAb group (Fig. 3C), which is necessary to account for the similar reductions in volumetric growth in the ACT+mAb treated tumours whether treated on d3 or d7 (Fig. 2B, blue lines), despite a much lower E:T ratio in the d7 treated group. The second possibility our model highlights stems from the different dynamics of the CTL population between ACT-only and ACT+mAb treated groups. At late times the population dynamics of the CTLs was an important determinant of the E:T ratio, due to a combination of slow dynamics for CTL mitosis (Figs. 5A-B, row 3) and a delayed onset of CTL apoptosis (Figs. 5A-B, row 4). Notably, although the fitted rate parameter controlling the increase in CTL mitosis ( $k_i$ ) was substantially larger for the ACT-only condition than for the ACT+mAb condition (Fig. 3C), this did not reduce CTL mitosis overall - instead the peak of CTL mitosis simply shifted to later time points. These altered dynamics led to significant improvement in E:T ratio for the ACT+mAb group at late time points after treatment. Overall, our model indicates that ACT+mAb costimulation resulted in CTLs which were able to more rapidly prevent tumour cell mitosis after administration of ACT. Moreover, the dynamics of both CTL proliferation and apoptosis were delayed, resulting in a CTL population which remained inside the tumours for longer and therefore increasing the period of time in which CTLs could exert control of the tumour.

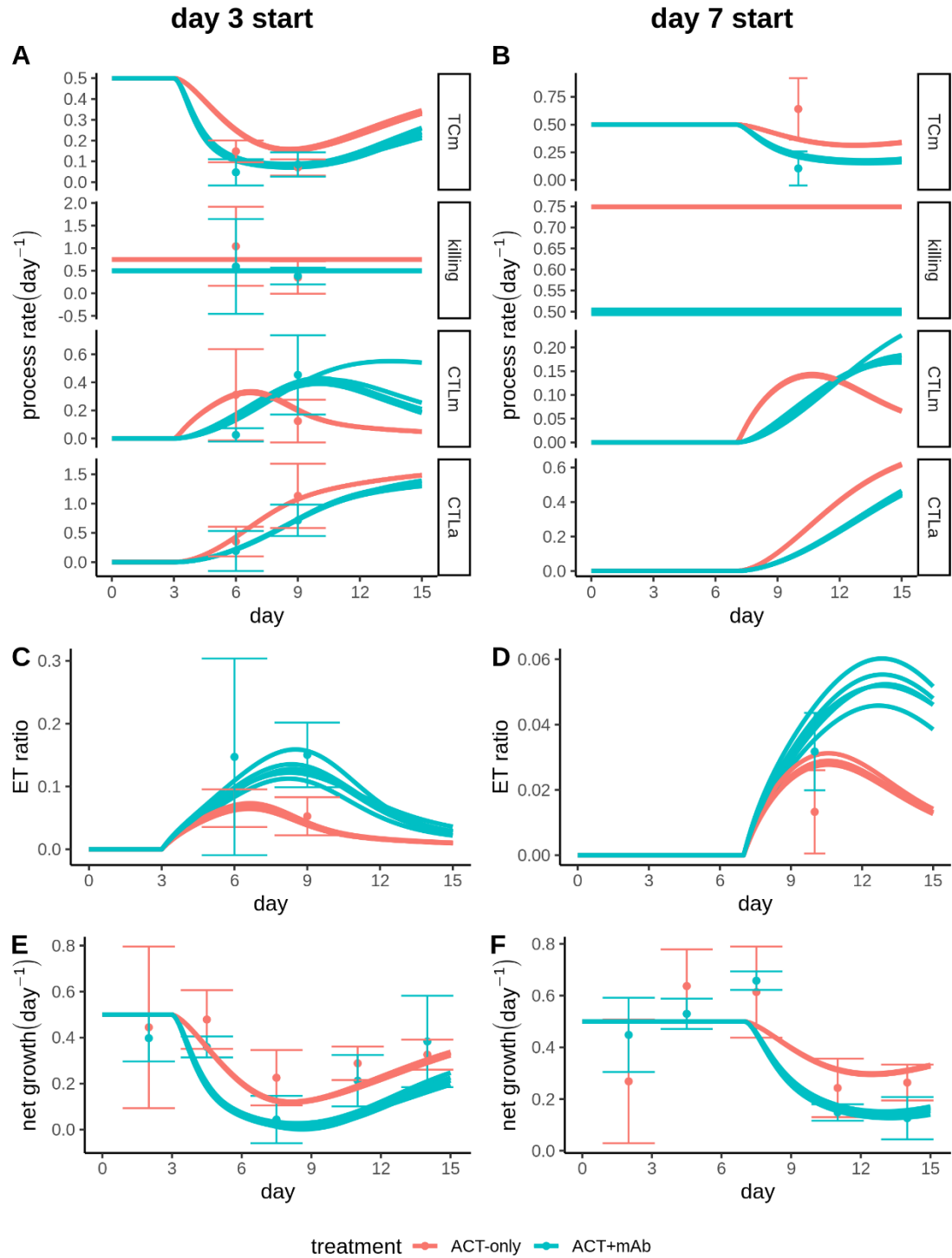


**Figure 5.** Enhanced antiproliferative effect and extended effector window of CD137 stimulated CTLs. A-F) Results of parameter estimation. Model output represented by lines, data plotted as mean and s.d. Shown are observed and fitted process rates (A-B), effector:target ratio (C-D) and net tumour growth (E-F) for either tumours treated on day 3 (A, C, E) or day 7 (B, D, F). Process rates considered in (A-B) are: Tcm (Tumour Cell mitosis); killing (of tumour cells by CTLs); CTLm (CTL mitosis); CTLa (CTL apoptosis).



**Table 1** Best fitting model parameter values and their explanations

Parameter name	Explanation	ACT+mAb	ACT-only
$g(day^{-1})$	TC mitosis rate	0.5	0.5
$s(TC^{-2/3} day^{-1})$	Rate constant for CTL infiltration into tumour	0.9	0.75
$k_e(CTL^{-1} day^{-1})$	Rate at which CTLs kill tumour cells	0.5	0.75
$k_i(day^{-1})$	Rate of CTL-induced increase in CTL mitosis	1	45
$d_i(day^{-1})$	Rate of decrease in CTL-induced CTL mitosis	0.25	10
$k_r(day^{-1})$	Rate of CTL-induced CTL apoptosis (resistance).	1.3	3.4
$k_q(day^{-1})$	Rate at which CTLs induce antiproliferative effect	45	9
$d_q(day^{-1})$	Rate at which CTL induced antiproliferative effect disappears	1.3	0.38

## Discussion

Here we used an ODE model to quantify the effector functions and population dynamics of CTLs and tumour cells, following ACT therapy within murine melanoma tumours. To parameterise our models we used data where mice were treated in the presence or absence of anti-CD137 [13]. The data consisted of counts of the number of CTLs/tumour cells and the number of apoptosis/mitosis events associated with each respective cell type, at various locations within the melanoma tumours being attacked by CTLs. We used our models to investigate the means by which adoptively transferred CTLs controlled the tumours, and also what caused the improved tumour control after anti-CD137 costimulation. We found that the apoptosis rates of tumour cells were well fitted by a linear dependency on the number of CTLs, indicating that local presence of

CTLs was required for TC apoptosis. However, we found that the CTL killing rate was very low and contributed little to tumour reduction overall. Instead, the antiproliferative effect had a large effect, with tumour cell mitosis rates observed *in vivo* being far below those needed to explain the growth of the untreated tumours. We found that almost all of the reduction in tumour growth after CTL treatment could be explained by decreased TC mitosis.

Importantly, we also sought to understand mechanistically what caused the improved tumour control after treatment with anti-CD137. Killing per CTL was unchanged after anti-CD137 stimulation and hence still contributed little to tumour control, so the improvement in tumour control was largely due to an enhanced antimitotic effect after anti-CD137 treatment. Our model suggested that this enhanced antimitotic effect could be explained either by an increased per-capita ability of CTLs to exert an antimitotic effect, or simply by a numeric increase of CTLs inside the tumour (each with similar antimitotic effects to unstimulated CTLs when considered per-capita). In our model these effects were difficult to separate, since increased mitotic effect of CTLs (on a per-capita basis) should also have the effect of increasing E:T ratio, by reducing the denominator. However, differences in E:T ratio between ACT-only and ACT+mAb treated groups emerged later than the differences in tumour cell proliferation and tumour size, which were already apparent by day 6 after tumour inoculation. Thus the data from early time points suggest a more rapid per-capita ability of anti-CD137 stimulated CTLs to prevent proliferation of tumour cells, compared to their unstimulated counterparts. Additionally, our model predicted that the increased E:T ratio, which was most apparent at late time points after ACT, should also play a role in improved tumour control. Although the rates of CTL mitosis were generally low and the net CTL population growth (mitosis minus apoptosis) was negative in almost all videos, the overall dynamics of the anti-CD137 stimulated CTL populations appeared different to their unstimulated counterparts. Specifically, the peak rate of CTL mitosis occurred later in the ACT+mAb treated group, which together with a delayed onset of apoptosis led to a more sustained presence in the tumour. In summary, after anti-CD137 treatment CTLs were able to rapidly shut down mitosis of tumour cells, but also remained present in the tumour for longer, both contributing to the improvement in tumour control.

Our results fit well with other reports about the effects of anti-CD137 stimulatory effects on CTL function in the literature. To our knowledge, there are no clear reports that CD137 enhances the cytotoxicity of CTLs. Instead, in agreement with our findings, studies which have directly measured CTL cytolytic activity have found similar killing after blockade of CD137 signalling [17], and CAR T cells engineered with a CD137 costimulatory module did not exhibit superior cytotoxic potential compared to CAR T cells lacking the CD137 module [18]. Several studies have found that CD137 costimulation induces IFN- $\gamma$  production by CTLs [17–19]. Enhanced IFN- $\gamma$  production by CTLs provides a possible mechanism for the increased ability of CTLs to prevent tumour cell proliferation suggested by our models, since IFN- $\gamma$  has been shown to play an important role in control of B16F10 melanoma tumours via arrest of the tumour cell cycle [20]. The prolonged presence of CTLs inside the tumour for the anti-CD137 treated group due to delayed apoptosis is in agreement with reports of anti-apoptotic effects of CD137 signalling on activated T cells [21,22].

One limitation of our model is that there is no representation of space, so the tumour is treated as homogeneous throughout. The B16F10 melanoma tumours are highly invasive [23] and events at the invading margins may be more important than events elsewhere in determining tumour growth, with tumour cells near the periphery having more space and more opportunities for proliferation. Anti-CD137 treatment reduced CTL migration inside the tumour resulting in long-lasting interactions with tumour cells [13], so it may be that CTLs remained near the tumour border or tumour vasculature and were more effective here than the control cells which migrated deeper into the tumour. Our model would not be sensitive to such an effect. Furthermore, we took the tumour cell density as constant but in reality this may have reduced if tumour cells continued to migrate outwards but proliferation was inhibited and killing occurred. In this case our estimates of the number of tumour cells are too high and our model underestimates the impact of the antiproliferative effect on the tumour, possibly explaining the remaining error in the tumour cell mitosis rate for our best fitting models. A spatially explicit model such as a partial differential equation model [24,25] could be developed, to take into account these limitations. This would however increase the complexity of the model, so more detailed measurements from the tumour would be required in order to determine the model parameters. Specifically, measurements of mitosis and killing rates categorised based on the distance to the center or periphery of the tumour would be useful to parameterise such a spatial model. Another useful measurement would be the net migration rate of both CTLs and tumour cells, along with the direction of migration.

Our model predictions can be tested in various ways. Although we included the tumours treated on day 7 in our analysis, we were not able to determine the number of TC apoptosis events or the apoptosis/mitosis of CTLs. That was because, whilst absolute cell numbers or TC mitosis events were relatively easy to detect, the other events were ambiguous. Nevertheless, our model does make predictions for these values which could in principle be checked. Moreover, our model predicts the arrival rate of new CTLs into the tumours which could be checked against time-lapse images. In our data CTL apoptosis increased over time, so we introduced a resistance variable  $R$  to account for this. This is consistent with recent reports that long range IFN- $\gamma$  signalling can cause upregulation of PD-L1 in cells across distances of up to  $800\mu m$  [26]; or that IFN- $\gamma$ -dependent invasion of myeloid-derived suppressor cells could be the major source of suppression [27]; or other immune checkpoint death receptors such as FAS-L [28]; or perhaps competition between tumour cells and CTLs for nutrients was a primary mediator of CTL apoptosis in our model, since both activated CTLs and tumour cells rely heavily on anaerobic glycolysis or glycolysis as sources of fuel [29], and interactions between CTLs and stromal cells resulted in catastrophic destruction of tumour vasculature [30], which ought to result in a reduction in glucose supply to the tumour and might account for increased apoptosis of CTLs over time. It would be useful to acquire more experimental data which could shed light on the reasons for this apparent time-increasing apoptosis rate.

Overall, our modelling study provides insights into the mechanisms CTLs use to control tumours, as well as insights into how these mechanisms may have changed upon costimulation with agonist antibody targeting the CD137 receptor. Moreover, the results of our model identify specific directions for future experimental work which would help elucidate the effect of CD137 stimulation upon CTLs.

## Models and Methods

### Experimental data

The experimental data we have used derives from a previously published study where mice were inoculated with B16F10 melanoma tumours, which were then studied over a period of up to 15 days post-inoculation through dorsal imaging windows, by means of two-photon microscopy [13]. In total there were 6 distinct experimental conditions. There were two control conditions, one with OVA antigen expressing tumour cells where ACT was not administered, and another with tumour cells not expressing OVA, but with ACT administered. A further two conditions had OVA expressing tumour cells, with ACT administered on either day 3 or day 7 post tumour inoculation. Finally, there were two conditions where ACT was administered to mice bearing OVA expressing tumours, together with costimulation using agonist anti-CD137 (clone 1D8), again on either day 3 or day 7 post tumour inoculation. For these costimulated conditions, anti-CD137 was delivered intraperitoneally, on the same day as ACT.

The dataset comprises estimates of tumour volume measured at days 1, 3, 6, 9, 13 and 15 in all mice. Moreover, for the mice treated with ACT on day 3 and bearing OVA expressing tumours, statistics were available for the number of CTLs and tumour cells, as well as their mitosis and apoptosis rates, on either day 6 or day 9 after tumour inoculation (days 3 and 6 after CTL transfer). These statistics are samples from imaging volumes of size  $0.35 \cdot 0.35 \cdot 0.1mm$  which were imaged for 1-3h (See Fig. 6B,6D of ref: [13]). Finally, intravital images were available for the mice treated on day 7, although no statistics for these images had yet been recorded. We therefore quantified the number of CTLs and tumour cells, and the number of tumour cell mitosis events in these images as well. The number of CTLs and TC mitosis events was determined via manual counting, whereas the number of tumour cells was determined automatically using ImageJ as follows: we first processed images using a 3D gaussian blur ( $\sigma=2$  in the x-y directions, and  $\sigma=0.2$  in the z direction). Then, we selected every third slice in the Z direction to avoid repeated counting of the same cell. Remaining slices were then thresholded using the Li method [31]. Following thresholding, the watershed method [32] was used to separate touching cells. Finally, the “analyse particles” plugin was used to quantify cells, excluding particles of less than 10 pixels in area.

To determine the killing rate from the experimental data we considered the number of apoptosis events counted per position as a Poisson distributed random variable. We evaluated two possibilities for the Poisson rate parameter, which we termed “linear” or “mass-action”. For the linear model, we considered the rate parameter to be proportional to the number of CTLs counted at the position. For the mass-action model, we considered the rate parameter to be proportional to the product of the number of CTLs and the number of tumour cells counted at the position. For either model, we determined the rate parameter which maximised the likelihood of the counted apoptosis events from the Poisson distribution. We considered all samples together, or alternatively samples grouped by treatment, resulting in different numbers of fitted rate

parameters required to describe the data. To compare the quality of fits while accounting for different numbers of parameters, we used Akaike's and Bayes' information criteria.

## Ordinary Differential Equation model CTLs v.s. B16F10 Melanoma

We used ODE models for tumour growth, CTL population dynamics and the effect of the CTLs on tumours, thus approximating tumours as well-mixed entities. Although some degree of intratumoural heterogeneity can be expected, considering them to be spatially homogeneous is a reasonable initial approach given the small size of the tumours.

### Tumour growth in the absence of CTLs

The available tumour growth data derives from B16F10 murine melanoma tumours recorded for 15 days after their implantation [13]. We opted for the simplest possible model for tumour growth in the absence of CTLs, i.e., the exponential growth model which considers a volume of tumour ( $V$ ) made of tumour cells who undergo mitosis with an average rate  $g$ , because it was sufficient to describe the part of the data without ACT very well. Indeed, within the 15 day time period we studied, tumours remained small: the median tumour volume (considering all our data) was  $0.04\text{mm}^3$  on day 3 and  $0.93\text{mm}^3$  on day 15. Thus, there was no need to take into account a reduction in TC proliferation as the tumour volume increases, as is commonly seen when models are applied to large malignancies and the logistic growth model is applied [33–36]. For all our simulations we took  $g = 0.5(\text{day}^{-1})$  in the absence of CTLs, based on growth rates for tumours in the data for conditions either without ACT or periods before CTL transfer in the ACT treated groups. This corresponds to a doubling time of 1.4 days for the tumour cell population, and it is approximately consistent with doubling times in the region  $1.7 - 2 (\text{day}^{-1})$  reported for B16F10 tumours growing up to  $100\text{mm}^3$  in another study, where B16F10 cells were implanted into the ears of mice [37] (instead of the deep dermis as was the case for the data we studied here).

### Effects of CTLs on tumours

In our data the frequency of tumour cell apoptosis was low, so in our models we included an antiproliferative effect of CTLs on the tumour. For this, we denote separately  $T_p$ , the subset of tumour cells which are proliferating and  $T_q$ , a subset of “quiescent”, non-proliferating tumour cells:

$$T_p + T_q = T, \tag{Eq. 1}$$

where  $T$  is the total number of tumour cells in the tumour. Invading CTLs have 2 different effects on tumour cells: either killing which occurs at rate  $k_e (\text{CTL}^{-1} \text{ day}^{-1})$ , or induction of the quiescent state which happens at rate  $k_q (\text{CTL}^{-1} \text{ day}^{-1})$ . Our quiescent state is motivated by observations of an  $IFN\gamma$ -dependent cell-cycle arrest in B16F10 melanoma after ACT [20], which we previously implicated in control of murine EL4 lymphoma [6] and for which there is also evidence in ovarian and breast carcinoma models [26]. In B16F10 melanoma, quiescent tumour cells recover from

CTL induced cell cycle arrest after a few days [20]. In our model recovery occurs with rate  $d_q$  ( $\text{day}^{-1}$ ). The dynamics of proliferating and quiescent tumour cells can thus be described as:

$$\frac{dT_p}{dt} = gT_p - (k_e + k_q) (T_p/T) E + d_q T_q \quad \text{Eq. 2}$$

$$\frac{dT_q}{dt} = k_q (T_p/T) E - k_e (T_q/T) E - d_q T_q. \quad \text{Eq. 3}$$

Note that we found no evidence in the data to suggest that killing of tumour cells by CTLs might depend on the number of tumour cells (S1. Fig). Therefore, we considered the sum of all CTL killing activity to be  $k_e E$  ( $\text{day}^{-1}$ ) in our ODE model, i.e. the killing rate is independent of the number of tumour cells and is shared between proliferating and quiescent tumour cells in accordance with their fraction in the tumour.

### CTL population dynamics

Our model considers only transferred CTLs (since only these could be seen with the fluorescent reporter system), therefore neglecting any endogenous response. Although endogenous CTLs may have been present, robust tumour control in the presence of ACT was still achieved in RAG  $\pm$  mice (See Fig. 1H [13]) for approximately 30 days before tumours regrew. From this we concluded that endogenous CTLs did not contribute significantly to early tumour regression in the experimental set-up we are modeling here, but were required for long term tumour control. Negligible contribution of the endogenous (or innate) immune response are also consistent with our observation that TC apoptosis correlated strongly with the local number of transferred CTLs (See Fig 2C), although we cannot exclude that the local density of endogenous/innate effectors might also have correlated with the local density of transferred CTLs. The total number of tumour-infiltrating CTLs,  $E$ , inside the tumour is described by:

$$\frac{dE}{dt} = sT^{2/3} + E(I - R)/T. \quad \text{Eq.4}$$

The first term represents the net movement of transferred CTLs into the tumour. Since we have no measurements directly pertaining to CTL infiltration of the tumours, we opted for a simple model where CTLs infiltrate across the tumour boundary at a constant rate  $s$  (per unit area of the boundary). The  $2/3$  power can be interpreted as a constant rate of infiltration across the boundary of the tumour, which we consider to be approximately spherical [38]. To take the CTL population dynamics into account, the second term of Eq. 4 includes two additional variables  $I$  and  $R$  to describe the dynamics of CTL proliferation and apoptosis inside the tumour. The variable  $I$  represents an auto-inductive response of CTLs upon encounter with antigen expressing cells and

is based on other models which have included Interleukin-2 as a driver of CTL mitosis [34,39]. Such stimulatory signals could originate from other CD8<sup>+</sup> T cells by means of quorum regulation [40] or from other immune cells such as CD4<sup>+</sup> T cells. Our model accounts for either possibility:

$$\frac{dI}{dt} = k_I E - d_I I. \quad \text{Eq. 5}$$

Thus, CTLs induce their own mitosis at rate  $k_I$  and the stimulus disappears at rate  $d_I$ .

The second variable  $R$  represents a resistance acquired by the tumour in response to infiltrating CTLs. Pro-apoptotic signals through the PD-1 receptor are a candidate source of this resistance, since in other experiments with B16F10 tumours treated with agonist antibody for CD137 tumour rejection was enhanced when agonist anti-CD137 was coadministered with an antagonist antibody for PD1 [41]. However, since other possible explanations are equally consistent with our data (see Discussion), we used the general term “resistance” for this variable:

$$\frac{dR}{dt} = k_R E. \quad \text{Eq. 6}$$

Thus, CTLs induce resistance proportional to their number inside the tumour at a constant rate  $k_R$ . The  $I$  and  $R$  terms are divided by the number of tumour cells in Eq. 4, since if  $I$  and  $R$  represent e.g. stimulating or suppressive cell populations (respectively), then their frequency among tumour cells should determine their effect on CTLs.

## Model Fitting Procedure

Models are fit by minimising the Root Mean Square Error between model prediction and each individual data point. “Individual data points” are considered to be either one volumetric growth estimate, or one statistic estimated from one intravital position. Thus a single mouse where the tumour volume was measured on days 1, 3, 6, 9, 13 and 15 and where intravital data was recorded at four positions on days 6 and 9 would produce 5 volumetric growth estimates, plus 8 estimates for each intravital process rate (32 in total) and a further 8 E:T ratio estimates. The correspondence between the intravital process rates determined from the experimental dataset and those determined from the ODE model is given in table 2. Minimisation was performed using the a differential evolution algorithm with the DEoptim [42] package in R, using the local-to-best evolution strategy. Each parameter estimation was performed with 5 repeats, using different randomly selected starting parameter values for each repeat. Individual repeats had population sizes of 200, and ran for 500 generations. ACT-only and ACT+mAb groups were fit separately with no overlapping parameters, except for the tumour growth rate parameter ( $g$ ) which was fixed to the same value for both ACT-only and ACT+mAb conditions before fitting.

**Table 2** Calculation of intravital process rates from experimental data and from ODE model

Intravital process rate	Calculation from experimental data	Calculation from model
CTL killing rate	$\frac{\text{tumour cell apoptosis}}{CTLs}$	$k_e$
Tumour cell mitosis rate	$\frac{\text{tumour cell mitosis}}{\text{tumour cells}}$	$gT_p/T$
CTL mitosis rate	$\frac{CTL \text{ mitosis}}{CTLs}$	$I/T$
CTL apoptosis rate	$\frac{CTL \text{ apoptosis}}{CTLs}$	$R/T$

## Data Availability

Source code for this work is available (<https://doi.org/10.5281/zenodo.4443230>).

## References

1. Tang J, Pearce L, O'Donnell-Tormey J, Hubbard-Lucey VM. Trends in the global immunology landscape. *Nat Rev Drug Discov.* 2018;17: 783–784.
2. Tang J, Shalabi A, Hubbard-Lucey VM. Comprehensive analysis of the clinical immunology landscape. *Ann Oncol.* 2018;29: 84–91.
3. Hegde UP, Mukherji B. Current status of chimeric antigen receptor engineered T cell-based and immune checkpoint blockade-based cancer immunotherapies. *Cancer Immunol Immunother.* 2017;66: 1113–1121.
4. Sun L, Zhang L, Yu J, Zhang Y, Pang X, Ma C, et al. Clinical efficacy and safety of anti-PD-1/PD-L1 inhibitors for the treatment of advanced or metastatic cancer: a systematic review and meta-analysis. *Sci Rep.* 2020;10: 2083.

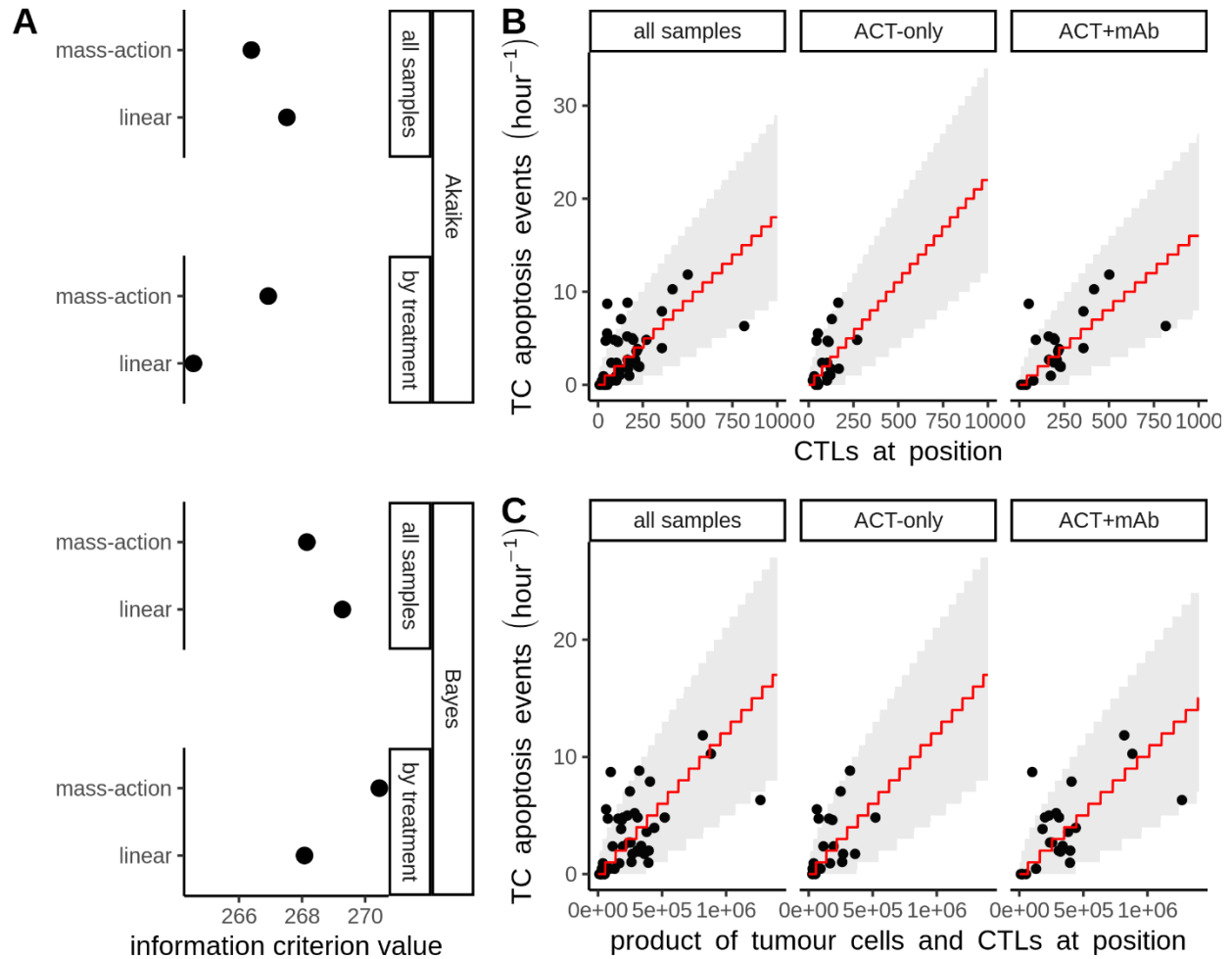


5. Rotte A. Combination of CTLA-4 and PD-1 blockers for treatment of cancer. *J Exp Clin Cancer Res.* 2019;38: 255.
6. Beck RJ, Slagter M, Beltman JB. Contact-dependent killing by cytotoxic T lymphocytes is insufficient for EL4 tumor regression in vivo. *Cancer Res.* 2019. doi:10.1158/0008-5472.CAN-18-3147
7. Hornberg JJ, Bruggeman FJ, Westerhoff HV, Lankelma J. Cancer: a Systems Biology disease. *Biosystems.* 2006;83: 81–90.
8. Stéphanou A, Fanchon E, Innominato PF, Ballesta A. Systems Biology, Systems Medicine, Systems Pharmacology: The What and The Why. *Acta Biotheor.* 2018;66: 345–365.
9. Etxeberria I, Glez-Vaz J, Teijeira Á, Melero I. New emerging targets in cancer immunotherapy: CD137/4-1BB costimulatory axis. *ESMO Open.* 2020;4. doi:10.1136/esmoopen-2020-000733
10. Kwon B. Anti-CD137 Cancer Immunotherapy Suppresses Tumor Growth-Response. *Cancer research.* 2018. pp. 1572–1573.
11. Dharmadhikari B, Zeng Q, Wu M, Schwarz H. Anti-CD137 Cancer Immunotherapy Suppresses Tumor Growth-Letter. *Cancer research.* 2018. p. 1571.
12. Yonezawa A, Dutt S, Chester C, Kim J, Kohrt HE. Boosting Cancer Immunotherapy with Anti-CD137 Antibody Therapy. *Clin Cancer Res.* 2015;21: 3113–3120.
13. Weigelin B, Bolaños E, Teijeira A, Martinez-Forero I, Labiano S, Azpilikueta A, et al. Focusing and sustaining the antitumor CTL effector killer response by agonist anti-CD137 mAb. *Proc Natl Acad Sci U S A.* 2015;112: 7551–7556.
14. Makkouk A, Chester C, Kohrt HE. Rationale for anti-CD137 cancer immunotherapy. *Eur J Cancer.* 2016;54: 112–119.
15. Cazaux M, Grandjean CL, Lemaître F, Garcia Z, Beck RJ, Milo I, et al. Single-cell imaging of CAR T cell activity in vivo reveals extensive functional and anatomical heterogeneity. *J Exp Med.* 2019; jem.20182375.
16. Perelson AS, Macken+ A. Kinetics of Cell-Mediated Cytotoxicity: Stochastic and Deterministic Multistage Models. *Math Biosci.* 1984;70: 161–194.
17. Cooper D, Bansal-Pakala P, Croft M. 4–1BB (CD137) controls the clonal expansion and survival of CD8 T cells in vivo but does not contribute to the development of cytotoxicity. *Eur J Immunol.* 2002;32: 521–529.
18. Song D-G, Ye Q, Carpenito C, Poussin M, Wang L-P, Ji C, et al. In vivo persistence, tumor localization, and antitumor activity of CAR-engineered T cells is enhanced by costimulatory signaling through CD137 (4-1BB). *Cancer Res.* 2011;71: 4617–4627.
19. Shuford WW, Klussman K, Tritchler DD, Loo DT, Chalupny J, Siadak AW, et al. 4-1BB costimulatory signals preferentially induce CD8+ T cell proliferation and lead to the amplification in vivo of cytotoxic T cell responses. *J Exp Med.* 1997;186: 47–55.

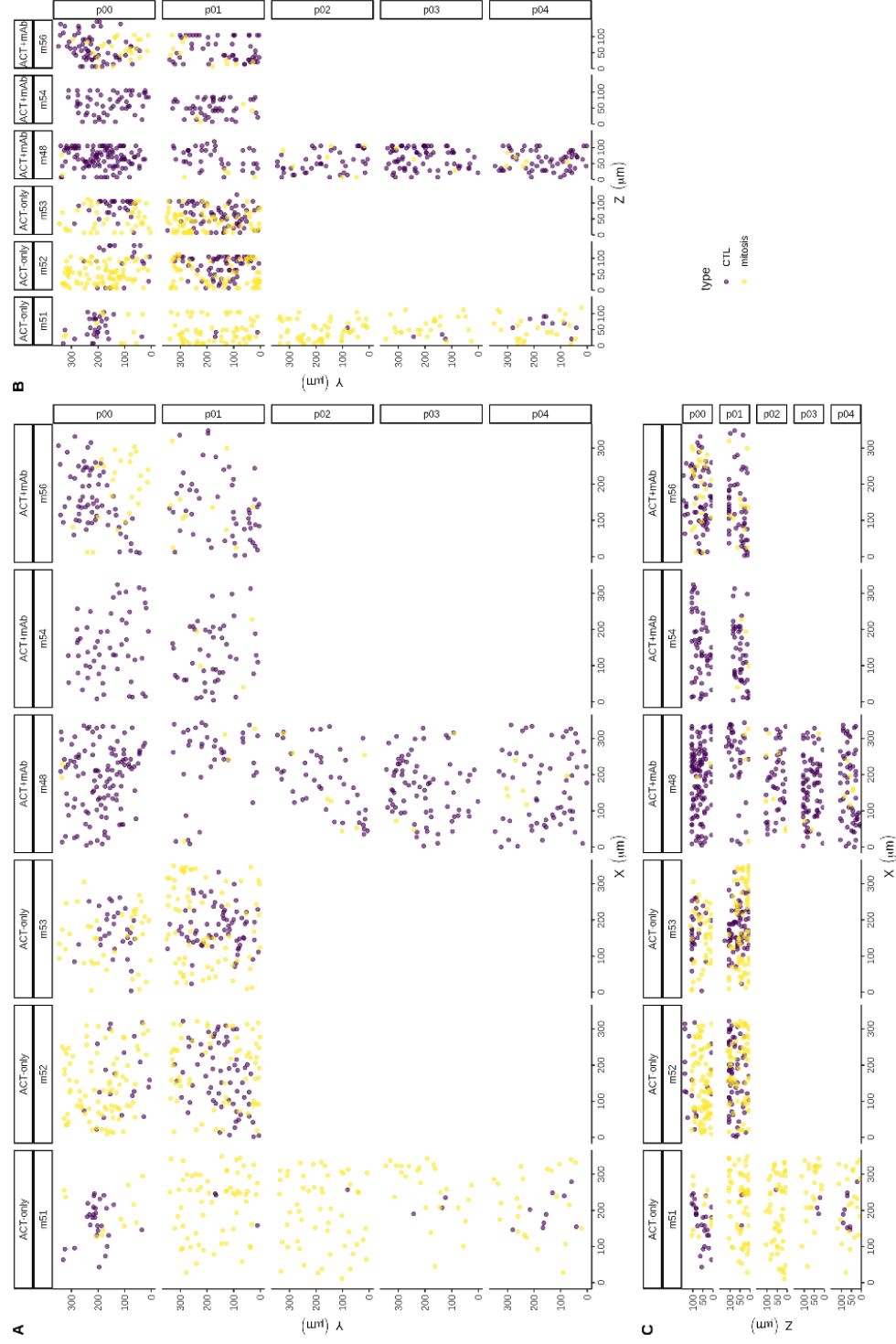
20. Matsushita H, Hosoi A, Ueha S, Abe J, Fujieda N, Tomura M, et al. Cytotoxic T lymphocytes block tumor growth both by lytic activity and IFN $\gamma$ -dependent cell-cycle arrest. *Cancer Immunol Res.* 2015;3: 26–36.
21. Lee H-W, Park S-J, Choi BK, Kim HH, Nam K-O, Kwon BS. 4-1BB promotes the survival of CD8+ T lymphocytes by increasing expression of Bcl-xL and Bfl-1. *J Immunol.* 2002;169: 4882–4888.
22. Hurtado JC, Kim YJ, Kwon BS. Signals through 4-1BB are costimulatory to previously activated splenic T cells and inhibit activation-induced cell death. *J Immunol.* 1997;158: 2600–2609.
23. Weigelin B, Bakker G-J, Friedl P. Intravital third harmonic generation microscopy of collective melanoma cell invasion: Principles of interface guidance and microvesicle dynamics. *Intravital.* 2012;1: 32–43.
24. Benzekry S, Lamont C, Beheshti A, Tracz A, Ebos JML, Hlatky L, et al. Classical mathematical models for description and prediction of experimental tumor growth. *PLoS Comput Biol.* 2014;10: e1003800.
25. Enderling H, Chaplain MAJ. Mathematical modeling of tumor growth and treatment. *Curr Pharm Des.* 2014;20: 4934–4940.
26. Hoekstra ME, Bornes L, Dijkgraaf FE, Philips D, Pardieck IN, Toebes M, et al. Long-distance modulation of bystander tumor cells by CD8+ T-cell-secreted IFN- $\gamma$ . *Nature Cancer.* 2020;1: 291–301.
27. Hosoi A, Matsushita H, Shimizu K, Fujii S-I, Ueha S, Abe J, et al. Adoptive cytotoxic T lymphocyte therapy triggers a counter-regulatory immunosuppressive mechanism via recruitment of myeloid-derived suppressor cells. *Int J Cancer.* 2014;134: 1810–1822.
28. Zhu J, Petit P-F, Van den Eynde BJ. Apoptosis of tumor-infiltrating T lymphocytes: a new immune checkpoint mechanism. *Cancer Immunol Immunother.* 2019;68: 835–847.
29. Kouidhi S, Elgaaied AB, Chouaib S. Impact of Metabolism on T-Cell Differentiation and Function and Cross Talk with Tumor Microenvironment. *Front Immunol.* 2017;8: 270.
30. Schietinger A, Arina A, Liu RB, Wells S, Huang J, Engels B, et al. Longitudinal confocal microscopy imaging of solid tumor destruction following adoptive T cell transfer. *Oncoimmunology.* 2013;2: e26677.
31. Li CH, Tam PKS. An iterative algorithm for minimum cross entropy thresholding. *Pattern Recognit Lett.* 1998;19: 771–776.
32. Soille P, Vincent LM. Determining watersheds in digital pictures via flooding simulations. *1990;1360: 240–250.*
33. Kuznetsov VA, Makalkin IA, Taylor MA, Perelson AS. Nonlinear dynamics of immunogenic tumors: parameter estimation and global bifurcation analysis. *Bull Math Biol.* 1994;56: 295–321.

34. Kirschner D, Panetta JC. Modeling immunotherapy of the tumor--immune interaction. *J Math Biol.* 1998;37: 235–252.
35. de Pillis LG, Radunskaya AE, Wiseman CL. A validated mathematical model of cell-mediated immune response to tumor growth. *Cancer Res.* 2005;65: 7950–7958.
36. Talkington A, Dantoin C, Durrett R. Ordinary Differential Equation Models for Adoptive Immunotherapy. *Bull Math Biol.* 2018;80: 1059–1083.
37. Potez M, Trappetti V, Bouchet A, Fernandez-Palomo C, Güç E, Kilarski WW, et al. Characterization of a B16-F10 melanoma model locally implanted into the ear pinnae of C57BL/6 mice. *PLoS One.* 2018;13: e0206693.
38. Frascoli F, Kim PS, Hughes BD, Landman KA. A dynamical model of tumour immunotherapy. *Math Biosci.* 2014;253: 50–62.
39. Lai X, Friedman A. Combination therapy of cancer with cancer vaccine and immune checkpoint inhibitors: A mathematical model. *PLoS One.* 2017;12: e0178479.
40. Zenke S, Palm MM, Braun J, Gavrilov A, Meiser P, Böttcher JP, et al. Quorum Regulation via Nested Antagonistic Feedback Circuits Mediated by the Receptors CD28 and CTLA-4 Confers Robustness to T Cell Population Dynamics. *Immunity.* 2020;52: 313–327.e7.
41. Chen S, Lee L-F, Fisher TS, Jessen B, Elliott M, Evering W, et al. Combination of 4-1BB agonist and PD-1 antagonist promotes antitumor effector/memory CD8 T cells in a poorly immunogenic tumor model. *Cancer Immunol Res.* 2015;3: 149–160.
42. Mullen K, Ardia D, Gil DL, Windover D, Cline J. DEoptim: An R Package for Global Optimization by Differential Evolution. 2009. Available: <https://papers.ssrn.com/abstract=1526466>

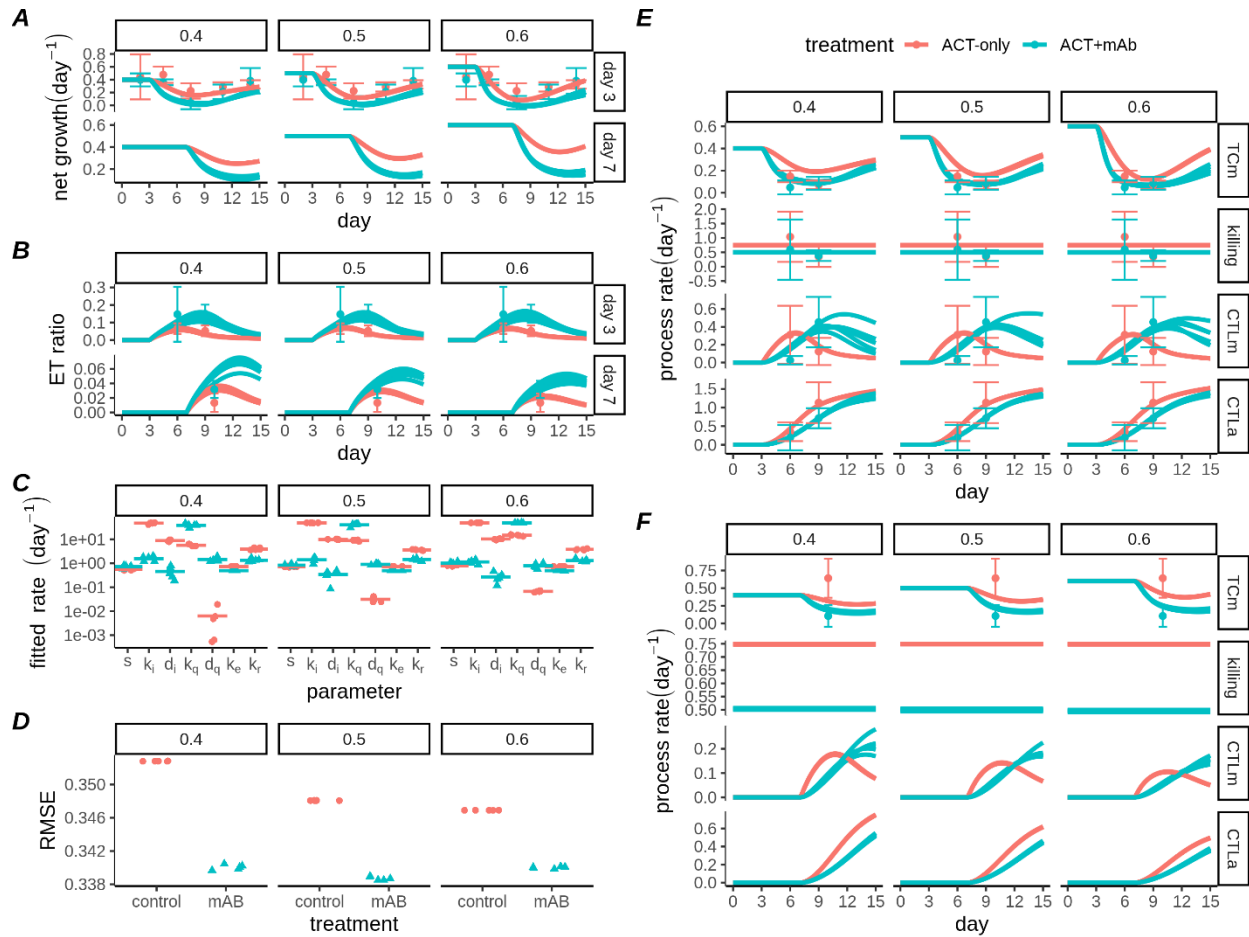
## Supplementary Data



**S1 Fig.** Information content of linear or mass-action CTL killing models. A) Akaike (top 2 rows) or Bayes (bottom 2 rows) information criteria values for either linear or mass-action killing models. For the linear model, the killing intensity is taken to be linearly proportional to the number of CTLs. For the mass-action killing model, the killing intensity is proportional to the product of the number of CTLs and tumour cells at each position. Fits were performed for either all the samples grouped together (rows 1&3), or separately for ACT+mAb and ACT-only treatment conditions (rows 2&4). B-C) Linear killing (B) or mass action killing (C) model fits for all samples grouped together (left columns), or ACT-only (central columns) and ACT+mAb (right columns) fitted separately.



**S2 Fig.** Quantification of CTLs and TC mitosis in day 7 treated data. A-C) Purple dots are the locations of individual CTLs in the first frame, and yellow dots are the locations of mitotic events (only frames 1-30 were counted, = 1 hour). Each image shows all points counted per position, thus A-C are three “max intensity” style views of a single point cloud per position (rows) and mouse (columns), i.e. views of the xy axes (A), yz axes (B) and xz axes (C). XYZ (z=slice) axes are shown with a fixed scaling relative to their length – 0.7 pixels (xy) = 1 μm, 1 slice = 7 μm. All points were determined manually.



**S3 Fig.** Sensitivity of ODE model fitting to the growth rate parameter,  $g$ . For all panels the preset growth rate parameter is indicated by the value across columns. A) Net tumour growth predicted by each of the best fitting parameter sets, for either tumours exposed to ACT on day 3 (top row) or day 7 (bottom row). B) Effector:target ratio predicted by each of the best fitting parameter sets, for either tumours exposed to ACT on day 3 (top row) or day 7 (bottom row). C) Best fitting parameters for the ODE model. Each point represents 1 of 5 fits using the stochastic evolutionary algorithm, and horizontal lines represent the mean fitted parameter for either ACT-only (red) or ACT+mAb (blue) conditions. D) Root Mean Square Error (RMSE) for each fitted parameter set. E-F) Intravital process rates predicted by each of the best fitting parameter sets for tumours exposed to ACT on day 3 (E) or day 7 (F). Process rates considered are: TCm (Tumour Cell mitosis); killing (of tumour cells by CTLs); CTLm (CTL mitosis); CTLa (CTL apoptosis).

# Chapter 5

## Quantification of T cell exhaustion in B16F10 melanoma through mathematical modeling

Richard J Beck<sup>1</sup>, Sander Sloot<sup>1</sup>, Hirokazu Matsushita<sup>2</sup>, Kazuhiro Kakimi<sup>2</sup>, Joost B Beltman<sup>1</sup>

1. Division of Drug Discovery and Safety, Leiden Academic Centre for Drug Research, Leiden University, Leiden, The Netherlands
2. Department of Immunotherapeutics, The University of Tokyo Hospital, Tokyo, Japan

### Abstract

Cytotoxic T Lymphocytes (CTLs) are an important component of the adaptive immune response and have an important role in controlling tumours. Improved understanding of CTL interactions within solid tumours will yield insights of benefit to the development of immunotherapeutic strategies against cancer. CTLs are best known for their ability to lyse antigen presenting targets, however they also secrete cytokines such as interferon- $\gamma$  (IFN- $\gamma$ ), which can inhibit cell cycle progression and thus block proliferation of neighbouring cells. In this study, we take a systems biology approach to compare the importance of cytolytic versus IFN- $\gamma$  mediated cytostatic effects in a murine melanoma model. We integrated measurements of tumour volume, fluorescent imaging data, and transcriptomics data to inform an ordinary differential equation (ODE) model of CTL activities inside the tumour. Our model predicted that the cytotoxic effects of CTLs were very small, and that the cytostatic effects of IFN- $\gamma$  were likely responsible for almost all of the observed difference in tumour growth between the CTL treated versus the untreated tumours. Moreover, our analysis and subsequent modelling revealed that the window of IFN- $\gamma$  production was much shorter than the period of CTLs infiltrating the tumour. This was consistent with the dynamics of delayed upregulation of CTL exhaustion markers TIM-3 and LAG-3 but not with the dynamics of PD-1 and PD-L1. This suggests that within B16F10 melanomas TIM-3 and LAG-3 have a more important role than the PD-1/PD-L1 axis in the development of a dysfunctional CTL phenotype, especially at late stages of anti-tumour T cell responses.

## Introduction

Immunotherapy is an emerging strategy for treatment of cancer, with an ever growing number of immunotherapies having reached clinical trials or been approved already[1]. Blood cancers were amongst the first to be successfully treated with immunotherapy[2]; to date solid tumours have proved more challenging. Despite this, several treatments are already available for solid tumours and many more are under trial[3]. Although there has been some success with immunotherapy so far, there is a pressing need for greater mechanistic understanding of the interactions of immune cells within solid tumours. Such understanding may help expand the scope of immunotherapies to different cancers, identify biomarkers to predict which patients might benefit from immunotherapy[4], optimise the dosing schedule for immunotherapies[5,6], or identify potential combination therapeutic strategies[7]. Mathematical or computational models are a useful tool to develop such understanding, since they can link data from different sources and make quantitative predictions for what we should expect under different conditions.

CD8<sup>+</sup> Cytotoxic T Lymphocytes (CTLs) are a key player in the anti-cancer immune response, and many immunotherapy strategies are focussed on these cells. Two prominent examples are blockade of inhibitory receptors such as PD-1 expressed on CTLs in hopes of “removing the brakes” on the immune response[8,9], or adoptive transfer of engineered (CAR) T Cells[10,11]. Therefore understanding the functioning of CTLs inside tumours is of foundational importance for the rational design of immunotherapies. Secretion of the cytokine IFN- $\gamma$  is a hallmark of activated CTLs, yet due to its pleiotropic effects the exact effects of this cytokine in solid tumours remain poorly understood. Indeed, some have even noted the “paradoxical” role of IFN- $\gamma$  in tumour progression[12], paradoxical in the sense that IFN- $\gamma$  can have both pro-tumour and anti-tumour effects. Amongst the pro-tumour effects, IFN- $\gamma$  can lead to recruitment of suppressive cells such as regulatory T cells or myeloid derived suppressor cells (MDSCs), or can induce expression of immune checkpoint ligands such as PD-L1 on tumour cells[13,14]. Amongst the anti-tumour effects, IFN- $\gamma$  can aid in the recruitment of innate immune effectors, kill tumour cells, or exert antiproliferative effects on tumour cells[15–17].

Here, we focus on the antiproliferative effects IFN- $\gamma$  has on tumour cells. The antiproliferative effects are mediated by inhibitors of cyclin dependent kinases which result in arrest of tumour cells at the G<sub>1</sub> phase of the cell cycle, which has been shown in a variety of cell lines[15–17]. However, IFN- $\gamma$  also has anti-angiogenic effects which may in part explain the reduction in tumour cell proliferation. Previously we have used computational models to demonstrate how an antiproliferative effect mediated by cytokines could have a very potent effect on tumour progression, since through cytokine signalling CTLs can control many tumour cells, thus stalling tumour growth and buying time for killing of tumour cells by CTLs [18,19]. However, in our previous modeling work no direct data linking the proliferation of tumour cells to IFN- $\gamma$  levels inside the tumours was available. Therefore, here we have used data from another study by Matshushita and coworkers where the antiproliferative effects of IFN- $\gamma$  were explicitly explored[15]. In that study, CTLs strongly inhibited B16F10 melanoma tumour growth, but this effect was reversed when adoptive T cell transfer was accompanied by administration of anti-IFN- $\gamma$  antibodies. In



addition, histological analysis of tumours expressing a cell cycle sensor revealed that most cells were arrested in the G<sub>1</sub>-phase after CTL transfer.

In the current study we sought to gain a quantitative understanding of the role of IFN- $\gamma$  mediated antiproliferative effects, hence we specifically quantified how important were the effects of IFN- $\gamma$  in tumour control relative to the canonical killing functions of CTLs. To answer that question, we developed an Ordinary Differential Equation model which integrated data from Matshushita et al.[15] to arrive at a coherent, quantitative description of the intratumoural activities of CTLs and their interactions with the tumour following adoptive transfer. Consistent with our previous study of B16F10 tumours[19], our model predicted that the cytotoxic effects of CTLs were very small, and that the cytostatic effects of IFN- $\gamma$  were responsible for almost all of the observed difference in tumour growth between the CTL treated versus the untreated tumours. Moreover, our analysis and subsequent modelling indicated that the window of IFN- $\gamma$  production was very short, with CTLs losing the ability to produce IFN- $\gamma$  within a few days of CTLs infiltrating the tumour. Markers of CTL exhaustion such as TIM-3 and LAG-3 were still increasing over this period, suggesting that CTLs had become exhausted inside the tumour. In contrast to TIM-3 and LAG-3, the dynamics of PD-1 and PD-L1 did not coincide with the dynamics of CTL exhaustion, suggesting a relatively minor role for these checkpoints as determinants of CTL exhaustion in the B16F10 melanoma model, at least at late stages of anti-tumour immune responses.

## Results

### Presence of CTLs correlates with cell cycle arrest in tumour cells

Previously, the adoptive transfer of CTLs was shown to induce G<sub>1</sub>-phase cell cycle arrest of B16F10 tumour cells in an IFN- $\gamma$  dependent manner[15], however the temporal evolution of this arrested state and correlation with the number of tumour infiltrating CTLs was not explicitly quantified. Therefore, we exploited previously unquantified images from the same study, taken at multiple time points after CTL transfer, to estimate the number of tumour infiltrating CTLs and B16F10 tumour nuclei. Moreover, due to the incorporated Fucci cell cycle sensor it was also possible to discriminate between B16F10 nuclei in the G<sub>1</sub>-phase and nuclei that were in other (S-G<sub>2</sub>-M) phases of the cell cycle. In order to quantify the number of B16F10 nuclei in either the G<sub>1</sub> phase or in the S-G<sub>2</sub>-M phases at different timepoints after CTL transfer, we developed automated pipelines using the ilastik[20] cell density estimation tool (see Methods). Comparison of the ilastik predictions for small subregions of sample images (Fig. 1A) selected across different time points to our own manual counts made for the same images demonstrated that our pipeline was reliable (Fig. 1B). Moreover, our estimated densities of G<sub>1</sub> phase (Fig. 1C) or S-G<sub>2</sub>-M phase (Fig. 1D) on day 3 were comparable to those in the study of Matsushita et. al[15], as were the ratios of cells in G<sub>1</sub>:S-G<sub>2</sub>-M phases (Fig. 1E). The number of CTLs per slide was far more difficult to determine automatically, which was likely due to the irregular morphology of the CTLs and their lack of a visible nucleus. Since the number of CTLs was much lower than the number of B16F10 nuclei, we instead performed a manual count of the number of CTLs across all images (Fig.1F). We found a strong negative correlation between the number of CTLs and the G<sub>1</sub>:S-G<sub>2</sub>-M ratio in the sample images (Fig. 1G), with a Pearson's correlation coefficient of -0.60 (95% confidence

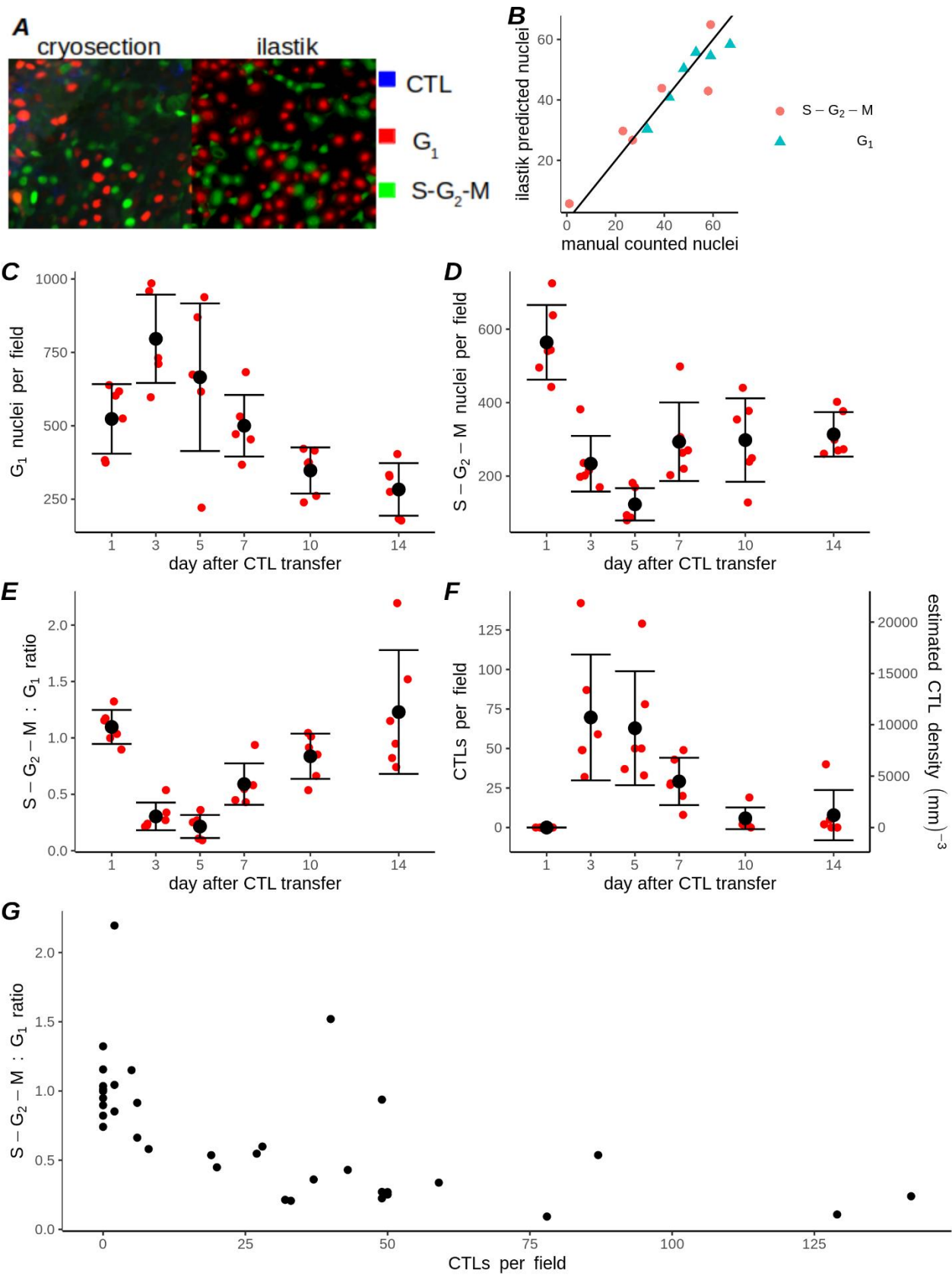


**Figure 1.** (displayed on previous page) Dynamics of tumour cell cycle arrest correlates closely with CTL presence. A) Comparison of cryosection image (left), with probabilities predicted by ilastik (right). G<sub>1</sub> and S-G<sub>2</sub>-M phase nuclei are shown (respectively) in red or green. CTLs appear blue in the cryosection image and were not quantified using ilastik. Image shown is an example of a subregion (175x175µm) of one complete cryosection (750x550µm), which was used for training the classifier. B) Number of nuclei in cryosection subregions used for training the classifier, comparing manually counted (horizontal axis) nuclei with the ilastik estimate (vertical axis). C-D) Results of automated quantification of the number of B16F10 nuclei in the G<sub>1</sub> phase (C) or in the S-G<sub>2</sub>-M phases (D), applied to the full set of cryosection images. E) Ratio of cells in S-G<sub>2</sub>-M:G<sub>1</sub> phases determined from the automated density estimation results (shown in C-D). F) Number of CTLs manually counted in each cryosection. Each small red point in C-F represents the total number of cells counted per cryosection, large black points and error bars are (respectively) mean  $\pm$  standard deviation. G) Comparison of the number of CTLs (horizontal axis) with the tumour cell S-G<sub>2</sub>-M:G<sub>1</sub> ratio (vertical axis) for each available fluorescent image.

interval between -0.7757570 and -0.3289711) allowing us to reject the null hypothesis of no correlation ( $p=0.00015$ ). In summary, the G<sub>1</sub> cell cycle arrest following CTL transfer lasted for up to 5 days and its temporal dynamics were closely linked to the presence of CTLs inside the tumour.

### **Tumour cell cycle arrest correlates with tumour growth reduction**

To check if the temporary G<sub>1</sub> cell cycle arrest was consistent with tumour volume progression, we also incorporated tumour volume measurements into our analysis. An exponential model of tumour growth was sufficient to describe tumour progression over the studied interval (Fig. 2A), i.e. within the observed range of tumour sizes there was not yet any indication for a potential carrying capacity limiting tumour growth. Volume estimates were available from three separate experiments with CTL treatment (Fig. 2B). We noted some minor yet apparent systematic differences between experiments. For instance, almost all volumes recorded on day -1 were larger in one of the biological replicates (compare red and green points in Fig. 2A-B, day -1). Despite these minor discrepancies, the broad pattern of tumour progression was similar across replicates, with substantially arrested growth between days 3-7. Nevertheless, such systematic differences between experiments could potentially distort our results, for example because the switching from 12 mice to 2 mice between measurements going from days 7-10 (Fig. 2B) would artificially introduce a period of tumour growth above even the untreated growth rate into our data. To avoid this issue, we converted the data into estimates of the tumour growth rate between measurement intervals for both the data without CTL transfer (Fig. 2C) and those with CTL transfer (Fig. 2D). For the experiments where CTLs were transferred, this resulted in consistent values between experiments and allowed us to safely incorporate the additional measurements from the 2 mice that were recorded up until day 14. From this analysis, reduced tumour growth was apparent between days 3-7 (Fig. 2D; points centred on days 4 and 6), but growth recovery in the measurement interval between days 7-10 (Fig. 2D; point centred on day 8.5). Therefore the period of tumour growth reduction was coincident with the period of G<sub>1</sub> phase tumour cell cycle arrest (Fig. 1E), and by extension also coincident with the presence of CTLs within the tumour (Fig. 1F).

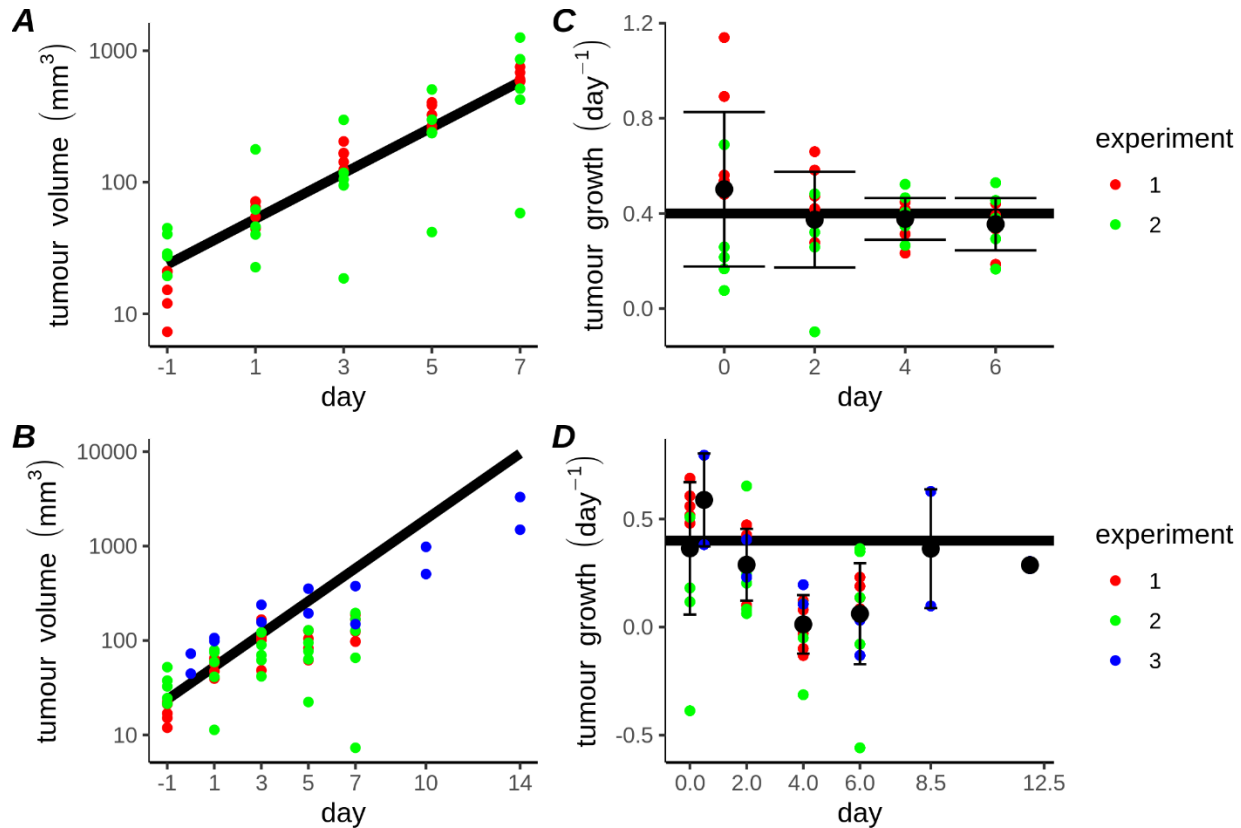


**Figure 2.** Tumour volume dynamics corresponds to G<sub>1</sub> cell cycle arrest and CTL presence. A) Tumour volume progression from 2 different experiments (n=5 mice per experiment) without CTL treatment. B) Tumour volume progression from 3 different experiments (n=5 mice in experiments 1&2, n=2 mice in experiment 3) with CTLs transferred on day 0. C) Untreated tumour growth rate estimates for each mouse taken across each of the measurement intervals shown in A. D) Tumour growth rate estimates for each mouse receiving CTL transfer on day 0. Solid black lines in A-D show results of fitting an exponential growth model ( $g=0.4 \text{ day}^{-1}$ ) to the untreated data (A,C) and are shown alongside CTL treated data (B,D) for comparison. Black points and error bars in C-D represent (respectively) mean  $\pm$  standard deviation of all points. Points in C-D are shown at the midpoint of the interval over which they were estimated. Coloured dots in all panels indicate the independent experiments consisting of multiple mice.

### Loss of IFN- $\gamma$ production precedes loss of CTLs from tumours

IFN- $\gamma$  secreted by CTLs was the putative agent which led to cell cycle arrest and the transient reduction of tumour progression in our studied data[15]. As a proxy for IFN- $\gamma$  levels inside the tumour we used mRNA expression data recorded within the same experiments as the previously analysed image (Fig. 1) and volume progression data (Fig. 2). We found that Cd8a transcription dynamics (Fig.3A row 1) matched the CTL dynamics measured in the images (Fig. 1F), indicating agreement between the transcriptomics data and the imaging data with respect to CTL abundance. However, the dynamics of IFN- $\gamma$  transcription appeared much different to those of the CTLs (Fig.3A, row 2). IFN- $\gamma$  transcription peaked sharply on day 3 after CTL transfer, but had dropped sharply by day 5 and returned to basal levels on day 7, when CTLs still remained inside the tumour. To verify the dynamics of IFN- $\gamma$ , we also checked Stat1 and Socs1 (Fig 3A, rows 3-

4) which are downstream of the IFN- $\gamma$  receptor[21] in the IFN- $\gamma$  signalling pathway. These followed very similar dynamics to IFN- $\gamma$  mRNA, lending support to the idea that the IFN- $\gamma$  mRNA expression data was a suitable proxy for IFN- $\gamma$  signalling dynamics inside the tumour.

We hypothesized that the difference in dynamics between CTLs and IFN- $\gamma$  transcription was due to a gradual CTL exhaustion inside the tumour, leading to a loss of their effector functions. Exhausted T Cells display hierarchical loss of effector functions including secretion of cytokines such as proliferative ability, capacity to kill target cells, and secretion of IFN- $\gamma$ [22,23]. Several genes are associated with the exhausted T Cell state[24,25], and as T Cells become progressively more exhausted they express a greater diversity of inhibitory receptors[23]. Indeed, we could identify transcripts for a number of well described immune checkpoint molecules in the mRNA dataset, including PD1, its ligand PD-L1, LAG-3, and TIM-3 (Fig. 3B). Overall, our analysis suggests that the pulse of IFN- $\gamma$  transcription remains brief despite CTLs still being present within the tumour and is due to development of an exhausted phenotype amongst the transferred CTLs.

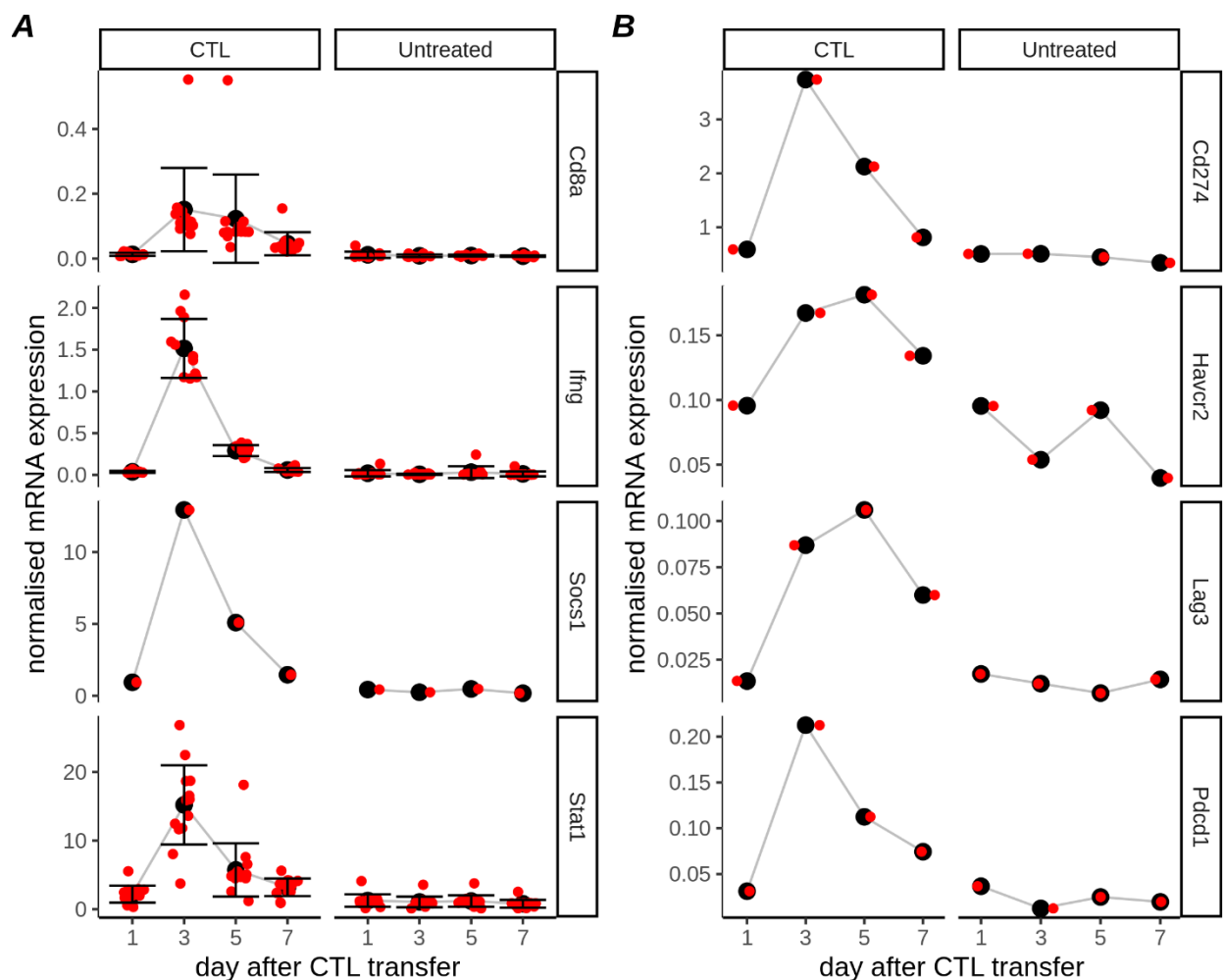


**Figure 3.** Dynamics of selected genes from microarray dataset. A) Comparison of dynamics of probes specific for Cd8a (row1), Ifng (row 2), Socs1 (row 3), or Stat1 (row 4) between CTL treated and untreated mice (across columns). Black points and error bars in A represent (respectively) mean  $\pm$  s.d for all probes

at a given time point. B) Comparison of dynamics of probes specific for mRNA coding PD-1 (Pdc1) and PD-L1 (Cd274), TIM-3 (Havcr2) and LAG-3 (Lag3) (along rows), between CTL treated and untreated mice (across columns). Red points in A-B represent expression values after normalisation at the 75th percentile.

## IFN- $\gamma$ transcription dynamics are compatible with G<sub>1</sub> phase tumour cell cycle arrest

Due to the early reduction in IFN- $\gamma$  signalling, it is unclear whether IFN- $\gamma$  can be entirely responsible for the G<sub>1</sub> phase tumour cell cycle arrest which followed highly similar dynamics to the CTLs. To test the compatibility of the IFN- $\gamma$  transcription data with the dynamics of the CTLs and the tumour cell cycle dynamics, we developed an ODE model. Our ODE model describing the interactions between CTLs and the tumour (Fig. 4A) features an explicit description of the cell cycle of tumour cells, in which they cycle from G<sub>1</sub> phase into S-G<sub>2</sub>-M phases at rate  $k_{gs}$ , and then back into G<sub>1</sub> phase at rate  $k_{sg}$ . The model also features CTLs which kill tumour cells at rate  $k_e$  and produce IFN- $\gamma$ , which precludes tumour cells from transferring from G<sub>1</sub> phase to S phase. The sensitivity of tumour cell cycle arrest to IFN- $\gamma$  is determined by the parameter  $k_i$ . To test the contribution of the two CTL effector functions to tumour control (i.e., killing and antiproliferative effect), we linearly interpolated between the experimental data for the number of CTLs (Fig. 4B) and for IFN- $\gamma$  expression (Fig. 4C), and used these interpolations directly as inputs to our model. Subsequently, we tested different combinations of the parameters  $k_e$  and  $k_i$  (Fig. 4D) to find the best fit to the tumour growth rate (Fig. 4E, red line) and the S-G<sub>2</sub>-M : G<sub>1</sub> ratios (Fig. 4F, red line) determined from the experimental data. Our best fitting parameter set (Fig. 4D; marked with black circle) had a value of  $k_e=1$  (CTL<sup>-1</sup> day<sup>-1</sup>) although other values for  $k_e$  in the range 0-3 (CTL<sup>-1</sup> day<sup>-1</sup>) led to relatively low errors, consistent with killing rates we have previously estimated for CTLs against B16F10 melanoma tumours[19]. The best fitting value for the antiproliferative effect ( $k_i=8.5$  IFN<sup>-1</sup> mm<sup>3</sup>) led to sharp reductions in the transition rate of tumour cells out of the G<sub>1</sub> phase for the IFN- $\gamma$  expression levels found in our data (Fig. 4G). At the peak of IFN- $\gamma$  expression on day 3, the transition rate from G<sub>1</sub> to S-G<sub>2</sub>-M phases ( $k_{gs}$ ) was reduced to 7% of its original value, and even at the lower IFN- $\gamma$  expression levels measured on other days  $k_{gs}$  was significantly reduced (Figs. 4C, 4G; dashed lines). Thus our best fitting parameters implied that cycling tumour cells are sensitive to IFN- $\gamma$  even at low expression levels. When we took the best fitting parameters and disabled killing by setting  $k_e=0$  (Fig. 4D; marked with black square), most of the tumour growth reduction was preserved (Fig. 4E, blue dashed line). In contrast, taking our best fitting parameters and disabling the antiproliferative effect of IFN- $\gamma$  (Fig. 4D; marked with triangle) resulted in only a very small reduction in the net growth rate of the tumours (Fig. 4E, green dashed line). Overall, these results support our previous analysis showing that an antiproliferative effect of IFN- $\gamma$  is more important than CTL cytotoxicity to control B16F10 tumours[19]. Moreover, these results show that the dynamics of IFN- $\gamma$  are compatible with the dynamics of the tumour cell cycle arrest, despite the apparently short duration of IFN- $\gamma$  production.

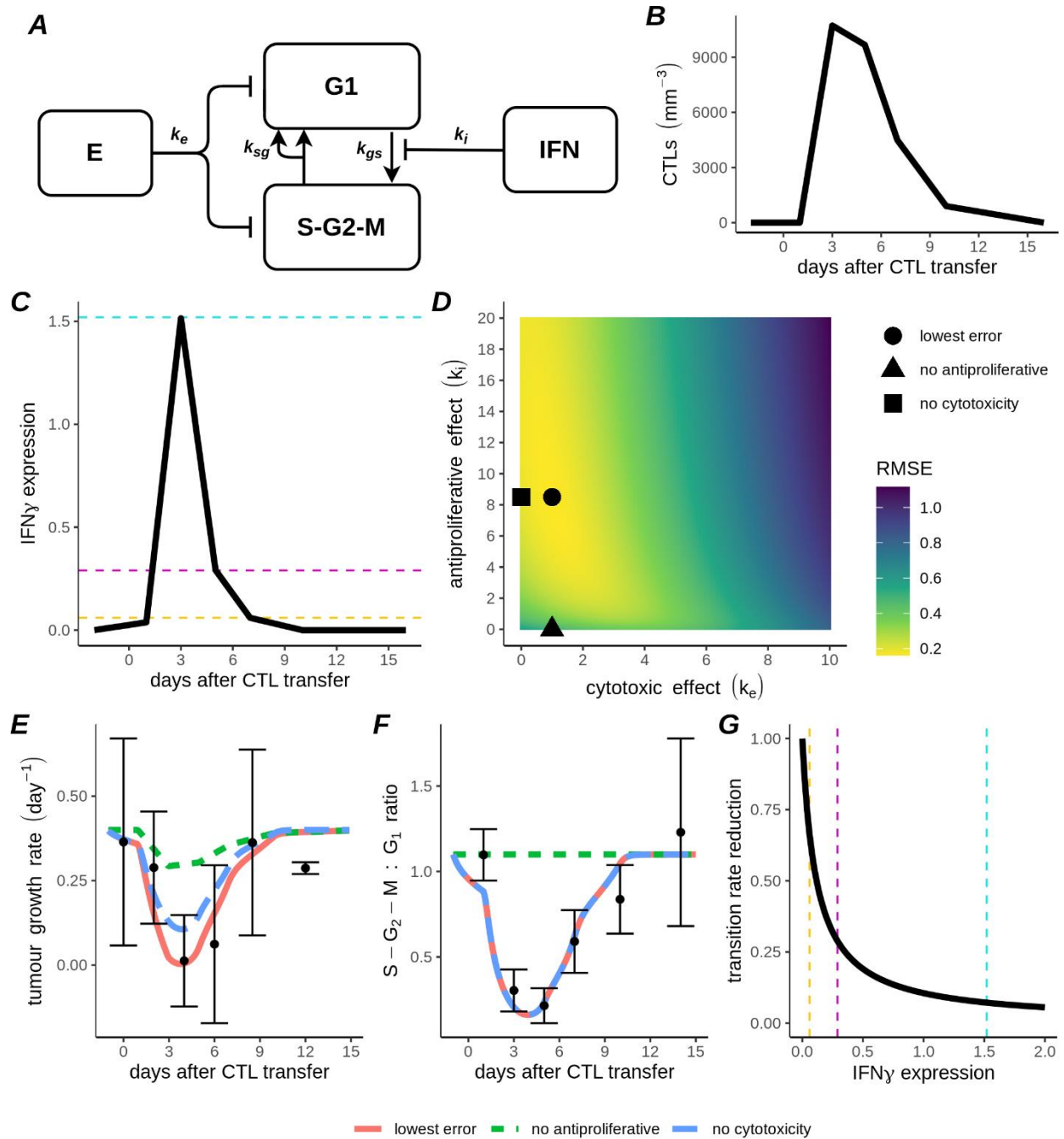


**Figure 4.** Compatibility of IFN- $\gamma$  transcription dynamics with tumour cell cycle arrest. A) Schematic for ODE model to compare CTL killing and IFN- $\gamma$  mediated antiproliferative effect in B16F10 melanoma. B-C) Linear interpolation of mean CTL density (B) and mean IFN- $\gamma$  expression (C). D) Heatmap showing root-mean-square error (RMSE) for different combinations of the CTL killing rate parameter ( $k_e$ ) and the parameter controlling the sensitivity of cell-cycle arrest to IFN- $\gamma$  ( $k_i$ ). E-F) Predictions for tumour growth rate (E) and ratio of tumour cells in S-G<sub>2</sub>-M : G<sub>1</sub> states (F) for the combination of parameters with the lowest RMSE (solid red line). In addition, simulations are shown with either the best fitting  $k_i$  parameter and  $k_e=0$  (blue long dashed line), or with the best fitting  $k_e$  parameter and  $k_i=0$  (green short dashed line). G) Fractional reduction in transition rate from G<sub>1</sub> to S-G<sub>2</sub>-M phase with varying IFN- $\gamma$  expression levels, for the best-fitting

parameter value  $k_i=8.5 \text{ IFN}^{-1} \text{ mm}^3$ . Dashed lines in C and G highlight the predicted reduction in transition rate from  $G_1$  to S-G<sub>2</sub>-M phase for the mean IFN- $\gamma$  expression levels measured on days 3 (cyan), 5 (magenta) and 7 (yellow).

## CTL exhaustion quantitatively explains IFN- $\gamma$ transcription dynamics

In order to explain the dynamics of CTLs and IFN- $\gamma$  and to quantify the importance of different immune checkpoints in these dynamics, we extended our ODE model (Fig. 5A). In this extended model, CTLs infiltrate the tumour at a basal rate  $s_0$ , expand within the tumour at rate  $s_e$ , and die with rate  $d_e$ . In addition to their killing of tumour cells, CTLs inside the tumour produce IFN- $\gamma$ . Finally our model includes the immune checkpoints LAG-3, TIM-3, PD1, and its ligand PDL1, which decrease the activity of CTLs (see Methods). We fit this ODE model simultaneously to all the experimental data discussed in Figures 1-3, using Min-Max feature scaling to surmount the issue of comparing measurements from different modalities (see Methods), which resulted in an excellent model fit (Fig. 5B-C, magenta lines). Importantly, without using any checkpoints, we could not obtain a good fit to any of the experimental measurements (Fig. 5B, red lines), demonstrating that T cell exhaustion is required to explain the T cell anti-tumour response.

In order to identify which of the identified immune checkpoint (IC) molecules is the most important determinant of the exhausted CTL state in the *in vivo* experimental setting with B16F10 tumours, we tried fitting our model with each IC separately. Including only PD1-PDL1 as an inhibitor (green lines; Fig. 5B-C), the fits improved compared to our model with no ICs, however we were still not able to achieve a good fit to the number of CTLs counted inside the tumour, nor to the dynamics of PD-1 and PD-L1 themselves. We achieved equally good fits with LAG-3 (Fig 5B-C, dark blue lines), with TIM-3 (Fig. 5B-C, cyan lines), and with the combination model including all checkpoints together (Fig 5B-C, magenta lines). Note that these model variants gave similar predictions to the simplified model, where CTLs and IFN- $\gamma$  were used as inputs to the model, in terms of the relative importance of cytotoxic effects versus antiproliferative effects (Fig. S1). We also examined the dynamics of the exhausted state, comparing the level of exhaustion for each inhibitor (Fig. 5D). When fit individually, exhaustion due to LAG-3 increased throughout the simulated period (Fig. 5D, row 1); for TIM-3, exhaustion (Fig. 5D, row 3) increased and then remained constant from day 5 until the end of the simulated period; and for PD-1/PD-L1, exhaustion peaked on day 5 and then declined afterwards (Fig. 5D, row 2). We also investigated how much the individual ICs contributed to the evolution of CTL exhaustedness for models fit with all inhibitors simultaneously, which resulted in similar exhaustion dynamics for each IC as when they were fit individually (Fig. 5E). However, the relative contributions of each individual inhibitor to the overall exhausted state was clearly different. For the best fitting parameter set (Fig. 5E, row 1), the contributions of TIM-3 and PD-1/PD-L1 towards exhaustion became negligible compared to that of LAG-3, which we verified by removing each IC individually from this best fitting parameter set (Fig. 5F, column 1). Compared to the situation with all ICs in place the model dynamics were virtually unaffected by knockout of PD-1/PD-L1 or TIM-3, whilst knockout of LAG-3 completely disrupted the model dynamics.



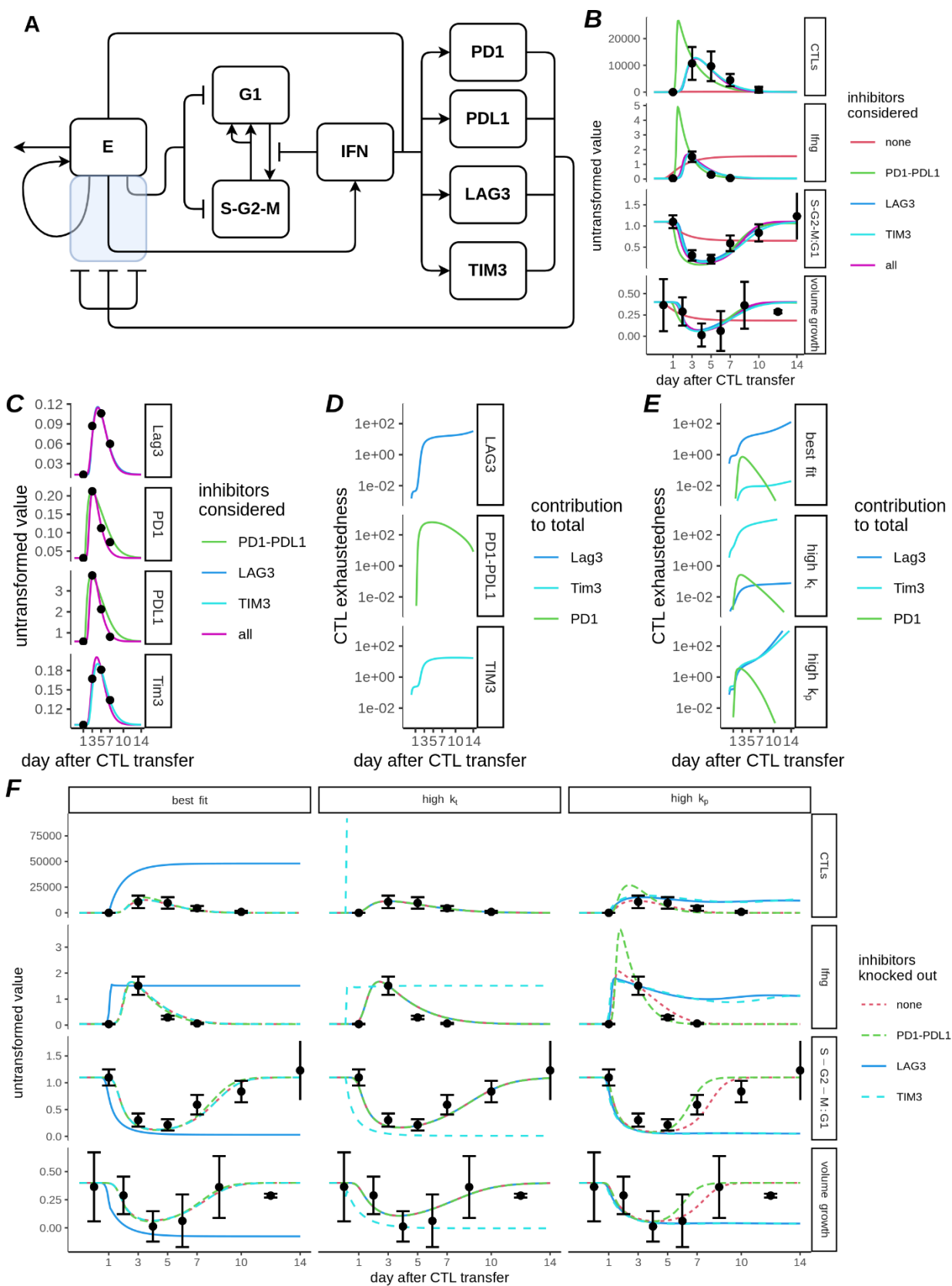


**Figure 5.** (displayed on previous page) Early cessation of IFN- $\gamma$  is quantitatively compatible with the development of CTL exhaustion. A) Schematic for ODE model of CTLs versus B16F10 melanoma. Pointed arrows represent a positive effect (i.e. transfer, production, recruitment), whilst flat-headed arrows represent an inhibiting effect. CTL functions that are reduced due to CTL exhaustion are represented by lines passing through the translucent blue box. B) Model fits to CTL density (top row), IFN- $\gamma$  mRNA expression (2nd row), ratio of S-G<sub>2</sub>-M:G<sub>1</sub> nuclei (3rd row), or volumetric tumour growth (bottom row). C) Model fit to ICs for each considered combination of ICs used for fitting the model. Different ICs are shown in each row as indicated by facet label. Colored lines in B-C represent model output, and model fits with different ICs are indicated by colour. D) CTL exhaustion level, when individual ICs were used to fit the model (as indicated in rows). Different coloured lines are the contribution for each term in Eq. 11 (see Methods), i.e: dark blue -  $k_L L/E$ ; cyan -  $k_H H/E$ ; green -  $k_p(P/E)(P_L V/V_0)$ . E) Contribution of different ICs to CTL exhaustion level, when all ICs were used to fit the model. Shown are results from the best fitting parameter set (top row), and two selected parameter sets with the highest contributions towards exhaustion from TIM-3 (middle row) or from PD-1/PD-L1 (bottom row). F) Results of knocking out individual inhibitors (as indicated by color and linetype) when all inhibitors were initially included in the fit: for either the best fitting model (column 1), the model with highest contribution from TIM-3 (column 2), or the model with highest contribution from PD-1/PD-L1 (column 3). In all panels, points and error bars represent (respectively) mean  $\pm$  s.d. of experimental data used to fit the model, and lines represent model simulations. Parameter values for best fitting models are given in Table 1.

Since our fitting procedure generated a range of parameter sets, we checked whether any of the other generated parameter sets might permit a larger role for TIM-3 or PD-1/PD-L1. To this end we selected the best fitting 20% of parameter sets amongst the final generation of our evolutionary algorithm, all of which resulted in reasonably good fits to the experimental data (Fig. S2). From this subset, we selected the parameter sets with either the highest value of  $k_L$  relative to the other exhaustion parameters or the highest relative value of  $k_p$ , i.e. the parameters which (respectively) controlled the contribution of TIM-3 and PD-1/PD-L1 towards exhaustion. The parameter set with a high value for  $k_L$  resulted in development of an exhausted state that was dominated by the contribution of TIM-3 (Fig. 5E, row 2), and knockout of TIM-3 in this model completely disrupted model dynamics (Fig. 5F, column 2). This supports the result from the individual fits because it shows that TIM-3, similarly to LAG-3, correlates well with the exhausted CTL state. The parameter set with a high value for  $k_p$  resulted in development of an exhausted state that had initially approximately equal contributions from all ICs, before PD-1/PD-L1 dropped and LAG-3 and TIM-3 took over the role as determinants of exhaustion (Fig. 5E, row 3). There, knockout of any of the ICs disrupted the dynamics of the model, although PD1/PD-L1 knockout led to disruption of early dynamics and LAG-3 or TIM-3 knockout to disruption of late dynamics (Fig. 5F, column 3). Overall, these results show that the brief window of IFN- $\gamma$  production is quantitatively consistent with development of an exhausted state amongst CTLs, and that expression of the immune checkpoint molecules LAG-3 and TIM-3 correlate best with the development of this exhausted state. Our analysis suggests that of the three ICs considered, PD-1/PD-L1 is the least important determinant of the exhausted CTL state, however our model remains compatible with PD-1/PD-L1 playing a role in CTL exhaustion at early time points after CTL infiltration of the tumour.

## Discussion

In a previous study on which our work was built, Matsushita et. al. found that tumour control of B16F10 melanoma by CTLs was mediated by a combination of cytotoxic and cytostatic effects, with the cytostatic effects being due to IFN- $\gamma$  mediated cell cycle arrest of the melanoma cells[15]. However, the progression of cytostatic and antiproliferative effects over time was not explicitly explored. Here, we analysed image data, tumour volume measurements, and transcriptomics data from the study by Matsushita et. al[15], using data acquired at multiple timepoints after CTL transfer. We found that the presence of CTLs inside the tumour strongly correlated with tumour cell cycle arrest, as well as with the inhibition of volumetric tumour growth. However, IFN- $\gamma$  signalling within the tumours followed early dynamics, with CTLs primarily producing IFN- $\gamma$  early after arrival in the tumours. Since the loss of IFN- $\gamma$  preceded the recovery of tumour cell proliferation, it was unclear whether IFN- $\gamma$  signalling could completely account for the observed tumour cell cycle arrest, and what role T cell exhaustion had in these processes. Therefore, we developed an ODE model to describe tumour growth, CTL infiltration, CTL production of IFN- $\gamma$  and subsequent interference with cell cycle progression, and also killing of tumour cells by CTLs. Using this model we were able to describe all the experimental data, which led us to conclude that IFN- $\gamma$  mediated tumour cell cycle arrest, together with killing of tumour cells by CTLs, were sufficient mechanisms to account for the experimental data. We also used our models to compare the contribution of CTL mediated cytotoxic or cytostatic effects towards tumour control. Our model predicted CTL killing rates ( $k_e$ ) between 0-3 CTL<sup>-1</sup> day<sup>-1</sup>, which resulted in only a minor contribution of CTL killing towards tumour control compared to the IFN- $\gamma$  mediated cell cycle arrest, consistent with our findings from a B16F10 tumour we have previously analysed[19].

As part of our study, we developed a model describing the dynamics and effector functions of tumour infiltrating CTLs. Based on mRNA expression data, IFN- $\gamma$  transcription peaked on day 3, had fallen sharply by day 5, and was virtually zero on day 7. This was in contrast to the number of CTLs which remained present in similar numbers on days 3 and 5, and were still observable in reasonable numbers at late time points. Therefore, our model required inclusion of the development of CTL exhaustion in order to account for this loss in ability to produce IFN- $\gamma$ . CTL exhaustion is identified by a progressive increase in the number and diversity of inhibitory receptors expressed by CTLs[23,26,27]. We identified four well known inhibitory molecules amongst the available transcriptomics data: LAG-3, TIM-3, PD-1, and the PD-1 ligand PD-L1. With our model we were able to obtain good fits if the exhausted state was correlated with TIM-3 or LAG-3, but not with PD-1/PD-L1, which was due to the early peak of PD-1 and PD-L1 transcription that was already well in decline on day 5 whilst CTL numbers in the tumour remained high. This early peak was not compatible with the idea that CTLs were becoming gradually more exhausted over time. On the other hand, LAG-3 and TIM-3 increased relative to the CTLs over time and therefore correlated most with the loss of IFN- $\gamma$  transcription. Consistent with our model prediction, LAG-3 and TIM-3 have been previously shown to have high correlation with dysfunctional “exhausted” phenotype in CD8<sup>+</sup> CTLs in melanoma[24]. Our model was not compatible with the dynamics of PD-1/PD-L1 as sole correlates of the exhausted state, which appears at first sight to contradict reports indicating that PD-1/PD-L1 signalling is relevant for immunosuppression in melanoma[28,29], although our result agrees with others showing the

B16F10 cell line in particular may be resistant to PD-1 antagonist monotherapy[30,31] . Since our model was compatible with PD-1/PD-L1 signalling making a partial contribution to CTL exhaustion at early time points, it may be that PD-L1/PD-1 plays only an initial role in immune suppression and that this role is taken over later by other checkpoints, which is consistent with findings that blockade of LAG-3 as well as PD-1 receptors is required to prevent relapse in melanoma[28]. One caveat for the data employed to fit our model is that only one probe was available per checkpoint. Therefore future experiments should confirm the dynamics of the expression of these immune checkpoint molecules and further investigate their contribution to T cell exhaustion.

Our model implies that the reduced activity of CTLs and in particular the apparent reduction in IFN- $\gamma$  which preceded the disappearance of CTLs in the tumour by several days, could be explained by the development of an exhausted phenotype in the tumour infiltrating CTLs. Moreover, in our model IFN- $\gamma$  played an important role in driving this exhausted phenotype. For exhaustion related to the PD-L1/PD-1 axis, this is clearly justified, because IFN- $\gamma$  can induce upregulation of PD-L1 on tumour cells[13]. Moreover, IFN- $\gamma$  induces increased antigen presentation on tumour cells[12], which should lead to increased stimulation of CTLs via their T cell receptors. This could explain the contribution of IFN- $\gamma$  towards upregulation of the other immune checkpoints included in our model, which are more commonly associated with excessive and prolonged exposure to antigen[27]. In order to further study the dynamics of the CTL population in the tumour it would be useful to perform a second transfer of CTLs, which may help elucidate the extent to which the mechanisms of decline in CTL function are due to transferred CTLs becoming exhausted (and therefore a second transfer of “fresh” CTLs should result in similar anti-tumour effects) or are due to resistive mechanisms deployed by the tumour (in which case a second transfer of CTLs would be expected to provide only limited benefit).

Our study was limited by a lack of direct data concerning several important aspects of the CTL dynamics within the tumour. First, we had no direct data on the killing rate ( $k_e$ ) of the CTLs inside the tumour, so this parameter was allowed to vary freely during the fitting process. Depending on which immune checkpoint molecules were included in the fitting process, we recovered a range of different values for  $k_e$ , although these parameters were all plausible and comparable with other values for the killing rate of tumour cells by CTLs *in vivo* reported elsewhere[32], including that for attack of B16F10 cells[19]. Importantly, however, the choice of immune checkpoint molecules and the resultant values of  $k_e$  did not impact our conclusion that IFN- $\gamma$  mediated cell cycle arrest was the main determinant of tumour control. A second limitation surrounds our model of CTL exhaustion inside the tumours. Two specific questions we could not address due to the whole-tumour microarray data we used were: 1) which cells were expressing inhibitory molecules and 2) whether our results would have been different had we included ‘missing’ relevant molecules from the transcriptomics data, e.g. the immune checkpoint CTLA-4. Unbiased gene expression data generated at the single cell level, using single cell RNA-Seq techniques, would therefore be interesting to incorporate into similar modelling strategies in future. A third limitation is the possible presence of other tumour infiltrating cells, such as MDSCs which are recruited to B16F10 tumours after adoptive transfer of CTLs and exert suppressive effects on the tumour infiltrating CTLs[33]. The frequency of various immune cell types can be inferred from either single cell, or bulk transcriptomic data using computational methods[34], and it would be interesting to extend our modelling approach to include other relevant immune cells using such methods in future.

In our analysis, we used mRNA expression as a substitute for protein expression. Previous studies report that mRNA levels are substantially predictive of protein expression levels[35,36]. Moreover, although some delay should be expected between mRNA expression and protein expression, this delay has been estimated to last for only a few hours[36] and thus should not have a significant impact on our data, which consists of measurements made across several days. For the *in vivo* setting we studied, the rapid decline in the S-G<sub>2</sub>-M : G<sub>1</sub> ratio after transfer of CTLs indeed suggests that protein expression rapidly follows mRNA expression. Conversely, the S-G<sub>2</sub>-M : G<sub>1</sub> ratio does not appear to recover immediately upon downregulation of IFN- $\gamma$  mRNA. One explanation could be that the effect of IFN- $\gamma$  lasts longer than the protein due to downstream signaling. Another is that tumour cells are very sensitive to low levels of IFN- $\gamma$ , therefore the effect could persist even after IFN- $\gamma$  synthesis has substantially declined. The latter explanation seems to be in line with a study which found that bystander sensing of IFN- $\gamma$  could occur at distances of over 40 cell lengths[13], implying high sensitivity of tumour cells to this cytokine.

In summary, we have presented a mathematical model that can successfully predict inhibition of tumour growth following adoptive T cell transfer. We used this model to quantify the contribution of IFN- $\gamma$  and cytotoxicity to the antitumour activity of CTLs, which led to the conclusion that IFN- $\gamma$  contributes most to tumour growth blockade by CTLs. Our model also includes anti-tumourigenic (antiproliferative, enhancing recruitment of CTLs) and pro-tumourigenic (driver of CTL exhaustion) effects of IFN- $\gamma$ . The presence of opposing effects of IFN- $\gamma$  have led to descriptions of an “IFN- $\gamma$  paradox”[12]. Our model, by including these different effects associated with IFN- $\gamma$ , can serve as a quantitative baseline to be augmented in future, and may help guide further experimental work.

## Methods

### Data Summary

For the development of the mathematical model, data from the paper by Matsushita et al.[15] were used. In brief, the experimental protocol in that previous study involved inoculation with  $10^7$  B16F10 melanoma cells into C57BL/6 mice, followed 9 days later by adoptive transfer of  $10^6$  activated pmel-1 transgenic T cells recognising the gp100 peptide (note that throughout the current study, the day of CTL transfer is designated “day 0”). The data included measurements of tumour volume from experiments in mice either with or without subsequent adoptive transfer of CTLs. From the same experiments we also used fluorescence microscope images of cryosections of B16F10 tumours expressing the fucci cell cycle sensor, taken on days 1,3,5,7,10 & 14 following CTL transfer. Finally, the data set included microarray RNA expression data from B16F10 tumours at days 1, 3, 5 & 7 after CTL transfer.

### Image analysis

Automated estimates of the number of G<sub>1</sub> or S-G<sub>2</sub>-M phase nuclei were produced using the ilastik (version 1.1.3) cell density estimation tool. Training and classification was performed using merged (RGB) images. For training the classifier we selected subregions ( $100\text{--}200\mu\text{m}^2$ ) from the larger ( $750\times 550\mu\text{m}$ ) cryosections. One subregion was selected from each available time point to

ensure a representative training set. Pipelines for different nuclei ( $G_1$  or S- $G_2$ -M ) were trained separately. Training was performed by manually labelling training images until the classifier estimated numbers of cells achieved a satisfactory match with manual counts for the same data.

## Analysis of gene expression data

Microarray data were downloaded from the Gene Expression Omnibus (GEO) database (series GSE57304; samples GSM1379331– GSM1379344). These data correspond to the same set of experiments as the image and tumour volume progression data we have used, and the methodology for acquisition of these data has been described previously[15]. Briefly, tumour tissues from mice were harvested on different days (1,3,5,7) after CTL transfer, or on the same days in the untreated (without CTLs) condition. Each sample contained 500ng of pooled RNA from 3-4 different tumours, and microarray analysis was performed with 45,018 probes to quantify expression levels of the targeted genes. We performed similar data processing steps to the original publication: probes were discarded when their `glbWellAboveBG` flag was zero at all samples, and we normalised different samples at the 75th percentile.

## Basic ODE Model

We developed an ODE model to describe the intratumoral activities of the transferred CTLs. The basic model of tumour growth (in the absence of CTLs) considers two possible states for alive tumour cells: they can be either in the  $G_1$  phase of the cell cycle (denoted in the equation as  $G$ ), or else in the S,  $G_2$ , or M phase (together denoted  $S$  in the model equations). The reason for choosing these states as explicit model variables was because the Fucci cell cycle reporter used in the experiments, which our model is based upon, could distinguish only between  $G_1$  or S- $G_2$ -M phases. Cells move from the  $G_1$  state into the S- $G_2$ -M state at rate  $k_{gs}$ , and leave the S- $G_2$ -M state at rate  $k_{sg}$  (Eq. 1):

$$\frac{dS}{dt} = k_{gs}G - k_{sg}S. \quad \text{Eq 1}$$

The S- $G_2$ -M state concludes when a tumour cell undergoes mitosis. To include this increase in tumour cells in our model, we consider that for every cell which leaves the S- $G_2$ -M state, two cells enter the  $G_1$  state (Eq 2):

$$\frac{dG}{dt} = -k_{gs}G + 2k_{sg}S. \quad \text{Eq 2}$$

The resulting tumours grow exponentially when the ratio of cells in  $G$  and  $S$  states is at its steady state value. When CTLs ( $E$ ) are introduced into the tumours, our basal model of tumour growth (Eq's 1-2) is modified to include two possible effects CTLs can have on the tumour. The first of these effects is direct killing of tumour cells, which occurs with a constant rate  $k_e$  (per CTL). As

we have done previously[18,19], we take the total killing activity of CTLs to be directly proportional to the number of CTLs inside the tumour, such that the total killing activity of the CTLs is given by  $\alpha k_e E$  (note that  $\alpha$  is a scalar used to modify the effector functions of CTLs if their activity is reduced due to being exhausted: see Eq's 7-12). We consider that killing is directed equally towards cells in  $G_1$  or S-G<sub>2</sub>-M phases, so that the fraction of tumour cells in either state (i.e.  $G (S + G)^{-1}$  or  $S (S + G)^{-1}$ , respectively) determines the fraction of the total killing activity that each subset of tumour cells receives.

The second effect that CTLs can have on the tumour is an antiproliferative effect, mediated by IFN- $\gamma$ , which results in an arrest of the cell cycle in the  $G_1$  phase. To include this effect in our model we reduce the transition of cells out of the  $G_1$  phase by scaling with the term  $(1 + k_i I / V)^{-1}$ . Here, the variable  $I$  represents the total quantity of IFN- $\gamma$  inside the tumour and  $V$  is the variable representing tumour volume. Thus, the term  $I / V$  represents the concentration of IFN- $\gamma$  inside the tumours, and  $k_i$  determines the concentration dependence of the IFN- $\gamma$  dependent reduction in the rate at which tumour cells can leave the  $G_1$  phase. The equations to describe the evolution of the number of tumour cells in  $G_1$  or S-G<sub>2</sub>-M phases become:

$$\frac{dS}{dt} = k_{gs} G (1 + k_i I / V)^{-1} - k_{sg} S - \alpha k_e E S (S + G)^{-1}, \quad \text{Eq 3}$$

$$\frac{dG}{dt} = -k_{gs} G (1 + k_i I / V)^{-1} + 2k_{sg} \cdot S - \alpha k_e E G (S + G)^{-1}. \quad \text{Eq 4}$$

To test the compatibility of IFN- $\gamma$  transcription dynamics with  $G_1$  tumour cell cycle arrest Eq's 3-4 were used directly.  $I$  and  $E$  were estimated by linearly interpolating between the mean of the experimental data at each available time point, and these linear interpolations were used as inputs to the model.

### ODE Model with CTL dynamics

To describe the dynamics of the CTL population and their production of IFN- $\gamma$ , we extended our basic ODE model with further equations. We consider that after transfer, CTLs would begin to arrive in any given region of the tumour at a constant rate  $s_0$ . We take a constant rate of CTL arrival per unit volume of tumour, hence the rate at which CTLs can find the tumour scales with tumour volume. Moreover, we consider that CTLs expand within the tumour at rate  $s_e$ , and die at a constant rate,  $d_E$ . CTL expansion inside the tumour is also reduced according to the level of CTL exhaustion ( $\alpha$ ). Thus, CTL dynamics is described by the following equation:

$$\frac{dE}{dt} = s_0 V + \alpha s_e E - d_E E. \quad \text{Eq 5}$$

We consider CTLs to be the major source of IFN- $\gamma$  inside the tumours, therefore IFN- $\gamma$  production is proportional to the number of CTLs, but is reduced according to their level of exhaustion ( $\alpha$ ), and IFN- $\gamma$  disappears from the system with a rate  $d_i$ :

$$\frac{dI}{dt} = \alpha E - d_i I. \quad \text{Eq 6}$$

Finally, we include a mechanism whereby CTLs become exhausted inside the tumour. T cell exhaustion is characterised by a loss of effector functions along with a progressive increase in the amount and diversity of inhibitory receptors expressed by T cells[23,26,27]. We used the well described PD1, PD-L1, LAG-3 & TIM-3 inhibitory molecules as indicators of exhausted T cells[24], which in our model appear with variable names P, P<sub>L</sub>, L, and H (respectively):

$$\frac{dP}{dt} = E(1 + k_A I/V) - d_p P, \quad \text{Eq 7}$$

$$\frac{dP_L}{dt} = E(1 + k_A I/V) - d_{pl} P_L, \quad \text{Eq 8}$$

$$\frac{dL}{dt} = E(1 + k_A I/V) - d_l L, \quad \text{Eq 9}$$

$$\frac{dH}{dt} = E(1 + k_A I/V) - d_t H. \quad \text{Eq 10}$$

We tested several model variants, one with no immune checkpoints, three in which we consider one checkpoint at a time, and one considering all checkpoints simultaneously. All inhibitory molecules follow similar dynamics, increasing in proportion to the number of CTLs inside the tumour and disappearing from the system with different rate constants  $d_p, d_{pl}, d_l$ , and  $d_t$  (respectively). Production is increased proportional to the term  $(1 + k_A I/V)$ , which allows for a contribution of IFN- $\gamma$  to the exhausted state. Note that the IFN- $\gamma$  induction of exhaustion may be direct or indirect, e.g. by increasing antigenicity of tumour cells and thereby increasing stimulation of T cells via the T cell receptor. In our model, we consider PD1, LAG-3, and HAVCR2 as expressed on the membrane of CTLs, so the ratio of each of these checkpoint molecules to the number of CTLs determines the overall level of exhaustion of the CTLs in our model. PDL1 is modelled differently, being a ligand for the PD1 receptor, and the concentration of PDL1 in our model is multiplied together with the membrane density of PD1 expressed on CTLs to determine



the contribution from PD1-PDL1 signalling (see Eq. 11 in ref: [37]). To describe the joint effect of these inhibitory molecules on the CTLs, we consider a weighted sum  $R$ :

$$R = k_l L/E + k_t H/E + k_p (P/E)(P_L/V). \quad \text{Eq 11}$$

$R$  represents the total “exhaustedness” of the CTL population inside the tumour. The parameters  $k_l$ ,  $k_t$ , and  $k_p$  represent the individual contribution of (respectively) LAG-3, TIM-3, and PD-1/PD-L1 signalling towards the level of exhaustion of CTLs. In absence of detailed information about the impact of exhaustion level on CTL functions (killing, IFN- $\gamma$  production, expansion), we take all these functions to be equally reduced with the level of CTL exhaustion:

$$\alpha = 1 - (1 + k_{ex}/R)^{-1}. \quad \text{Eq 12}$$

Here,  $k_{ex}$  is the level of exhaustion at which all effector functions are half of their maximum value. Thus, Equation 12 scales the exhaustion level to a scaled term  $\alpha$  which can range from 0 to 1 and is applied to the relevant rate constants in Equations 3-6.

### Parameter estimation

Parameter estimation for the two parameters in the basal tumour growth model was performed separately from the other parameters. We consider that the density of the tumour cells remained constant over time, so that volumetric tumour growth rate could be taken as a proxy for the expansion rate of the tumour cell population. We obtained an estimate for the untreated tumour growth rate ( $g$ ) from fitting an exponential model of tumour growth to the volumetric growth data for the untreated tumours. Moreover, estimates of the ratio of tumour cells in the S-G<sub>2</sub>-M : G<sub>1</sub> phase gave a second measurement allowing the two parameter ( $k_{gs}$ ,  $k_{sg}$ ) basal model of tumour growth to be completely defined, considering that the ratio of S-G<sub>2</sub>-M : G<sub>1</sub> phase tumour cells has reached a steady state (which is reasonable since we deal with data two weeks after tumour inoculation). Then, using the equation for exponential growth:

$$\frac{d(S+G)}{dt} = g (S + G), \quad \text{Eq 13}$$

where  $g$  is the tumour growth rate, one can substitute the left hand side of Eq.13 with  $k_{sg}S$ , noting that  $k_{sg}S$  is the total rate of new tumour cell production obtained from summing Eq's. 1-2. Following the substitution, an expression for  $g$  can be found in terms of  $S$  and  $G$ :

$$g = k_{sg}S / (S + G). \quad \text{Eq 14}$$

Since our model results in an exponentially growing tumour with a constant ratio of cells in S:G states, explicit equations for the growth of the populations in each state can be written separately:

$$S(t) = S_{ss}e^{gt}, \quad \text{Eq 15}$$

$$G(t) = G_{ss}e^{gt}, \quad \text{Eq 16}$$

with the subscript (SS) indicating validity of these equations when the initial populations are at their steady state ratio. Following differentiation of each equation:

$$\frac{dS}{dt} = gS_{ss}e^{gt}, \quad \text{Eq 17}$$

$$\frac{dG}{dt} = gG_{ss}e^{gt}, \quad \text{Eq 18}$$

the resulting equations (17-18) can be combined to remove the common terms ( $ge^{gt}$ ). This leads to the following:

$$\frac{1}{S} \frac{dS}{dt} = \frac{1}{G} \frac{dG}{dt}, \quad \text{Eq 19}$$

where we have omitted the subscript with the understanding that Eq. 19 is valid only when the tumour is growing exponentially with the ratio S/G at a steady state value. Therefore, by substituting the expressions for  $\frac{dG}{dt}$  and  $\frac{dS}{dt}$  given in Eq's 1-2, the Eq's 14 & 19 can be rearranged to express the  $k_{sg}$  and  $k_{gs}$  parameters for the basal tumour growth model as a function of tumour growth rate ( $g$ ) and the ratio of S-G<sub>2</sub>-M : G<sub>1</sub> phase tumour cells at steady state:

$$k_{sg} = g (1 + S/G)(S/G)^{-1}, \quad \text{Eq 20}$$

$$k_{gs} = g (1 + 2S/G). \quad \text{Eq 21}$$

The remaining model parameters which relate to the dynamics of the CTLs and their effects on the tumours were obtained together, by fitting to all available data over time simultaneously (i.e. the CTL counts; the S/G ratios; the volumetric growth data; the IFN- $\gamma$  expression data; the immune checkpoint expression data). The measurements derived from the experimental data are multivariate and do not have the same dimension or scale. To avoid the set of measurements with the largest numerical values from dominating the fit, we could not easily use studentized residuals (i.e. dividing residuals by the estimated standard deviation of the measurements) to remove the dimensionality of each measurement, because for a number of experimental observations (CTLs on day 1, all immune checkpoints) the estimated standard deviation would be zero. Instead, we opted to apply Min-Max feature scaling. For a given set of experimental measurements of the same type denoted  $X$  (where  $X$  could be, for example, the number of CTLs counted on each different day of measurement), the equation for the transform is given by the following:

$$X_s = (X - \min(X))/(\max(X) - \min(X)), \quad \text{Eq 22}$$

where  $X_s$  is the set of Min-Max rescaled measurements and  $\min(X)$  and  $\max(X)$  are the smallest and largest values for the subset of experimental data under consideration. Thus, all experimental data is linearly rescaled to the range between 0-1. The same transformation is applied to the measurements sampled from the model,

$$Y_s = (Y - \min(X))/(\max(X) - \min(X)). \quad \text{Eq 23}$$

Note that the model output is scaled relative to the experimental data, thus rescaled values for modelled variables are allowed to take values outside the range 0-1. Finally, the root-mean-square error (RMSE) is calculated:

$$RMSE = \sqrt{\frac{\sum^n (x_n - y_n)^2}{n}}, \quad \text{Eq 24}$$

where  $n$  is the total number of measurement points used in the fitting and  $x_n$  and  $y_n$  are the individual measurements taken from the experimental data and the model output, respectively. After fitting the reverse calculation is applied to convert back to the original scaling for the

experimental data. For the basic model with I and E used as inputs, there were only two parameters ( $k_i$  and  $k_e$ ) to be estimated, therefore we tested all combinations of the parameters in the range 0-20 at intervals of 0.1 and selected the combination with the lowest RMSE. For the model including CTL dynamics we used an evolutionary algorithm[38] to minimise the RMSE, following the local-to-best strategy, with a population size of 500 and lasting for 1500 generations. Best-fitting parameter sets are provided in Table 1.

**Table 1.** Description of model parameters, with best fitting parameter values. Columns 2-4 give values for ICs fit individually, columns 5-7 give values for fits with all ICs included.

symbol	Best (LAG)	Best (TIM)	Best (PD)	Best (all)	Best (all-high $k_i$ )	Best(all-high $k_p$ )	Units	Description
$s_0$	0.011	0.087	0.007	0.032	0.04	0.008	( $\text{mm}^{-3} \text{day}^{-1}$ )	Infiltration rate of CTLs into tumour
$s_e$	8.39	9.10	13.56	14.97	116	17.97	( $\text{day}^{-1}$ )	Expansion rate of CTL population within tumour
$d_e$	0.91	0.89	0.47	1.19	0.4	1.23	( $\text{day}^{-1}$ )	Death rate of CTLs inside tumour
$d_i$	4.74	3.87	0.80	25.1	1.06	10.1	( $\text{day}^{-1}$ )	Rate at which IFN- $\gamma$ disappears from the system.
$k_{gs}$	1.64						( $\text{day}^{-1}$ )	Basal tumour cell transition rate from $G_1$ to S-G <sub>2</sub> -M cell cycle phases
$k_{sg}$	0.66						( $\text{day}^{-1}$ )	Basal tumour cell transition rate from S-G <sub>2</sub> -M to $G_1$ cell cycle phase
$k_i$	0.011	0.035	0.063	0.038	0.18	0.35	(IFN $^{-1} \text{mm}^3$ )	Determines the concentration of IFN- $\gamma$ required to prevent transfer of tumour cells from $G_1$ to S-G <sub>2</sub> -M cell cycle phases. $k_i^{-1}$ is the concentration of IFN- $\gamma$ required to reduce the transition rate by 50%.
$k_e$	3.57	4.20	0.007	2.72	1.44	0.007	(CTL $^{-1} \text{day}^{-1}$ )	Rate at which CTLs kill tumour cells
$k_A$	0.69	0.013	0.011	0.025	0.016	0.012	(IFN $^{-1} \text{mm}^3$ )	Relative contribution of IFN- $\gamma$ to immune checkpoint expression
$k_{ex}$	22.4	28.9	13.6	7.92	0.9	0.067	CTL $^{-1}$	Determines level of immune checkpoint expression required to decrease CTL function
$k_l$	0.78	NA	NA	52.5	0.02	0.13	(LAG $^{-1}$ )	Contribution of LAG3 towards CTL exhaustion
$k_t$	NA	48.6	NA	0.043	104	0.21	(TIM $^{-1}$ )	Contribution of TIM3 towards CTL exhaustion
$k_p$	NA	NA	0.007	0.10	0.009	0.01	(PD1 $^{-1}$ PDL1 $^{-1} \text{mm}^3$ )	Contribution of PD-1/PD-L1 towards CTL exhaustion
$d_l$	0.41	NA	NA	0.74	0.053	0.37	( $\text{day}^{-1}$ )	Disappearance rate of LAG3 inside the system
$d_t$	NA	0.51	NA	1.18	0.3	0.57	( $\text{day}^{-1}$ )	Disappearance rate of TIM3 inside the system
$d_p$	NA	NA	0.22	67.3	13.7	125	( $\text{day}^{-1}$ )	Disappearance rate of PD-1 inside the system
$d_{pl}$	NA	NA	0.26	15.1	116	20.4	( $\text{day}^{-1}$ )	Disappearance rate of PD-L1 inside the system

## References

1. Tang J, Pearce L, O'Donnell-Tormey J, Hubbard-Lucey VM. Trends in the global immunoncology landscape. *Nat Rev Drug Discov.* 2018;17: 783–784.
2. Liu Y, Bewersdorf JP, Stahl M, Zeidan AM. Immunotherapy in acute myeloid leukemia and myelodysplastic syndromes: The dawn of a new era? *Blood Rev.* 2019;34: 67–83.
3. Nixon NA, Blais N, Ernst S, Kollmannsberger C, Bebb G, Butler M, et al. Current landscape of immunotherapy in the treatment of solid tumours, with future opportunities and challenges. *Curr Oncol.* 2018;25: e373–e384.
4. Gibney GT, Weiner LM, Atkins MB. Predictive biomarkers for checkpoint inhibitor-based immunotherapy. *Lancet Oncol.* 2016;17: e542–e551.
5. Ribba B, Boetsch C, Nayak T, Grimm HP, Charo J, Evers S, et al. Prediction of the Optimal Dosing Regimen Using a Mathematical Model of Tumor Uptake for Immunocytokine-Based Cancer Immunotherapy. *Clin Cancer Res.* 2018;24: 3325–3333.
6. Qomlaqi M, Bahrami F, Ajami M, Hajati J. An extended mathematical model of tumor growth and its interaction with the immune system, to be used for developing an optimized immunotherapy treatment protocol. *Math Biosci.* 2017;292: 1–9.
7. Melero I, Berman DM, Aznar MA, Korman AJ, Pérez Gracia JL, Haanen J. Evolving synergistic combinations of targeted immunotherapies to combat cancer. *Nat Rev Cancer.* 2015;15: 457–472.
8. Sharpe AH, Pauken KE. The diverse functions of the PD1 inhibitory pathway. *Nat Rev Immunol.* 2018;18: 153–167.
9. Salmaninejad A, Valilou SF, Shabgah AG, Aslani S, Alimardani M, Pasdar A, et al. PD-1/PD-L1 pathway: Basic biology and role in cancer immunotherapy. *J Cell Physiol.* 2019;234: 16824–16837.
10. Hegde UP, Mukherji B. Current status of chimeric antigen receptor engineered T cell-based and immune checkpoint blockade-based cancer immunotherapies. *Cancer Immunol Immunother.* 2017;66: 1113–1121.
11. Cazaux M, Grandjean CL, Lemaître F, Garcia Z, Beck RJ, Milo I, et al. Single-cell imaging of CAR T cell activity in vivo reveals extensive functional and anatomical heterogeneity. *J Exp Med.* 2019;216: 1038–1049.
12. Zaidi MR. The Interferon-Gamma Paradox in Cancer. *J Interferon Cytokine Res.* 2019;39: 30–38.
13. Hoekstra ME, Bornes L, Dijkgraaf FE, Philips D, Pardieck IN, Toebes M, et al. Long-distance modulation of bystander tumor cells by CD8+ T-cell-secreted IFN- $\gamma$ . *Nature Cancer.* 2020;1: 291–301.

14. Garcia-Diaz A, Shin DS, Moreno BH, Saco J, Escuin-Ordinas H, Rodriguez GA, et al. Interferon Receptor Signaling Pathways Regulating PD-L1 and PD-L2 Expression. *Cell Rep.* 2017;19: 1189–1201.
15. Matsushita H, Hosoi A, Ueha S, Abe J, Fujieda N, Tomura M, et al. Cytotoxic T lymphocytes block tumor growth both by lytic activity and IFN $\gamma$ -dependent cell-cycle arrest. *Cancer Immunol Res.* 2015;3: 26–36.
16. Harvat BL, Seth P, Jetten AM. The role of p27Kip1 in gamma interferon-mediated growth arrest of mammary epithelial cells and related defects in mammary carcinoma cells. *Oncogene.* 1997;14: 2111–2122.
17. Chin YE, Kitagawa M, Su WC, You ZH, Iwamoto Y, Fu XY. Cell growth arrest and induction of cyclin-dependent kinase inhibitor p21 WAF1/CIP1 mediated by STAT1. *Science.* 1996;272: 719–722.
18. Beck RJ, Slagter M, Beltman JB. Contact-Dependent Killing by Cytotoxic T Lymphocytes Is Insufficient for EL4 Tumor Regression In Vivo. *Cancer Res.* 2019;79: 3406–3416.
19. Beck RJ, Weigelin B, Beltman JB. CD137-stimulated cytotoxic T lymphocytes exert superior tumour control due to an enhanced antimitotic effect on tumour cells. *bioRxiv.* 2020. p. 2020.12.15.411538. doi:10.1101/2020.12.15.411538
20. Berg S, Kutra D, Kroeger T, Straehle CN, Kausler BX, Haubold C, et al. ilastik: interactive machine learning for (bio)image analysis. *Nat Methods.* 2019;16: 1226–1232.
21. Morris R, Kershaw NJ, Babon JJ. The molecular details of cytokine signaling via the JAK/STAT pathway. *Protein Sci.* 2018;27: 1984–2009.
22. Thommen DS, Schumacher TN. T Cell Dysfunction in Cancer. *Cancer Cell.* 2018;33: 547–562.
23. Wherry EJ. T cell exhaustion. *Nat Immunol.* 2011;12: 492–499.
24. Li H, van der Leun AM, Yofe I, Lubling Y, Gelbard-Solodkin D, van Akkooi ACJ, et al. Dysfunctional CD8 T Cells Form a Proliferative, Dynamically Regulated Compartment within Human Melanoma. *Cell.* 2019;176: 775–789.e18.
25. Singer M, Wang C, Cong L, Marjanovic ND, Kowalczyk MS, Zhang H, et al. A Distinct Gene Module for Dysfunction Uncoupled from Activation in Tumor-Infiltrating T Cells. *Cell.* 2016;166: 1500–1511.e9.
26. Blank CU, Haining WN, Held W, Hogan PG, Kallies A, Lugli E, et al. Defining “T cell exhaustion.” *Nat Rev Immunol.* 2019;19: 665–674.
27. Wherry EJ, Kurachi M. Molecular and cellular insights into T cell exhaustion. *Nat Rev Immunol.* 2015;15: 486–499.
28. Goding SR, Wilson KA, Xie Y, Harris KM, Baxi A, Akpinarli A, et al. Restoring immune function of tumor-specific CD4<sup>+</sup> T cells during recurrence of melanoma. *J Immunol.* 2013;190: 4899–4909.

29. Hu Z, Ye L, Xing Y, Hu J, Xi T. Combined SEP and anti-PD-L1 antibody produces a synergistic antitumor effect in B16-F10 melanoma-bearing mice. *Sci Rep*. 2018;8: 217.
30. Chen S, Lee L-F, Fisher TS, Jessen B, Elliott M, Evering W, et al. Combination of 4-1BB agonist and PD-1 antagonist promotes antitumor effector/memory CD8 T cells in a poorly immunogenic tumor model. *Cancer Immunol Res*. 2015;3: 149–160.
31. Garriss CS, Arlauckas SP, Kohler RH, Trefny MP, Garren S, Piot C, et al. Successful Anti-PD-1 Cancer Immunotherapy Requires T Cell-Dendritic Cell Crosstalk Involving the Cytokines IFN- $\gamma$  and IL-12. *Immunity*. 2018;49: 1148–1161.e7.
32. Breart B, Lemaître F, Celli S, Bousso P. Two-photon imaging of intratumoral CD8+ T cell cytotoxic activity during adoptive T cell therapy in mice. *J Clin Invest*. 2008;118: 1390–1397.
33. Hosoi A, Matsushita H, Shimizu K, Fujii S-I, Ueha S, Abe J, et al. Adoptive cytotoxic T lymphocyte therapy triggers a counter-regulatory immunosuppressive mechanism via recruitment of myeloid-derived suppressor cells. *Int J Cancer*. 2014;134: 1810–1822.
34. Chen B, Khodadoust MS, Liu CL, Newman AM, Alizadeh AA. Profiling Tumor Infiltrating Immune Cells with CIBERSORT. *Methods Mol Biol*. 2018;1711: 243–259.
35. Guo Y, Xiao P, Lei S, Deng F, Xiao GG, Liu Y, et al. How is mRNA expression predictive for protein expression? A correlation study on human circulating monocytes. *Acta Biochim Biophys Sin*. 2008;40: 426–436.
36. Liu Y, Beyer A, Aebersold R. On the Dependency of Cellular Protein Levels on mRNA Abundance. *Cell*. 2016;165: 535–550.
37. Lai X, Friedman A. Combination therapy of cancer with cancer vaccine and immune checkpoint inhibitors: A mathematical model. *PLoS One*. 2017;12: e0178479.
38. Mullen K, Ardia D, Gil DL, Windover D, Cline J. DEoptim: An R Package for Global Optimization by Differential Evolution. 2009. Available: <https://papers.ssrn.com/abstract=1526466>



## Supplementary Data

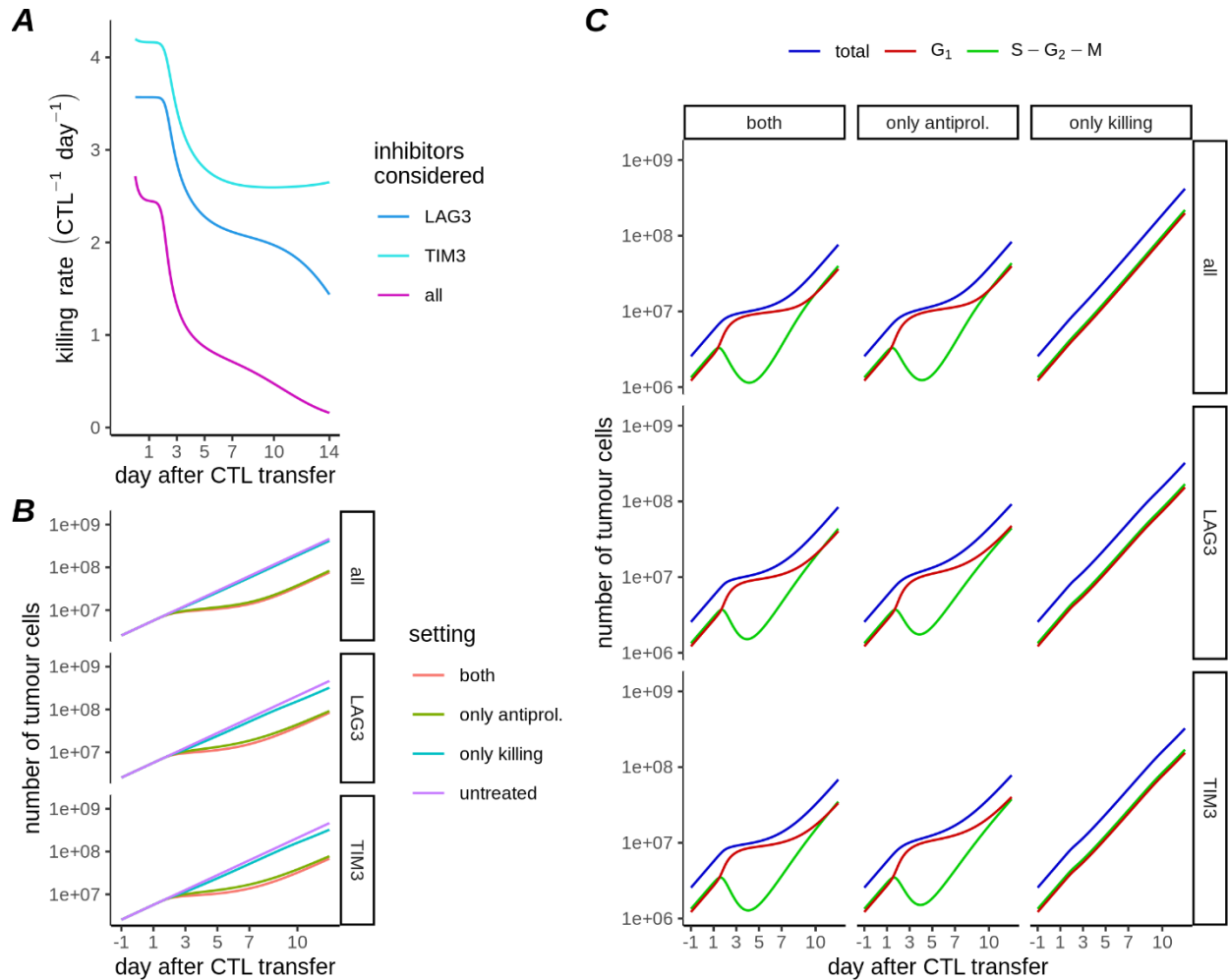


**Figure S1.** Relative effects of killing and IFN- $\gamma$  in the fitted models. A) Different CTL killing rates predicted using the best fits for three IC combination models (only LAG-3, only TIM-3, or the combination of LAG-3, TIM-3 and PD-1/PD-L1), each of which resulted in a good fit to the experimental data. Each fitted combination is represented by a different color. B) Comparison of the number of tumour cells, predicted over time for each of the three selected IC combinations (along rows). Total cells (blue), G<sub>1</sub> phase cells (red), or S-G<sub>2</sub>-M phases (green) are shown separately for each condition. Along columns are simulations with either all parameters as fitted (left), with killing disabled (middle), or with the antiproliferative effect disabled (right). C) Comparison of total number of tumour cells in the model for the 9 conditions simulated in B. An additional line (“untreated”, purple) shows the growth of the tumour simulated without any CTLs.

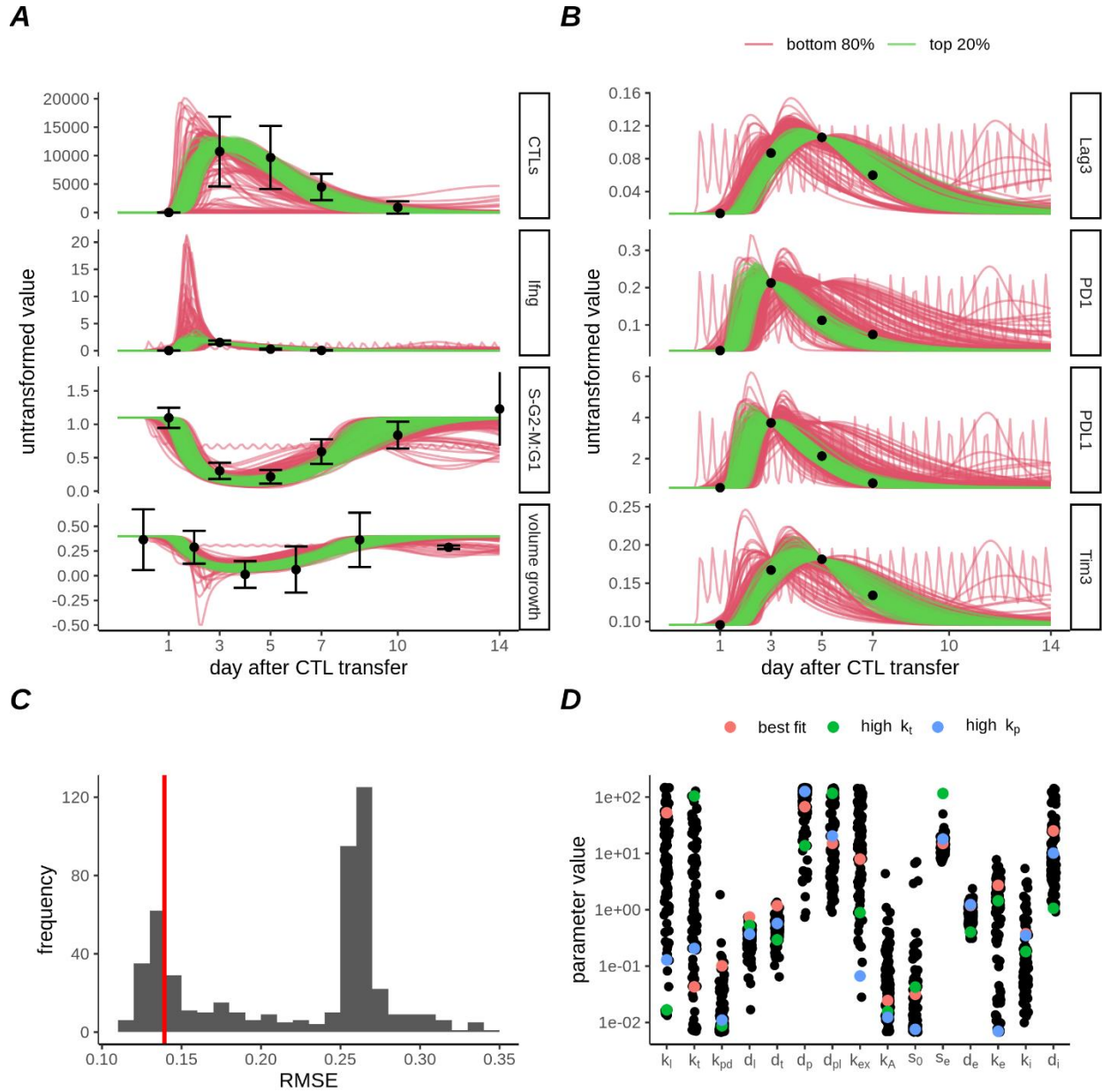


**Figure S2.** Parameter variability amongst the final generation of the evolutionary algorithm, when all ICs were used to fit the model. A) Model fits to CTL density (top row), IFN- $\gamma$  mRNA expression (2nd row), ratio of S-G2-M:G1 nuclei (3rd row), or volumetric tumour growth (bottom row). B) Model fit to each IC as indicated by facet labels per row. Symbols and error bars in A-B represent experimental measurements and SD, whereas lines represent model output, and are coloured according to whether they were in the top 20% of the best fitting parameter sets. C) Distribution of root-mean-square-error (RMSE) for parameter sets in the final generation. Red line indicates the cutoff for the top 20% of parameter sets. D) Parameter values for the top 20% of parameter sets in the final generation of the evolutionary algorithm. Coloured dots indicate parameter sets for best fit (red) and for high relative values of  $k_t$  (green) and of  $k_p$  (blue) compared to other exhaustion parameters (these sets are used in Fig. 5E-F in main text).

# Chapter 6

## Discussion

### Summarizing discussion

In this thesis we have studied the effector functions of cytotoxic T lymphocytes in various *in vitro* and *in vivo* experiments, with emphasis on the role of CTLs as mediators of immunotherapies for cancer. To study CTL effector functions, we analysed experimental data in order to derive statistics and parameters informative about CTL function. Moreover, using these parameters, we developed mechanistic models and studied them in order to obtain insights about the behaviour of CTLs. In the following sections, we revisit the questions originally posed in the introduction to this thesis.

### **How can the rate at which CTLs kill target cells be quantified and what is the rate at which CTLs kill tumour cells?**

In chapter 2, we used stochastic models and bayesian inference to study the expected kinetics of CTL killing when observed under the microscope. In particular, we sought to define the measurements required in order to accurately determine the killing rate of cells based on imaging data. Early models treated CTL cytotoxicity as a Poisson process<sup>1</sup>, but others have suggested that multiple hits from CTLs may be required in order to effectively lyse target cells (i.e., the multiple-hitting hypothesis)<sup>2-4</sup>. We found that the multiple hitting hypothesis was compatible with recent unexplained observations of non-Poisson killing dynamics for CTLs *in vitro*<sup>5</sup>, and established a bayesian inference procedure which could be applied to test the multiple-hitting hypothesis. We also determined that the ability to track the contact history of CTLs with individual target cells was a requirement for accurate assessment of multiple hitting based on imaging data.

We had data available from three different cell lines with which we could address the question of CTL killing rate. In an *in vitro* assay in which CTLs killed Epstein-Barr virus transformed B cells presenting the pp65 peptide<sup>5</sup> (chapter 2), CTLs killed with an average rate of  $k=8$  (kills CTL<sup>-1</sup> day<sup>-1</sup>). In an *in vivo* setup employing EL4 lymphoma<sup>6</sup> (chapter 3), CTLs killed with an average rate of  $k=4$  (kills CTL<sup>-1</sup> day<sup>-1</sup>). In *in vivo* experiments using the B16F10 melanoma cell line<sup>7</sup> (chapter 4), CTLs killed with an average rate of  $k=0.75$  (kills CTL<sup>-1</sup> day<sup>-1</sup>). These estimates for CTL killing rates towards tumour cells are comparable to other reports in the literature. In another murine experiment we have analysed<sup>8</sup> (not included in this thesis), CTLs were estimated to kill B cell lymphoma cells in the bone marrow at a rate of  $k=4.8$  (kills CTL<sup>-1</sup> day<sup>-1</sup>). Another study using the B16F10 melanoma cell line reported different rates of killing depending on the site of injection<sup>9</sup>, with  $k=1.24$  (kills CTL<sup>-1</sup> day<sup>-1</sup>) when melanoma cells were injected into the liver, but  $k=3.18$  (kills CTL<sup>-1</sup> day<sup>-1</sup>) when cells were injected into the spleen. Overall, in this thesis we have studied the killing rate of CTLs in two tumour cell lines *in vivo*, as well as one cell line in *an vitro* setting. Moreover, we have laid out a framework for analysing the killing kinetics of CTLs in imaging data in future.

## How important is the contribution of CTL mediated killing towards control of tumours?

An important focus of this thesis was to assess the sufficiency of CTL killing to account for tumour control. In chapter 3, we investigated *in vivo* experiments employing the EL4 lymphoma cell line which underwent rapid regression following adoptive transfer of CTLs<sup>6</sup>. For these EL4 tumours, conflicting reports existed in the literature regarding the mechanisms used by adoptively transferred CTLs to eliminate the tumours. Imaging of mixed tumours, containing both patches of antigen-positive and antigen-negative tumour, showed selective elimination of antigen-positive regions after CTL transfer<sup>6</sup>. This result from mixed tumours suggested an important role for contact dependent, antigen specific recognition and destruction of tumour cells by the transferred CTLs. However, another study using the same EL4 tumour cell line showed that perforin and FAS-L doubly deficient T cells were not significantly compromised in their ability to control the same tumours<sup>10</sup>. Since either perforin or FAS-L are expected to be required for contact dependent killing, effective tumour control in the absence of both mechanisms seemed incompatible with the imaging study using mixed tumours.

Estimates for the killing rate of CTLs were available from two photon imaging of the regressing EL4 tumours, with a value for the killing rate of  $k=4$  (kills CTL<sup>-1</sup> day<sup>-1</sup>). Thus, we asked whether the observed CTL killing rate was sufficient to explain the rapid tumour regression which was also reported. To address this question we developed both an ordinary differential equation model and a spatially explicit agent based model, to describe CTL killing inside the tumours. We found that the observed rates of CTL killing were well below those required to explain the rapid tumour regression evident in the data. This was true even when we simulated multiple-hitting CTLs, for which the associated variable killing rate over time<sup>11</sup> (chapter 2) could have implied that the reported killing rate ( $k=4$  kills CTL<sup>-1</sup> day<sup>-1</sup>) was an underestimate due to imaging being performed at an early time point. However, the discrepancy between the measured killing rate and the killing rate we predicted necessary to result in tumour regression was too large to be accounted for by multiple-hitting.

In chapters 4-5, we studied two datasets derived from the B16F10 melanoma model after adoptive CTL transfer. The different datasets were generated by two different experimental groups, with each group having adopted a slightly different experimental setup. In one series of experiments<sup>7</sup> (used in chapter 4) tumours were injected and then observed by means of long (1-4 hours) three-dimensional two-photon microscopy imaging through dorsal skinfold windows implanted into the mice. CTLs recognised ovalbumin (OVA) expressed by the B16F10 melanoma cells. Data from this series of experiments had the advantage that direct measurements of the killing rate of tumour cells by CTLs could be made ( $k=0.75$  kills CTL<sup>-1</sup> day<sup>-1</sup>), along with measurements of the mitosis rate of tumour cells. However, the presence of the imaging windows limited the size of tumours that could be studied and it was unclear whether the presence of the windows influenced the growth of the tumours or the response of the CTLs.

Complementing these data were data from other experiments<sup>12</sup> (used in chapter 5) using the B16F10 melanoma cell line, except with pmel-1 transgenic T cells recognising the gp100 peptide expressed on the tumour cells. In this series of experiments, *ex vivo* cryosections rather than an

imaging window was used, permitting study of larger tumours but having the disadvantage that no direct measurements of CTL killing rate or tumour mitosis rate were available. Nevertheless, using model fitting we were able to infer values for these parameters from the available data. In these data, immunofluorescence imaging of the cryosections was used to quantify the number of tumour infiltrating CTLs. Moreover, in combination with the Fucci cell cycle reporter, the *ex vivo* sections allowed discrimination between tumour cells in the G<sub>1</sub> phase of the cell cycle and tumour cells in other (S-G<sub>2</sub>-M) phases, which made it possible to estimate the rate of tumour cell mitosis. Since we could infer the tumour mitosis rate from the ratio of tumour cells in G<sub>1</sub>:S-G<sub>2</sub>-M phases, we were able to make an estimate of the CTL killing rate: we did this by asking how much additional CTL killing, in addition to the reduced mitosis, would be needed in order to explain the volumetric progression of the tumours. By comparing the estimate of tumour cell mitosis to the volumetric progression of the tumours, we inferred a value for the killing rate of the CTLs, i.e.,  $k=1$  kill CTL<sup>-1</sup> day<sup>-1</sup>. Interestingly, in spite of the different antigen (gp100) recognised by CTLs in these experiments, this killing rate estimate was consistent with the experiments where CTLs recognised the OVA antigen (chapter 4), suggesting that the exact antigen recognised by CTLs does not have a major impact on the rate at which they can kill target cells.

We developed ODE models to describe the data generated by each set of B16F10 experiments. Despite the differences in experimental settings, our analysis and modelling of each set of data gave consistent conclusions: in each case the cytotoxic function of CTLs had only a small effect on tumour progression. Thus our results from studying the B16F10 melanoma cell line (chapters 4-5) were consistent with those obtained in our study of the EL4 lymphoma cell line (chapter 3), i.e. CTL killing was insufficient to account for the majority of the reduction in tumour size or progression concomitant with the adoptive transfer of CTLs.

### **How important are the antiproliferative effects that CTLs exert upon tumour cells?**

Since in each of the *in vivo* experiments studied (chapters 3-5) we found that CTL mediated killing at the reported or inferred rates was insufficient to explain the extent of the tumour regression reported, we asked in each case to what extent an antiproliferative effect of the transferred CTLs could explain the data. In chapter 3, we used our spatial agent based model, but applied a constraint that our model should also be able to describe the results from mixed EL4 tumours where selective destruction of antigen expressing cells was observed. We found that including a mechanism whereby CTLs secrete a soluble cytokine with antiproliferative effects on tumour cells would allow us to simultaneously describe all the available data. Our model suggested that the antiproliferative effect of the cytokine was quantitatively more important, due to the ability of CTLs to control the proliferation of many tumour cells, given that the antiproliferative effect is mediated by a soluble molecule which can diffuse away from CTLs. This would explain how double knockout of perforin and FAS-L had little impact on tumour control, as shown experimentally in an earlier study<sup>10</sup>. Nevertheless, our model also explained the selective destruction of antigen expressing cells in mixed tumours, which occurred for two reasons. Firstly, the antiproliferative effect would affect the OVA-expressing cells more strongly than non-OVA-expressing bystander cells, due to the selective localisation of CTLs leading to high concentrations of cytokine in areas inhabited by antigen expressing tumour cells. Second, although the reported CTL killing rates were quite low, they eventually led to appreciable reduction in the number of tumour cells, provided the tumour

cells could not proliferate. Together these two effects impose a strong selection pressure on the tumour cells, explaining the selective elimination of antigen expressing cells.

A limitation of our study in EL4 tumours (chapter 3) was lack of any direct data concerning the proliferation rate of tumour cells. This limitation was addressed in chapters 4-5, since in both datasets estimates of tumour cell mitosis were available. By examining hypothetical deviations in the estimated rates of tumour cell mitosis after adoptive transfer of CTLs, we were able to make inferences about the impact of CTL transfer on the proliferation rate of the tumour cells. After incorporating these data into our ODE models, we saw in each case the mitosis rate of tumour cells was substantially diminished concomitant with the presence of the CTLs. Indeed, we found that the reduced mitosis rates after CTL transfer were quantitatively sufficient to account for the majority of reduced volume progression. Overall, we again found that the cytotoxic function of CTLs had a negligible effect on tumour progression when quantitatively compared with the antiproliferative effect. Thus in all the *in vivo* data we studied, we reached the conclusion that an antiproliferative effect associated with transferred CTLs is more important than any direct killing of tumour cells by CTLs.

Since we identified a potential antiproliferative effect of CTLs as having a large effect on tumour progression, it is important to understand the mechanisms through which such an effect occurs. Based on reports that the CTL secreted cytokine interferon- $\gamma$  (IFN- $\gamma$ ) can cause cell cycle arrest<sup>12-14</sup>, and also because the antiproliferative effect of IFN- $\gamma$  was explicitly explored and confirmed in one of the studies we used to develop our models<sup>12</sup> (chapter 5), it seems that the cytokine IFN- $\gamma$  is an important mediator of the antiproliferative effect in the B16F10 cell line. Although IFN- $\gamma$  was shown to have no effect on the proliferation of EL4 cells *in vitro*<sup>12</sup>, when we simulated a similar antiproliferative effect from IFN- $\gamma$  in our spatial ABM (chapter 3) we were able to describe the time course of the EL4 lymphoma tumour size. This result suggests that there may be other means, in addition to IFN- $\gamma$  mediated cell cycle arrest, by which transferred CTLs can reduce the proliferation of tumour cells. There are plausible mechanisms by which this could occur - for example IFN- $\gamma$  promotes expression of the chemokines CXCL9, CXCL10, and CXCL11, which all have angiostatic effects<sup>15</sup>. As another example, nitric oxide is secreted by stromal cells after exposure to IFN- $\gamma$ <sup>16</sup> and can reduce proliferation of EL4 cells *in vitro*. Due to the importance of antiproliferative effects of CTLs suggested and highlighted by our models, an important focus of future work should be to clarify and quantify these effects.

### **What is the effect of CTL stimulation on their *in vivo* functionality?**

In addition to quantifying the relative importance of killing and antiproliferative effects of CTLs towards tumour regression in the B16F10 tumours, additional data available from the studies used in chapters 4-5 allowed us to further investigate other aspects of CTL function. In the series of experiments where CTLs were observed through dorsal imaging windows using two photon microscopy (chapter 4), an additional experimental condition was studied in which CTLs were adoptively transferred in the presence of an agonist antibody targeting the costimulatory CD137 receptor<sup>7</sup>. CD137 is expressed on both innate and adaptive immune cells and stimulation of CD8<sup>+</sup> T cells via the CD137 receptor may improve their proliferation and resistance to apoptosis<sup>7,17,18</sup>. In the data we studied<sup>7</sup>, several differences had already been observed in the CD137 stimulated

condition compared to the unstimulated condition: increased tumour cell apoptosis and reduced tumour cell mitosis after CD137 stimulation, alterations in the apoptosis and mitosis kinetics of the CTLs, and improved tumour control in the CD137 stimulated case. Moreover, CD137 stimulation led to increases in expression of molecules related to enhanced CTL cytolytic function, such as the transcription factors T-bet and eomesodermin<sup>7</sup>. It was therefore suggested that CD137 improved the *in vivo* killing capacity of the transferred CTLs. However, there had been no attempt to integrate these differences into a coherent model and thus it was not clear which of the differences in dynamics at the cellular level accounted for enhanced tumour control. Thus, we utilised our ODE model describing the behaviour of the CTLs inside the tumour, and fit our model separately to each condition in order to explore differences in the fitted model parameters and resulting dynamics between the CD137-stimulated and non-CD137-stimulated CTLs. With our modelling approach we found that enhanced antiproliferative effects of the CTLs at the site of the tumour were likely to account for the majority of the improvement in tumour control after stimulation with the CD137 targeted agonist antibody. Thus our overall conclusion was that stimulation of T cells via the CD137 axis did not have an appreciable impact on their cytolytic function *in vivo*. Rather, the most important impact of stimulation upon CTL function was an improvement in their ability to prevent tumour cells from proliferating.

### **What is the contribution of immune checkpoint molecules towards CTL exhaustion?**

In chapter 5, we exploited the availability of gene expression data at multiple time points for the B16F10 melanoma tumours to derive further insights about the behaviours of the tumour infiltrating CTLs<sup>12</sup>. Interestingly, according to the expression data, IFN- $\gamma$  signalling decreased whilst CTLs were still present in the tumour, indicating a loss of function for the CTLs. By examining the gene expression data for candidate explanations for these dynamics, we found upregulation of several immune checkpoint molecules which suggested the development of an exhausted CTL phenotype<sup>19–21</sup> as a potential explanation for the loss of effector function. Thus we included CTL exhaustion in our model, in which the effector functions of the CTLs were reduced as the levels of the immune checkpoint transcripts increased. Our model showed that such a mechanism of CTL exhaustion was indeed able to account for the observed CTL and tumour dynamics. We also used our model to compare between different checkpoint molecules to identify which might be the most important determinants of the exhausted CTL state in the setting with B16F10 tumours. Interestingly, we found that the PD-1/PD-L1 axis alone was not compatible with the exhausted state, since according to the transcript data these molecules were only transiently expressed and therefore not able to explain the progressive deterioration in CTL production of IFN- $\gamma$  and the progressive reduction of CTLs inside the tumour. Instead, we found that LAG3 and TIM3 were most consistent with being determinants of CTL exhaustion in B16F10 tumours. Taken together these results suggest that immune checkpoint molecules do contribute towards CTL exhaustion, however expression of PD-1 and its ligand PD-L1 do not appear to be sufficient to explain the exhausted state. Other molecules such as TIM3 and LAG3 likely also play a role and are candidates for further study.

## Perspectives

In the following sections, some limitations of the work presented in this thesis are discussed. Suggestions are made for how some of those limitations might be addressed in future work, and possible avenues for extending the work in this thesis are presented.

### Importance of killing in other types of tumour

Since the ability of CTLs to recognise and kill antigen presenting target cells is their most well known function, it was perhaps surprising to discover that our models predicted a negligible contribution of CTL mediated killing of tumour cells in two different *in vivo* tumour cell lines studied in this thesis (EL4 lymphoma, B16F10 melanoma). The relative importance of CTL mediated killing versus an antiproliferative effect of CTLs upon tumour cells is likely to depend on the characteristics of the tumour in question. For example, in slow-growing tumours one might expect the killing of CTLs to have a large relative contribution, simply because in such tumours there is little mitosis to suppress. This observation highlights one limitation of our studies, which is that they were based on extremely rapidly growing experimental tumour models, with growth rates of 0.4-0.9 day<sup>-1</sup> corresponding to tumour cells undergoing mitosis every 1-2 days. These are not necessarily reflective of the tumour growth rates found in human cancer patients. A recent study comparing growth rates in five cohorts of human cancer patients with different types of cancer<sup>22</sup> found much lower growth rates, with doubling times ranging from 70-3050 days. Therefore, although our findings relating to the importance of an antiproliferative effect associated with CTL infiltration will certainly help to interpret and contextualise findings based from studies using preclinical mouse models, it is unclear whether they will also hold true in human tumours with much slower growth.

Due to the difficulties inherent in obtaining data from human cancer patients, it is important to find other ways to address the question on the contribution of killing and antiproliferative effects to tumour control, for example by using murine tumours (although it remains important to find ways to link data from animal studies to human patients - see section below on extension to human studies). A starting point would be to characterise the importance of an antiproliferative effect in murine tumours with a broader spectrum of growth rates. In one experiment we have analysed (not included in this thesis) where B cell lymphomas grew in the bone marrow of mice, the estimated doubling time of the tumour was 14 days<sup>8</sup>; there we found that tumour eradication was entirely consistent with the estimated killing rate of the CTLs, although we could not exclude the possibility that cell cycle arrest may have also played a role in the control of those tumours. Future work should therefore continue to analyse additional experimental tumours with a broad spectrum of growth rates in order to clarify whether the relative importance of an antiproliferative effect compared to CTL killing is indeed dependent on tumour growth rate.

### Improved quantification of CTL killing

Another avenue for future work centres on the quantification of tumour cell death in the presence of CTLs. In chapter 2 we addressed how a requirement for multiple hits for CTLs to kill tumour cells might confound estimates of the CTL killing rate. This is relevant because some evidence



suggests that melanoma cells require multiple hits for annihilation by CTLs<sup>3</sup>. Moreover, as has been pointed out previously<sup>11</sup> and in chapter 2 of this thesis, multiple-hitting should lead to a variable observed rate at which CTLs kill target cells, which depends on the number of hits targets have already received. Our investigation of the requirements for quantifying the killing rate of CTLs based on microscopy data in the presence of multiple-hitting highlighted the importance of studying the interaction history of CTLs with tumour cells. By studying the risk of tumour cell death as a function of time spent in contact with CTLs, one can very directly assess whether target cells' risk of dying increases after having spent a significant time in contact with the CTL, or whether targets instead face a constant risk of death whilst in contact with a CTL. Although in chapter 2 we focussed on characterising multiple hitting, the principle of studying target cell risk of death in the presence of CTLs has more general applications. For example, it has been suggested that tumour infiltrating CTLs recruit innate effector immune cells and that these play a significant role in killing tumour cells<sup>10</sup>. In addition, cytokines secreted by CTLs may also increase the risk of death experienced by targets not directly contacted by CTLs<sup>10,23,24</sup>. These questions could be addressed directly by looking at the risk of tumour cell death in the absence of CTL transfer, and comparing it to the risk of death experienced by uncontacted tumour cells in tumours following adoptive CTL transfer. If innate effectors or CTL-secreted cytokines are indeed relevant, one should expect an increased risk of death even amongst uncontacted tumour cells following adoptive CTL transfer, with risk of death likely varying as a function of distance to the CTLs, since uncontacted tumour cells ought to be at enhanced risk of being killed by the innate effectors or cytokines. Future work applying similar analysis as presented in chapter 2 of this thesis to a variety of imaging datasets will thus be useful to better understand how the presence of CTLs influences target cell's risk of death in various contexts.

## **Modulation of CTL effector functions**

The models and approach developed in this thesis establish a quantitative baseline for several important aspects of CTL effector function in tumours. We established dynamical equations and estimated the rates of several important functions, such as CTL killing of tumour cells, changes to the mitosis rate of tumour cells following adoptive CTL transfer, and also the dynamics of the CTL populations. Although our modelling approach is clearly a simplification, in which we reduce the complex dynamics occurring inside tumours to just a few equations, this is already a substantial refinement on existing frequently used methods of quantifying CTL performance, like measuring the volume progression of tumours after CTL transfer. As such, our modelling approach is highly useful for studying the effect of different modulators of CTL function. We studied costimulation of CTLs via the CD137 receptor, however there are a number of other modulators which similarly stimulate the priming and activation of CTLs. For example, OX40 (CD134), CD27, and CD28 are similar to CD137 in that they are all members of the tumour necrosis factor family of receptors, they all provide costimulatory signals to T cells, and they are all linked to enhanced T cell functions<sup>25–27</sup>. Thus these molecules are also candidates for future study using similar methods as those outlined in this thesis.

## Extension to human studies

In a previous section (Importance of killing in other tumour models) we discussed the representability of our results based on murine models and in particular whether they might be relevant to human cancer patients. The ultimate aim of our research is to provide insights that might inform strategies for treating human cancer patients, therefore it is important to explicitly seek ways to link research in murine models to the human patient. Recent studies have examined biopsies from patients undergoing immunotherapy, to identify mechanisms underlying success or failure of treatment<sup>28</sup>, or identify biomarkers predicting which patients are likely to respond to a particular immunotherapy<sup>29,30</sup>. Examples of biomarkers which have been repeatedly associated with response to immunotherapies are the tumour mutational burden<sup>31,32</sup>, cytotoxic gene signature<sup>33,34</sup>, or density of infiltrating immune cells<sup>35,36</sup>. However, the predictive value of such biomarkers and their applicability to different types of cancer is debated.

Mathematical and computational models such as those developed in this thesis are appropriate tools for linking observations in murine models to human data. A prerequisite for making this comparison is the development of mathematical and computational models which can be defined in terms of measurements which can feasibly be made in human patients. For many of the variables used in our models this should be feasible. For example, all our models rely on quantification of the frequency of tumour infiltrating CTLs, which can be obtained from tumour biopsies using immunofluorescence techniques. Given our findings that tumour infiltrating CTLs may have a potent antiproliferative effect on tumour cells (chapters 3-5), it would also be of interest to determine whether such antiproliferative effects occur and are important in cancer patients receiving immunotherapy. Single cell sequencing of cell populations from human tumours is a possible means of testing this finding<sup>37</sup>, since cell cycle markers might reveal differences in the proportion of tumour cells in various cell cycle stages before and after immunotherapy (in case longitudinal samples from the same patients were available), or between immunotherapy treated and untreated patients (in case longitudinal samples from the same patients were not available). Future work should thus aim to validate our findings about the relevance of antiproliferative effects of CTLs, by searching for evidence of decreased tumour cell mitosis and arrested cell cycle in data from immunotherapy patients.

1. Perelson, A. S. & Macken+, A. Kinetics of Cell-Mediated Cytotoxicity: Stochastic and Deterministic Multistage Models. *Math. Biosci.* **70**, 161–194 (1984).
2. Gadhamsetty, S., Marée, A. F. M., Beltman, J. B. & de Boer, R. J. A general functional response of cytotoxic T lymphocyte-mediated killing of target cells. *Biophys. J.* **106**, 1780–1791 (2014).
3. Caramalho, I., Faroudi, M., Padovan, E., Müller, S. & Valitutti, S. Visualizing CTL/melanoma cell interactions: multiple hits must be delivered for tumour cell annihilation. *J. Cell. Mol. Med.*

- 13**, 3834–3846 (2009).
4. Halle, S. *et al.* In Vivo Killing Capacity of Cytotoxic T Cells Is Limited and Involves Dynamic Interactions and T Cell Cooperativity. *Immunity* **44**, 233–245 (2016).
  5. Vasconcelos, Z. *et al.* Individual Human Cytotoxic T Lymphocytes Exhibit Intracloal Heterogeneity during Sustained Killing. *Cell Rep.* **11**, 1474–1485 (2015).
  6. Breart, B., Lemaître, F., Celli, S. & Bousso, P. Two-photon imaging of intratumoral CD8+ T cell cytotoxic activity during adoptive T cell therapy in mice. *J. Clin. Invest.* **118**, 1390–1397 (2008).
  7. Weigelin, B. *et al.* Focusing and sustaining the antitumor CTL effector killer response by agonist anti-CD137 mAb. *Proc. Natl. Acad. Sci. U. S. A.* **112**, 7551–7556 (2015).
  8. Cazaux, M. *et al.* Single-cell imaging of CAR T cell activity in vivo reveals extensive functional and anatomical heterogeneity. *J. Exp. Med.* jem.20182375 (2019).
  9. Liu, L., Dai, B., Li, R., Liu, Z. & Zhang, Z. Intravital molecular imaging reveals the restrained capacity of CTLs in the killing of tumor cells in the liver. *Theranostics* **11**, 194–208 (2021).
  10. Hollenbaugh, J. A., Reome, J., Dobrzanski, M. & Dutton, R. W. The rate of the CD8-dependent initial reduction in tumor volume is not limited by contact-dependent perforin, Fas ligand, or TNF-mediated cytotoxicity. *J. Immunol.* **173**, 1738–1743 (2004).
  11. Gadhamsetty, S., Marée, A. F. M., Beltman, J. B. & de Boer, R. J. A Sigmoid Functional Response Emerges When Cytotoxic T Lymphocytes Start Killing Fresh Target Cells. *Biophys. J.* **112**, 1221–1235 (2017).
  12. Matsushita, H. *et al.* Cytotoxic T lymphocytes block tumor growth both by lytic activity and

- IFN $\gamma$ -dependent cell-cycle arrest. *Cancer Immunol Res* **3**, 26–36 (2015).
13. Harvat, B. L., Seth, P. & Jetten, A. M. The role of p27Kip1 in gamma interferon-mediated growth arrest of mammary epithelial cells and related defects in mammary carcinoma cells. *Oncogene* **14**, 2111–2122 (1997).
  14. Chin, Y. E. *et al.* Cell growth arrest and induction of cyclin-dependent kinase inhibitor p21 WAF1/CIP1 mediated by STAT1. *Science* **272**, 719–722 (1996).
  15. Keeley, E. C., Mehrad, B. & Strieter, R. M. Chemokines as mediators of tumor angiogenesis and neovascularization. *Exp. Cell Res.* **317**, 685–690 (2011).
  16. Hollenbaugh, J. A. & Dutton, R. W. IFN- $\gamma$  Regulates Donor CD8 T Cell Expansion, Migration, and Leads to Apoptosis of Cells of a Solid Tumor. *The Journal of Immunology* **177**, 3004–3011 (2006).
  17. Yonezawa, A., Dutt, S., Chester, C., Kim, J. & Kohrt, H. E. Boosting Cancer Immunotherapy with Anti-CD137 Antibody Therapy. *Clin. Cancer Res.* **21**, 3113–3120 (2015).
  18. Makkouk, A., Chester, C. & Kohrt, H. E. Rationale for anti-CD137 cancer immunotherapy. *Eur. J. Cancer* **54**, 112–119 (2016).
  19. Wherry, E. J. T cell exhaustion. *Nat. Immunol.* **12**, 492–499 (2011).
  20. Wherry, E. J. & Kurachi, M. Molecular and cellular insights into T cell exhaustion. *Nat. Rev. Immunol.* **15**, 486–499 (2015).
  21. Blank, C. U. *et al.* Defining ‘T cell exhaustion’. *Nat. Rev. Immunol.* **19**, 665–674 (2019).
  22. Talkington, A. & Durrett, R. Estimating Tumor Growth Rates In Vivo. *Bull. Math. Biol.* **77**, 1934–1954 (2015).

23. Selleck, W. A. *et al.* IFN-gamma sensitization of prostate cancer cells to Fas-mediated death: a gene therapy approach. *Mol. Ther.* **7**, 185–192 (2003).
24. Nagoshi, M., Sadanaga, N., Joo, H. G., Goedegebuure, P. S. & Eberlein, T. J. Tumor-specific cytokine release by donor T cells induces an effective host anti-tumor response through recruitment of host naive antigen presenting cells. *Int. J. Cancer* **80**, 308–314 (1999).
25. Croft, M., So, T., Duan, W. & Soroosh, P. The significance of OX40 and OX40L to T-cell biology and immune disease. *Immunol. Rev.* **229**, 173–191 (2009).
26. Hendriks, J. *et al.* CD27 is required for generation and long-term maintenance of T cell immunity. *Nat. Immunol.* **1**, 433–440 (2000).
27. Esensten, J. H., Helou, Y. A., Chopra, G., Weiss, A. & Bluestone, J. A. CD28 Costimulation: From Mechanism to Therapy. *Immunity* **44**, 973–988 (2016).
28. Grasso, C. S. *et al.* Conserved Interferon- $\gamma$  Signaling Drives Clinical Response to Immune Checkpoint Blockade Therapy in Melanoma. *Cancer Cell* (2020) doi:10.1016/j.ccell.2020.08.005.
29. Havel, J. J., Chowell, D. & Chan, T. A. The evolving landscape of biomarkers for checkpoint inhibitor immunotherapy. *Nat. Rev. Cancer* (2019).
30. Braun, D. A. *et al.* Interplay of somatic alterations and immune infiltration modulates response to PD-1 blockade in advanced clear cell renal cell carcinoma. *Nat. Med.* **26**, 909–918 (2020).
31. Hellmann, M. D. *et al.* Tumor Mutational Burden and Efficacy of Nivolumab Monotherapy and in Combination with Ipilimumab in Small-Cell Lung Cancer. *Cancer Cell* **33**, 853–861.e4 (2018).

32. Goodman, A. M. *et al.* Tumor Mutational Burden as an Independent Predictor of Response to Immunotherapy in Diverse Cancers. *Mol. Cancer Ther.* **16**, 2598–2608 (2017).
33. Jiang, P. *et al.* Signatures of T cell dysfunction and exclusion predict cancer immunotherapy response. *Nat. Med.* **24**, 1550–1558 (2018).
34. Hwang, S. *et al.* Immune gene signatures for predicting durable clinical benefit of anti-PD-1 immunotherapy in patients with non-small cell lung cancer. *Sci. Rep.* **10**, 643 (2020).
35. Mlecnik, B. *et al.* Integrative Analyses of Colorectal Cancer Show Immunoscore Is a Stronger Predictor of Patient Survival Than Microsatellite Instability. *Immunity* **44**, 698–711 (2016).
36. Pagès, F. *et al.* International validation of the consensus Immunoscore for the classification of colon cancer: a prognostic and accuracy study. *Lancet* **391**, 2128–2139 (2018).
37. Hsiao, C. J. *et al.* Characterizing and inferring quantitative cell cycle phase in single-cell RNA-seq data analysis. *Genome Res.* **30**, 611–621 (2020).

# Thesis Summary

Immunotherapies for cancer are an emerging class of therapeutic strategies which aim to treat cancer via augmentation of the immune system. Despite significant success of immunotherapies in the past decade, not all patients will respond to these treatments and the reasons why immunotherapies are successful in some patients, but not others, remain incompletely understood. The immune response to cancer is a complex, multistage process, and mathematical and computational models are a useful tool for understanding such complex systems. In this thesis, I develop mathematical and computational models of Cytotoxic T Lymphocytes (CTLs), who are key players in the immune system due to their ability to recognise, destroy, and provide long lasting protection against malignant or virally infected cells.

Since the rate at which CTLs can kill tumour cells is a crucial parameter determining their efficacy in immunotherapies, in chapter 2, I ask how the killing rate of CTLs is best quantified based on imaging data. By developing Monte Carlo simulations of CTLs killing target cells, I show that population-level killing statistics can give misleading conclusions about the killing behaviour of CTLs. Specifically, I show how the results of an *in vitro* killing assay, purporting to demonstrate the existence of a subpopulation of “high rate killer” CTLs, could alternatively be explained by a homogeneous population of CTLs which require multiple hits with cumulative damage before target cells can be killed. I develop a bayesian inference procedure for estimating CTL killing parameters from imaging data, and validate this inference procedure using artificial data created with an agent based model.

In chapter 3, I ask whether the rate at which CTLs kill EL4 lymphoma cells, determined from *in vivo* two photon imaging experiments, is sufficient to explain EL4 tumour regression. To test this, I develop both an Ordinary Differential Equation (ODE) model and an Agent Based Model (ABM) to describe the interaction of adoptively transferred CTLs with the EL4 tumours. Based on the results of both models, I find that the measured killing rate of the CTLs is not compatible with tumour regression in the EL4 tumours. Using the ABM, I test alternative hypotheses which might explain how transferred CTLs could have led to tumour regression. I conclude that an antiproliferative effect associated with the transferred CTLs is compatible with the experimental data.

In chapter 4, I examine an *in vivo* data set of B16F10 melanoma treated with adoptively transferred CTLs that were stimulated with an agonist antibody targeting the CD137 receptor. I ask what were the primary mechanisms CTLs used to control the tumours, and also how the stimulation via the CD137 receptor altered the functions of the transferred CTLs. To address these questions, I developed an ODE model of the interaction between the transferred CTLs and the B16F10 tumours. Similarly to the EL4 tumours examined in chapter 3, I find that the killing rate of the transferred CTLs is insufficient to account for the reduced tumour progression after CTL transfer, and that a substantial antiproliferative effect exerted upon tumour cells is necessary to explain the data. Moreover, the results of the modelling study indicate that stimulation of the CTLs via their CD137 receptor enhances this antiproliferative effect, explaining the reduced tumour size in the CD137 stimulated condition relative to the non-CD137-stimulated control tumours.

In chapter 5 I revisit the B16F10 melanoma model using a different set of experimental data. Similarly to chapter 4, I develop an ODE model and apply it to the experimental data, confirming that the control of these B16F10 melanoma tumours after CTL transfer can largely be explained by an antiproliferative effect associated with the transferred CTLs. Accompanying the experimental data I employ in chapter 5 are longitudinal measurements of gene expression taken from the tumours. By integrating these gene expression data in the ODE model, I ask whether the transcriptional dynamics of the cytokine IFN- $\gamma$  are compatible with the dynamics of the antiproliferative effect. This analysis shows that these dynamics are indeed compatible with each other, indicating that IFN- $\gamma$  is plausibly the sole mediator of the antiproliferative effect in this *in vivo* set-up. IFN- $\gamma$  transcription did not last for more than a few days in the data, indicating that the CTLs had lost their ability to control the tumours. Therefore I also searched within the gene expression data for the transcription of molecules that might explain the deactivation of the CTLs. I conclude that the dynamics of a number of immune checkpoint molecules are compatible with their role in shutting down the antitumour functions of the CTLs.

Overall, the results in this thesis suggest that computational models are a useful and appropriate tool for understanding the immune response to cancer. Moreover, I establish a framework for examining the effector functions of CTLs in the context of cancer immunotherapy. Using this framework, I identify an important contribution of a CTL mediated antiproliferative effect in two different experimental tumour cell lines. In the B16F10 melanoma model, I characterise the antiproliferative effect in further detail. I find it is consistent with CTL secretion of the cytokine IFN- $\gamma$ , that it is enhanced by stimulation of CTLs via their CD137 receptor, but that it is also short-lived. Finally, I identify several immune checkpoint molecules associated with the termination of IFN- $\gamma$  production.



## Nederlandse samenvatting

Immuuntherapie voor kanker is in opkomst als klasse van therapeutische strategieën die gericht zijn op de behandeling van kanker via stimulatie van het immuunsysteem. Ondanks het beduidende succes van immuuntherapie in het afgelopen decennium reageren niet alle patiënten op dit type behandeling en de redenen waarom er wel of geen succes mee wordt geboekt bij sommige patiënten blijven onvoldoende begrepen. De immuunrespons op kanker is een complex proces dat bestaat uit meerdere fasen, en wiskundige en computermodellen zijn een effectief hulpmiddel om dergelijke complexe systemen te begrijpen. In dit proefschrift ontwikkel ik wiskundige en computationele modellen van cytotoxische T-lymfocyten (CTL's), hetgeen zeer belangrijke componenten zijn in het immuunsysteem vanwege hun vermogen om kwaadaardige of viraal geïnfekteerde cellen te herkennen, te vernietigen en er langdurige bescherming tegen te bieden.

Aangezien de snelheid waarmee CTL's tumorcellen kunnen doden een cruciale parameter is die hun werkzaamheid bij immuuntherapieën bepaalt, onderzoek ik in hoofdstuk 2 hoe de snelheid waarmee CTL's tumorcellen doden het best kan worden gekwantificeerd op basis van gegevens van microscopische beelden. Door Monte Carlo-simulaties te ontwikkelen van CTL's die 'target cellen' doden, laat ik zien dat statistieken over het aantal dode cellen op populatieniveau misleidende conclusies kunnen geven over het vernietigingsproces van target cellen door CTL's. In het bijzonder laat ik zien hoe de resultaten van *in vitro* 'killing assays', welke lijken te wijzen op het bestaan van een subpopulatie van CTL's die extreem snel target cellen doden, kunnen worden verklaard door een homogene populatie van CTL's die meerdere treffers nodig hebben om voldoende cumulatieve schade aan target cellen aan te richten om deze te doden. Ik ontwikkel een Bayesiaanse inferentie procedure voor het schatten van parameters gerelateerd aan het vernietigingsproces door de CTL's op basis van microscopische beelden, en valideer deze inferentie procedure met behulp van simulatie data die zijn gemaakt met een 'agent-based' model (ABM).

In hoofdstuk 3 onderzoek ik of de snelheid waarmee CTL's EL4 lymfoomcellen doden, bepaald met *in vivo* two-photon microscopie, voldoende is om EL4-tumorregressie te verklaren. Om dit te testen, ontwikkel ik zowel een 'Ordinary Differential Equation' (ODE) model als een ABM om de interactie van in het bloed geïnjecteerde CTL's met de EL4 tumoren te beschrijven. Op basis van de resultaten van beide modellen concludeer ik dat de gemeten snelheid waarmee de CTL's tumorcellen doden niet overeenstemt met tumorregressie in de EL4 tumoren. Met behulp van het ABM test ik alternatieve hypothesen die zouden kunnen verklaren hoe ingebrachte CTL's tot de waargenomen tumorregressie kunnen leiden. Ik concludeer dat een antiproliferatief effect geassocieerd met de ingebrachte CTL's compatibel is met de experimentele gegevens.

In hoofdstuk 4 onderzoek ik een *in vivo* dataset van B16F10 melanoom behandeld met in de bloedbaan geïnjecteerde CTL's die gestimuleerd zijn met een agonist antilichaam dat is gericht tegen de CD137 receptor. Ik analyseer wat de belangrijkste mechanismen waren die CTL's

gebruikten om de tumoren in bedwang te houden, en ook hoe de stimulatie via de CD137 receptor de functies van de overgedragen CTL's veranderde. Om deze vragen te beantwoorden, heb ik een ODE-model ontwikkeld van de interactie tussen de ingebrachte CTL's en de B16F10 tumoren. Net als bij de EL4 tumoren die in hoofdstuk 3 zijn onderzocht, concludeer ik dat de snelheid waarmee de ingebrachte CTL's tumorcellen doden onvoldoende is om de verminderde tumorgroei na overdracht van de CTL's te verklaren, en dat een substantieel antiproliferatief effect op tumorcellen nodig is om de gegevens te verklaren. Bovendien geven de resultaten van het model aan dat stimulatie van de CTL's via hun CD137 receptor dit antiproliferatieve effect versterkt. Dit verklaart de kleinere tumoren na stimulatie met CD137 ten opzichte van de controle situatie waarbij niet via de receptor gestimuleerd werd.

In hoofdstuk 5 bekijk ik het B16F10 melanoom systeem opnieuw met behulp van een andere set experimentele gegevens. Net als in hoofdstuk 4 ontwikkel ik een ODE-model en pas het toe op de experimentele data, waarmee ik bevestig dat het in bedwang houden van deze B16F10 melanomen na CTL overdracht grotendeels verklaard kan worden door een antiproliferatief effect geassocieerd met de overgedragen CTL's. Longitudinale metingen van genexpressie van de tumoren zijn toegevoegd aan de experimentele gegevens die ik in hoofdstuk 5 gebruik. Door deze genexpressie gegevens te integreren in het ODE model onderzoek ik of de transcriptionele dynamiek van het cytokine IFN- $\gamma$  compatibel is met de dynamiek van het antiproliferatieve effect. De analyse laat zien dat dit inderdaad het geval is, wat aangeeft dat IFN- $\gamma$  mogelijk de enige mediator is van het antiproliferatieve effect in deze experimentele opzet. IFN- $\gamma$  transcriptie duurde niet langer dan een paar dagen volgens de gegevens, wat aangeeft dat de CTL's hun vermogen om de tumoren te beheersen over de tijd verloren. Daarom heb ik binnen de genexpressie data ook gezocht naar moleculen die de deactivatie van de CTL's zouden kunnen verklaren. Ik concludeer dat de dynamiek van een aantal 'immuun checkpoint' moleculen compatibel is met de afnemende antitumor functionaliteit van de CTL's.

Over het algemeen suggereren de resultaten in dit proefschrift dat computationele modellen een waardevol en geschikt hulpmiddel zijn om de immuunrespons op kanker te begrijpen. Bovendien stel ik een raamwerk op voor het onderzoeken van de effectorfuncties van CTL's in de context van kanker immuuntherapie. Met behulp van dit raamwerk identificeer ik een belangrijke bijdrage van antiproliferatieve effecten door CTL's in twee verschillende experimentele tumor cellijnen. In het B16F10 melanoommodel verklaar ik het antiproliferatieve effect in meer detail. Ik concludeer dat het consistent is met secretie van het cytokine IFN- $\gamma$  door CTL's, dat dit effect wordt versterkt door stimulatie van CTL's via hun CD137-receptor, maar dat het ook van korte duur is. Ten slotte identificeer ik verschillende immuun checkpoint moleculen die geassocieerd zijn met de beëindiging van IFN- $\gamma$  productie.

# Curriculum Vitae

Richard Beck was born in Whitehaven, England on February 2nd 1993. In 2011, he began his studies in Engineering Science at the University of Oxford. At Oxford, Richard specialised in biomedical engineering and during his Masters he developed mathematical models of the acid-sensing ion channel. He graduated with the degree Master of Engineering in 2015, whereupon he immediately began his PhD at the Leiden Academic Centre for Drug Research, on the project: "Modelling the role of cytotoxic T lymphocytes in tumour regression". The research was conducted under the supervision of Prof. Bob van de Water and Dr. Joost B. Beltman. From August 2021 Richard will begin a postdoctoral position at the department of integrated mathematical oncology at the Moffit cancer center in Florida.

## List of publications

**Beck, Richard J.**, Maarten Slagter, and Joost B. Beltman. "Contact-dependent killing by cytotoxic T lymphocytes is insufficient for EL4 tumor regression in vivo." *Cancer research* 79, no. 13 (2019): 3406-3416.

Cazaux, Marine, Capucine L. Grandjean, Fabrice Lemaître, Zacarias Garcia, **Richard J. Beck**, Idan Milo, Jérémy Postat, Joost B. Beltman, Eleanor J. Cheadle, and Philippe Bousso. "Single-cell imaging of CAR T cell activity in vivo reveals extensive functional and anatomical heterogeneity." *Journal of Experimental Medicine* 216, no. 5 (2019): 1038-1049.

**Beck, Richard J.**, Dario I. Bijker, and Joost B. Beltman. "Heterogeneous, delayed-onset killing by multiple-hitting T cells: Stochastic simulations to assess methods for analysis of imaging data." *PLoS computational biology* 16, no. 7 (2020): e1007972.

**Beck, Richard J.**, Bettina Weigelin, and Joost B. Beltman. "Mathematical modelling based on in vivo imaging suggests CD137-stimulated cytotoxic T lymphocytes exert superior tumour control due to an enhanced antimitotic effect" *Cancers*, in press.

# Acknowledgements

I am most grateful for the help and support of numerous others, without whom this thesis would not have been possible.

First and foremost Joost, my supervisor and co-promotor. Your patience, support, and wisdom have been invaluable over these past five years. I have learned so much from you about how to approach research in a critical and methodical manner. You were always available to help me when I needed it. I could not have asked for a better supervisor.

To Bob, my promotor. I am grateful to have had the opportunity to work in your department. Your relentless drive and hunger for science is awesome. Thank you for inspiring me and for keeping me on my toes.

To Bettina W., Loic D., Kazu K., and Philippe B.. Thank you for sharing the experimental data which made this research possible. I am most grateful for all the emails and skype discussions where you answered my questions and helped me understand your data.

To my computational colleagues Margriet, Gerhard, Isoude, Huan, and Muriel. Thank you for all the feedback and the different perspectives you gave on my research these past few years. Margriet and Gerhard, you were always happy to help answer my questions about computers and coding. I'm grateful that you were both so generous with your time, I would never have made it through without you!

To all my colleagues in DDS2, thank you for the support, the fun times, and for making me feel welcome in the department. To Esmee, Bas, Britt, Luc, Linda, Matthijs, Johannes, Nanette & Muriel - it was great to participate in all the different sporty activities with you, whether it was swimming, cycling, football or skiing! Steven W. - our triathlon battles were truly epic. You were the ultimate competitor and you really showed me how to push past my limits.

To my family, thank you for the unwavering support and encouragement you have given me all these years. Mam, dad, and nana - your pride and interest in my work has been amazing. Mam and dad - you are both fantastic role models and I would be nowhere without you.